# AIR QUALITY DEGRADATION IN ALASKA WILDERNESS AREAS DUE TO

# EMISSION CHANGES

By

Trang T. Tran

RECOMMENDED: _____
Dr. Peter Webley

_____
Dr. Gregory Newby

_____
Dr. William Simpson

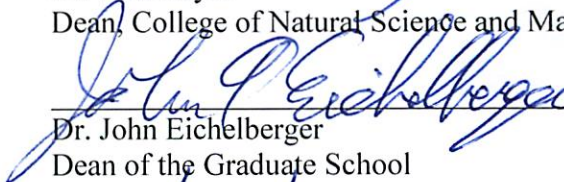_____
Dr. Catherine Cahill, Advisory Committee Chair

_____
Dr. William Simpson
Chair, Department of Chemistry and Biochemistry

APPROVED: _____
Dr. Paul Layer
Dean, College of Natural Science and Mathematics

_____
Dr. John Eichelberger
Dean of the Graduate School

_____
8/20/2013
Date

AIR QUALITY DEGRADATION IN ALASKA WILDERNESS AREAS DUE TO

EMISSION CHANGES


A

DISSERTATION



Presented to the Faculty

of the University of Alaska Fairbanks



in Partial Fulfillment of the Requirements

for the Degree of



DOCTOR OF PHILOSOPHY



By

Trang T. Tran, B.S., M.S.



Fairbanks, Alaska

August 2013

**Abstract**

The increasing trends in aerosol concentrations observed by the Interagency Monitoring of Protected Visual Environments (IMPROVE) network in the wilderness areas along the Gulf of Alaska during low insolation periods and in Denali National Park and Preserve (Denali NP) during high insolation periods have raised the concerns about air quality degradation and visibility impairment in these pristine areas. This dissertation aims to investigate the reason for those observed increases in aerosol concentrations in Alaska wilderness areas by performing a series of simulation sets with the Weather Research and Forecasting model coupled with Chemistry (WRF-Chem). These simulation sets use the same meteorological conditions but change the emission scenarios.

The model evaluation analysis showed that WRF-Chem performed well in simulating meteorological conditions over Alaska and the North Pacific under both low and high insolation conditions. Performance skill-scores of the WRF-Chem model in simulating aerosol concentrations for the coastal monitoring sites along the Gulf of Alaska were consistent with state-of-the-science air-quality model performance.

During low insolation periods, domestic and international ship emissions were the most important contributors to aerosol concentrations in the coastal regions along the Gulf of Alaska. The increases/decreases in ship emissions led to subsequent increases/decreases in aerosol concentrations in the coastal areas along the Gulf of Alaska during low insolation periods. During high insolation periods, in Interior Alaska, the contributions of local wildfire emissions to aerosol concentrations were notable even

during the weak Alaska fire activity scenario. Under the strong Alaska fire activity scenario, local wildfire emissions were the dominant source of aerosols in Interior Alaska. The increases in Alaskan wildfire emissions led to significant increases in aerosol concentrations in Interior Alaska.

During both low and high insolation periods, Japanese anthropogenic and Siberian wildfire emissions were not important contributors to total aerosol concentrations in all regions of Alaska.

Overall in the wilderness areas along the Gulf of Alaska, the increases in aerosol concentrations observed during low insolation periods stemmed from increases in domestic and international ship emissions in the North Pacific. In contrast, the increases in aerosol concentrations observed at Denali NP during high insolation periods stemmed from increases in Alaskan wildfire emissions.

# Table of Contents

# List of Tables

# List of Figures

**Acknowledgement**

I would like to take this opportunity to deeply acknowledge the generous supports from many kind people who help to make my "Ph.D. dream" come true.

First of all, I would like to express my deep sense of gratitude to my advisor, Dr. Catherine F. Cahill for her continuous guidance, kind understanding, encouragement and excellent advice for my research and writing of this dissertation. I would not have gotten to this point without her support.

I gratefully acknowledge my committee members: Dr. William R. Simpson, Dr. Gregory B. Newby and Dr. Peter Webley for their constructive comments and encouragement. My gratitude also goes to Dr. Nicole Mölders, Dr. Georg A. Grell and Dr. Martin Stuefer for their valuable instructions in solving technical questions and other fruitful discussion for my research. I also own many thanks to Ms. Carol Holz, Ms. Laura Bender and Ms. Sue Wolfe for encouraging me to stay strong and overcome some important obstacles during my Ph.D. program.

I am thankful to all funding resources contributed to my research and dissertation writing. The exact funding sources that supported each study are acknowledged in each corresponding chapter. I would like to thank Arctic Region Supercomputing Center and Dr. Christopher R. Iceman for their computational support.

My sincere thanks are sent to faculty and staff of the Department of Chemistry and Biochemistry and Department of Atmospheric Sciences at UAF for their generous assistance during my time here. My special thanks are also sent to my research colleagues, labmates and friends: Huy N.Q. Tran, Taryn Lopez, Jennifer Bell, Peter

xiv

**Chapter 1 Introduction**

Alaska is one of the most pristine areas of the United States (Karl et al., 2011). Three of the four monitoring sites of Interagency Monitoring of Protected Visual Environments (IMPROVE) air monitoring network in Alaska, including Denali National Park and Preserve (Denali NP), Simeonof and Tuxedni Wilderness Ares are located in areas defined as Class I by the Clean Air Act and protected by the Regional Haze Rule (EPA, 2013a). In these areas, a national visibility goal is stated as "the prevention of any future and remedying of any existing impairment of visibility in mandatory Class I Federal areas, which impairment results from man-made air pollution." These mandates are obligatory in the Clean Air Act Amendments of 1977 and must be attained (ADEC, 2012a). However, the IMPROVE data indicate that fine sulfate aerosol concentrations have increased over the last decades at the three monitoring sites in Class I Areas and at Trapper Creek, another IMPROVE site (Malm et al., 1994; Mölders et al., 2010; IMPROVE, 2013). Increases in fine aerosol concentrations in Alaska wilderness areas are of concern as increasing aerosol concentrations will lead to visibility degradation. Moreover, the increasing acidic aerosol (e.g., sulfate) concentrations also will lead to acid deposition that may harm the ecosystem in these wilderness areas. Improved knowledge and understanding of the major contributors to particulate pollution and the impact of increased emissions could help policy makers in their cost-efficient decision making and help prevent the degradation of air quality in the wilderness areas of Alaska.

According to Environmental Protection Agency's (EPA) definition (EPA, 2013b), fine aerosols are particulate matter, which can be solid particles or liquid droplets with

diameter $\leq 2.5$ µm ($PM_{2.5}$). $PM_{2.5}$ can be directly emitted to the atmosphere by emission sources (primary aerosols) or can be formed by precursor gases via gas-to-particle conversions (secondary aerosols) (Finlayson-Pitts and Pitts, 1999; Seinfeld and Pandis, 2006). $PM_{2.5}$ can cause adverse impacts to human health such as heart and lung diseases and premature deaths (Kappos et al., 2004; Dominici et al., 2006; Pope and Dockery, 2006). $PM_{2.5}$ may also cause adverse impacts to the ecosystem such as increasing acid deposition onto vegetation or acid loading in water bodies. $PM_{2.5}$ additionally decreases visibility (Bulger et al., 1998; NAPAP, 2005; Han et al., 2012). In the wilderness areas in Alaska where population density is extremely low but wildlife is valuable as a food source and tourist draw, the environmental impacts of $PM_{2.5}$, such as increased acid deposition and impaired visibility, are of greater concern than their human health impacts.

Alaska differs from the rest of the U.S. in its remote location and unique climate of long, dark, cold winters contrasted with endless sunlight in warm summers. Among winter and summer months, January and June, respectively, remain of special interest since they are the most extreme insolation periods in Alaska. In January, daylight hours range from 0 hrs in the north to 7 hrs in the south of Alaska (Shulski and Wendler, 2007), leading to predominantly nighttime atmospheric chemistry. In June, daylight hours range from 18 hrs in the south to 24 hrs in the north of Alaska (Shulski and Wendler, 2007), favoring a dominance of daytime atmospheric chemical processes. Under these extreme insolation conditions, photochemical mechanisms of aerosol formation in the Arctic and sub-Arctic regions of Alaska differ from those in mid-latitudes. Hence, one cannot assess

the impact of emissions on aerosol concentrations in Alaska from previous studies performed for mid-latitudes.

The strong variations in insolation and temperature conditions yield very distinct annual cycles for emission sources of aerosols in Alaska, such as wildfires, dimethyl sulfide (DMS) from the ocean, residential combustions and cruise ship emissions. During low insolation periods, local emissions from residential combustions, car exhausts, industrial productions and long-range transport of anthropogenic pollutants to the state are sources of aerosols in Alaska. During high insolation periods, wildfire emissions are another source of aerosols.

The trends in aerosol concentrations vary across different geographic regions of Alaska and vary between low and high insolation periods. As a high lattitude region, Alaska has large charge in solar irradiation (i.e. insolation) among seasons due to large differences in the amount of daylight (Shulski and Wendler, 2007). In Alaska, during late fall and winter (Nov-Feb), daylight hours are at a minimum whereas during summer (Jun-Aug) daylight hours are at a maximum (Shulski and Wendler, 2007). For low insolation conditions (Nov - Feb), sulfate concentrations measured at the IMPROVE network sites have increased at the coastal sites along the Gulf of Alaska and decreased in Denali NP in Interior Alaska (Fig. 1.1a, b). For high insolation conditions (Jun-Aug), sulfate concentrations have increased in Denali NP and decreased at the coastal sites (Fig. 1.1c, d). The small slope values of the observed sulfate concentration trend lines indicate the slow rate of change in sulfate concentrations for both low and high insolation conditions (Fig. 1.1a, b, c, d). The observed trends were statistically significant for low insolation

conditions and insignificant for high insolation conditions at the 95% confidence level (Fig. 1.1a, b, c, d). The large variability of wildfire emissions during high insolation conditions might affect the statistical significance of the linear trends. The differences in photochemical mechanisms and emission variations between low and high insolation periods, as discussed previously, may contribute to the different behavior of aerosol concentration trends observed in different regions of Alaska. Therefore, investigating the relationship between emission changes and aerosol concentration changes in Alaska must be conducted for both low and high insolation periods, for which January and June serve as temporal bookends in this study.

In Alaska natural sources of $PM_{2.5}$ include volcanic eruptions (Cahill et al., 2010; Webley et al., 2006), oceanic emissions such as DMS (Ferek et al., 1995), sea salt (Shaw, 1991) and biogenic emissions from boreal forests (Spracklen et al., 2008). Lightning and human-initiated wildfires are also the sources of $PM_{2.5}$ in Alaska (Duck et al., 2007; Grell et al., 2011; Hecobian et al., 2011). Anthropogenic sources can be local emission sources of Alaska especially from major cities (e.g., Anchorage, Fairbanks and Juneau) (Tran and Mölders, 2012a, b; Department of Health and Human Services, 2011). The long-range transports of the pollutants from the anthropogenic sources outside of the state such as ship emissions (Geiser et al., 2010; Mölders et al., 2010) or Asian emissions (Shaw and Khalil, 1989; Quinn et al., 2007; ADEC, 2012a) also brings $PM_{2.5}$ to Alaska. Observed increases in aerosol concentrations may stem from the increases in emissions of either local or out-of-state sources.

The number of volcanic eruptions in Alaska has showed no trends during the last decades (Mölders et al., 2011a), suggesting volcanic emissions cannot be responsible for any observed trends in aerosol concentration. Alaska forested acreage declined by ~1% between 1953 and 2007 (Smith et al., 2009), suggesting a slight decrease in biogenic emissions. DMS concentrations in sea water in the Gulf of Alaska showed decreasing trends over the last decade, implying decreases in DMS emissions (Fig. 1.2). Therefore, the steady volcanic emissions, decreased biogenic and DMS emissions should not be contributing factors to the increases in aerosol concentrations observed at IMPROVE monitoring sites.

Alaska anthropogenic emissions are extremely low in most areas of the state, except for oil operations on the North Slope of Alaska and human activities in a few of the largest cities of the state (Blake et al., 1992; Hoefler Consulting Group and Sierra Research Green Engineering, 2001). Oil production on the North Slope and emissions from Alaska's fossil fuel industry have been in decline since 1988 (ADEC, 2008; EIA, 2012). Although the Alaskan population has grown continuously from from 401,000 in 1980 to 731,000 in 2012 (U.S. Census Bureau, 2013), Alaska's population density is still the lowest in the US (i.e. 1.2 persons per square miles in 2010 in Alaska compared with 87.4 persons per square miles averaged over the U.S). About 60% of Alaska's population is concentrated in the three largest cities: Anchorage, Fairbanks and Juneau (U.S. Census Bureau, 2013). In Fairbanks, local emission sources coupled with strong inversions under low insolation conditions (due to its special location and topography) have caused local $PM_{2.5}$ pollution in Fairbanks (Tran et al., 2012; Tran and Mölders,

2012a; Mölders, 2013). Reported measurements of $PM_{10}$ pollution in Anchorage are related to natural sources (volcanic ash, dust) rather than anthropogenic sources (Gordian et al., 1996; Department of Health and Human Services, 2011; ADEC, 2012b). Juneau air quality is within the EPA's National Air Quality Standards (ADEC, 2010). The impacts of local anthropogenic emissions on $PM_{2.5}$ concentrations in the entire state of Alaska are minimal, except for local $PM_{2.5}$ pollution in Fairbanks, which is enhanced by local meteorological conditions, such as strong inversions under low insolation conditions (see ADEC, 2012b). Anchorage has experienced dramatic improvements in air quality in recent years (Genova et al., 2006). Conversely, the air quality in Fairbanks has decreased considerably, during the past several years, with more days showing $PM_{2.5}$ concentrations exceeding the national standard of 35.5 µg m$^{-3}$ (ADEC, 2013). However, polluted air in Fairbanks occurs during strong inversions when the air is not moving out of the Fairbanks area; hence there is no transport of the pollutants to the Denali NP or wilderness areas along the Gulf of Alaska. Therefore, the changes in local anthropogenic emissions across Alaska are not the causes of the increases in aerosol concentrations observed at the IMPROVE monitoring sites.

Alaska's air quality is well-known to be impacted by long-range transports from anthropogenic sources in Europe and Russia especially during the Arctic haze season (late winter and spring) (Shaw and Khalil, 1989; Polissar et al., 2001; Quinn et al., 2007; ADEC, 2012a). In Alaska, only the North Slope falls within the Arctic climate region (Stafford et al, 2000; Wendler and Shulski, 2009). All of the IMPROVE network monitoring sites fall within the sub-Arctic regions which are less impacted by Arctic haze

than the Arctic regions (ADEC, 2012a). In addition, the observational data at Barrow on the North Slope indicates that aerosol concentrations stemming from Arctic haze have decreased markedly over the last decades (Bodhaine and Dutton, 1993; Quinn et al., 2009). Therefore, the decreases in aerosol concentrations during Arctic haze events would not cause the observed increases in aerosol concentrations at sites south of the North Slope, such as Denali NP and the coastal regions along the Gulf of Alaska.

Asian dust events are also found to impact aerosol concentrations and speciation in the Arctic and sub-Arctic regions of Alaska during local spring time (Rahn et al., 1977; Barrie and Barrie, 1990; Cahill, 2003). Their impacts on aerosol concentrations in Alaska under extreme insolation conditions (i.e., January and June) are weak (Wilcox II and Cahill, 2003). Moreover, the IMPROVE monitoring data for local spring time (March, April and May) in Denali NP and at the coastal sites along the Gulf of Alaska indicate that fine soil aerosol concentrations have decreased over the last decades (IMPROVE, 2013), suggesting that the observed increases in aerosol concentrations at these sites are not related to the changes in Asian dust emissions.

Asian anthropogenic emissions in China and Japan have increased over the last decades (Tanimoto et al., 2009). Transport of pollutants from East Asia to North America usually occur only at high altitudes due to air mass uplift near the emission source regions (Shaw and Khalil, 1989; van Curen, 2003; Shindell et al., 2008). Typically, pollution from China and Japan is emitted at low altitudes, follows a northeastern track towards the Arctic, encounters the Aleutian Low, and are is scavenged before reaching

Alaska (ADEC, 2011). Therefore, Asian emission changes are unlikely to affect aerosol concentration at surface sites.

Due to its pristine environment, abundant wildlife and natural landscapes of mountains and glaciers, Alaska has been an attractive place for cruise tourism (Alaska Resource Development Council, 2013). Other commercial marine vessel types, such as tugs, fishing vessels and ferries, are also an essential part of the intrastate and interstate transportation system for Alaska (MXAK, 2005). International ship traffic significantly affects air quality along the West Coast of the contiguous U.S. (Capaldo et al., 1999) and Alaska. Both international and domestic marine traffic emissions have been proved to impact the air quality of the coastal areas along the Gulf of Alaska (Geiser et al., 2010; Graw et al., 2010; Mölders et al., 2010; 2011a). Marine travel is an important contributor to the state's economy with the number of marine vehicles and passengers using Alaska marine highway system have been increasing since 1963 (Metz et al., 2011). This increased usage of the marine highway suggests increases in ship emissions in Alaska. Mölders et al. (2011a) showed increasing $PM_{2.5}$ and $SO_2$ emissions from shipping lanes in the Gulf of Alaska. The increase in ship emissions, therefore, is a potential cause of observed increases in aerosol concentrations under low insolation conditions in the coastal regions along the Gulf of Alaska.

In Alaska, the wilderness environment is strictly protected from impacts of anthropogenic activities, but the impacts of wildfire emissions on air quality are unavoidable under high insolation periods, especially because most of the wildfires in Alaska are due to lightning ignitions (Barney, 1971; Bieniek, 2007). Wildfire plumes

undergo long-range transports, especially at upper altitudes due to the high injection height of fire emissions (Grell et al., 2011; Hecobian et al., 2011; Sessions et al., 2011). Many studies show that boreal forest fires impact air quality on regional (Tanimoto et al., 2000; Kato et al., 2002), continental and even hemispheric scales (Wotawa and Trainer, 2000; Copper et al., 2001; Forster et al., 2001). Located downwind of the prevailing westerlies from Siberia, Alaska's air quality can be impacted not only by local wildfire emissions but also by Siberian wildfire emissions. However, since Siberian wildfires are mostly surface fires. For a typical year in Siberia, Belov (1976) and Furyaev (1996) reported that 80% of all fires were surface fires with relatively low injection heights (~1300 m above sea level (Jet Propulsion Laboratory, 2013)), advection of Siberian wildfire plumes to Alaska would be subject to more intense lower atmospheric scavenging mechanisms, and less impact on Alaskan aerosol particle concentrations may be expected. Wildfire emissions in both Alaska and Siberia have increased over the few last decades (Barney, 1971; Soja et al., 1997; Juday et al., 2004) partly due to climate change effects including increases in temperature and decreases in summer precipitation in the boreal regions (Stocks et al., 1998; Stafford et al., 2000). The increase in wildfire emissions, mainly in Alaska, is a potential cause of the observed increase in aerosol concentrations under high insolation episodes over Interior Alaska.

Modeling simulations of the impacts of emission changes on aerosol concentrations have been conducted at hemispheric and global scales, including covering the state of Alaska (Saikawa et al., 2009; Lei et al., 2011; Hedegaard et al., 2012). These studies mostly discussed the relationship between anthropogenic emission changes and

air quality changes in densely populated areas. Because these modeling studies were conducted at hemispheric and global scales, the modeling grid resolutions were too coarse to answer the questions about air quality degradation in the national parks and wilderness areas in Alaska. Previous studies of aerosols in Alaska focus on specific aerosol pollution events (e.g., Fairbanks $PM_{2.5}$ pollution (Tran and Mölders, 2012a,b; Leelasakultum et al., 2012; Mölders, 2013), Asian dust events (Cahill, 2003), or typical wildfire events (Duck et al., 2007; Grell et al., 2011; Hecobian et al., 2011), or the changes of aerosol concentrations related to Arctic haze in Barrow, North Slope (Bodhaine and Dutton, 1993; Quinn et al., 2009)). The reasons for the increasing trends in aerosol concentrations in the Alaska wilderness areas in the Interior Alaska and the coastal areas along the Gulf of Alaska still have not been investigated.

This dissertation aims to investigate the impacts of emission changes on aerosol concentrations in the wildernesses and other areas of Alaska under low and high insolation conditions, with a focus on ship and wildfire emission changes, respectively. The research hypothesis is: *the observed increases in aerosol concentrations in the wilderness areas along the Gulf of Alaska under low insolation periods are due to increases in ship emissions; whereas the observed increases in aerosol concentrations in Denali NP under high insolation conditions are due to the increases in Alaskan wildfire emissions.* To test this hypothesis, four scientific questions will be addressed:

1) Which emission sectors are the important contributors to aerosol concentrations in the coastal areas along the Gulf of Alaska under low insolation conditions?

2) How do emission changes from the important contributors affect aerosol concentrations in the coastal areas along the Gulf of Alaska under low insolation conditions?

3) Which emission sectors are the important contributors to aerosol concentrations in Interior Alaska under high insolation conditions?

4) How do emission changes from the important contributors affect aerosol concentrations in the Interior Alaska under high insolation conditions?

To answer these questions and test the hypothesis, the impacts of various emission sources and their impacts on aerosol concentrations are quantified for various regions of Alaska. In Alaska, the experimental measurement stations are too scarce to provide answers to such questions, so a numerical modeling approach with the Alaska-adapted (Mölders et al., 2011b) version of the Weather Research and Forecasting model (WRF; Skamarock et al., 2008) inline coupled with chemistry packages (WRF-Chem; Grell et al., 2005; Peckham et al., 2009) was selected for this study. WRF-Chem allows different emission scenarios to be switched on or off and meteorology kept the same to isolate the emission impacts for a specific source or group of sources. WRF-Chem has been applied as a state-of-the-science chemistry transport model for many locations (Gustafson et al., 2007; Barnard et al., 2009; Yang et al., 2012). Moreover, the many sophisticated physics and chemistry schemes developed for WRF-Chem make it possible to capture the extreme weather and chemistry in the Arctic and sub-Arctic regions (Mölders, 2008; Hines and Bromwich, 2008; Mölders and Kramm, 2010; Mölders et al., 2011b; 2012; Wilson et al., 2011; PaiMazumder et al., 2012). Therefore, the WRF-Chem

model, with modifications for Alaska conditions introduced by Mölders et al (2011b), is a suitable choice for the research methodology of this dissertation. The main purpose of using WRF-Chem in this study is to capture the long-range transports of pollutants from potential emission sources to Alaska as well as the impact of local sources. Therefore, WRF-Chem simulations are performed with 30 km grid-increments over the model domain that encompasses Alaska, Japan, Siberia and the North Pacific (figures indicating model domain are shown in Chapter 4, 5 and 6).

The answers to questions (1) and (2) serve to identify whether ship emissions are the major contributor to the aerosol concentrations and the main cause for the increased aerosol concentrations observed in the wilderness areas along the Gulf of Alaska during low insolation periods. Similarly, the answers to question (3) and (4) serve to identify the roles of wildfire emissions on increased aerosol concentrations observed in the Denali NP during high insolation periods.

To answer question (1), WRF-Chem simulations were performed for January 2000 (hereafter referred as REF_Jan) taking into account the emissions inside Alaska (i.e., local anthropogenic sources) and outside Alaska (i.e., shipping lanes and other anthropogenic sources from Asia and Siberia). The relative importance of ship emissions versus Alaskan and Asian anthropogenic emissions on aerosol concentrations in various regions of Alaska was examined by determining the prevailing winds for various regions of Alaska and identifying the potential emission sources of aerosol concentrations located upwind of the regions of interest. The multi-correlation coefficients of $SO_2$ or sulfate aerosol concentrations for each region of interest in Alaska versus $SO_2$ emission and

wind speed at each grid-cell over the entire WRF-Chem domain at various time-lags were calculated to check whether there was advection of aerosols from the potential sources to the receptor (i.e., regions of Alaska). Chapter 4 addresses the results used to answer this question.

To answer question (2), Student's t-tests with a 95% significance level were applied for the differences in hourly averaged sulfate aerosol and its precursors concentrations between REF_Jun simulations and the other simulations that used the same meteorological conditions of January 2000 but with the emissions of January 1990. These tests examined whether the increase in ship emissions could have caused the increases in observed aerosol concentrations at wilderness areas along the Gulf of Alaska under low insolation conditions. The statistical test was also applied to the differences in hourly averaged aerosol precursor emissions and aerosol concentrations between REF_Jan simulations and the other simulations that had the same starting parameters as REF_Jan except for the ship emissions.  Nautical emissions were reduced in the simulations in accordance with the reduction rates proposed for the shipping lanes inside and outside the North American Emission Control Area (ECA) to examine if reductions in ship emissions improve air quality of Alaska. The ECA, under the International Convention for the Prevention of Pollution from Ships (MARPOL), comes into effect on 1 August 2012 and regulates stricter controls on emissions of $SO_2$, NOx and particulate matter for ships trading off the coasts of Canada, the United States and the French overseas collectivity of Saint-Pierre and Miquelon (IMO, 2013). Chapters 4 and 5 discuss

the impacts of ship emission changes on aerosol concentration changes in the coastal regions along the Gulf of Alaska under low insolation conditions.

To answer question (3), WRF-Chem simulations were performed for June 2008 (REF_Jun) to investigate the importance of Alaskan wildfire emissions versus Siberian wildfires, Japanese anthropogenic sources, shipping sources and Alaskan anthropogenic emissions on aerosol concentrations in Interior Alaska and the coastal regions of Alaska. In June 2008, Alaska had minimum levels of fire activity (Alaska Department of Forestry, 2012) while Siberia had normal levels of fire activity (MODIS burned area product; Roy et al., 2005; 2008) according to the historical record. Therefore, the emission situation for June 2008 is an appropriate scenario to use to explicitly examine the long-range transports of Siberian wildfire plumes to Alaska. The important emission sectors affecting $PM_{2.5}$ concentrations in Alaska were identified by comparing the daily-averaged wind patterns with the horizontal distributions of daily-averaged $PM_{2.5}$ concentrations over the entire WRF-Chem domain in the near-surface layer and above the atmospheric boundary layer (~2 km). This identified the advection pathways from emission sources to Interior Alaska and the coastal regions of Alaska.

Unlike other sources considered in this dissertation, wildfire emissions had a large interannual variability; therefore, the relative importance of all potential wildfire sources versus anthropogenic sources on aerosol concentrations in Interior Alaska strongly varied with respect to wildfire activities in this region. The relative contributions of wildfire ( or anthropogenic) emissions to $PM_{2.5}$ concentrations in Alaska was calculated by comparing the model results of the simulations with and without wildfire (or anthropogenic)

emissions to address the relative importance between these two sectors. Such calculations were conducted for a weak Alaska fire activity scenario (June 2008; hereafter referred as REF_Jun) and an increased Alaska fire activity scenario (June 2004; hereafter referred as IFA). 2004 was selected to represent the strong fire activity scenario because it was the worse fire year during the last decade (Alaska Department of Forestry, 2012). IFA simulations were performed with the same setup as REF_Jun except that wildfire emissions were obtained from June 2004 data. Unlike the Alaskan wildfires, Siberian wildfire activities were strong in REF_Jun and weak in IFA (MODIS burned area product; Roy et al., 2005; 2008). Chapter 6 discusses the relative importance of Alaskan versus Siberian wildfires and anthropogenic emissions on $PM_{2.5}$ concentrations.

To answer question (4), in Interior Alaska, the temporal evolutions of daily, regionally-averaged $PM_{2.5}$ precursor emissions, $PM_{2.5}$ concentrations and $PM_{2.5}$ speciation were compared between the IFA and REF_Jun simulations to investigate the changes in $PM_{2.5}$ concentrations and speciation in response to the increases in Alaskan wildfire emissions. The Student's t-test with a 95% significance level was applied to the differences in hourly averaged $PM_{2.5}$ concentrations between IFA and REF_Jun to examine whether the increases in Alaskan wildfire emissions may have caused the increases in observed aerosol concentrations at the Denali NP under high insolation conditions. The results discussed in Chapter 6 serve to answer this question.

Chapter 2 of this dissertation describes the physical/chemistry packages of WRF-Chem model, model setup and model evaluation methods. It also includes a summary of the evaluations of model performances from previous studies and an analysis of the

impacts of various emission sources and their changes on aerosol concentrations in various regions of Alaska. Chapter 3 presents the emission inventories prepared for carrying out the WRF-Chem simulations performed for this dissertation. The overall conclusions of this study are presented in Chapter 7.

**References**


ADEC, 2008. Improvements to the Alaska greenhouse gas emission inventory. Summary report. Available at http://www.climatechange.alaska.gov/docs/ghg_ei_rpt.pdf

ADEC, 2010. Juneau air quality monitoring report. Air Quality Division, Air Monitoring and Quality Assurance Program.
Available at http://dec.alaska.gov/air/am/projects&Reports/FDMS_rpt_93-09.pdf

ADEC, 2011. Overview of Alaska and air quality. Amendments to state air quality control plan, appendix to Section III.K: Areawide pollutant control program for regional haze. Available at http://dec.alaska.gov/air/anpms/rh/rhdoc2/Appendix%20III.K.3.pdf

ADEC, 2012a. Regional haze trans-boundary monitoring study report. Air Quality Division, Air Monitoring and Quality Assurance Program. Available at http://www.dec.state.ak.us/air/am/Haze%20report/Final%20Regional%20Haze%20Trans -Boundary%20Monitoring%20Project.pdf

ADEC, 2012b. State of Alaska 2010 ambient air quality network assessment. Monitoring and Quality Assurance, Division of Air Quality, Department of Environmental Conservation. Available at
http://www.dec.state.ak.us/air/am/Alaska%202010%20Ambient%20Air%20Quality%20 Network%20Assessment.pdf

ADEC, 2013. $PM_{2.5}$ and Fairbanks. Retrieved March 12, 2013, from http://www.dec.state.ak.us/air/anpms/pm/pm2-5_fbks.htm

Alaska Department of Forestry, 2012. Fire statistics. Retrieved June 17, 2012, from http://forestry.alaska.gov/firestats/index.htm

Alaska Resource Development Council, 2013. Alaska's Tourism Industry. Retrieved March 17, 2013, from http://www.akrdc.org/issues/tourism/overview.html

Barnard, J.C., Fast, J.D., Paredes-Miranda, G.L., Arnott, P.W., Laskin, A., 2009. Technical Note: Evaluation of the WRD-Chem 'aerosol chemical to aerosol optical properties' module using data from the MILAGRO campaign. Atmos. Chem. Phys., 10, 8927-8961.

Barney, R.J., 1971. Wildfires in Alaska-some historical and projected effects and aspects. Proceedings of Fire in the Northern Environment - A Symposium - Fairbanks, AK 13-14 April 1971. 51-59.

Barrie, L. A., Barrie, M. J., 1990. Chemical components of lower tropospheric aerosols in the high arctic: six years of observations. J. Atmos. Chem., 11, 211-226.

Belov, S.V., 1976. Forest Pyrology. Leningrad Forestry Academy of the USSR, St. Petersburg, Russia.

Bieniek, P., 2007. Climate and predictability of Alaska wildfires. Master thesis, Uni. of Alaska Fairbanks.

Blake, D. R., Hurst, D.F., Smith, T.W., Whipple, W.J., Chen, T.-Y., Blake, N.J., Rowland, F.S., 1992. Summertime measurements of selected nonmethane hydrocarbons in the arctic and subarctic during the 1988 Arctic Boundary Layer Expedition (ABLE3A). J. Geophys. Res., 97, 16559-16588.

Bodhaine, B., Dutton, E., 1993. A long-term decrease in Arctic haze at Barrow, Alaska. Geophys. Res. Lett., 20, 947-950.

Bulger, A., Cosby, J., Webb, R., 1998. Acid Rain: current and projected status of coldwater fish communities in the Southeastern US in the context of continued acid deposition. Coldwater conservation fund report for Trout Unlimited. Available at http://swas.evsc.virginia.edu/Assests/Docs/Current-and-Projected-Status.pdf

Cahill, C.F., 2003. Asian aerosol transport to Alaska during ACE-Asia. J. Geophys. Res., 108(D23), 8664.

Cahill, C.F., Rinkleff, P.G., Dehn, J., Webley, P.W., Cahill, T.A., Barnes, D.E., 2010. Aerosol measurements from a recent Alaskan volcanic eruption: Implications for volcanic ash transport predictions. J. Volcanol. Geotherm. Res, 198, 76-80.

Capaldo, K., Corbett, J.J., Kasibhatla, P., Fischbeck, P.S., Pandis, S.N., 1999. Effects of ship emissions on sulfur cycling and radiative climate forcing over the ocean. Nature, 400, 743-746.

Copper, O.R., Moody, J.L., Thornberry, T.D., Town, M.S., Carroll, M.A., 2001. PROPHET 1998 meteorological overview and air-mass classification. J. Geophys. Res., 106, 24289-24299.

Department of Health and Human Services, 2011. Air quality in Anchorage – A summary of air monitoring data and trends 1980-2010. Air Quality Program of Municipality of Anchorage, Public Health Division. Available at
 http://www.dec.alaska.gov/air/anpms/doc-anpms/2011%20AQ%20report%20-%20final.pdf

Dominici, F., Peng, R.D., Bell, M.L., 2006. Fine particulate air pollution and hospital admission for cardiovascular and respiratory diseases. J. Ameri. Med. Assoc., 295(10), 1127-1134.

Duck, T.J., Firanski, B.J., Millet, D.B., Doldstein, A.H., Holzinger, R., Worsnop, D.R., White, A.B., Stohl, A., Dickinson, C.S., van Donkelaar, A., 2007. Transport of forest fire emissions from Alaska and the Yukon Territory to Nova Scotia during summer 2004. J. Geophys. Res., 112, doi:10.1029/2006JD007716.

EIA, 2012. Annual energy outlook 2012 with projections to 2035. DOE/EIA-0383(2012). Retrieved Febuary 10, 2013, from http://www.eia.gov/forecasts/aeo/

EPA, 2013a. List of 156 Mandatory Class I Federal Areas. EPA's website, retrieved Feb 5th 2013 from http://www.epa.gov/visibility/class1.html

EPA, 2013b. Particulate matter. EPA's website, retrieved March 20th 2013 from http://www.epa.gov/pm/

Ferek, R.J., Hobbs, P.V., Radke, L.F., Herring, J.A., Sturges, W.T., Cota, G.F., 1995. Dimethyl sulfide in the arctic atmosphere. J. Geophys. Res., 100, 26093-26104.

Finlayson-Pitts, B.J., Pitts, J.N.Jr, 1999. Chemistry of the upper and lower atmosphere: theory, experiments and applications. Academic Press. ISBN-13: 978-0122570605.

Forster C, Wandinger U, Wotawa G, James P, Mattis I, Althausen D, Simmonds P, O'Doherty S, Jennings SG, Kleefeld C, Schneider J, Trickl T, Kreipl S, Jager H,Stohl A, 2001. Transport of boreal forest fire emissions from Canada to Europe. J. Geophys. Res., 106, 22887-22906.

Furyaev, V.V., 1996. Fire Ecology of Siberian Boreal Forests. Fire in Ecosystems of Boreal Eurasia. Eds: Goldammer, J.G., Furyaev, V.V.. Kluwer Academic Publishers, Netherlands, 168–185.

Geiser, L., Schirokauer, D., Bytnerowicz, A., Dillman, K., Fenn, M., 2010. Effects of cruise ship emissions on air quality and terrestrial vegetation in Southeast Alaska. In: Shah, M. (Ed), Alaska park science, ISSN 1545-4967.

Genova, F. D., Dulla, R., Carlson, T., 2006. Tier 2 gasoline emission benefits in Alaska. Report prepared for ADEC, Report No. SR2006-09-01.

Gordian, M.E., Ozkaynak, H., Xue, J., Morris, S.S., Spengler, J.D., 1996. Particulate air pollution and respiratory disease in Anchorage, Alaska. Environ. Health Persp., 104, 290-297.

Graw, R., Faure, A., Schirokauer, D., 2010. Air pollution emissions from tourist actitities in Klondike Gold Rush National Historical Park. In: Shah, M. (Ed), Alaska park science, ISSN 1545-4967.

Grell, G.A., Peckham, S.E., Schmitz, R., McKeen, S.A., Frost, G., Skamarock, W.C., Eder, B., 2005. Fully coupled "online" chemistry within the WRF model. Atmos. Environ., 39, 6957-6975

Grell, G.A., Freitas, S.R., Stuefer, M., Fast, J., 2011. Inclusion of biomass burning in WRF-Chem: impact of wildfires on weather forecasts. Atmos. Chem. Phys., 11, 5289–5303.

Gustafson, W.I. Jr., Chapman, E.G., Ghan, S.J., Fast, J.D., 2007. Impact on modeled cloud characteristics due to simplified treatment of uniform cloud condensation nuclei during NEAQS 2004. J. Geophys. Res. Lett., 34, L19809.

Han, S., Bian, H., Zhang, Y.m Wu, J., Wang, Y., Tie, X., Li, Y., Li, X., Yao, Q., 2012. Effect of aerosols on visibility and radiation in spring 2009 in Tianjin, China. Aeros. A.Q. Res., 12, 211–217.

Hines, K.M., Bromwich, D.H., 2008. Development and testing of Polar Weather Research and Forecasting (WRF) model. Part I: Greenland ice sheet meteorology. Mon. Wea. Rev., 136, 1971-1989.

Hecobian, A., Liu, Z., Hennigan, Z., Huey, L. G., Jimenez, J. L., Cubison, J. L., Vay, S., Diskin, G. S., Sachse, G. W., Wisthaler, A., Mikoviny, T., Weinheimer, A. J., Liao, J., Knapp, D. J., Wennberg, P. O., K¨urten, A., Crounse, J. D., St. Clair, J., Wang, Y., Weber, R. J., 2011. Comparison of chemical characteristics of 495 biomass burning plumes intercepted by the NASA DC-8 aircraft during the ARCTAS/CARB-2008 field campaign. Atmos. Chem. Phys., 11, 13325–13337.

Hedegaard G.B., Christensen, J.H., Brandt, J., 2012. The relative importance of impacts from climate change vs. emissions change on air pollution level in the 21st century. Atmos. Chem. Phys. Discuss., 12, 24501–24530.

Hoefler Consulting Group and Sierra Research Green Engineering, 2001. 1999 air toxics emission inventory for Anchorage, Fairbanks and Juneau, Alaska. Final report prepared for ADEC under Contract #18-4014-00.

IMO, 2013. North American emission control area comes into effect on 1 August 2012. Retrieved March 15, 2013, from
 http://www.imo.org/mediacentre/pressbriefings/pages/28-eca.aspx

Interagency Monitoring of Protected Visual Environments (IMPROVE), 2013. Online IMPROVE Database Access; retrieved in Mar 2009 and Oct 2012 from IMPROVE website at http://views.cira.colostate.edu/fed/DataWizard/Default.aspx

Jet Propulsion Laboratory, 2013. MISR plume height project − Siberia 2008. Retrieved July 24, 2013, from http://www-misr.jpl.nasa.gov/getData/accessData/MisrMinxPlumes/projectArea/index.cfm?ProjectArea=16

Juday, G.P., Barber, V., Duffy, P., Linderholm, H., Rupp, S., Sparrow, S., Vaganov, E., Yarie, J., 2004. Forests, land management, and agriculture. Chapter 14 − Arctic climate impact assessment. Cambridge University Press. ISBN 0-521-86509-3.

Kappos, A.D., Bruckmann, P., Eikmann, T., Englert, N., Heinrich, U., Höppe, P., Koch, E., Krause, G.H.M., Kreyling, W.G., Rauchfuss, K., Rombout, P., Schulz-Klemp, V., Thiel, W.R., Wichmann, H.-E., 2004. Health effects of particles in the ambient air. Inter. J. Hyg. Environ. Heal., 207, 399-407.

Kato, S., Pochanart, P., Hlrokawa, J., Kajii, Y., Akimoto, H., Ozaki, Y., Obi, K., Katsuno, T., Streets, D.G., Minko, N.P., 2002. The influence of Siberian forest fires on carbon monoxide concentrations at Happo, Japan. Atmos. Environ., 36, 385-390.

Karl J., Morrison, P., Swope, L., Ackley, K., 2011. Wildlands of the United States. Pacific Biodivesity Institute's report for the Pew Wilderness Center.

Leelasakultum, K., Mölders, N., Tran, H.N.Q., Grell, G.A., 2012. Potential impacts of the introduction of low-sulfur fuel on $PM_{2.5}$ concentrations at breathing level in a subarctic city. Adv. Meteo., 2012, 12 p.

Lei, M., Duval, E., Chin, M., 2011. Impact of changes in future anthropogenic aerosol emmissions on the northern hemispheric regional air quality and climate. J. Exp. Sec. Sci., 1, 25-32.

Malm, W.C., Sisler, J.F., Huffman, D., Eldred, R.A., Cahill, T.A., 1994. Spatial and seasonal trends in particle concentration and optical extinction in the United States. J. Geophys. Res., 99, 1347-1370.

Metz, P., Brigham, T., Larocque, S., Pierce, J., Arledge, A., Calvin, J., Harrington, E., Miller, S., Lingwood, B., Marshall, D., Watts, T., 2011. Alaska marine highway system analysis. Alaska Department of Transportation and Public Facilities. Retrieved from http://www.dot.state.ak.us/amhs/reports.shtml

Mölders, N., 2008. Suitability of the Weather Research and Forecasting (WRF) model to predict the June 2005 fire weather for Interior Alaska. Wea. Forecast., 23, 953-973.

22

Mölders, N., Kramm, G., 2010. A case study on wintertime inversions in Interior Alaska with WRF. Atmos. Res., 95, 314-332.

Mölders, N., Porter, S.E., Cahill, C.F., Grell, G.A., 2010. Influence of ship emissions on air quality and input of contaminants in southern Alaska National Parks and Wilderness Areas during the 2006 tourist season. Atmos. Environ., 44, 1400-1413.

Mölders, N., Porter, S.E., Tran, T.T., Cahill, C.F., Mathis, J., Newby, G.B., 2011a. The effect of unregulated ship emissions for aerosol and sulfur-dioxide concentrations in southwestern Alaska. In: Criddle, K., Eicken, H., Lovecraft, A., Metzger, A. (Eds.), North by 2020: Perspectives on a Changing North. Alaska University Press, Fairbanks, 14 p.

Mölders, N., Tran, H.N.Q., Quinn, P., Sassen, K., Shaw, G.E, Kramm, G., 2011b. Assessment of WRF/Chem to capture sub-Arctic boundary layer characteristics during low solar irradiation using radiosonde, SODAR, and station data. Atmos. Poll. Res., 2, 283-299.

Mölders, N., Tran, H.N.Q., Cahill, C.F., Leelasakultum, K., Tran, T.T., 2012. Assessment of WRF/Chem $PM_{2.5}$-forecasts using mobile and fixed location data from the Fairbanks, Alaska winter 2008/09 field campaign, Atmos. Pol. Res., 3, doi: 10.5094/APR.2012.018

Mölders, N., 2013. Investigations on the impact of single direct and indirect, and multiple emission-control measures on cold-season near-surface $PM_{2.5}$-concentrations in Fairbanks, Alaska, Atmos. Poll. Res., 6, 87-100.

MXAK, 2005. Marine Exchange of Alaska, Alaska Port Maritime Traffic and Air Emissions, Juneau, AK, June 13, 2005.

NAPAP, 2005. National acid precipitation assessment program report to Congress: an integrated assessment. Available at http://ny.water.usgs.gov/projects/NAPAP/NAPAPReport2005.pdf

PaiMazumder, D., Henderson, D., Mölders, N., 2012. Evaluation of WRF-forecasts over Siberia: Air mass formation, clouds and precipitation. The Open Atmos. Sci. J., 6, 93-110.

Peckham, S.E., Fast, J.D., Schmitz, R., Grell, G.A., Gustafson, W.I., McKeen, S.A., Ghan, S.J., Zaveri, R., Easter, R.C., Barnard, J., Chapman, E., Salzmann, M., Wiedinmyer, C., Freitas, S.R., 2009. WRF/Chem Version 3.1 User's Guide. 78p.

Polissar, A.V., Hopke, P., K., Harris, J.M., 2001. Source regions for atmospheric aerosol measured at Barrow, Alaska. Environ. Sci. Technol., 35 (21), 4214–4226.

Pope, C.A., Dockery, D.W., 2006. Health effects of fine particulate air pollution: Lines that connect. J. Air & Waste Manag. Assoc., 56, 709-742.

Quinn, P. K., Shaw, G., Andrews, E., Dutton, E. G., Ruoho-Airola, T., Gong, S. L., 2007. Arctic haze: Current trends and knowledge gaps. Tellus, 59B, 99–114.

Quinn, P.K., Bates, T.S., Schulz, K., Shaw, G.E., 2009. Decadal trends in aerosol chemical composition at Barrow, Alaska: 1976-2008. Atmos. Chem. Phys., 9, 8883–8888.

Rahn, K.A., Borys, R., Shaw, G.E., 1977. The Asian source of Arctic haze bands. Nature 268, 713–715.

Roy, D.P., Jin, Y., Lewis, P.E., Justice, C.O., 2005. Prototyping a global algorithm for systematic fire-affected area mapping using MODIS time series data. Remo. Sens. Environ., 97, 137-162.

Roy, D.P., Boschetti, L., Justice, C.O., Ju, J., 2008. The collection 5 MODIS burned area product - Global evaluation by comparison with the MODIS active fire Product. Remo. Sens. Environ., 112, 3690-3707.

Saikawa, E., Naik, V., Horowitz, L.W., Liu, J., Mauzerall, D.L, 2009. Present and potential future contributors of sulfate, black and organic carbon aerosols from China to global air quality, premature mortality and radiative forcing. Atmos. Environ., 43, 2814-2822.

Seinfeld, J.H., Pandis, S.N., 2006. Atmospheric chemistry and physics − From air pollution to climate change (2nd edition). John Wiley & Sons.

Sessions, W. R., Fuelberg, H. E., Kahn, R. A., Winker D. M., 2011. An investigation of methods for injecting emissions from boreal wildfires using WRF-Chem during ARCTAS. Atmos. Chem. Phys., 11, 5719–5744.

Shaw, G.E., Khalil, M.A.K., 1989. Arctic Haze. The Handbook of Environmental Chemistry, Springer-Verlag, Berlin, 69-111.

Shaw, G.E., 1991. Aerosol chemical components in Alaska air masses: 2. Sea salt and marine product. J. Geophys. Res., 96(D12), 22369–22372.

Shindell, D.T., Chin, M., Dentener, F., Doherty, R.M., Faluvegi, G., Fiore, A.M., Hess, P., Koch, D.M., MacKenzie, I.A., Sanderson, M.G., Schultz, M., Stevenson, D.S., Teich, H., Textor, C., Wild, O., Bergmann, D.J., Bey, I., Bian, H., Cuvelier, C., Duncan, B.N., Folberth, G., Horowitz, L.W., Jonson, J., Kaminski, J.W., Marmer, E., Park, R., Pringle, K.J., Schroeder, S., Szopa, S., Takemura, T., Zeng, G., Keating, T.J., Zuber, A., 2008. A multi-model assessment of pollution transport to the Arctic. Atmos. Chem. Phys., 8, 5353–5372.

Shulski, M., Wendler, G., 2007. The climate of Alaska. University of Alaska Press, ISBN 978-1-60223-007-1.

Skamarock, W.C., Klemp, J.B., Dudhia, J., Gill, D.O., Barker, D.M., Duda, M.G., Huang, X.-Y., Wang, W., Powers, J.G., 2008. A description of the Advanced Research WRF version 3. NCAR/TN, 125p.

Smith, W.B., Miles, P.D., Perry, C.H., Pugh, S.A., 2009. Forest resources of the United States, 2007. A technical document supporting the forest service 2010 RPA assessment. Available at http://www.fs.fed.us/nrs/pubs/gtr/gtr_wo78.pdf

Soja, A.J., Tchebakova, M.N., French, N.H.F., Flannigan, M.D., Shugart, H.H., Stocks, B.J. Sukhinin, A.I. Parfenova, E.I., Chapin III F.S., Stackhouse Jr.P.W., 1997. Climate-induced boreal forest change: predictions versus current observations. Glob. Planet. Chan., 56, 274–296.

Spracklen, D.V., Bonn, B., Carslaw, K.S., 2010. Boreal forests, aerosols and the impacts on clouds and climate. Phil. Trans. R. Soc. A, 366, 4613-4626.

Stafford, J.M., Wendler, G., Curtis, J., 2000. Temperature and precipitation of Alaska: 50 year trend analysis. Theor. Appl. Climatol., 67, 33-44.

Stocks, B.J., Fosberg, M.A., Lynham, T.J., Mearns, L., Wotton, B.M., Yang, Q., Jin, J.Z., Lawrence, K., Hartley, G.R., Mason, J.A., McKenney, D.W., 1998. Climate Change and Forest Fire Potential in Russian and Canadian Boreal Forests. Clim. Chan., 38, 1-13.

Tanimoto, H., Kajii, Y., Hirokawa, J., Akimoto, H., 2000. The atmospheric impact of boreal forest fires in far eastern Siberia on the seasonal variation of carbon monoxide: Observations at Rishiri, a northern remote island in Japan. Geophys. Res. Lett., 27, 4073-4076.

Tanimoto, H., Ohara, T., Uno, I., 2009. Asian anthropogenic emissions and decadal trends in springtime tropospheric ozone over Japan: 1998-2007. Geophys. Res. Lett., 36, L23802.

Tran, H.N.Q., Leelasakultum, K., Mölders, N., 2012. A tool for public PM$_{2.5}$-concentration advisory based on mobile measurements. J. Enivorn. Protection, 3, 1671-1688.

Tran, H.N.Q., Mölders, N., 2012a. Numerical investigations on the contribution of point-source emissions to the PM2.5-concentrations in Fairbanks, Alaska Atmos. Poll. Res., 5, doi: 10.5094/APR.2012.022.

Tran, H.N.Q., Mölders, N., 2012b. Wood-burning device changeout: Modeling the impact on PM$_{2.5}$-concentrations in a remote subarctic urban nonattainment area. Adv. Meteo., 2012, 12p.

U.S. Census Bureau, 2013. State & County QuickFacts. Retrieved March 15, 2013, from   http://quickfacts.census.gov/qfd/states/02000.html

van Curen, R.A., 2003. Asian aerosols in North America: extracting the chemical composition and mass concentration of the Asian continental aerosol plume from long-term aerosol records in the western United States. J. Geophys. Res., 108, 4623-4639.

Webley, P.W., Dean, K.G., Dehn, Jonathan, Bailey, J.E., Peterson, R., 2006. Volcanic-ash dispersion modeling of the 2006 eruption of Augustine Volcano Using the Puff Model, chapter 21 of Power, J.A., Coombs, M.L., and Freymueller, J.T., eds., The 2006 eruption of Augustine Volcano, Alaska: U.S. Geological Survey Professional Paper 1769, 507-526.

Wendler, G., Shulski, M., 2009. A century of climate change for Fairbanks, Alaska. Arctic,  62(3), 295–300.

Wilson, A.B., Bromwich, D.H., Hines, K.M., 2011. Evaluation of Polar WRF forecasts on the Arctic System Reanalysis domain: Surface and upper air analysis. J. Geophys. Res., 116, doi:10.1029/2010JD015013.

Wilcox II, W.J., Cahill, C.F., 2003. Regional Haze Trends in Alaska: Implications for Protected Class I Visibility Areas. EM, Dec 2003, 34-39.

Wotawa, G., Trainer, M., 2000. The influence of Canadian forest fires on pollutant concentrations in the United States. Sci., 14, 288-324.

Yang, Q., Gustafson, W.I.Jr., Fast, J,D., Wang, H., Easter, R.C., Wang, M., Ghan, S.L., Berg, L.K., Leung, L.R., Morrison, H., 2012. Impact of natural and anthropogenic aerosols on marine stratocumulus and precipitation in the Southeast Pacific: A regional modelling study using WRF-Chem. Atmos. Chem. Phys. Discuss., 12(6), 14622-14667.
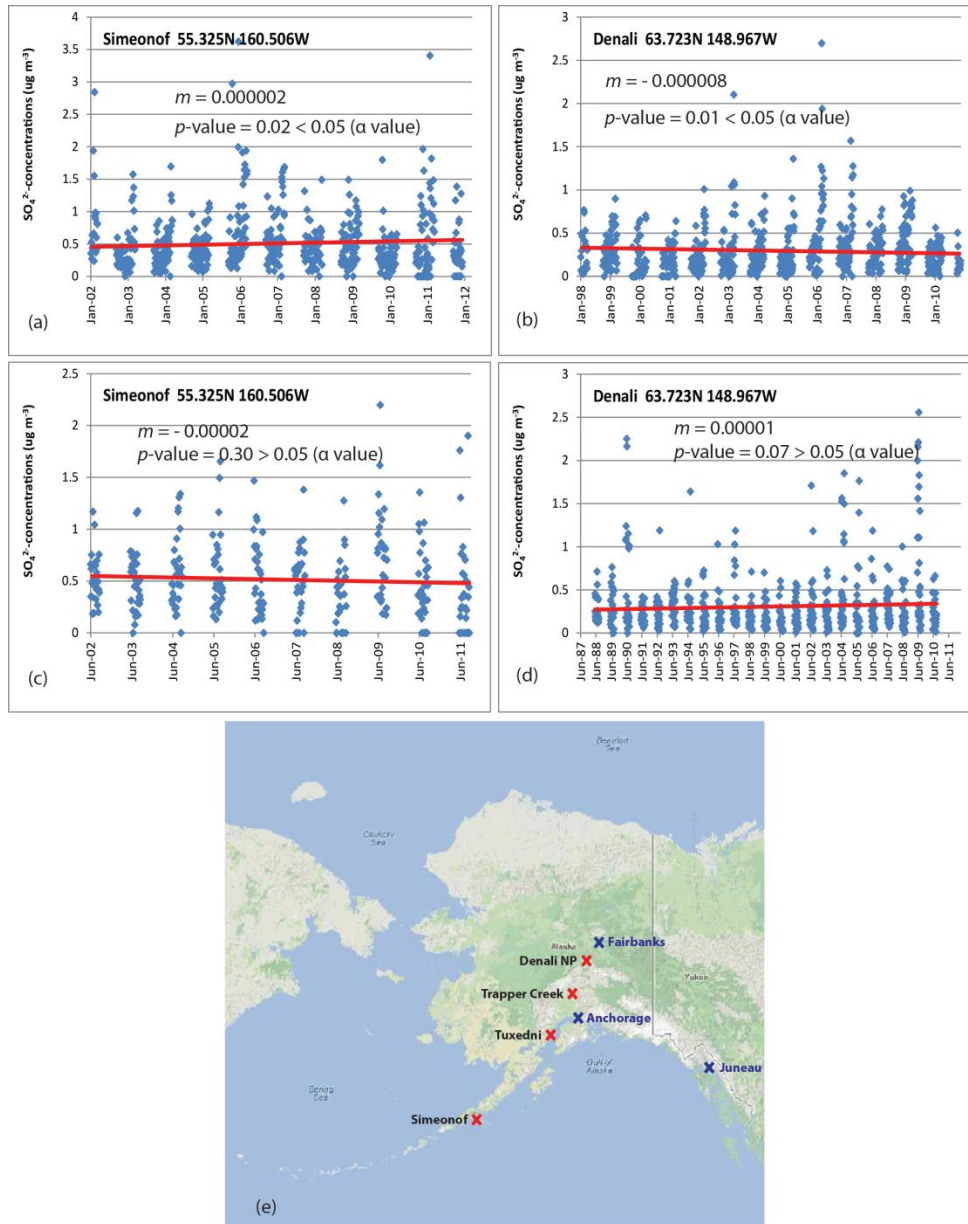
Fig. 1.1. Observed sulfate concentrations (blue dots) and linear trends (red lines) at the Denali NP and Simeonof sites. Data are from the IMPROVE network extracted for low insolation periods November-February (a, b) and high insolation periods June-August (c, d). Tuxedni and Trapper Creek sites have similar trends as in Simeonof for both low and high insolation periods, therefore not shown. The panel (e) shows locations of monitoring sites and the major cities of Alaska. Noted that Fig. are shown in different timescales due to more data available at Denali NP than at Simeonof site. *m* indicated slope of the linear trends. Probability (*p*-value) was calculated to examine the statistical significance of the trends at the 95% confidence level (i.e. α=0.05).
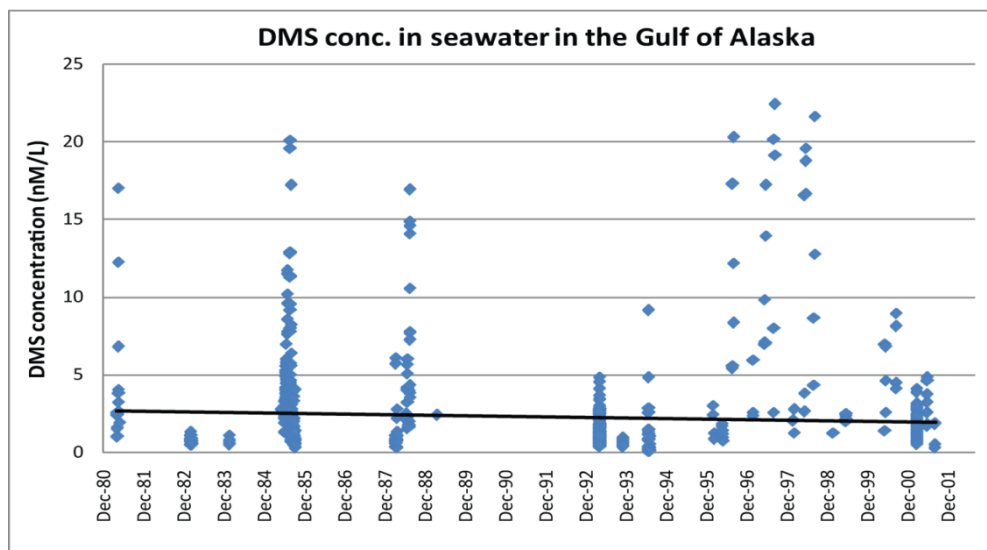
Fig. 1.2. Temporal evolution of DMS concentrations in sea water in the Gulf of Alaska as obtained from global database available at http://saga.pmel.noaa.gov/dms/.

## Chapter 2 Experimental design and methodology

The Weather Forecasting and Research model (WRF; Skamarock et al., 2008) inline coupled with chemistry packages (WRF-Chem; Peckham et al., 2009) was used to perform simulations over a domain covering Alaska, Japan, and parts of Canada, Siberia, China, and the North Pacific (Fig. 2.1). The same meteorological initial and boundary conditions were used for each simulations, with various emission scenarios to investigate whether emission changes may be the reasons for observed changes in aerosol concentrations in Alaska. WRF-Chem has been applied as a state-of-the-science chemistry transport model (Gustafson et al., 2007; Barnard et al., 2009; Yang et al., 2012). Moreover, the sophisticated physics and chemistry schemes developed for WRF-Chem allow extreme weather conditions and chemistry in Arctic and sub-Arctic regions to be captured (Mölders, 2008; Hines and Bromwich, 2008; Mölders and Kramm, 2010; Mölders et al., 2011; Wilson et al., 2011; PaiMazumder et al., 2012). Therefore, the WRF-Chem model with modifications for Alaska conditions introduced by Mölders et al (2011) becomes the suitable choice for the research methodology presented in this dissertation. A summary on evaluation of WRF's (WRF-Chem's) performance from previous studies for Arctic and sub-Arctic regions is presented in section 2.3. The model's performance evaluation for simulations performed for this study is presented in Chapter 4, 5 and 6.

## 2.1 Model description

WRF-Chem is an Eulerian model with a staggered Arakawa C-grid  (Arakawa and Lamb, 1977). This grid provides more accurate results at fine resolutions than to unstaggered grids such as Arakawa A-grid (Warner, 2011). A mass-based terrain following coordinate is used for the vertical coordinate system.

The two components considered in WRF-Chem are meteorology and chemistry. They could be treated independently from each other (known as offline), where the transport of chemicals is driven by meteorology without any feedback on meteorology; or they can be treated dependently of each other, i.e. inline. The latter implies that the meteorology is affected by the chemistry and vice versa (Grell et al., 2005). The former approach is more computationally attractive than the latter one. Therefore, the former method was preferred in the past. However, since chemistry does feedback to the meteorology via interaction between cloud microphysics, radiation and chemistry, ignoring this interaction in offline simulations could limit the accuracy of the air quality prediction. Moreover, some of these aerosol-radiation and aerosol-cloud feedbacks have strong impacts on weather and climate (e.g. Mölders and Olson, 2004; Yarker et al., 2010; Grell et al., 2011). The rapid development of computational resources makes inline WRF-Chem more attractive than ever before.

Furthermore, offline calculations may lead to inconsistencies with consequences for simulated air quality as discussed in detail, for instance, in Mölders et al. (1994) and Mölders and Laube (1994). In inline simulations, there is no need for spatial or temporal interpolation between the two components, since they use the same grid, but perform the

integration at the individual timesteps needed by the processes using the operator splitting method. Both components also use the same transport schemes and physical packages for sub-grid scale processes (Grell et al., 2005).

The physical and chemical packages chosen for this study are briefly reviewed and the reasoning for their choice is discussed in the following sections.

### 2.1.1 Physics packages

In the Arctic region, cloud processes involve both the cold and warm pathways of precipitation formation and super-cooled water and ice may co-exist. Furthermore, aqueous chemical reactions are important processes for this aerosol study. The modified cloud microphysical parameterization by Lin et al. (1983) accounts for six classes of hydrometeors: water vapor, cloud-water, rain, cloud-ice, snow and hail (i.e. graupel). Cloud-ice transforms to snow, as an intermediate step, before transforming to hail. The formation of virga from cloud anvils, the relationship between snow and amount of cloud-ice, rain, hails are also assessed. As such this scheme is able to simulate the co-existance of solid and liquid cloud particles and cold cloud processes occurring in the Arctic. It is also coupled to the aqueous phase module and it recommended for simulating aqueous chemical reactions that occur in cloud droplets (Peckham et al., 2009).

Since the simulations for this study were setup at 30 km grid-increment, cumulus convection is of sub-grid scale and needs to be parameterized. The modified 3 dimentions (3D)-version of the Grell-Dévényi ensemble scheme (Grell and Dévényi, 2002) was

chosen. This ensemble method takes into account the differing entrainment/detrainment of updraft/downdraft, and precipitation efficiencies of convective clouds.

The Rapid Radiative Transfer Model (RRTM) developed by Mlawer et al. (1997) and the Goddard shortwave scheme (Chou and Suarez, 1994) were selected for the treatment of long-wave and shortwave radiation, respectively. The RRTM is a spectral-band scheme using the correlated-k method that involves infrared and thermal radiation absorbed and emitted by gases and surfaces. The emissivity of the surface is considered based on the land-use type, which followed the U.S. Geological Survey land use data. The RRTM determines the upward long-wave radiative flux. The absorptions and emissions of gases including water vapor, ozone, carbon dioxide and trace gases (e.g. methane, nitrous oxide and the common halocarbons) determine the downward flux. A major advantage of the RRTM comes from its use of look-up tables for representing the long-wave processes to save computational time. The Goddard shortwave scheme considers 11 spectral bands including the visible range and surrounding wavelengths. The abilities of absorbing, reflecting and scattering the incoming solar radiation of atmospheric gases are included in Goddard scheme. These processes determine the downward shortwave radiation flux while the upward flux is also determined by the reflection from the surface. Surface albedo is considered depending on land-use type and the fractional snow-cover if snow exists. Over the ocean, surface albedo depends on the fractional cover of the ocean by sea-ice. Note that in the model domain, a large part of the Arctic Ocean, Bering and Chukchi Seas and some parts along the Gulf of Alaska are ice-covered in January.

Janjić's (2002) scheme was selected for the parameterization of the processes in the surface layer. This scheme calculates friction velocities and exchange coefficients that serve as input for determining surface heat and moisture fluxes in land-surface model (LSM) or surface stress in the atmospheric boundary layer (ABL) scheme. The viscous sub-layer is treated depending on the surface types (i.e. land, sea-ice or water).

In the studies for the Arctic, for the land surface model which simulate the exchange of heat and moisture at the land-atmosphere interface, permafrost is of importance to be considered. Thus, either a modified version of Rapid Update Cycle (RUC) (Smirnova et al., 2000) or NOAH scheme (Chen and Dudhia, 2001) LSM is appropriate as these models allow considering frozen soil processes. The NOAH scheme was selected for this study since it includes sea-ice treatment, which is essential for Alaska regional domains. This feature is not considered by the RUC. The NOAH scheme considers four soil layers for the calculation of the soil temperature and moisture states, one canopy layer with canopy moisture, and snow cover. It only considers one snow-layer and assumes a homogeneous snowpack, but allows that the snowpack covers only a fraction of the grid-cell. The sensible and latent heat fluxes calculated by the NOAH scheme serve as input for the ABL scheme.

The Mellor-Yamada-Janjic (MYJ) scheme was selected for parameterizing the turbulence in the ABL and free atmosphere (Janjić, 2002; Mellor and Yamada, 1982). This scheme considers the one-dimensional prognostic turbulent kinetic energy equation that describes the local vertical mixing.

**2.1.2 Chemistry packages**

Atmospheric gas phase reactions are described in WRF-Chem by the Regional Acid Deposition Model version 2 (RADM2; Chang et al., 1989) gas-phase mechanisms (Stockwell et al., 1990). Inorganic reactions and constants follow the scheme developed by DeMore et al. (1988), which involves 14 stable inorganic compounds, four inorganic short-lived intermediates and three abundant stable species (i.e. oxygen, nitrogen, water). In the orgranic chemistry scheme, 26 groups of stable organic compounds and 16 groups of organic short-lived intermediates (peroxy radicals) are included following Middleton et al. (1990). Photolysis rates are calculated in accord with Madronich (1987). Photolysis processes take into account 21 photo-chemical reactions.

Aerosols can be categorized as two types depending on how they were formed in the atmosphere: 1) primary aerosols which stem directly from emissions; 2) Secondary aerosol builds in the atmosphere and emission plumes (Finlayson-Pitts and Pitts, 1999; Seinfeld and Pandis, 2006). Its formation depends on the availability of precursors and atmospheric conditions. The Modal Aerosol Dynamics Model for Europe (MADE) (Ackermann et al., 1998) in conjunction with the Secondary Organic Aerosol Model (SORGAM) (Schell et al., 2001) were chosen to describe the aerosol physical, chemical and dynamical processes. The MADE module is a modification of the original Regional Particulate Model described by Binkowski and Shankar (1995), which predicts the aerosol-size distributions, aerosol formation by nucleation, condensation, coagulation, and chemical transformation processes including aqueous-phase reactions as well as aerosol transport and removal by dry deposition. The SORGAM simulates the physical

and chemical properties of secondary organic aerosols. These two schemes are referred to as a conjunctive module named MADE/SORGAM in WRF-Chem.

The treatment of dry deposition is based on Wesely (1989) with the modifications introduced for Alaska by Mölders et al. (2011). The scheme considers various factors such as surface temperature, stomata response to environmental parameters, the wetting of surface by dew and rain and the covering of surface by snow. The surface resistance of gases against deposition is computed using Henry's Law constants and chemical reactivity of different water-soluble substances. The modifications include the treatment of dry deposition over snow in accord with Zhang et al. (2003) and the lowering of the threshold at which stomata close. In Alaska, stomata of coniferous trees are still open at -5$^{o}$C (Mölders et al., 2011).

**2.1.3 Model domain**

The model domain was set up with a 30 km grid-increment and 240×120 grid points, centered at (59.0°N, 179.0°E) to cover entire Alaska, East Asia and West Canada (Fig 2.1). The 28 vertical levels reach from the surface to 0hPa. The eta-levels are 1.000, 0.993, 0.983, 0.970, 0.954, 0.934, 0.909, 0.880, 0.830, 0.779, 0.729, 0.678, 0.592, 0.514, 0.443, 0.380, 0.324, 0.273, 0.228, 0.188, 0.153, 0.121, 0.094, 0.069, 0.048, 0.030, 0.014 and 0.000. This vertical grid permits resolving the processes in the ABL well. The simulated thickness of the first layer above the Earth's surface is about 25 and 27m for low insolation and high insolation simulations, respectively. The thickness of the vertical layers increases with height.

**2.1.4 Initialization**

The WRF-Chem simulations used the National Center for Atmospheric Research (NCAR) and National Centers for Environmental Prediction (NCEP) 1.0°×1.0°, six-hour, global final analysis data (FNL) as initial and boundary conditions for the meteorological fields and sea-ice, soil and snow conditions.

The chemical fields were initialized by idealized profiles of Alaska/North Pacific background concentrations following Mölders et al. (2011) for the first simulation of each episode. The following simulations used the chemical distributions obtained at the end of the previous run as initial conditions. Background concentrations served as lateral boundary conditions.

Limited area models, like WRF, lose their predictability after approximately 10 days of simulation (e.g. Pielke, 2002; Jacobson, 2005). Therefore, the meteorological fields need to be re-initialized every 5-10 days. Mölders (2008) has indicated that when FNL-data was used as initial/boundary conditions, the quality of 5-day simulations only marginally differed from that of 1-day simulations (i.e. daily initializations). Therefore, in this study, initializations were conducted for the meteorological fields every five days.

**2.2 Analysis method**

Model evaluations were conducted for Alaska for January 2000 (REF_Jan) and June 2008 (REF_Jun) on both meteorological and chemical aspects.

To evaluate the model's performance with respect to meteorology, simulated results were compared with hourly Western Regional Climate Center (WRCC)

observations of temperature (T), dew-point temperature ($T_d$), wind-speed (v) and direction (dir), sea-level pressure (SLP), relative humidity (RH), precipitation (RR) and downward shortwave radiation (SW). During January 2000 and June 2008, WRCC data were available for 59 and 83 sites within Alaska, respectively. Standard meteorological data including T, SLP, v and dir from National Data Buoy Center (NDBC; 2012) available at 15 sites over the North Pacific were used for evaluating model performance over the oceanic regions for REF_Jun.

Performance skill-scores (bias, root-mean-square error (RMSE), standard deviation of error (SDE) and correlation skill-score (R)) (Table 2.1) were calculated in accordance with Anthes (1983) and Anthes et al. (1989) to evaluate the simulated meteorological fields.

To evaluate the model's performance with respect to predicted chemistry, simulated $SO_2$, sulfate- and nitrate-aerosol concentrations were compared with observations available at Denali Park and Poker Flat from the Clean Air Status and Trends Network (CASTNET) campaign and at Denali Park headquarters from the IMPROVE network. CASTNET provided weekly average concentration, while IMPROVE provided daily averages every third day.

The fractional bias (FB), normalized mean square error (NMSE), correlation skill-score (R) and fraction within a factor of two (FAC2) (Table 2.1) were calculated following Chang and Hanna (2004) to evaluate model performance with respect to chemistry. For a perfect model, FB, NMSE, $|R|$ and FAC2 equal to 0.0, 0.0, 1.0 and 100%, respectively. An air quality model is considered as a good model if it has about

approximately 50% of the predictions within a factor of two of the observations and FB within ±0.30 (Chang and Hanna, 2004).

Multi-correlation coefficients (Eq. 2.1) of concentrations averaged over the regions of interest in Alaska versus emissions and wind speed at each grid cell were calculated following Cohen et al. (2003) to investigate the role of emissions and meteorological conditions for the distribution of pollutants as simulated by REF_Jan.

$$R_{Y.X_1X_2} = \sqrt{\frac{(R_{YX_1})^2 + (R_{YX_2})^2 - 2(R_{YX_1})(R_{YX_2})(R_{X_1X_2})}{1-(R_{X_1X_2})^2}} \quad \text{(Eq. 2.1)}$$

where

$R_{YX_1}$ are the correlation coefficients of regional averaged concentrations versus emissions,

$R_{YX_2}$ are the correlation coefficients of regional averaged concentrations versus wind-speed, and

$R_{X_1X_2}$ are the correlation coefficients of emissions versus wind-speed.

Hourly average concentration differences between the results of simulations with emissions of reference simulations (e.g, REF_Jan, REF_Jun) and simulations with various substituted emission scenarios were examined to investigate the impacts of emission changes on the changes of aerosol concentrations in Alaska. A student's t-test at the 95% confidence level was applied to the aerosol concentration differences between the reference and the changing emission simulations to test the null-hypothesis that the changes in emissions do not cause any changes in aerosol concentrations like those found by the IMPROVE network.

**2.3 Summary on evaluation of WRF's (WRF-Chem's) performance in previous studies for Arctic and sub-Arctic regions**

The performance of WRF-Chem in simulating meteorological and chemical fields is key factor in determining whether the model results are reliable to serve as the basis for raising further scientific questions on the impact of various emission sources.

Performance of WRF in simulating meteorological quantities had been extensively investigated by various sensitivity studies using different WRF configurations (e.g., Chigullapalli and Mölders, 2008; Hines and Bromwich, 2008; Bromwich et al., 2009; Gaudet and Stauffer, 2010; Mölders and Kramm, 2010; Hines et al., 2011; Cassano et al., 2011) in order to determine a configuration that has best performance. As the results, each study suggested a combination of parameterizations that produced the best performance. However, the preferred model setup combination tends to depend on the application, and there is no one model setup that gave the best performance in all case studies (Bromwich et al., 2009). The common features shared by those studies were that WRF captured the temporal evolutions of meteorological quantities well with comparable performance skill-scores. More details of their common features with respect to WRF's performance is summarized as follows.

**Temperature:** The performance skill-score of the WRF model strongly depended on the selection of physical packages (Mölders and Kramm, 2010). In most of the case studies, WRF yielded warm biases for temperature (Hines and Bromwich, 2008; Mölders and Kramm, 2010; Hines et al., 2010). WRF tended to have warm bias in simulating 2m temperature and 2m dew-point temperature. Its performance in simulating temperature

weakened when there were sudden change in temperature due to a frontal passage, (i.e. increasing atmospheric stability) or over regions having erroneous land-cover distribution (Porter, 2009; PaiMazumder et al., 2012).

**Wind speed:** Overestimation of wind-speed was commonly found in all case studies. The main reason for discrepancy in simulating wind-speed resulted from the mis-representing the complex terrain and other local effects such as drainage flows (Mölders, 2008; Mölders et al., 2011; Wilson et al., 2011). Positive biases occurred at all simulation sites for simulation in both polar and mid-latitude regions: overestimated by 1.1 m s$^{-1}$ on average in simulations for southern Alaska in January 2006 (Wilson et al., 2011); positive biases of 1.55 m s$^{-1}$ and 0.98 m s$^{-1}$ on average were found for two simulations with different WRF setups for interior Alaska (Mölders and Kramm, 2010); and for simulation for Mexico City in March 2006, WRF overestimated wind-speed by 28% on average (Zhang et al., 2009).

**Downward shortwave radiation**: WRF's performance on simulating radiation highly depended on its performance in simulating cloud coverage. Discrepancy in simulating radiation balance led to discrepancies in simulating other parameters such as temperature, moisture and atmospheric stability (Bromwich et al., 2009; Mölders and Kramm, 2010; PaiMazumder et al., 2012). For simulations for Interior Alaska, daily accumulated downward shortwave radiation was overestimated by 10% on average for WRF simulation for Interior Alaska in June 2005 (Mölders, 2008), overestimated by 33 W m$^{-2}$ in December 2009 – January 2010 (Tran et al., 2012).

**Sea-level pressure:** WRF usually captured the temporal evolution of sea-level pressure very well with small biases of $\pm$ 3 hPa. WRF underestimated sea-level pressure by -3.2 hPa for simulation for northern polar region (Wilson et al., 2011); negative bias of -1.1 hPa was found for simulation for southest Alaska (Yarker et al., 2010); sea-level pressure was overestimated by 0.4-1.2 hPa on average for simulations over the Arctic Ocean (Bromwich et al., 2009).

**Precipitation**: Discrepancy in the microphysic scheme, and incorrect land-use type in the case of convective precipitation contributed to errors in simulating precipitation. In addition, the catch deficits and poor representation of the monitoring network would also contributed to the low performance results. Temporal evolution of hourly precipitation was captured relatively well. However, WRF had difficulty in capturing the temporal and spatial evolution of the daily accumulated precipitation (Mölders, 2008; PaiMazumder and Mölders , 2009; Yarker et al., 2010; PaiMazumder et al., 2012).

**Temperature and wind vertical profile**: WRF-Chem captured the occurrence of surface inversions throughout the simulation episodes, but failed to fully capture their magnitude. The reason for this behavior may be due to the land-surface model that typically predicted a warmer surface condition than observed during local Alaskan winter. For Interior Alaska, simulations with WRF-Chem in winter 2005/2006 and winter 2008/2009 captured the frequency of the inversion layers (Mölders et al., 2011; Mölders et al., 2012); inversion layers with strong temperature gradient (>8 K/100 m) were not well captured; wind-speed below (above) 600 m above ground level was overestimated

(underestimated) (Mölders et al., 2011). Similarly, for simulations over Greenland for December 2002, WRF captured the vertical profiles of temperature and wind-speed in the middle and upper troposphere (above 700 hPa) relatively well, but was relatively weak in doing so below 700 hPa (Hines et al., 2011). These behaviors show WRF tends to over predict the mixing strength in the atmospheric boundary layer.

Evaluation of WRF-Chem's performance in simulating chemical species in the Artic and sub-Arctic regions had been performed by various studies (Mölders and Kramm, 2010; Mölders et al., 2011; 2012). Chang and Hanna (2004) and Boylan and Russell (2006) proposed several skill-scores and criteria based on which a model can be evaluated for its performance. Those skill-scores include the fractional bias (FB), fractional error (FE), normalized mean bias (NMB), normalized mean error (NME), mean fractional bias (MFB) and mean fractional error (MFE). In overall, WRF-Chem had good to acceptable performance in capturing the observed $PM_{2.5}$ concentrations. Mölders et al. (2011) reported that for simulations for Interior Alaska in winter 2005/2006, WRF-Chem had FB and FAC2 of 20% and 41%, respectively in simulating $PM_{2.5}$ concentrations. For simulations for similar domain and for winter 2008/2009, WRF-Chem had FB, FE, NMB, NME, and FAC2 of 22%, 67%, 13%, 71%, and 56%, respectively, in simulating 24h-average $PM_{2.5}$ concentrations (Mölders et al. , 2012). The above skill-cores showed that WRF-Chem had good performance in simulating $PM_{2.5}$ concentrations based on the criteria suggested by Chang and Hana (2004) and Boylan and Russell (2006). For WRF-Chem simulation over the Southern Alaska and the Gulf of Alaska in May 2006, Mölders et al. (2010) reported that WRF-Chem broadly captures the temporal evolution of aerosol

concentrations, and underestimated $PM_{2.5}$ and $PM_{10}$ by 2.3 µg m$^{-3}$ and 5.8 µg m$^{-3}$, respectively, on average over two monitoring sites.

Except for sulfate aerosols concentrations, WRF-Chem commonly had a relatively weak performance in simulating nitrate and ammonium aerosol concentrations. Emissions of ammonia being too low in the emission inventories was attributed to this discrepancy (Mölders et al., 2011; Mölders et al. , 2012).

Performance of WRF-Chem in simulating chemical species highly depended on its performance in simulating meteorological fields (Mölders et al., 2011; Mölders et al., 2012). Accuracy in simulating temperature is one of the most important factors that affected WRF-Chem performance to simulate $PM_{2.5}$. Large uncertainty in simulating $PM_{2.5}$ concentrations was often associated with discrepancies in capturing the inversion strength and/or the temporal/spatial distribution of temperature, wind-speed and other meteorological parameters. WRF-Chem's had a weak performance in capturing the temporal evolution of $PM_{2.5}$ typically when it underestimated inversion strength, missed frontal passage, or when there were sudden temperature changes (Mölders et al., 2012).

# References

Ackermann, I.J., Hass, H., Memmesheimer, M., Ebel, A., Binkowski, F.S., Shankar, U., 1998. Modal aerosol dynamics model for Europe: Development and first applications. Atmos. Environ., 32, 2981-2299.

Anthes, R.A., 1983. Regional models of the atmosphere in middle latitudes. Mon. Wea. Rev., 111, 1306-1335.

Anthes, R.A., Kuo, Y.H., Hsie, E.Y., Low-Nam, S., Bettge, T.W., 1989. Estimation of skill and uncertainty in regional numerical models. Quart. J. Roy. Meteor. Soc., 115, 763-806.

Arakawa, A., Lamb, V.R., 1977. Methods of computational physics. Academic Press, New York, 17, 174-265.

Barnard, J.C., Fast, J.D., Paredes-Miranda, G.L., Arnott, P.W., Laskin, A., 2009. Technical Note: Evaluation of the WRD-Chem 'aerosol chemical to aerosol optical properties' module using data from the MILAGRO campaign. Atmos. Chem. Phys., 10, 8927-8961.

Binkowski, F. S., and U. Shankar, 1995. The regional particulate matter mdel, 1. Mode description and preliminary results. J. Geophys. Res., 100, 26191-26209.

Boylan, J.W., Russell, A.G., 2006. PM and light extinction model performance metrics, goals, and criteria for three-dimensional air quality models. Atmos. Environ., 40, 4946-4959.

Bromwich, D.H., Hines, K.M., Bai, L.-S., 2009. Development and testing of Polar Weather Research and Forecasting model: 2. Arctic Ocean. Journal of Geophysical Research, 114, 22p.

Cassano, J.J., Higgin, M.E., Seefeldt, M.W., 2011. Performance of the Weather Research and Forecasting Model for month-long pan-Arctic simulations. Ameri. Meteo. Soc., 139, 3469-3488.

Chang, J. S., Binkowski, F.S., Seaman, N.L.,McHenry, J.N., Samson, P.J., Stockwell, W.R., Walcek, C.J., Madronich, S., Middleton, P.B., Pleim, J.E., Lansford, H.H., 1989. The Regional Acid Deposition Model and Engineering Model. State-of-Science/Technology, Report 4, National Acid Precipitation Assessment Program, Washington D.C.

Chang, J. C., Hanna, S. R., 2004. Air quality model performance evaluation. Meteorol. Atmos. Phys., 87, 167–196.

Chen, F., Dudhia, J., 2001. Coupling an advanced land-surface/ hydrology model with the Penn State/ NCAR MM5 modeling system. Part I: Model description and implementation. Mon. Wea. Rev., 129, 569–585.

Chigullapalli, S., Mölders, N., 2008. Sensitivity studies using the Weather Research and Forecasting (WRF) model. REU-report, Fairbanks, 15p.

Chou, M.-D., Suarez, M.J., 1994. An efficient thermal infrared radiation parameterization for use in general circulation models. NASA Tech. Memo., 104606, 85p.

Cohen, J., Cohen, P., West, S. G., Aiken, L. S., 2003. Applied multiple regression/correlation analysis for the behavioral sciences, 3rd Ed.  Mahwah, NJ: Lawrence Erlbaum Associates.

DeMore, W. B., Sander, S. P., Molina, M. J., Golden, D. M., Hampson, R. F., Kurylo, M. J.,  Howard, C. J., Ravishankara, A. R., 1988. Chemical kinetics and photochemical data for use in stratospheric modeling. Evaluation Number 8, National Aeronautics and Space Administration, Jet Propulsion Laboratory, California Institute of Technology, Pasadena.

Finlayson-Pitts, B.J., Pitts, J.N.Jr, 1999. Chemistry of the upper and lower atmosphere: theory, experiments and applications. Academic Press. ISBN-13: 978-0122570605.

Gaudet, B.J., Stauffer, D.R., 2010. Stable boundary layers representation in meteorological models in extremely cold wintertime conditions. Report to the Environmental Protection Agency, 60p.

Grell, G.A., Dévényi, D., 2002. A generalized approach to parameterizing convection combining ensemble and data assimilation techniques. Geophys. Res. Lett., 29, 1693, doi:10.1029/2002GL015311.

Grell, G. A., Peckham, S. E., Schmitz, R.,  McKeen, S. A., Frost, G., Skamarock, W. C., Eder, B., 2005. Fully coupled "online" chemistry within the WRF model. Atmos. Environ., 39, 6957-6975.

Grell, G., Freitas, S. R., Stuefer, M., Fast, J., 2011. Inclusion of biomass burning in WRF-Chem: impact of wildfires on weather forecasts. Atmos. Chem. Phys., 11, 5289–5303.

Gustafson, W.I. Jr., Chapman, E.G., Ghan, S.J., Fast, J.D., 2007. Impact on modeled cloud characteristics due to simplified treatment of uniform cloud condensation nuclei during NEAQS 2004. J. Geophys. Res. Lett., 34, L19809.

Hines, K.M., Bromwich, D.H., 2008. Development and testing of Polar Weather Research and Forecasting (WRF) model. Part I: Greenland ice sheet meteorology. Mon. Wea. Rev., 136, 1971-1989.

Hines, K.M., Bromwich, D.H., Bai, L.-S., Barlage, M., Slater, A.G., 2011. Development and testing of Polar WRF. Part III: Arctic land. J. Cli., 24, 26-48.

Jacobson, M. Z., 2005. Fundamentals of atmospheric modeling. Cambridge University Press, New York, 813p.

Janjić, Z.I., 2002. Nonsingular implementation of the Mellor-Yamada level 2.5 scheme in the NCEP meso model. NCEP Office Note. 437, 61p.

Lin, Y.-L., Rarley, R.D., Orville, H.D., 1983. Bulk parameterization of the snow field in a Cloud Model. J. Appl. Meteor., 22, 1065-1092.

Madronich, S., 1987. Photodissociation in the atmosphere, 1, actinic flux and the effects of ground reflections and clouds. J. Geophys. Res., 92, 9740-9752.

Mellor, G. L., Yamada, T., 1982. Development of a turbulence closure model for geophysical fluid problems, Rev. Geophys. Space Phys., 20, 851-875.

Middleton, P., Stockwell, W. R., Carter, W. P. L., 1990. Aggregation and analysis of volatile organic compound emissions for regional modeling, Atmos. Environ., 24A, 1107-1133.

Mlawer, E.J., Taubman, S.J., Brown, P.D., Iacono, M.J., Clough, S.A., 1997. Radiative transfer for inhomogeneous atmospheres: RRTM, a validated correlated-k model for the longwave. J. Geophys. Res., 102D, 16663-16682.

Mölders, N., Laube, M., 1994. A numerical study on the influence of different cloud treatment in a chemical transport model on gas phase distribution. Atmos. Res., 32, 249-272.

Mölders, N., Hass, H., Jakobs, H.J., Laube, M., Ebel, A., 1994. Some effects of different cloud parameterizations in a mesoscale model and a chemistry transport model. J. Appl. Meteor., 33, 527-545.

Mölders, N., Olson, M.A., 2004. Impact of urban effects on precipitation in high latitudes. J. Hydrometeor., **5**, 409-429.

Mölders, N., 2008. Suitability of the weather research and forecasting (WRF) model to predict the June 2005 fire weather for Interior Alaska. Weather Forecasting 23, 953-973.

Mölders, N., Kramm, G., 2010. A case study on wintertime inversions in Interior Alaska with WRF. Atmos. Res., 95, 314-332.

Mölders, N., Tran, H.N.Q., Quinn, P., Sassen, K., Shaw, G.E, Kramm, G., 2011. Assessment of WRF/Chem to capture sub-Arctic boundary layer characteristics during low solar irradiation using radiosonde, SODAR, and station data, Atmos. Pol. Res., 2, 283-299.

Mölders, N., Tran, H.N.Q., Cahill, C.F., Leelasakultum, K., Tran, T.T., 2012. Assessment of WRF/Chem PM2.5-forecasts using mobile and fixed location data from the Fairbanks, Alaska winter 2008/09 field campaign. Atmos. Poll. Res., 3, 180-191.

National Data Buoy Center (NDBC), 2012. Alaska Historical Marine Data. Retrieved at http://www.ndbc.noaa.gov/maps/alaska_hist.shtml

PaiMazumder, D., Mölders, N., 2009. Theoretical assessment of uncertainty in regional averages due to network density and design. J. App. Meteo. Cli., 48, 1643-1666.

PaiMazumder, D., Henderson, D., Mölders, N., 2012. Evaluation of WRF-forecasts over Siberia: Air mass formation, clouds and precipitation. The Open Atmos. Sci. J., 6, 93-110.

Peckham, S.E., Fast, J.D., Schmitz, R., Grell, G.A., Gustafson, W.I., McKeen, S.A., Ghan, S.J., Zaveri, R., Easter, R.C. , Barnard, J., Chapman, E., Salzmann, M., Wiedinmyer, C. and Freitas, S.R., 2009. WRF/Chem Version 3.1 User's Guide. 78p.

Pielke, R.A., 2002. Mesoscale Meteorological Modeling. Academic Press, New York, 676p.

Porter, S.E., 2009. Investigation of the impact of ship emissionson atmospheric composition and deposition into remote, coastal landscapes of southwest Alaska. University of Alaska Fairbanks, M.S. thesis. Available at htpp://www.gi.alaska.edu/~molders/porter_final_thesis.pdf.

Schell, B., Ackermann, I.J., Hass, H., Binkowski, F.S., Ebel, A., 2001. Modeling the formation of secondary organic aerosol within a comprehensive air quality model system. J. Geophys. Res., 106, 28275-28293.

Seinfeld, J.H., Pandis, S.N., 2006. Atmospheric chemistry and physics − From air pollution to climate change (2nd edition). John Wiley & Sons.

Simpson, D., Guenther, A., Hewitt, C.N., Steinbrecher, R., 1995. Biogenic emissions in Europe 1. Estimates and uncertainties. J. Geophys. Res., 100D, 22875-22890.

Skamarock, W.C., Klemp, J.B., Dudhia, J., Gill, D.O., Barker, D.M., Duda, M.G., Huang, X.-Y., Wang, W., Powers, J.G., 2008. A description of the Advanced Research WRF version 3. NCAR/TN, 125pp.

Smirnova, T. G., Brown, J. M., Benjamin, S. G., Kim, D., 2000. Parameterization of cold season processes in the MAPS land-surface scheme, J. Geophys. Res., 105D, 4077-4086.

Stockwell, W.R., Middleton, P., Chang, J.S., Tang, X., 1990. The second-generation regional acid deposition model chemical mechanism for regional air quality modeling. J. Geophys. Res., 95, 16343-16367.

Tran, H.N.Q., Leelasakultum, K., Mölders, N., 2012. A tool for public $PM_{2.5}$-concentration advisory based on mobile measurements. J. Eviron. Protec., 3, 1671-1688.

Wesely, M.L., 1989. Parameterization of surface resistances to gaseous dry deposition in regional-scale numerical models. Atmos. Environ., 23, 1293-1304.

Wilson, A.B., Bromwich, D.H., Hines, K.M., 2011. Evaluation of Polar WRF forecasts on the Arctic System Reanalysis domain: Surface and upper air analysis. . J. Geophys. Res., 116, doi:10.1029/2010JD015013.

Yang, Q., Gustafson, W.I.Jr., Fast, J,D., Wang, H., Easter, R.C., Wang, M., Ghan, S.L., Berg, L.K., Leung, L.R., Morrison, H., 2012. Impact of natural and anthropogenic aerosols on marine stratocumulus and precipitation in the Southeast Pacific: A regional modelling study using WRF-Chem. Atmos. Chem. Phys. Discuss., 12(6), 14622-14667.

Yarker, M.B., PaiMazumder, D., Cahill, C.F., Dehn, J., Prakash, A., Mölders, N., 2010. Theoretical investigations on potential impacts of high-latitude volcanic emissions of heat, aerosols and water vapor and their interactions on clouds and precipitation. The Open Atmos. Sci. J., 4, 12-23.

Zhang, L., Brook, J.R., Vet, R., 2003. A revised parameterization for gaseous dry deposition in air-quality models. Atmos. Chem. Phys., 3, 2067-2082.

Zhang, Y., Dubey, M.K., Olsen, S.C., Zheng, J., Zhang, R., 2009. Comparisons of WRF/Chem simulations in Mexico City with ground-based RAMA measurements during the 2006-MILAGRO. Atmos. Chem. Phys., 9, 3777-3798.

Table 2.1 Equations to calculate performance measures of WRF/Chem (e.g. Anthes, 1983; Anthes et al., 1989; Chang and Hanna, 2004). Here, $\phi_i = (x_i - y_i)$ is the different between $i^{th}$ predicted (x) and observed (y) meteorological quantities and n is the number of observations. Here, $C_p$ and $C_o$ stand for predicted and observed concentrations, respectively; and $\sigma_C$ stands for standard deviation over the dataset

| Skill scores for evaluating model performance with respect to meteorology | |
|---|---|
| Skill score | Equation |
| Bias | $$\bar{\phi} = \frac{1}{n}\sum_{i=1}^{n}\phi_i = \frac{1}{n}\sum_{i=1}^{n}(x_i - y_i)$$ |
| Root-mean-square error | $$RMSE = \left[\frac{1}{n}\sum_{i=1}^{n}(\phi_i)^2\right]^{1/2}$$ |
| Standard deviation of error | $$SDE = \left[\frac{1}{n-1}\sum_{i=1}^{n}(\phi_i - \bar{\phi})^2\right]^{1/2}$$ |
| Correlation skill-score | $$R = \frac{\sum_{i=1}^{n}x_iy_i - \frac{\sum_{i=1}^{n}x_i \sum_{i=1}^{n}y_i}{n}}{\sqrt{\left[\sum_{i=1}^{n}x_i^2 - \frac{(\sum_{i=1}^{n}x_i)^2}{n}\right]\left[\sum_{i=1}^{n}y_i^2 - \frac{(\sum_{i=1}^{n}y_i)^2}{n}\right]}}$$ |

| Skill scores for evaluating model performance with respect to chemistry | |
|---|---|
| Skill score | Equation |
| Fractional bias | $$FB = \frac{\overline{C_o} - \overline{C_p}}{0.5(\overline{C_o} + \overline{C_p})}$$ |
| Normalized mean square error | $$NMSE = \frac{\overline{(C_o - C_p)^2}}{\overline{C_o}\,\overline{C_p}}$$ |
| Correlation skill-score | $$R = \frac{\overline{(C_o - \overline{C_o})(C_p - \overline{C_p})}}{\sigma_{C_p}\sigma_{C_o}}$$ |
| Fraction within a factor of two | FAC2 = fraction of data that satisfy $0.5 \le \frac{C_p}{C_o} \le 2.0$ |
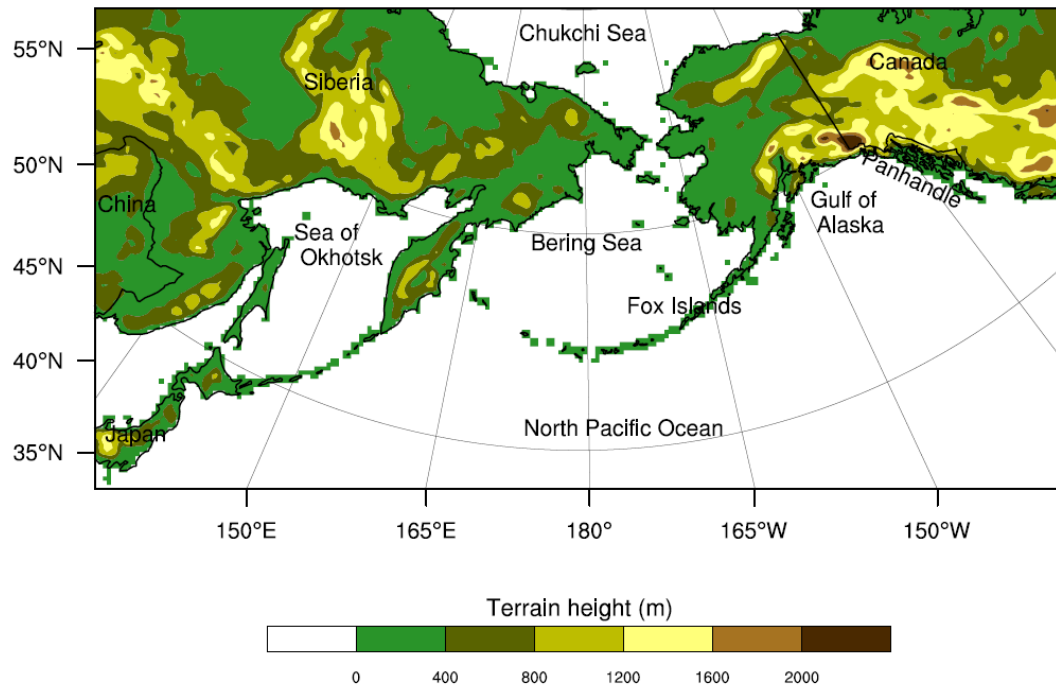
Fig. 2.1 Domain and terrain height for WRF-Chem simulations. The 28 vertical levels reach from the surface to 0hPa with eta-levels of 1.000, 0.993, 0.983, 0.970, 0.954, 0.934, 0.909, 0.880, 0.830, 0.779, 0.729, 0.678, 0.592, 0.514, 0.443, 0.380, 0.324, 0.273, 0.228, 0.188, 0.153, 0.121, 0.094, 0.069, 0.048, 0.030, 0.014 and 0.000.

**Chapter 3 Emission inventory**

**3.1 Global emission data set**

According to Peckham et al. (2009), there are several emission datasets available for WRF-Chem's users to prepare emission input for the simulations. They include (1) the standard 4-km resolution data based upon the U.S. Environmental Protection Agency (EPA) National Emissions Inventory (NEI) inventory available every three years (e.g., 1999, 2002, 2005, 2008); (2) the REanalysis of the TROpospheric (RETRO) chemical composition over the past 40 years and (3) the Emission Database for Global Atmospheric Research (EDGAR) global emission inventories. Depending on the specific characteristics of the model domain (e.g location, resolution of the domain), a particular dataset would be chosen for the simulations. For simulations conducted over other regions of the world, global emission datasets have to be used (Peckham et al., 2009). In this study, the model domain has a 30 km grid increment and covers East Asia and Alaska. Therefore, global emission datasets were selected (i.e. RETRO and EDGAR).

**3.1.1 Anthropogenic emissions**

The anthropogenic emissions discussed in this section refers only to in-land anthropogenic emissions. For WRF-Chem simulations, global emission data sets are provided by the RETRO (Pulles et al., 2005) or EDGAR emission inventory (Oliver et al., 1996; Olivier et al., 2005; EC-JRC/PBL, 2011). The EDGAR inventory is available as gridded data with a 0.1°×0.1° (most updated, version 4.2) or 1°×1° (version 2.0 and 3.2FT2000) spatial and yearly mean resolution. The RETRO inventory is available as

gridded data with a 0.5°×0.5° spatial and monthly mean resolution except for ship emissions that have a 1°×1° resolution. Both the RETRO and EDGAR inventories store global emission data of direct and indirect greenhouse gases (e.g., carbon dioxide ($CO_2$), methane ($CH_4$), nitrous oxide ($N_2O$)) as well as some precursor gases (e.g., sulfur dioxide ($SO_2$), carbon monoxide (CO), $NO_x$ (= NO (nitric oxide) + $NO_2$ (nitrogen dioxide)), Non-Methane Volatile Organic Compounds (NMVOC)) from anthropogenic sources. In this study, only emission of CO, $NO_x$, $SO_2$ and NMVOC have been considered in the simulations.

Activity data from the International Energy Agency (IEA) are used as original data for both RETRO and EDGAR (Olivier et al., 1996; Schultz et al., 2007). Because of sharing the same data source, these datasets are not completely independent from each other. According to a study by Butler et al. (2008), the EDGAR and RETRO datasets are generally very similar, though there are some differences due to the slightly different purposes for which the inventories were designed. Sometimes differences are due to different methodologies used in the construction of the inventories. Tables 3.1 and 3.2 show some key differences between the RETRO and EDGAR global emission inventories (Butler et al., 2008).

Table 3.2 shows that CO and $NO_x$ emissions of the EDGAR inventory are about 10% higher than those of the RETRO inventory. Conversely, the NMVOC emission in the RETRO is 10% higher than that in the EDGAR inventory. However, these variances are still in the range of the high global uncertainty of each dataset, which is about 50%-100% (Olivier et al., 2001). Therefore, the total emissions for these pollutants are

considered to be the same among the two inventories. There is no comparison for $SO_2$ because $SO_2$ emission data is only available for the EDGAR and not for the RETRO inventory. In this study for Alaska, $SO_2$ is a key pollutant which plays an important role in the formation of aerosols. Therefore, the EDGAR datasets were selected for the anthropogenic emissions because the EDGAR data includes emissions of more relevant pollutant species for this study than does the RETRO data.

The latest EDGAR dataset (EDGAR v4.2) comprises the annual emission inventories on a $0.1° \times 0.1°$ grid. This data was used for the anthropogenic emissions for simulations in high insolation periods. It provides annual global anthropogenic emissions for in-land sources for 2008 as the most updated year that data is available (EC-JRC/PBL, 2011).

For simulations in low insolation periods, since this latest data set was not available at the time those simulations were performed, the older EDGAR data set was used with emission inventoried on a $1° \times 1°$ grid. The EDGAR Version 2.0 dataset and the EDGAR 3.2 Fast Track 2000 dataset (32FT2000) which provide annual global emissions for the year 1990 and 2000, respectively, were used in this study.

EDGAR data were jointly conducted by Netherlands Organization for Applied Scientific Research and Netherlands National Institute for Public Health and the Environment in cooperation with Global Emissions Inventory Activity (GEIA) of the International Atmospheric Chemistry Programme (IGAC) to meet the urgent need of atmospheric chemistry and climate modelers and the need of policy-makers. The inland anthropogenic emissions of EDGAR consist of: (i) fossil-fuel related sources; (ii) biofuel

combustion; (iii) industrial production and consumption processes (including solvent use) and (iv) landuse-related sources, including waste treatment (Olivier et al., 1996; van Aardenne et al., 2005). Hereafter, a brief description is given on the original sources from which the EDGAR data were compiled (Olivier et al., 1996; Olivier et al., 2001).

**Fossil fuel related sources**: The energy data of 112 countries (year 1990) or 136 countries (year 2000) are from the International Energy Agency (IEA) energy statistic. Emission factors comply with the GEIA data.

**Biofuel combustion**: Most of the country activity levels are from the Biomass Users Network (BUN), except for some Organization for Economic Co-operation and Development (OECD) countries, for which the original data comes from the IEA data. Emission factors are based on different previous studies conducted by many experts in the field (Builtjes, 1992; Veldt and Berdowski, 1995).

**Industrial processes**: Activity data are generally taken from the United Nations statistics. Exceptions are solvent use, for which a number of specific activity levels for a certain year were taken from published industrial data and estimates for per-country-use of solvents based on economic characteristics. Emission factors comply with the GEIA data.

**Landuse and waste treatment**: Activity data per country are generally from the Food and Agriculture Organization of the United Nations (FAO) statistics.

It must be noted that 32FT2000 (emissions in 2000) use different emission factors than EDGAR 2.0 (emissions in 1990). For 2000, anthropogenic emission inventories take into account emission reductions that have occurred due to control measures

implemented since 1995. There are many sectors in which important emission reduction measures have been implemented, such as coal mining, gasoline cars, shifting type of rice cultivation, landfills with gas recovery. In addition, also for power plants and some industries in countries where additional control technology (e.g. for $SO_2$ and $NO_x$) has been installed, updated emission factors were considered (Olivier et al., 2001; van Aardenne et al., 2005).

### 3.1.2 Ship emissions

To be consistent with other anthropogenic emissions, ship emission data was also taken from EDGAR data. For low insolations periods, the EDGAR data version 2.0 (emission in 1990) and EDGAR 3.2 Fast Track 2000 dataset (emission in 2000) were used for ship emissions. The EDGAR ship emission inventories provide gridded data with $1^o$x$1^o$ and annual resolution. They were developed based on the IEA fuel statistics. However, this data only includes the international ship emissions without any domestic ship emissions (Fig. 3.1). Fortunately, the RETRO ship emission data, which is based on the ship emission inventory approach of Endresen et al. (2003), includes domestic ship emissions (van het Bolscher et al., 2008). This dataset is also on a $1^o$x$1^o$ grid and comprises monthly values (uniform variation). Therefore, the input for ship emission in this study is the combination of both the EDGAR and RETRO inventories. Within the model domain, the EDGAR international ship emissions are kept the same. Any grid cell having no EDGAR ship emission data is assigned the RETRO ship emission data (Fig. 3.2).

For high insolation period (June 2008), ship emission data of most updated EDGAR v4.2 has spatial resolution of $0.1° \times 0.1°$ and is fine enough to represent emissions from both domestic and international shipping lanes. Therefore, this dataset was used for high insolation simulations.

*Comparison between top-down and bottom-up approach for ship emission*

Generally, global ship emission inventories (EDGAR and RETRO) are developed by applying top-down approaches: the emissions are estimated based on the total fuel consumption. On the other hand, regional ship emissions are calculated by bottom-up approaches, (e.g., Porter, 2009; Mölders et al., 2010) and so can provide finer resolution and more accurate spatial distribution of emission. However, by applying a bottom-up approach for global ship inventory would be very limited due to unavailability of ship movement data (Marmer et al., 2009). Figures 3.3 and 3.4 show the framework of top-down and bottom-up approach, respectively.

Figure 3.5 presents ship emissions for CO, $NO_x$, $SO_2$ for 2000 as obtained by two inventories that use different approaches: a top-down (left) and bottom-up (right) approach for comparison. Data are shown exemplarily for the same domain as used by Porter (2009). Note that this domain is smaller than the domain used in this study, which covers a larger area where data is not available for applying a bottom-up approach. Based on the trend of ship activity from 2002 to 2004 reported by the Marine Exchange of Alaska (MXAK, 2005) and commercial marine inventories for selected Alaska ports developed by Pechan (2005), an emission factor ratio E2004/E2002 was calculated for each pollutant (Table 3.3). Using these factors, the emission data derived for 2006 by

Porter (2009) was projected to 2000 for comparison with the RETRO data, assuming the same emission factors for two periods: 2000 - 2002 and 2004 -2006.

Figure 3.5 clearly illustrates that the finer resolution and more accurate spatial distribution of emission obtained by the bottom-up approach inventory shows the major shipping lanes. On the contrary, in the RETRO ship-emission inventory, it is difficult to identify the shipping lanes due to the coarse resolution of the emission data ($1^{o}$x$1^{o}$). However, despite being developed by two different methods, the amount of pollutants emitted in both two cases is of the same order of magnitude (Fig. 3.5). The same is true for NMVOC.

### 3.1.3 Biogenic emissions

For biogenic emission, Guenther et al.'s (1994) and Simpson et al.'s (1995) biogenic emission schemes were used to calculate the emissions of isoprene, monoterpenes, other volatile organic compound (VOCs) from vegetation and nitrogen emission from soil. This biogenic emission module calculates the emissions inline and considers the simulated temperature and photosynthetic active radiation conditions. It uses the U.S Geological Survey (USGS) land-use classification to consider land-use type.

### 3.1.4 Wildfire emissions

Wildfire emissions were estimated by the Brazilian Biomass Burning Emissions Model (3BEM) (Freitas et al., 2005; Longo et al., 2010). 3BEM used near real-time remote sensing fire products as the source for determining fire locations. In our study,the

MOderate-Resolution Imaging Spectrometer (MODIS; Giglio et al., 2003) dataset was used for wildfire locations due to its high spatial resolution raging from 0.25 to 1 km. For each fire pixel detected, the mass of a certain emitted tracer (i) is calculated by Eq. 3.1(see Longo et al. (2010) for more detail).

$$M_i = \alpha_{veg} \times \beta_{veg} \times EF^i_{veg} \times a_{fire} \qquad \text{(Eq 3.1)}$$

Where $M_i$ is the mass of emitted tracer (*i*), $\alpha_{veg}$ is the amount of above-ground biomass available for burning, $\beta_{veg}$ is the combustion factor (fuel loading which can be derived from a land cover classification), $EF^i_{veg}$ is the emission factor for a certain species (i) from the appropriate type of vegetations, and $a_{fire}$ is burned area.

3BEM uses land use (Belward, 1996; Sestini et al., 2003) and carbon in vegetation (Olson et al., 2000) datasets to determine emission factors, combustion factors and carbon densities for each vegetation type in accordance with the approaches of Ward et al. (1992) and Andreae and Merlet (2001). Uniform hourly emissions during each 24h period were applied for wildfire emissions.

Anthropogenic and biogenic emissions were assigned as surface fluxes in the lowest layer above the ground since these sources emit pollutants at a temperature close to the ambient air temperature resulting in negligible buoyancy. However, wildfire emissions are always emitted with strong buoyancy due to the hot air released by the burns. Therefore, the effect of plume rise on our wildfire emissions needs to be included. In this study, a one dimension time-dependent entrainment plume model originally developed by Latham (1994) coupled in WRF-Chem by Freitas et al. (2007) with appropriate boundary conditions provided by WRF-Chem (the host model) was applied

to explicitly simulate the plume rise and determine the injection height of the fire smoke plumes. Wildfire emissions were then assigned throughout the vertical column at fire locations from the near-surface layer up to the layer corresponding to the simulated injection height.

## 3.2 Allocation functions

As stated previously, the emission datasets of the EDGAR (anthropogenic and ship emissions) and RETRO (ship emission) are annual and monthly totals, respectively. To use these datasets in the WRF-Chem simulations, temporal allocation functions including monthly, weekly and hourly profiles were used to consider the actual variation of emissions in time.

### 3.2.1 Allocation functions for anthropogenic emission sectors

Based on the similarity in activity frequency variation, anthropogenic emission sectors of EDGAR (except ship emissions) were categorized into six typical groups, which are: (1) industrial processes, (2) power plants, (3) residential combustion, (4) petroleum production, (5) waste treatment and (6) road transportation following Mölders (2009).

The temporal profiles (Fig.3.6) were applied separately for each of these groups. Table 3.4 presents the grouping of the EDGAR emission sectors.

Activity allocation functions generally follow the temporal profiles developed by Veldt (1991) for the Europe climate model LOng Term Ozone Simulation (LOTOS).

However, some profiles, which were developed or modified for Alaska (Mölders, 2009), were used instead. Table 3.5 indicates the selection of temporal profiles for each group of emissions.

Figure 3.6 shows that the monthly variations strongly differ among groups of emission sectors due to the different activity in winter/summer. Except for petroleum production and waste treatment, which are assumed to be uniform in the weekly temporal variation profile, most emission sources have lower activity frequency on weekends than on weekdays. Hourly allocation functions also differ among emission sources due to their activity characteristics in the diurnal course. Applying activity-allocation functions of emissions into the simulations has to be conducted with caution to minimize uncertainties in model results. However, although impacts of emissions depend on temporal profiles, only very small differences are found in simulations that apply different weekday/weekend and hourly variation profiles (Vutukuru and Dabdub, 2008; Fortun and Mölders, 2009).

### 3.2.2 Allocation functions for ship emissions

The monthly allocation functions for shipping in North America developed by Wang et al. (2007) (Fig. 3.7) were used in this study. This profile is very similar to other temporal allocation functions for global ship emissions (e.g. Corbett et al., 2007). Since the assumption of uniform rates of ship emission serves well in the absence of high temporal resolution emission datasets (Vutukuru and Dabdub, 2008), uniform allocation functions were used for weekday/weekend and hourly variations.

### 3.3 Volatile organic compound (VOC) speciation

The term VOCs refers to a variety of gases. The most common compound, methane ($CH_4$), is assumed to a fix value of 1.7ppm in WRF-Chem simulations. $CH_4$ emission variations were neglected. Only other VOCs (also called non-methane VOCs or NMVOCs) are considered for emissions. EDGAR provides VOC emissions from anthropogenic sources as aggregated data (emission of total NMVOCs per year), which need to be split into specific species.

For anthropogenic emissions, there is no NMVOCs speciation for Alaska available. Therefore, the NMVOCs speciation developed by Theloke and Friedrich (2007) for atmospheric dispersion models in Europe is used instead. The NMVOCs of ship emission were split into specific species in accordance with Eyring et al. (2005). The speciation of VOCs from biogenic emissions was conducted inline automatically by WRF/Chem following Guenther et al. (1994). Tables 3.6 and 3.7 present the speciation of NMVOCs for anthropogenic and ship emissions.

### 3.4 Preparation of emissions for WRF-Chem simulation

The WRF-Chem simulations require hourly input data in netcdf format with speciation of VOCs. Therefore, the preparation of this input dataset was conducted externally from the simulations. A package of programs named emission_readin was created to read in the raw data provided by the EDGAR and RETRO inventories, split the NMVOCs into species and combine the data from these two sources into aggregated data files. Another package of programs called prep_chem_sources, which was developed by

CPTEC (Centro de Previsao de Tempo e Estudos Climaticos) of Brazil (Freitas et al., 2011), maps the emission data onto the WRF-Chem domain. Modifications were made to this package to involve the activity allocation functions and include the right target chemical pollutants for specific design of the simulations. A binary data file was then created by processing these programs. It was finally converted to netcdf data format, which is ready for WRF/Chem simulations by a program named "convert_emiss.exe" available in WRF/Chem model package (Fig. 3.8).

# References

Andreae, M., Merlet, P., 2001. Emission of trace gases and aerosols from biomass burning, Glob. Biogeochem. Cy., 15(4), 955–966.

Belward, A., 1996. The IGBP-DIS global 1 km land cover dataset (DISCover)-proposal and implementation plans, IGBP-DIS Working Paper No. 13, Toulouse, France.

Builtjes, P.J.H., 1992. The LOTOS Long Term Ozone Simulation project. Summary Report. TNO-MW, Delft. TNOMW Techn. Report, R, 92/245.

Butler, T.M., Lawrence, M.G., Gurjar, B.R., van Aardenne, J., Schultz, M., Lelieveld, J., 2008. The representation of emissions from megacities in global emission inventories. Atmos. Environ., 42, 703–719.

Corbett, J.J., Firestone, J., Wang, C., 2007. Estimation, validation, and forecasts of regional commercial marine vessel inventories - Final report. California Air Resources Board, California Environmental Protection Agency and Commission for Environmental Cooperation of North America, 61p.

Endresen, Ø., Sørga˚ rd, E., Sundet, J.K., Dalsøren, S.B., Isaksen, I.S.A., Berglen, T.F., Gravir, G., 2003. Emission from international sea transportation and environmental impact. J. Geophys. Res., Vol. 108, 4560, 22p.

European Commission, Joint Research Centre / Netherlands Environmental Assessment Agency (EC-JRC/PBL), 2011. Emission Database for Global Atmospheric Research (EDGAR), release version 4.2. Available at http://edgar.jrc.ec.europa.eu.

Eyring, V., Köhler, H. W., Lauer, A., Lemper, B., 2005. Emissions from international shipping: 2. Impact of future technologies on scenarios until 2050. J. Geophys. Res., Vol. 110, D17306, 18p.

Fortun, T., Mölders, N., 2009. Investigations on the sensitivity of predicted air quality to the uncertainty in anthropogenic emissions. ARSC REU summer intern report, 18p.

Freitas, S. R., Longo, K. M., Silva Dias, M., Silva Dias, P., Chatfield, R., Prins, E., Artaxo, P., Grell, G., Recuero, F., 2005. Monitoring the transport of biomass burning emissions in South America, Environ. Fluid Mech., 5(1–2), 135–167.

Freitas, S. R., Longo, K. M., Chatfield, R., Latham, D., Silva Dias, M. A. F., Andreae, M. O., Prins, E., Santos, J. C., Gielow, R., Carvalho Jr., J. A., 2007. Including the sub-grid scale plume rise of vegetation fires in low resolution atmospheric transport models. Atmos. Chem. Phys., 7, 3385–3398.

64

Freitas, S. R., Longo, K.M., Alonso, M.F., Pirre, M., Marecal, V., Grell, G., Stockler, R., Mello, R.F., Sánchez Gácita, M., 2011. PREP-CHEM-SRC – 1.0: a preprocessor of trace gas and aerosol emission fields for regional and global atmospheric chemistry models. Geosci. Model Dev., 4, 419–433.

Giglio, L., Descloitres, J., Justice, C. O., Kaufman, Y. J., 2003. An enhanced contextual fire detection algorithm for MODIS. Remote Sens. Environ., 87, 273–282.

Guenther, A., Hewitt, C., Erickson, D., Fall, R., Geron, C., Graedel, T., Harley, P., Klinger, L., Lerdau, M., McKay, W., Pierce, T. and Zimmerman, P.R., 1994. A global model of natural volatile organic compound emissions. J. Geophys. Res., 100D, 8873-8892.

Latham, D., 1994. PLUMP: A one-dimensional plume predictor and cloud model for fire and smoke managers. Intermountain Research Station, USDA forest service, General Tech. R. INT-GTR-314.

Longo, K. M., Freitas, S. R., Andreae, M. O., Setzer, A., Prins, E., Artaxo, P., 2010. The Coupled Aerosol and Tracer Transport model to the Brazilian developments on the Regional Atmospheric Modeling System (CATT-BRAMS) – Part 2: Model sensitivity to the biomass burning inventories, Atmos. Chem. Phys., 10, 5785–5795.

Marmer E., Dentener, F., Aardenne, J. v., Cavalli, F., Vignati, E., Velchev, K., Hjorth, J., Boersma, F., Vinken, G., Mihalopoulos, N., Raes, F., 2009. What can we learn about ship emission inventories from measurements of air pollutants over the Mediterranean Sea? Atmos. Chem. Phys., 9, 6815–6831.

Mölders, N., 2009. Alaska Emission Model (AkEM) description. Internal Report. Fairbanks: 10p.

Mölders, N., Porter, S.E., Cahill, C.F., Grell, G.A., 2010. Influence of ship emissions on air quality and input of contaminants in southern Alaska National Parks and Wilderness Areas during the 2006 tourist season. Atmos. Environ., 44, 1400-1413.

MXAK, 2005. Marine Exchange of Alaska, Alaska Port Maritime Traffic and Air Emissions, Juneau, AK, June 13, 2005.

Olivier, J.G.J., Bouwman, A.F., Van der Maas, C.W.M., Berdowski, J.J.M., Veldt, C., Bloos, J.P.J., Visschedijk, A.J.H., Zandveld, P.Y.J. and Haverlag, J.L., 1996. Description of EDGAR Version 2.0: A set of global emission inventories of greenhous gases and ozone-depleting substances for all anthropogenic and most natural sources on a per country basis and on 1ox1o grid. National Institute of Public Health and the Environment (RIVM) report no. 771060 002 / TNO-MEP report no. R96/119.

Olivier, J.G.J., Berdowski, J.J.M., Peters, J.H.A.W., Bakker, J., Visschedijk, A.J.H., Bloos, J.P.J., 2001. Applications of EDGAR, including a description of version 3.0: reference database with trend data for 1970–1995. Technical Report 773301 001, National Institute of Public Health and the Environment (RIVM), The Netherlands.

Olivier, J.G.J., van Aardenne, J.A., Dentener, F., Ganzeveld, L.,  Peters, J.A.H.W., 2005. Recent trends in global greenhouse gas emissions: regional trends and spatial distribution of key sources. In: "Non-CO2 Greenhouse Gases (NCGG-4)", A. van Amstel (coord.), 325-330. Millpress, Rotterdam, ISBN 90 5966 043 9.

Olson, J. S.,Watts, J. A., Allison, L. J., 2000. Major world ecosystem complexes ranked by carbon in live vegetation: A database (revised November 2000), NDP-017, available at: http://cdiac.esd.ornl.gov/ndps/ndp017.html, Carbon Dioxide Information Analysis Center, Oak Ridge National Laboratory, Oak Ridge, Tennessee, USA.

Pechan, 2005. E.H. Pechan and Associates, Inc., Commercial Marine Inventories for Select Alaskan Ports, Final Report, Prepared by Pechan for the Alaska Department of Environmental Conservation, June 2005.

Peckham, S.E., Fast, J.D., Schmitz, R., Grell, G.A., Gustafson, W.I., McKeen, S.A., Ghan, S.J., Zaveri, R., Easter, R.C. , Barnard, J., Chapman, E., Salzmann, M., Wiedinmyer, C. and Freitas, S.R., 2009. WRF/Chem Version 3.1 User's Guide. 78p.

Porter, S.E., 2009. Investigation of the impact of ship emissionson atmospheric composition and deposition into remote, coastal landscapes of southwest Alaska. University of Alaska Fairbanks, M.S. thesis. Available at htpp://www.gi.alaska.edu/~molders/porter_final_thesis.pdf.

Pulles, T., Brand, R., van het Bolscher, M., Sørgård, E., Sundet, J., Dalsøren, S., Isaksen, I., Berglen, T., Gravir, G., Schultz, M., 2005. RETRO Emission Inventory: anthropogenic emission database, GEIA. Available at http://retro.enes.org/data_emissions.shtml.

Schultz M.G., Backman, L., Balkanski, Y., Bjoerndalsaeter, S., Brand, R., Burrows, J.P., Dalsoeren, S., de Vasconcelos, M.,  Grodtmann, B., Hauglustaine, D.A., Heil, A., Hoelzemann, J.J., Isaksen, I.S.A., Kaurola, J., Knorr, W., Ladstaetter-Weißenmayer, A., Mota, B., Oom, D., Pacyna, J., Panasiuk, D., Pereira, J.M.C., Pulles, T., Pyle, J., Rast, S., Richter, A., Savage, N., Schnadt, C., Schulz, M., Spessa, A., Staehelin, J., Sundet, J.K., Szopa, S., Thonicke, K., van het Bolscher, M., van Noije, T., van Velthoven, P., Vik, A.F., Wittrock, F., 2007. REanalysis of the TROpospheric chemical composition over the past 40 years (RETRO) - A long-term global modeling study of tropospheric chemistry - Final Report. Jülich/Hamburg. Published as report no. 48/2007 in the series "Reports on Earth System Science" of the Max Planck  Institute for Meteorology, Hamburg, ISSN 1614-1199. Available at http://www.knmi.nl/publications/fulltexts/retro_final_report.pdf

Sestini, M., Reimer, E., Valeriano, D., Alvalá, R., Mello, E., Chan, C., and Nobre, C., 2003. Mapa de cobertura da terra da Amazônia legal para uso em modelos meteorológicos, Anais XI Simpósio Brasileiro de Sensoriamento Remoto, 2901–2906.

Simpson, D., Guenther, A., Hewitt, C.N., Steinbrecher, R., 1995. Biogenic emissions in Europe 1. Estimates and uncertainties. J. Geophys. Res., 100D, 22875-22890.

Theloke, J., Friedrich, R., 2007. Compilation of a database on the composition of anthropogenic VOC emissions for atmospheric modeling in Europe. Atmos. Environ., 41, 4148–4160.

van Aardenne, J.A., Dentener, F., Olivier, J.G.J, Peters, J.A.H.W., 2005. The EDGAR 3.2 Fast Track 2000 dataset (32FT2000). Technical documentation available at http://themasites.pbl.nl/images/Description_of_EDGAR_32FT2000%28v8%29_tcm61-46462.pdf

van het Bolscher, M., Pulles T., Brand R., Pereira J., Mota B., Spessa A., Dalsøren S., Twan van Nojie, Szopa S., Schultz M.G, Rast S., 2008. REanalysis of the TROpospheric chemical composition over the past 40 years (RETRO) - A long-term global modeling study of tropospheric chemistry - RETRO deliverable D1-6: Emission data sets and methodologies for estimating emissions. Available at http://retro.enes.org/reports/D1-6_final.pdf

Veldt, C.1991. Emissions of SOx, NOx, VOC and CO from East European countries. Atmos. Environ., 25A, 2683–2700.

Veldt, C., Berdowski, J.J.M., 1995. GEIA-Note on the combustion of biomass fuels (Emission factors for CO, CH4 and NMVOC). TNO-MW, Delft. TNO Techn. Report 94/218.

Vutukuru, S., Dabdub, D., 2008. Modeling the effects of ship emissions on coastal air quality: a case study of southern California. Atmos. Environ., 42, 3751-3764.

Wang, C., Firestone, J., Corbett, J.J., 2007. Modeling Energy Use and Emissions from North American Shipping: Application of the Ship Traffic, Energy, and Environment Model. Environ. Sci. Technol., 41, 3226-3232.

Ward, E., Susott, R., Kaufman, J., Babbit, R., Cummings, D., Dias, B., Holben, B., Kaufman, Y., Rasmussen, R., Setzer, A., 1992. Smoke and fire characteristics for cerrado and deforestation burns in Brazil: BASE-B Experiment. J. Geophys. Res., 97(D13), 14601–14619.

Table 3.1 Comparison of original sources of the EDGAR and RETRO emission inventories (Butler et al., 2008)

| | EDGAR | RETRO |
|---|---|---|
| Energy activity data (including transport) | IEA: OECD (Organisation for Economic Co-operation and Development) and non-OECD | IEA: OECD and non-OECD |
| Industrial activity data | UN statistics, US Geological Survey minerals yearbook | Unknown |
| Waste activity data | Per capita calculation | Unknown |
| Population density | FAO (United Nations Food and Agriculture Organization) | CIESIN (Center for International Earth Science Information Network) |

Table 3.2 Comparison of total emissions for 2000 as provided by the EDGAR and RETRO inventories (Butler et al., 2008)

| Pollutant | EDGAR | RETRO |
|---|---|---|
| CO (Tg y$^{-1}$) | 531 | 477 |
| NO$_x$ (Tg y$^{-1}$) | 30.3 | 27.5 |
| NMVOC (Tg y$^{-1}$) | 136 | 152 |

Table 3.3 Temporal emission factors of ship emissions for the Alaska area  according to MXAK (2005)

| Emission factor ratio (E2004/E2002) | | | |
|---|---|---|---|
| | $NO_x$ Emissions | CO Emissions | $SO_2$ Emissions |
| Annual | 1.059 | 1.025 | 1.067 |
| Summer | 1.082 | 1.043 | 1.092 |
| Winter | 0.995 | 0.998 | 0.989 |

Table 3.4 Categorization of the EDGAR emission sectors

| Group of emission sources | EDGAR emission sectors |
|---|---|
| Industrial processes (IND) | Industries; Charcoal production; Ion & steel production; Non-ferrous production; Chemicals; Cement; Pulp & Paper; Food; Solvents; Miscellaneous |
| Power plant (POW) | Power generation |
| Residential combustion (RES) | Residential combustion |
| Petroleum production (PET) | Fossil fuel production; Oil and gas production |
| Waste treatment (WAS) | Waste Incineration; Waste handling |
| Road transportation (TRAN) | Road transportation; Land non-road transportation |

Table 3.5 Temporal profiles for groups of emission sources. AK: Temporal allocation functions developed for Alaska by Mölders (2009); (1): Data from GEVA; University of Alaska Fairbanks (UAF); (2): Data from the Department of Transportation of Alaska (DOT); EU: Temporal allocation functions developed by Veldt (1991) for the Europe climate model

| Group of emission sources | Monthly profile | Weekday/weekend profile | Hourly profile |
|---|---|---|---|
| Industrial processes | EU | EU | EU |
| Power plant | AK [1] | AK [1] | AK [1] |
| Residential combustion | EU | EU | EU |
| Petroleum production | EU | EU (Uniform) | EU (Uniform) |
| Waste treatment | EU | EU (Uniform) | EU (Uniform) |
| Traffic | EU | EU | AK [2] |

Table 3.6 Speciation of VOC emissions from anthropogenic sources. Values are percentages (%) of total VOC emissions in accordance with Theloke and Friedrich (2007)

| Class name/name | Solvent use/ petroleum | Land-transport | Combustion | Industry processes |
|---|---|---|---|---|
| Ethers | 1.30 | 0.00 | 0.00 | 2.40 |
| Alkenes | 0.28 | 4.00 | 4.75 | 3.75 |
| Aldehyde | 0.01 | 4.50 | 4.00 | 2.00 |
| Ethane (alkanes) | 14.00 | 20.50 | 14.50 | 15.50 |
| Xylenes | 7.33 | 9.00 | 12.33 | 1.67 |
| Toluenes | 7.33 | 9.00 | 12.33 | 1.67 |
| Alkenes | 12.28 | 4.00 | 4.75 | 18.25 |
| Propene | 0.28 | 4.00 | 4.75 | 3.75 |
| Ketones | 6.00 | 1.00 | 2.00 | 0.20 |
| Alkanes | 43.48 | 26.5 | 19.5 | 43.4 |
| Ethene (alkenes) | 0.28 | 4.00 | 4.75 | 3.75 |
| Phenols (aromatics) | 7.33 | 9.00 | 12.33 | 1.67 |
| Acids | 0.10 | 0.00 | 0.00 | 0.00 |
| Methanal (aldehydes) | 0.01 | 4.50 | 4.00 | 2.00 |

Table 3.7 Speciation of VOC emissions from ship emissions. Values are percentages of total VOC emissions in accordance with Eyring et al. (2005)

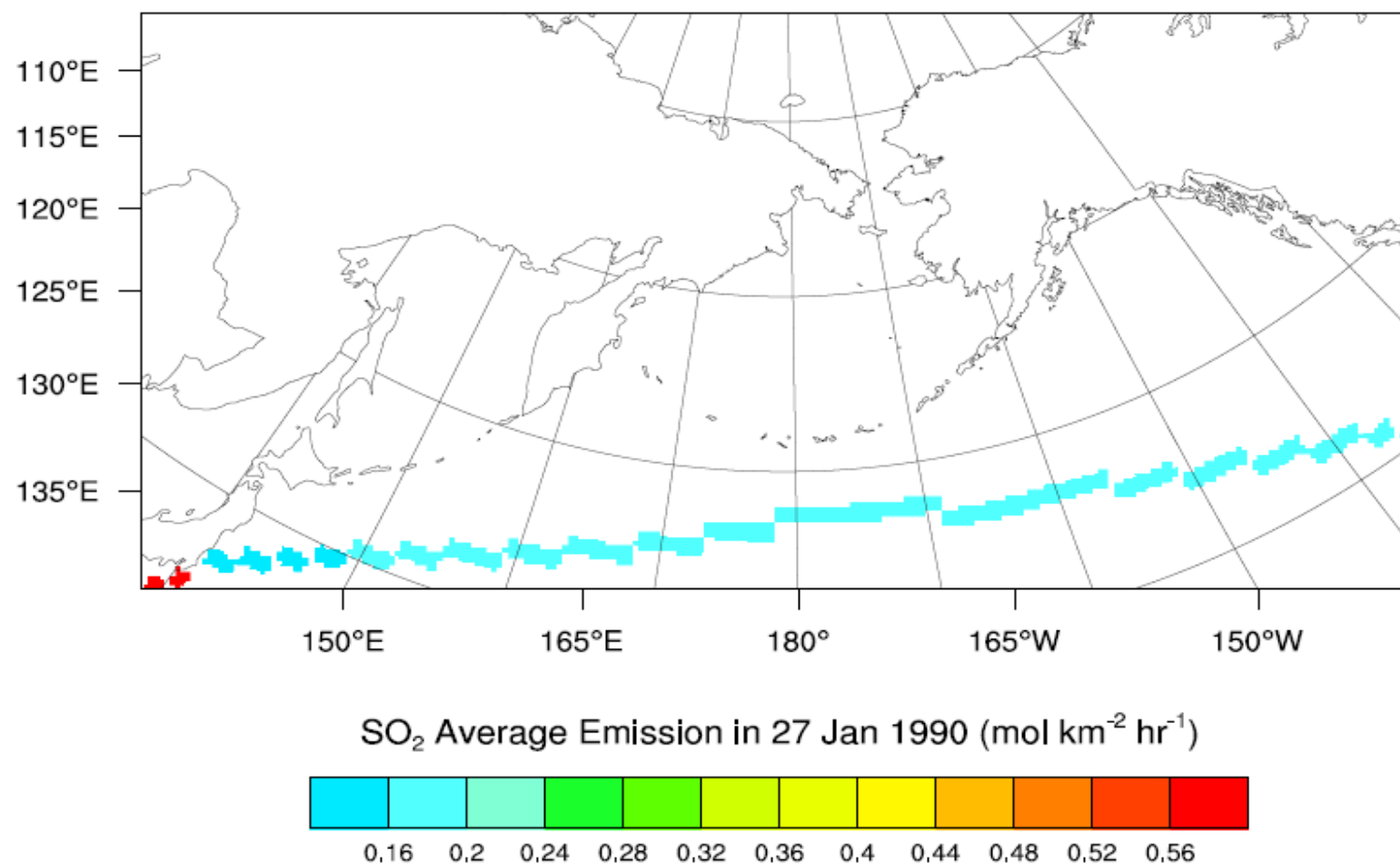| Class name/name | Operational modes | Tank loading |
| --- | --- | --- |
| Ethers | -- | -- |
| Alkenes | -- | -- |
| Aldehyde | -- | -- |
| Ethane (alkanes) | -- | 9.30 |
| Xylenes | 13.60 | 0.70 |
| Toluenes | 5.20 | 0.20 |
| Alkenes | 2.20 | -- |
| Propene | 22.90 | -- |
| Ketones | -- | -- |
| Alkanes | 30.20 | 73.20 |
| Ethene (alkenes) | 20.90 | -- |
| Phenols (aromatics) | -- | 7.60 |
| Acids | -- | -- |
| Methanal (aldehydes) | -- | -- |

Fig. 3.1 Average emissions of $SO_2$ for 27 January 1990 from international ship traffic derived from the EDGAR data.
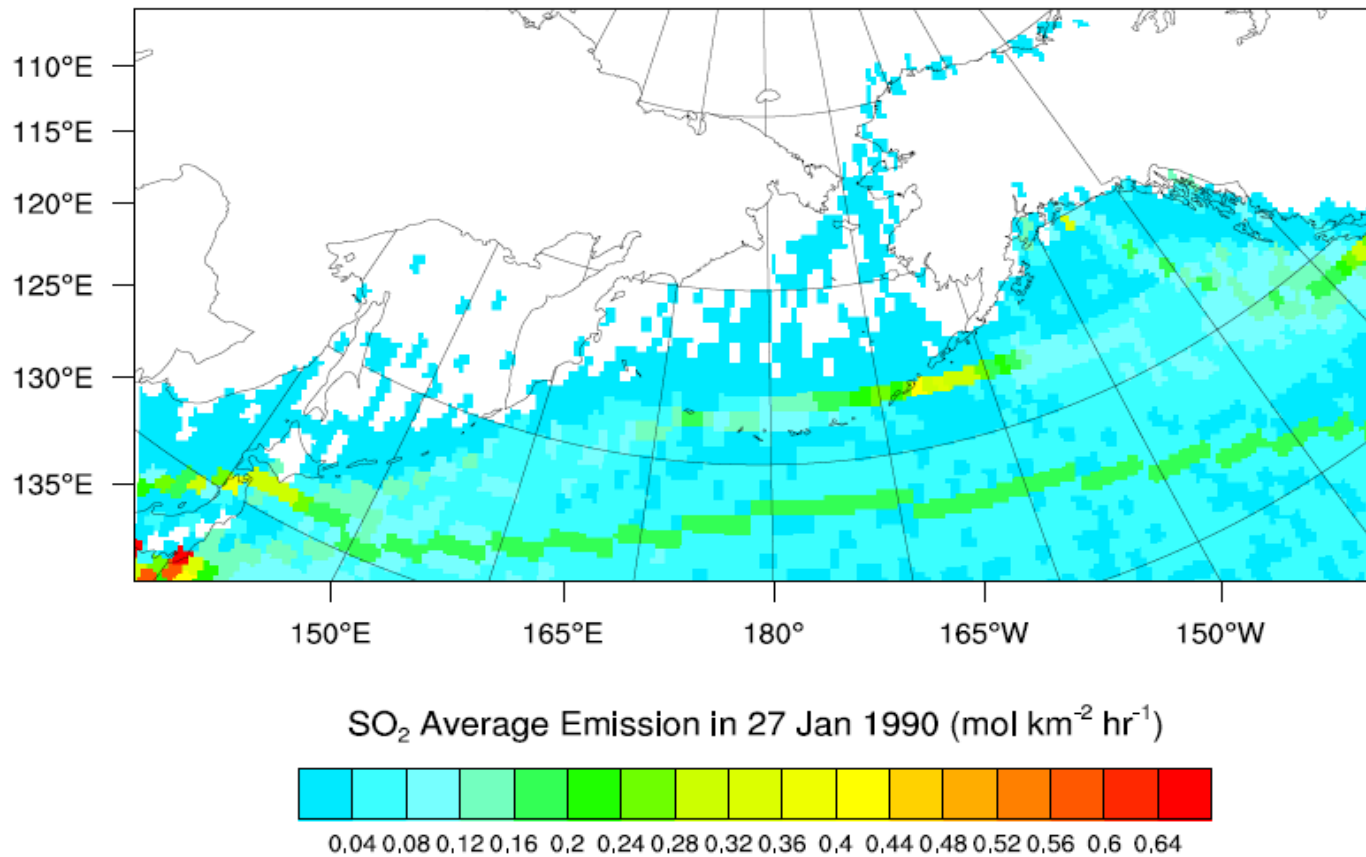
Fig. 3.2 Average emissions of $SO_2$ for 27 January 1990 as obtained from the combined data from the EDGAR and RETRO inventories using the method described in the text.

```
┌─────────────────────────────────────────────────┐
│                                                 │
│            IEA: Bunker fuel statistics          │
│                                                 │
└─────────────────────────────────────────────────┘
                         │
                         ▼
┌─────────────────────────────────────────────────┐
│                                                 │
│            Implied emission factors             │
│                                                 │
└─────────────────────────────────────────────────┘
                         │
                         ▼
┌─────────────────────────────────────────────────┐
│                                                 │
│         AMVER global distribution data          │
│                                                 │
└─────────────────────────────────────────────────┘
                         │
                         ▼
┌─────────────────────────────────────────────────┐
│                                                 │
│           1x1 degree global emissions           │
│                                                 │
└─────────────────────────────────────────────────┘
```
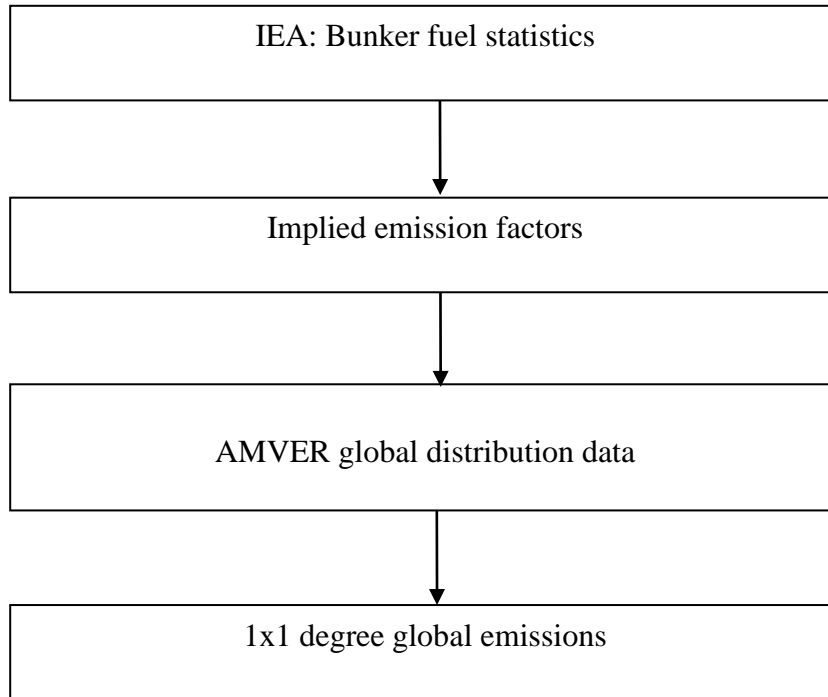
Fig. 3.3 Global ship emission inventory, classical top-down approach as applied for the EDGAR 32FT2000 from Marmer et al. (2009).

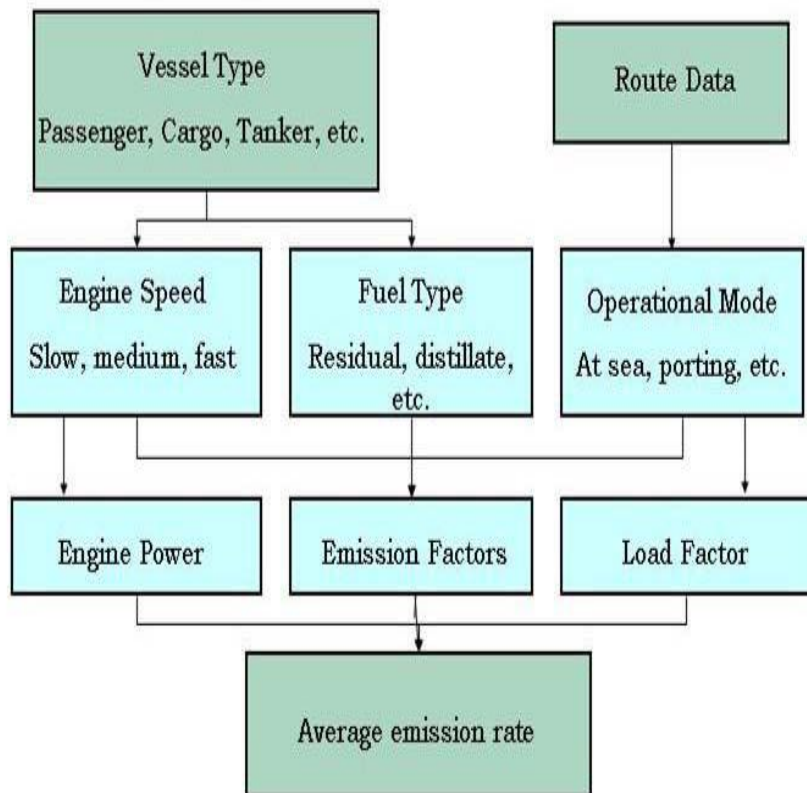*AMVER (Automated Mutual-Assistance Vessel Rescue System)*

Fig. 3.4 Regional ship emission inventory, using bottom-up approach (Porter, 2009).

**CO Emission**

**CO Emission**



**(a)**

**(b)**

Monthly CO emission (g/km²)

100  300  500  700  900  1100  1300  1500  1700  1900  2100  2300  2500  2700  2900  3100

**NO$_x$ emission**

**NO$_x$ emission**



**(c)**

**(d)**

Monthly NOx emission (kg/km²)

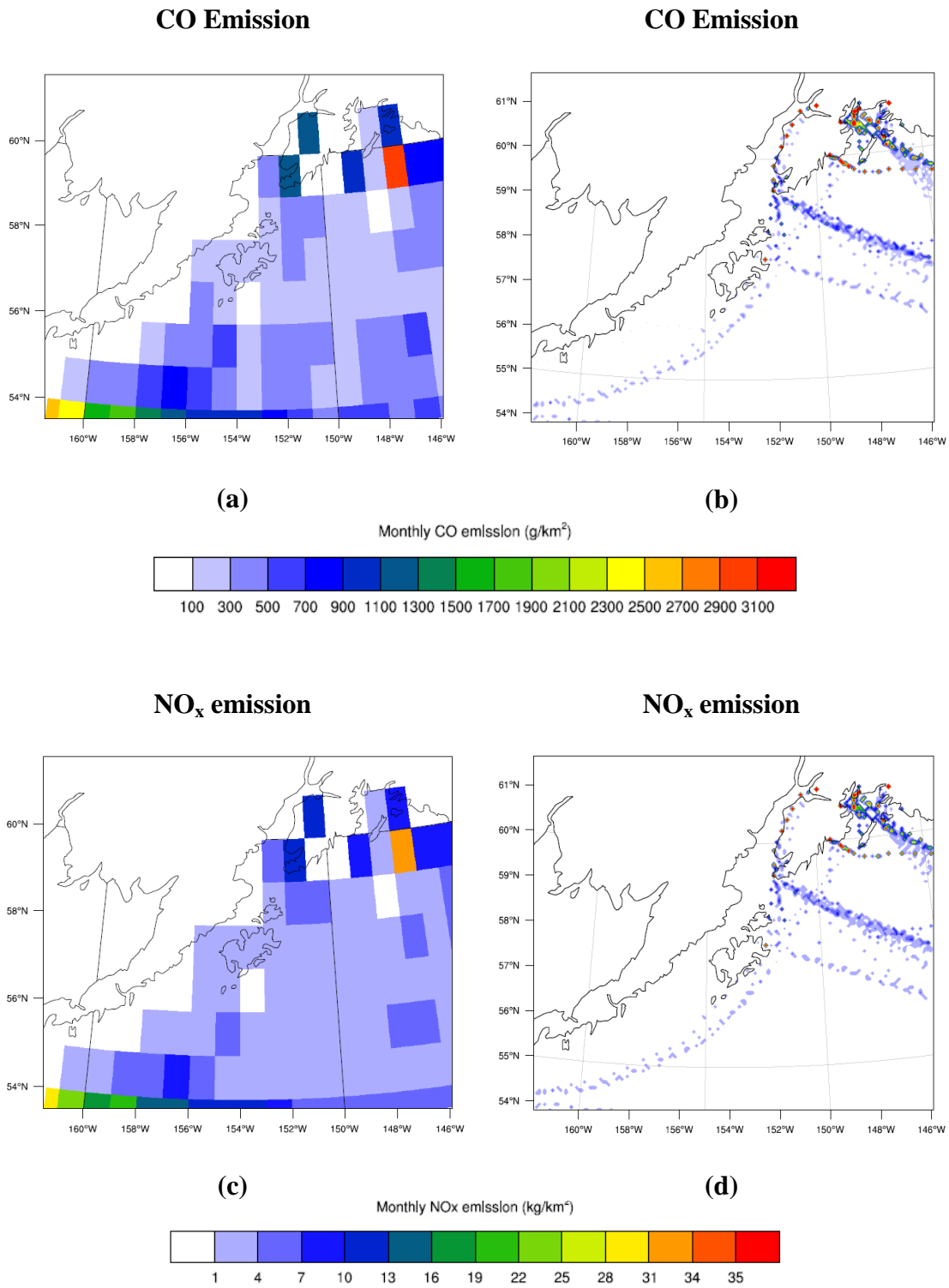1   4   7   10   13   16   19   22   25   28   31   34   35

Fig. 3.5 Total accumulated emissions of pollutants for June 2000. (a, c, e) top-down approach ship emission inventory (data from RETRO); (b, d, f) bottom-up approach ship emission inventory (modified after Porter, 2009).
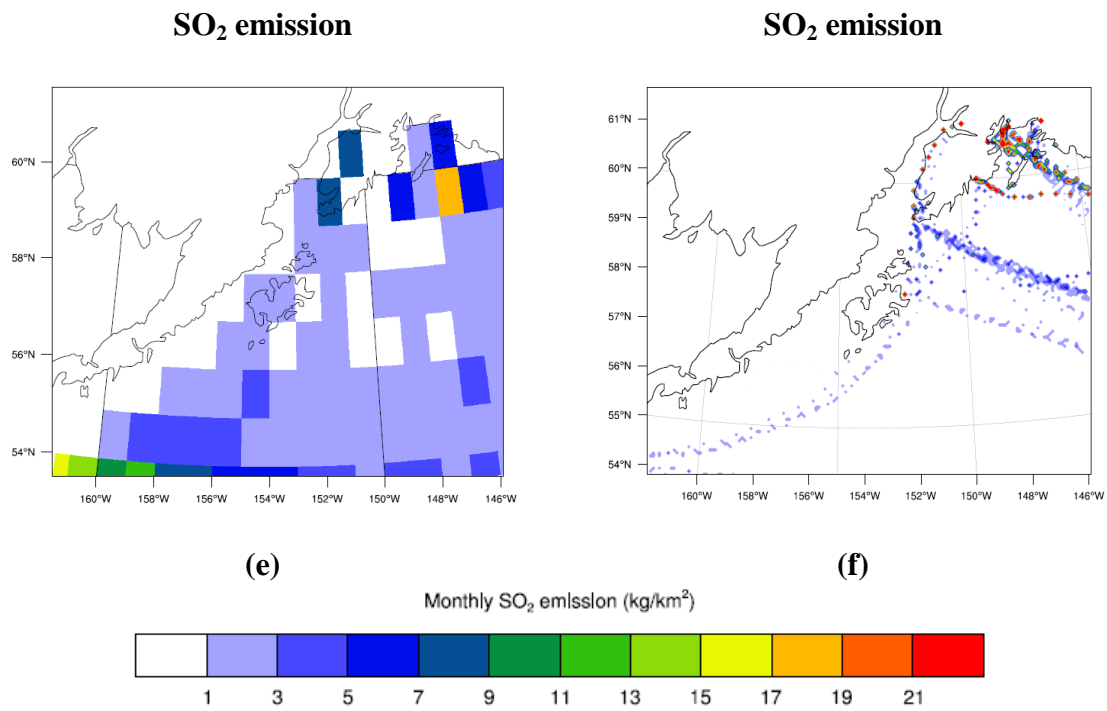
**SO₂ emission**

**SO₂ emission**



**(e)**

**(f)**

Monthly SO₂ emission (kg/km²)

Fig. 3.5 (Cont.)
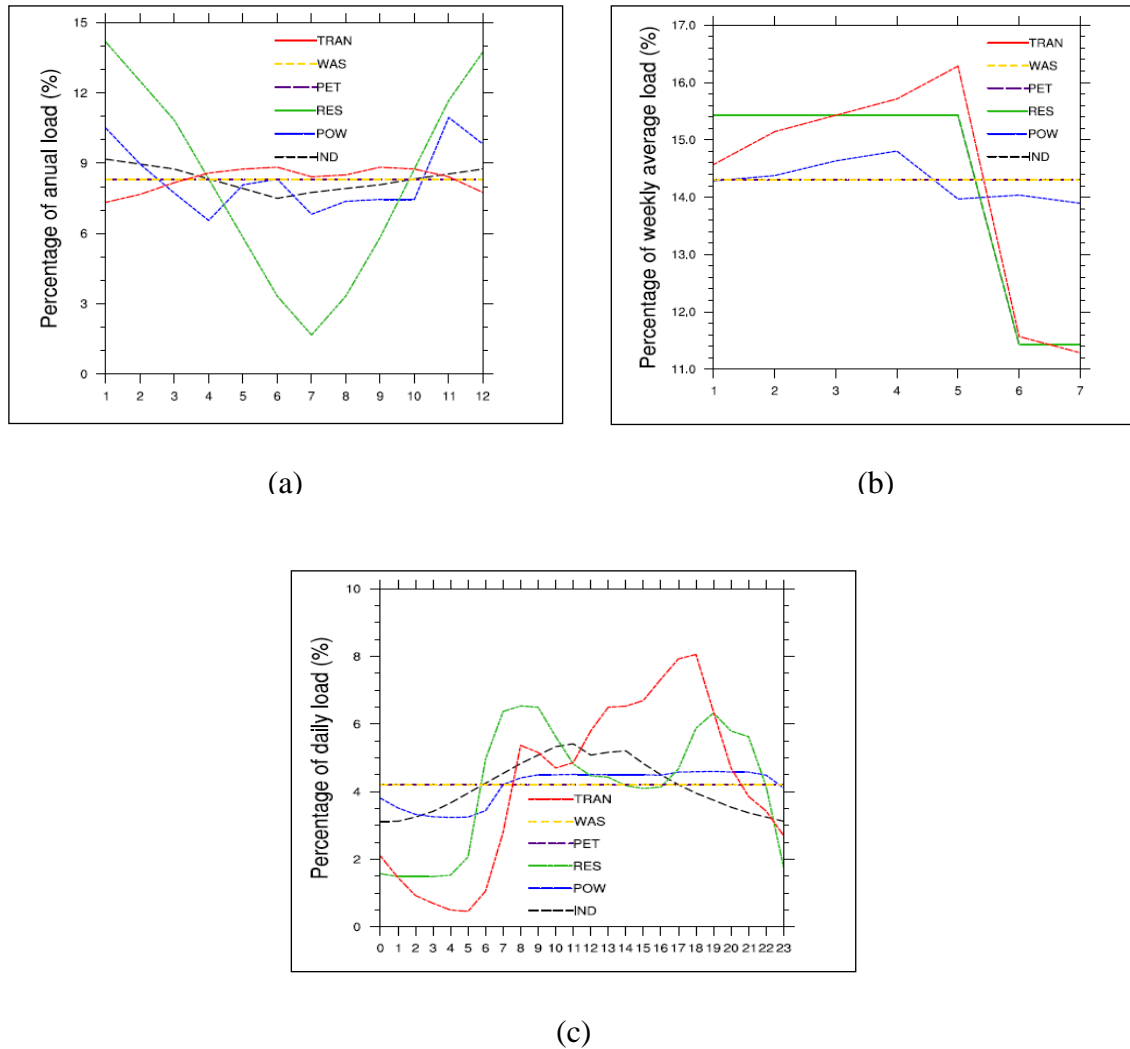
(a)

(b)



(c)

Fig. 3.6 Temporal variation of allocation functions for various anthropogenic sources: (a) monthly variation, (b) weekly variation, (c) hourly variation for each emission sector: road transportation (TRAN), waste treatment (WAS), petroleum production (PET), residential combustion (RES), power plant (POW) and industrial processes (IND) followed Veldt (1991) and Mölders (2009).
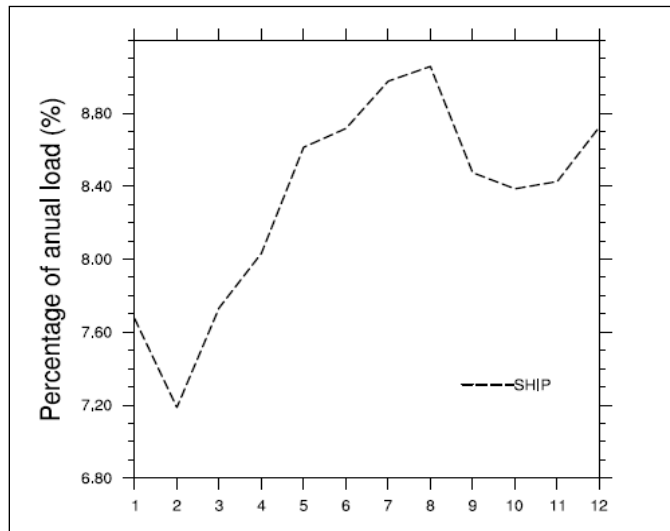
Fig. 3.7 Monthly variation of allocation functions of ship emission followed Wang et al. (2007).
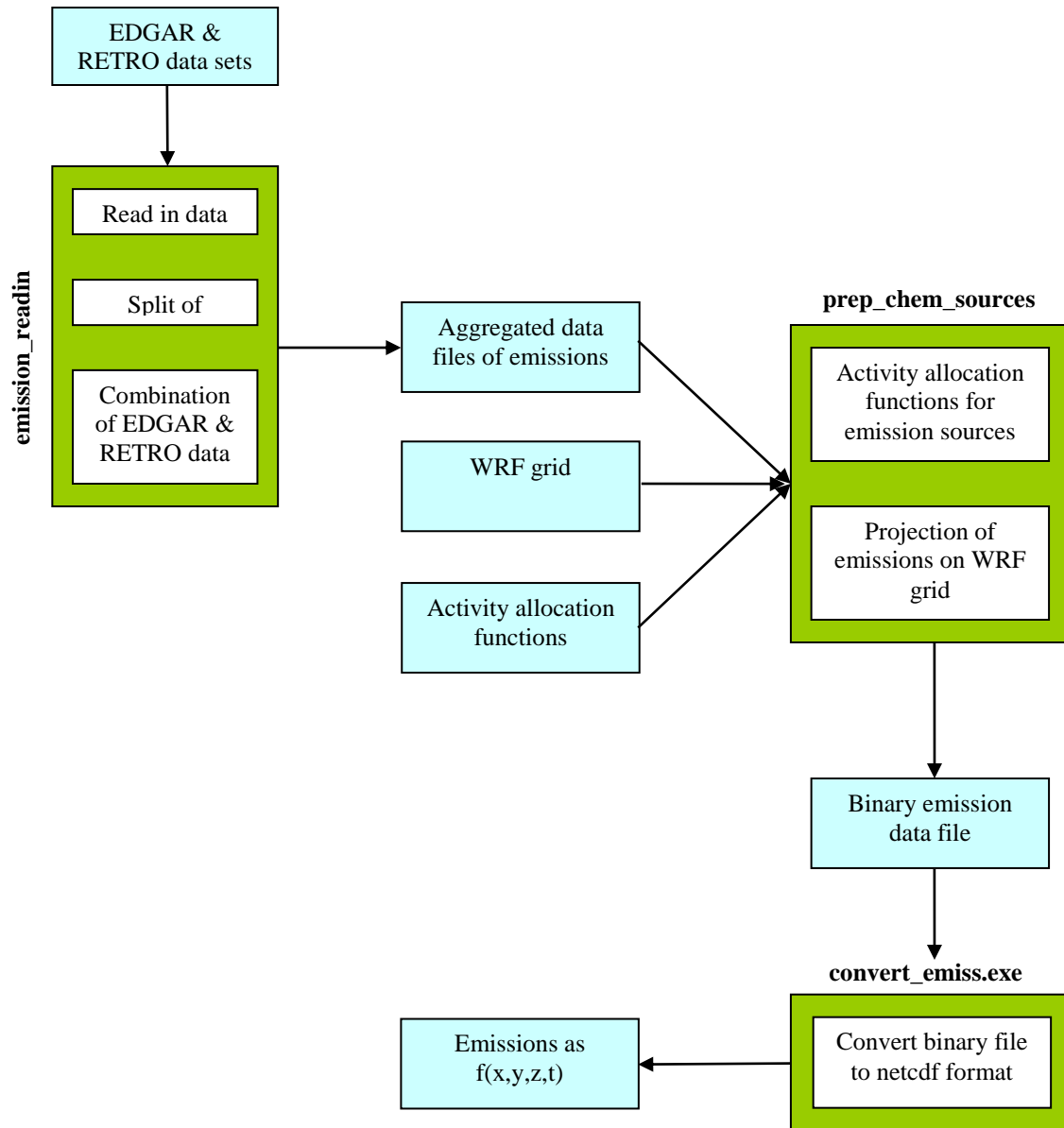
Fig. 3.8 Schematic view of emission data processing

**Chapter 4 Impacts of emission changes on sulfate aerosols in Alaska** [1]

**Abstract**

WRF-Chem simulations were performed using the meteorological conditions of January 2000 and alternatively the emissions between January 1990 and 2000 to examine whether increases in emissions may have caused the increasing trends in observed sulfate-aerosol concentrations at coastal Alaska sites. The analysis focused on six regions in Alaska that are exposed differently to the main emission sources. Meteorological observations at 59 sites and aerosol measurements at three sites showed that WRF-Chem model performed well to capture the meteorological situation over Alaska and simulated the aerosol concentrations acceptably. Generally, Alaska $SO_2$ and $SO_4^{2-}$-aerosol distributions are affected by long-range transport of $SO_2$ from ship emissions and/or emissions in Canada and southern Siberia except for the region adjacent to the Arctic Ocean that is influenced by local $SO_2$-emissions,. Local changes in emissions between 1990 and 2000 were not found to be the main cause for concentrations changes in the six regions. The increases of $SO_4^{2-}$-aerosols and $SO_4^{2-}$-in-cloud along the Gulf of Alaska are caused by increased ship or Canadian emissions. The study provides evidence that the increased ship and Canadian emissions during the last decades can cause increases in sulfate aerosols.

**4.1 Introduction**

The long-term observations of the Interagency Monitoring of Protected Visual Environment (IMPROVE) networks have shown notable increases in sulfate-aerosol concentrations at coastal sites of Alaska. On the contrary, decreases in concentrations were observed at the inland Denali National Park and Preserve site, located between the two largest Alaskan cities (Mölders et al., 2011a).

Sulfate aerosols are induced into the atmosphere via biological decay of dimethyl-sulphide (DMS) emitted from oceanic phytoplankton or oxidation of sulfur dioxide ($SO_2$) emitted in the gas phase from anthropogenic and natural sources (Seinfeld and Pandis, 2006). In Alaska, DMS-emissions and volcanic eruptions are natural sources of sulfate precursors in the atmosphere. The number of volcanic eruptions hardly changed in the last decades (Mölders et al., in 2011a) and DMS-emissions are negligibly small in Alaska coastal waters (Thomas et al., 2010). Anthropogenic emissions occur mainly in the only three cities across the state and due to oil production on the North Slope. Over the last few decades, various policies reduced emissions in many areas. In some regions of Alaska, however, emissions increased due to increased human activities. For instance, ship emissions on average increased since 1960 (Mölders et al., 2011a).

Recent studies on the sulfate-aerosol burden, long-range transport and the interactions between meteorological conditions and sulfate distributions have focused on mid-latitudes or the global scale. In the northeastern US, for instance, $SO_2$-emissions correlate linearly with downwind $SO_4^{2-}$-concentrations (van Dutkiewicz et al., 2000). The increases of $SO_2$-emissions from ships in the basin of southern California increased the $SO_4^{2-}$-concentrations in the coastal areas, and at some California inland locations due

to pollutant transport (Vutukuru and Dabdub, 2008). On the global scale, for instance, any change in precipitation, cloud cover or atmospheric circulation was found to alter the sulfate burden (Ackerley et al., 2009).

Transport of pollutants permits them to spread over large areas and affect pristine regions far remote from emission sources, even on an intercontinental scale. Long-range transport of $SO_2$, and $SO_4^{2-}$ from East Asia, for instance, contributes to the sulfur budget in Europe; the plume of $SO_2$ emitted in East Asia was advected across the North Pacific, North America and North Atlantic before reaching Europe (Fiedler et al., 2009). Analysis of satellite, aircraft, ground-based measurements over the North Pacific Ocean and western North America combined with chemical transport-model simulations indicated that 56% of the measured sulfate between 500 and 900 hPa over British Columbia has East-Asian sources (van Donkelaar et al., 2008). In north-american spring, anthropogenic sulfur emissions from East Asia increase the mean near-surface sulfate concentrations in western Canada by 30% and account for 50% of the overall regional sulfate burden between 1 and 5 km height. Empirical assessment of the frequency and intensity of dust transport from Asia to North America showed that the Asian aerosol plume contributes significantly to the aerosol loading at some high altitude sites across western North America (van Curen, 2003).

Since volcanic emissions remained constant (Mölders et al., 2011a), anthropogenic $SO_2$-emissions changed and ship emissions increased, local-emission changes and long-range transport may all be causes for the increasing sulfate-aerosol concentrations at Alaska coastal sites. This study focuses on examining the impacts of

emissions and their changes from 1990-2000 on sulfate gas and aerosols concentrations for six regions in Alaska.

## 4.2 Experimental design

### 4.2.1 Model description

The Weather Research and Forecasting model (WRF; Skamarock et al., 2008) was run inline with chemistry (WRF-Chem; Peckham et al., 2009) to examine the potential impacts of emission changes on sulfur components in Alaska. The model setup included: the cloud microphysical parameterization by Lin et al., (1983), Grell and Dévényi (2002) cumulus-ensemble scheme, the treatment of long-wave and shortwave radiation based on Mlawer et al. (1997) and Chou and Suarez (1994), respectively, Janjić's (2002) scheme for the viscous sub-layer and atmospheric boundary layer (ABL), the Mellor–Yamada–Janjić-scheme for describing the turbulence in the ABL and free atmosphere (Janjić, 2002), and the NOAH land-surface model (Chen and Dudhia, 2001).

The following well-tested setup for chemistry (McKeen et al., 2007; Mölders et al., 2010) was used, that allows interaction between cloud microphysics, radiation and chemistry. Gas-phase chemistry was considered by the Regional Acid Deposition Model version 2 (Stockwell et al., 1990). Photochemical reaction rates were calculated following Madronich's (1987) two-stream-method. The Modal Aerosol Dynamics Model for Europe (Ackermann et al., 1998) was used to predict the aerosol-size distributions, transport, nucleation, condensation, coagulation, dry deposition and chemical transformation processes including aqueous-phase reactions. The physical and chemical

properties of secondary organic aerosols including formation were simulated by the Secondary Organic Aerosol Model (Schell et al., 2001). Sulfates formed by oxidation of $SO_2$ in the gas phase and in the aqueous phase followed Stockwell et al. (1990) and Ackermann et al. (1998), respectively.

Dry deposition of pollutants followed Wesley (1989) with the modifications introduced by Mölders et al. (2011b). These modifications include the treatment of dry deposition over snow in accord with Zhang et al. (2003) and the lowering of the threshold at which stomata close. In Alaska, stomata of coniferous trees are still open at $-5\ ^{\circ}C$ (Mölders, 2011b).

The background concentrations were modified to represent the conditions over the North Pacific in accord with Mölders et al. (2011b).


**4.2.2 Emissions**

Biogenic emissions of isoprene, monoterpenes, and other volatile organic compounds from vegetation and nitrogen from soil based on temperature and photosynthetic active radiation were considered by the Model of Emissions of Gases and Aerosols from Nature (Guenther et al., 1994; Simpson et al., 1995).

The Emission Database for Global Atmospheric Research (EDGAR; http://www.mnp.nl/edgar/) data was used that comprises the annual anthropogenic emission inventories of carbon dioxide, methane, nitrous oxide, carbon monoxide, nitrogen oxide, and Non-Methane Volatile Organic Compounds on a $1^{\circ} \times 1^{\circ}$ grid. EDGAR provides international ship emissions, but no domestic ship emissions.

The Reanalysis of the Tropospheric (RETRO; http://retro.enes.org/data_emissions.shtml) chemical composition database provides both monthly international and domestic ship-emission inventories on a $1° \times 1°$ grid, but no anthropogenic $SO_2$-emissions. $SO_2$-emissions, however, are essential for the formation of sulfate aerosols. Therefore, the ship emissions of the EDGAR and RETRO data were merged. The EDGAR international ship emissions were used and assigned the RETRO ship-emission data to any grid-cell that has no EDGAR ship-emission data (Fig. 4.1). The emission data of EDGAR (anthropogenic and international ship emissions) and RETRO (domestic ship emission) are annual and uniform monthly totals, respectively. Thus, the same monthly, weekly and hourly allocation functions were used for the EDGAR and RETRO data. Allocation functions for anthropogenic emissions follow Mölders (2009) for Alaska, and Veldt (1991) else wise. For ship emissions, Wang et al.'s (2007) monthly allocation functions were used for shipping in North America. Since the assumption of uniform ship-emission rates serves well in the absence of high-temporal resolution emission datasets (Vutukuru and Dabdub, 2008), uniform profiles for weekday/weekend and hourly variations were used. For a comparison of RETRO and EDGAR data see Butler et al. (2008).

### 4.2.3 Simulations

The model domain was centered at 59°N, 179°E with 30 km spacing, $240 \times 120$ grid points in the horizontal and 28 in the vertical direction (Fig. 4.2). The thickness of vertical layers increases with height. The National Center for Atmospheric Research and National Centers for Environmental Prediction $1° \times 1°$, 6 h, global final analysis data (FNL) were used as initial and boundary conditions for the meteorological quantities. The meteorology was initialized every five days.

The chemical fields were initialized using idealized profiles of background concentrations for the first day of the simulation. All following simulations were initialized with the chemical distributions obtained at the end of the previous simulation.

WRF-Chem simulations were performed alternatively with the emission data of 2000 (REF) and 1990 (HIST) for January 1–31. The simulations are called REF and HIST hereafter. The first ten days as were discarded spin-up time for the chemical fields and used the rest of the simulation in the analysis. In both simulations, the model was run using the FNL-data of 2000 as initial and boundary conditions. This procedure ensures that differences are only in response to the emission changes.

### 4.2.4 Analysis

This study focuses on analyzing the distribution of sulfur components and changes therein over Alaska. Alaska was divided into six regions indicated as R1–R6 (Fig. 4.2). These regions differ with respect to their position to the main wind-direction (Fig. 4.3), their topography and climate. According to the Köppen–Geiger climate

classification updated by Kottek et al. (2006), R3 and R5 have mid-latitude oceanic climate in the southern parts and sub-Arctic oceanic climate in the northern parts with humid weather and mild winters. The climate of R2, R4 and R6 is sub-Arctic with dry and severe winters. R1 has an arid Arctic climate with extremely cold, dry winters. Complex mountainous terrain exists in R4, R5 and R6 (Interior Alaska), while R1, R2, and R3 have relatively flat terrain. Simulated average wind-speed varies from 6 to 11 m s$^{-1}$ for our episode. Average wind-speed is stronger in R3, R4, and R5 (11, 10, 8 m s$^{-1}$) than R1, R2, and R6 (6, 7, 7 m s$^{-1}$).

An evaluation was conducted for Alaska for January 2000 by comparing the simulated results with hourly observations of temperature, dew-point temperature, wind-speed and direction, and sea-level pressure (SLP) that are available at 59 sites (Fig. 4.2). For January 2000, sulfate observations are available at Denali Park and Poker Flat from the Clean Air Status and Trends Network (CASTNET) campaign and at Denali Park headquarters from the IMPROVE network. CASTNET provided weekly average concentration, while IMPROVE provided daily averages every third day.

Performance skill-score were calculated (bias, root-mean-square-error [RMSE], standard deviation of error [SDE] and correlation skill-score [R]) to evaluate the simulated meteorology. Fractional bias (FB), normalized mean-square-error (NMSE), correlation skill-score and fraction within a factor of two (FAC2) were calculated to evaluate model performance with respect to chemistry.

Multi-correlation coefficients of regional average concentrations of $SO_2$ or $SO_4^{2-}$-aerosols versus $SO_2$-emission or wind-speed at each grid-cell were calculated at various

time-lags for R1–R6 to investigate the role of emissions and meteorological conditions for the distributions of pollutants in Alaska.

Hourly average concentration differences (REF-HIST) of sulfur compounds were examined to assess the impacts of emission changes on $SO_2$ and $SO_4^{2-}$ in the gas phase, and $SO_4^{2-}$-aerosol and in-clouds. The discussion focuses on R1–R6, but results for other regions are discussed where required to explain the situation in the six regions. Student's t-tests were performed to assess the agreement between model and observed data, and to test the hypothesis that the changes in Asian, Canadian and ship emissions can cause changes as seen for January by the IMPROVE network. A confidence level of 95% was used from the t-tests.

The horizontal advection of $SO_2$, $SO_4^{2-}$-aerosol and $SO_4^{2-}$-in-cloud were calculated across the boundaries of each of the six regions in and out of the regions. The advection was determined for the entire atmospheric column of each region. No vertical transport exists at the top of the model.

## 4.3 Results

### 4.3.1 Evaluation

On average over Alaska, WRF-Chem overestimates air temperature (T), dew-point temperature ($T_d$) and wind-speed by 0.4 K, 0.4 K, and 4.3 m s$^{-1}$, respectively, while it slightly underestimates SLP by 2 hPa (Table 4.1). The discrepancies in T and $T_d$ are strongest after the passage of the cold fronts on January 13 and 16 (Fig. 4.4a, b, d). The

temporal evolutions of T, $T_d$, and SLP are captured acceptably to well leading to correlation skill-scores of 0.638, 0.654, and 0.922, respectively.

According to the hourly mean values of simulated and observed wind-direction, the main wind-direction for Alaska for 11 to 31 January 2000 was south-southeast. WRF-Chem captures successfully the overall wind-direction with a bias of 3°. However, WRF-Chem fails to capture the temporal behavior of wind-direction changes to their full extend.

Despite an evaluation at only three sites is limited, it is included for completeness. On average, WRF-Chem underestimates the sulfate concentrations at the Denali Park IMPROVE and Poker Flat sites, and overestimates them at the Denali Park CASTNET site; WRF/Chem overestimates $SO_2$ at both $SO_2$-sites (Fig. 4.5, Table 4.2). In Denali Park, 40% and 17% of the simulated concentrations fall within a factor of two for the CASTNET and IMPROVE observations, respectively. This different performance relates to the sites' locations. The IMPROVE site is close to a road that channels through the mountains and passes a small community (i.e. Healy) with a power plant, while the CASTNET site is in the park far away from any anthropogenic emission sources. WRF-Chem fails to capture the channeling of the dispersion plume from Healy to the monitoring site because channeling through mountains is of subgrid-scale like in other mesoscale models.

WRF-Chem captures well the temporal evolution of $SO_2$ for Poker Flat ($R = 0.800$). Simulated and observed $SO_2$ and sulfate concentrations agree within a factor of two in 50 and 75% of the time (Table 4.2).

**4.3.2 Description of the situation**

Ship traffic, the industrial centers in China and Japan, oil production, and Canadian emissions are the major contributors to $SO_2$-emissions in the domain (Fig. 4.6a). The hourly average $SO_2$-emissions in R1–R6 are 0.063, 0.002, 0.052, 0.040, 0.050 and 0.003 mol $km^{-2}$/h, respectively. Oil production in R1 causes this region to have the highest emissions in Alaska.

The ABL heights in R1–R6 are 682, 686, 1145, 1009, 1102 and 856 m, respectively. The potential temperature profiles indicate mostly stable conditions in the ABL of all six regions during the episode (Fig. 4.7). The same is true for the ABL of the adjacent Canada, Bering Sea, Siberia, and Gulf of Alaska.

$SO_4^{2-}$ gas-phase concentrations range from 0 to $6 \times 10^{-4}$ ppb and are low compared with other species, because the gas-phase oxidation of $SO_2$ to $SO_4^{2-}$ ($SO_2 + OH^-$) occurs during daylight at low rates ($\sim$1% $h^{-1}$; Newman, 1981). Despite actinic fluxes and photolysis-frequencies can have uncertainty of up to 50% at low insolation (Ruggaber et al., 1993), it can be assumed the impact of this error on the results to be small because gas-phase $SO_2$-oxidation rates and OH-radical concentrations available as precursors are low. In January, insolation is almost zero in northern Alaska (R1), 4–5 h in Interior Alaska (R6) and the west coast of Alaska (R2), about 5–7 h in the Aleutian (R3, R4) and the Panhandle (R5), and about 10 h in the mid-latitude region of the domain (http://www.absak.com/library/average-annual-insolation-alaska). Therefore, aqueous-phase oxidation of $SO_2$ to sulfates in-cloud droplets is the major reaction path. Advection in and out of Alaska is high below 4 km, which corresponds to the first 12

WRF-Chem layers above ground (Fig. 4.8). The highest advection occurs between layer 4 and 6 around 1 km above the ground, i.e. around the top of the ABL. The overestimated wind-speed by WRF-Chem may lead to transport of pollutants occuring too fast compared to observations, with consequences for chemical transformations at some places. However, since we discuss differences and use the same meteorology the impact on our overall conclusions can be negligible.

The pattern of $SO_2$-concentrations is quite similar with the local $SO_2$-emission pattern (Fig. 4.6a, b). Local emissions affect the $SO_2$-concentrations where $SO_2$-emissions are high (e.g. along the international shipping lane, in Japan, the northeast of China, the Northwest Territories, at Prudhoe Bay in R1). Here, $SO_2$-concentrations are relatively high as compared with other areas in the domain. Within Alaska, R1 has the highest $SO_2$-emissions and regional average concentrations (0.07 ppb). Regional average $SO_2$-concentrations amount 0.03, 0.02, 0.03, 0.05 and 0.02 ppb for R2–R6, respectively. In all six regions, $SO_2$-concentrations correlate statistically significantly with near-surface air temperatures ($-0.76 < R < -0.54$). Low $SO_2$-concentrations occur at high temperature and vice versa reflecting the temperature dependency of the oxidation reactions that are sinks for $SO_2$. In R1 and R2, $SO_2$-concentrations are not affected by long-range transport from the major shipping lanes in the Pacific Ocean and/or Asia ($R < 0.5$; Fig. 4.9). The notable amounts of $SO_2$ originate from emissions in adjacent areas (Fig. 4.8). The highest net inflow (advection in minus advection out) in R2 (Fig. 4.8a, g) yields relatively high $SO_2$-concentrations in R2, although R2 has the lowest $SO_2$-emissions. Relatively high correlations ($R > 0.6$) between $SO_2$-concentrations in R3–R6 and ship emissions in the

Bering Sea, along the Panhandle and international shipping lane and anthropogenic emissions in southern Siberia and Canada indicate long-range transport of $SO_2$ from these regions to R3–R6. The 21-day accumulated $SO_2$-advection in (out) of R3–R6 are 0.838 (0.735), 0.568 (0.315), 0.812 (0.407) and 0.461 (0.354) ppm, respectively. $SO_2$-advection is lowest in R6. The $SO_2$-emissions influence the local $SO_4^{2-}$-aerosol concentrations less than the $SO_2$ gas-phase concentrations as the different pattern of concentrations and emission evidence (Fig. 4.6a, c). Because the lifetime of sulfate aerosols in the atmosphere exceeds that of $SO_2$, transport processes affect the distribution of sulfate aerosols stronger than that of $SO_2$. In general, the regional averaged hourly concentrations of sulfur components remain relatively constant with time. For $SO_2$, emissions and chemical transformations to sulfate dominate the change of $SO_2$ in all regions rather than transport of $SO_2$ since the magnitudes of hourly regional average emissions and chemical transformations (thousands $ppb\,h^{-1}$) are much higher than the magnitude of the $SO_2$-transport (few $ppb\,h^{-1}$). $SO_2$-emissions (source) and chemical transformations ($SO_2$ loss) almost balance keeping the concentrations nearly unchanged. However, transport of sulfate aerosol and sulfate-in-cloud are important sources of sulfate content. Wet deposition is negligibly small as the regional daily averages are less than $1\,mm\,day^{-1}$ during 11–31 January. Neither the EDGAR nor RETRO inventory has data on primary sulfate emissions for which they were not considered in this study. Thus, absolute sulfate-transport is of same order of magnitude as the sulfate chemical transformations.

In R3, R4 and R5, winds from south-southwest dominated (Fig. 4.3), i.e. from regions with shipping lanes. Sulfate aerosol and its precursors are advected from these regions of high ship emissions. Therefore, $SO_4^{2-}$-aerosol concentrations (39, 24, 31 ng kg$^{-1}$ for R3, R4, R5) are higher in the coastal regions adjacent to the Gulf of Alaska than in R2 (18 ng kg$^{-1}$), and R6 (16 ng kg$^{-1}$). In R3, which is closest to the major shipping lanes, the $SO_4^{2-}$-aerosol concentrations are highest. In R2 and R6, winds from southeast and south-southeast, respectively, dominated, i.e. from regions with low $SO_2$-emissions. Therefore, R2, and R6 have lower $SO_4^{2-}$-aerosol concentrations than R3–R5. The relatively high $SO_4^{2-}$-aerosol concentrations of R1 (24 ng kg$^{-1}$) are due to high local $SO_2$-emissions or emissions transported from the offshore oil fields at the coast. Multi-correlation analysis (Fig. 4.10) shows that in R2–R6, $SO_4^{2-}$-aerosol concentrations at breathing level are related to $SO_2$ from domestic ship emissions in the Bering Sea, along the Panhandle, the international shipping lanes in the Pacific Ocean and/or anthropogenic emissions in Canada ($R > 0.6$). The high correlations in the 1 d or 2 d-time-lag indicate that $SO_2$ from emissions outside the regions has more time to be transformed into sulfate before arriving in Alaska. The long transport times of the 1 d or 2 d-time-lag imply time for chemical reactions that is not available in the 0 d-time-lag. In R1, long-range transport does not affect $SO_4^{2-}$-aerosol concentrations ($R < 0.5$ at various time-lags; therefore not shown). Advection into (out) R2, R3 and R5 are high (low). Thus, the net advection increases the $SO_4^{2-}$-aerosol concentration in R2, R3 and R5. On the contrary, advection out of R1 is higher than advection into R1. Advection into and out are relatively equal for

both R4 and R6. Note that R6 experiences the lowest advection of the six regions (Fig. 4.8b, h).

Sulfate-in-cloud concentrations (Fig. 4.6d) are high along the major shipping lanes where clouds are present. The hourly regional average $SO_4^{2-}$-in-cloud concentrations in the regions along the Gulf of Alaska, R3–R5, are 0.48, 0.30, 0.31 ng kg$^{-1}$, respectively. They exceed those of the inland region R6 (0.03 ng kg$^{-1}$) and the coastal regions R1 (0.02 ng kg$^{-1}$) and R2 (0.04 ng kg$^{-1}$) that are far away from high ship traffic. Advection of $SO_4^{2-}$-in-cloud in/out of the region is higher for R3, R4 and R5 than for R1, R2 and R6 (Fig. 4.8c, i).

Since the aqueous-phase oxidation reactions of $SO_2$ to sulfate occur in cloud droplets, cloud-water content affects sulfate production. The hourly regional vertically-averaged cloud-water content is $0.045 \times 10^{-6}$, $0.603 \times 10^{-6}$, $2.140 \times 10^{-6}$, $1.679 \times 10^{-6}$, $2.099 \times 10^{-6}$, $0.302 \times 10^{-6}$ g m$^{-3}$, respectively. Therefore, aqueous-phase oxidation reactions become more effective in R3, R4 and R5 than in R1, R2 and R6.

### 4.3.3 Effects of emission changes

Compared with 1990, the $SO_2$-emissions of 2000 increased in most of the domain, especially along the shipping lanes, in Japan, northeast China and in some areas in Canada (Fig. 4.12a). Wide areas of Alaska experienced no emission changes. On regional average, accumulated anthropogenic emissions increased by 387.9, 12.8, and 1.7 mol km$^{-2}$ in R1, R5, R6, while they decreased by 1.7, 0.5, and 4.1 mol km$^{-2}$ in R2, R3, and R4, respectively. R1 experienced the highest increase in $SO_2$-emissions due to

the growth of the oil industry in the 90s. The emissions of R2–R4 decreased due to pollution-control policies implemented between 1990 and 2000.

The correlation coefficients between emission changes and concentration changes of all sulfur components in the six regions are approximately zero and insignificant. This indicates that local-emission changes are not the main cause for the concentration changes in the six regions.

In R1, $SO_2$-emissions increased approximately five times whereas the accumulated regional average of $SO_2$-concentrations only increased by 1.5, i.e. the increased local emissions contributed not only to $SO_2$-increase inside, but also outside the region. In R2, $SO_2$-emissions decreased about 1.5 times, but the $SO_2$-concentrations remained almost constant between REF and HIST. The advection of $SO_2$ into R2 compensates for the decreases in emissions. In R5 and R6, emissions increased 1.5 and 13 times, respectively, while the $SO_2$-concentrations remained almost constant. Hence, the increased local emissions in R5 and R6 affect the $SO_2$-distributions outside these regions. The significantly increased emissions from international shipping increased the $SO_2$-concentrations significantly along the international shipping lanes (Fig. 4.12b) and affect the concentrations of pollutants in Alaska through being advected by cyclones.

$SO_4^{2-}$-aerosols increase notably along the Panhandle (R5). The $SO_4^{2-}$-aerosols increase slightly in R1, and increase significantly over the northeastern Pacific around 150°W, because of the increased emissions from international shipping (Fig. 4.12c). In R5, the regional average accumulated $SO_4^{2-}$-aerosol concentration is about 550 ng kg$^{-1}$ higher for REF than HIST. R5 is affected by winds from the south-southwest to

east-southeast (Fig. 4.3) that advect pollutants from increased ship and Canadian emissions. The significant increases of ship emissions, especially from international shipping, increased the $SO_4^{2-}$-aerosol concentrations in the Pacific Ocean south of 50°N. Decreases in $SO_4^{2-}$-aerosols concentrations occur over most of the Bering Sea, the Sea of Okhotsk and Chukchi Sea that have almost unchanged ship emissions.

The accumulated $SO_4^{2-}$-in-cloud concentrations increase about 9, 44 and 1 ng kg$^{-1}$ in R1, R5, R6, where $SO_2$-emissions increased; they decrease about 3, 7 ng kg$^{-1}$ in R2, R4, where $SO_2$-emission decreased. The $SO_4^{2-}$-in-cloud concentrations increased about 15 ng kg$^{-1}$ in R3 despite decreased $SO_2$-emissions. In R3, the increased $SO_4^{2-}$-in-cloud concentrations result from advection of polluted air with increased $SO_2$ and/or $SO_4^{2-}$-aerosol concentrations stemming from increased international ship emissions.

Since the same meteorology was used for REF and HIST, the general pollution-distribution patterns of HIST and REF are quite similar. The multi-correlation analysis at various time-lags showed the same features for REF and HIST in all regions. Consequently, the regions identified in REF as main source regions for pollution are again the main source regions in HIST. However, in all six regions, the changed emissions altered the absolute concentrations. Since long-range transport hardly affects concentrations in R1, the local-emission changes govern the concentration changes in R1. On the contrary, domestic and international shipping emissions and emissions in Canada and the changes therein affect R2–R6. Since R3–R5 are downwind of ship emissions, these regions experience advection of stronger polluted air. Therefore, concentrations of sulfate aerosols are higher in the REF than HIST simulations. The profiles for HIST show

the same behavior as for REF with highest advection around the top of the ABL except for marginal ($<3\%$) changes in magnitude of 21-day accumulated amounts of advected pollutants.

Despite the fact that REF and HIST used the same meteorological initial and boundary conditions, the cloud-water mixing ratio ($q_c$), air temperature and wind-speed marginally differ due to interaction between chemistry and physics (Fig. 4.13). The changes in $SO_4^{2-}$-aerosol concentrations alter cloud properties, and modify temperature via radiative and thermal effects. Changes in wind-speed result as secondary changes from altered interaction between cloud microphysics and meteorological dynamics. The highest temperature changes (up to $\pm1$ K) occur in R3 and R6. In R2, R3 and R4, wind-speed changes up to $\pm1$ m s$^{-1}$ and exceeds the changes in R1, R5 and R6 (up to $\pm0.6$ m s$^{-1}$). In R3, R4, and R5, cloud-water mixing ratios change up to $\pm0.006$ g kg$^{-1}$, where the changes of $SO_4^{2-}$-in-cloud concentrations are high. In R1, R2 and R6, changes of $SO_4^{2-}$-in-cloud concentrations are smaller than those in R3–R5.

## 4.4 Conclusions

WRF-Chem simulations were performed fixing the meteorological initial and boundary conditions to January 2000, but alternatively the emissions of 2000 (REF) and 1990 (HIST) to investigate whether emission changes may be the cause for the observed changes in $SO_2$ and $SO_4^{2-}$-aerosol concentrations in Alaska. The analysis focused on the sulfur compounds in six regions of Alaska (Fig. 4.3) that differ from each other with respect to their position to the main wind-direction, their topography and climate.

WRF-Chem performs well to capture the temporal evolution of the meteorological situation in Alaska. Here WRF-Chem, on average, overestimates temperature, dew-point temperature and wind-speed, while it slightly underestimates SLP. The few available observations of $SO_2$ and sulfate aerosols suggest that WRF-Chem underestimates $SO_2$-concentrations and overestimates $SO_4^{2-}$-aerosol concentrations. Model performance is worst where WRF-Chem fails to capture the dispersion of pollutants in extremely complex mountainous terrain. WRF-Chem simulates the $SO_2$ and sulfate concentrations at Poker Flat with good accuracy, where 50 and 75% of the simulated data being within a factor of two of the observations.

In all six regions, $SO_2$-concentrations are strongly, negatively correlated with temperature due to the temperature-dependent oxidation reactions that are the sinks for $SO_2$. In R1, local $SO_2$-emissions govern the $SO_2$-concentrations. Here and in R2, long-range transport does not affect the $SO_2$-concentrations. In the other regions, $SO_2$-distributions are associated with advection from the shipping lanes or Canada. Due to the longer lifetime than $SO_2$, $SO_4^{2-}$-aerosols are less sensitive to local emissions than to long-range transport. Being downwind of the shipping lanes and the Canadian emissions, R3, R4 and R5 have higher $SO_4^{2-}$-aerosol and $SO_4^{2-}$-in-cloud concentrations than R1, R2 and R6. In R2–R6, $SO_4^{2-}$-aerosols are associated with emissions from domestic and international shipping or Canada.

The analysis showed that local-emission changes between 1990 and 2000 are not the main cause for the observed concentration changes in Alaska. The significantly increased emissions from international shipping significantly increased the $SO_2$-

concentrations along the shipping lanes. The notable increase of $SO_4^{2-}$-aerosol concentrations in R5 results from advection of stronger polluted air from the international shipping lanes and Canada where the emissions increased between 1990 and 2000. In R3, the increase of $SO_4^{2-}$-in-cloud concentrations stems from advection of air with increased $SO_2$ and/or $SO_4^{2-}$-aerosol concentrations from the shipping lanes.

The changes in $SO_4^{2-}$-aerosol concentrations in response to the emission changes caused marginal, insignificant changes in the meteorological conditions between REF and HIST via radiative, thermal and cloud microphysical effects. This means that the altered emissions hardly affect meteorological conditions. In conclusion, the increasing trends in sulfate aerosols observed at some Alaska monitoring sites can be explained by the changes in ship emissions and emissions in Canada during the last decades.

## Acknowledgments

# References

Ackerley, D., Highwood, E.J., Frame, D.J., Booth, B.B.B., 2009. Changes in the global sulfate burden due to perturbations in global CO2 concentrations. Amer. Meteor. Soc., 22, 5421-5432.

Ackermann, I.J., Hass, H., Memmesheimer, M., Ebel, A., Binkowski, F.S., Shankar, U., 1998. Modal aerosol dynamics model for Europe: development and first applications. Atmos. Environ., 32, 2981-2999.

Butler, T.M., Lawrence, M.G., Gurjar, B.R., van Aardenne, J., Schultz, M., Lelieveld, J., 2008. The representation of emissions from megacities in global emission inventories. Atmos. Environ., 42, 703-719.

Chen, F., Dudhia, J., 2001. Coupling an advanced land-surface/hydrology model with the Penn State/NCAR MM5 modeling system. Part I: model description and implementation. Mon. Wea. Rev., 129, 569-585.

Chou, M.-D., Suarez, M.J., 1994. An efficient thermal infrared radiation parameterization for use in General Circulation Models, NASA Tech. Memo., 104606, 85p.

Fiedler, V., Arnold, F., Schlager, H., Dornbrack, A., Pirjola, L., Stohl, A., 2009. East Asian $SO_2$ pollution plume over Europe - part 2: evolution and potential impact. Atmos. Chem. Phys., 9, 4729-4745.

Grell, G.A., Dévényi, D., 2002. A generalized approach to parameterizing convection combining ensemble and data assimilation techniques. Geophys. Res. Lett., 29, 1693. doi:10.1029/2002GL015311.

Guenther, A., Hewitt, C., Erickson, D., Fall, R., Geron, C., Graedel, T., Harley, P., Klinger, L., Lerdau, M., McKay,W., Pierce, T., Zimmerman, P.R.,1994. A global model of natural volatile organic compound emissions. J. Geophys. Res., 100D, 8873-8892.

Janjić, Z.I., 2002. Nonsingular implementation of the MelloreYamada level 2.5 scheme in the NCEP Meso Model. NCEP Office Note, 437, 61p.

Kottek, M.,Grieser, J.,Beck,C.,Rudolf,B.,Rubel, F.,2006.World map of the Köppen-Geiger climate classification updated. Meteorol. Z., 15, 259-263.

Lin, Y.-L., Rarley, R.D., Orville, H.D., 1983. Bulk parameterization of the snow field in a cloud model. J. Appl. Meteor., 22, 1065-1092.

Madronich, S., 1987. Photodissociation in the atmosphere, 1, actinic flux and the effects of ground reflections and clouds. J. Geophys. Res., 92, 9740-9752.

McKeen, S.A., Chung, S.H., Wilczak, J., Grell, G.A., Djalalova, I., Peckham, S., Gong, W.,Bouchet, V., Moffet, R., Tang, Y., Carmichael, G.R., Mathur, R., Yu, S., 2007. The evaluation of several PM$_{2.5}$ forecastmodels using data collected during the ICARTT/NEAQS 2004 field study. J. Geophys. Res., 112, D10S20. doi:10.1029/2006JD007608.

Mlawer, E.J., Taubman, S.J., Brown, P.D., Iacono, M.J., Clough, S.A., 1997. Radiative transfer for inhomogeneous atmospheres: RRTM, a validated correlated-k model for the longwave. J. Geophys. Res., 102D, 16663-16682.

Mölders, N., Porter, S.E., Cahill, C.F., Grell, G.A., 2010. Influence of ship emissions on air quality and input of contaminants in southern Alaska National Parks and wilderness areas during the 2006 tourist season. Atmos. Environ., 44, 1400-1413.

Mölders, N., Porter, S.E., Tran, T.T., Cahill, C.F., Mathis, J., Newby, G.B., 2011a. The effect of unregulated ship emissions for aerosol and sulfur-dioxide concentrations in southwestern Alaska. In: Criddle, K., Eicken, H., Lovecraft, A., Metzger, A. (Eds.), North by 2020: Perspectives on a Changing North. Alaska University Press, Fairbanks, 14p.

Mölders, N., Tran, H.N.Q., Quinn, P., Sassen, K., Shaw, G.E, Kramm, G., 2011b. Assessment of WRF/Chem to capture sub-Arctic boundary layer characteristics during low solar irradiation using radiosonde, SODAR, and station data. Atmos. Poll. Res., 2, 283-299.

Mölders, N., 2009. Alaska Emission Model (AkEM) Description Internal Report, Fairbanks, 10p.

Newman, L., 1981. Atmospheric oxidation of sulfur dioxide: a review as viewed from power plant and smelter plume studies. Atmos. Environ., 15, 2231-2239.

Peckham, S.E., Fast, J.D., Schmitz, R., Grell, G.A., Gustafson, W.I., McKeen, S.A., Ghan, S.J., Zaveri, R., Easter, R.C., Barnard, J., Chapman, E., Salzmann, M., Wiedinmyer, C., Freitas, S.R., 2009. WRF/Chem Version 3.1 User's Guide, 78p.

Ruggaber, A., Forkel, R., Dlugi, R., 1993. Spectral actinic flux and its ratio to spectral irradiance by radiation transfer calculations. J. Geophys. Res., 98, 1151-1162.

Schell, B., Ackermann, I.J., Hass, H., Binkowski, F.S., Ebel, A., 2001. Modeling the formation of secondary organic aerosol within a comprehensive air quality model system. J. Geophys. Res., 106, 28275-28293.

Seinfeld, J.H., Pandis, S.N., 2006. Atmospheric chemistry and physics − From air pollution to climate change (2nd edition). John Wiley & Sons.

Simpson, D., Guenther, A., Hewitt, C.N., Steinbrecher, R., 1995. Biogenic emissions in Europe 1. Estimates and uncertainties. J. Geophys. Res., 100D, 22875-22890.

Skamarock, W.C., Klemp, J.B., Dudhia, J., Gill, D.O., Barker, D.M., Duda, M.G., Huang, X.-Y., Wang, W., Powers, J.G., 2008. A description of the Advanced Research WRF Version 3, NCAR/TN, 125p.

Stockwell, W.R., Middleton, P., Chang, J.S., Tang, X., 1990. The second-generation regional acid deposition model chemical mechanism for regional air quality modeling. J. Geophys. Res., 95, 16343-16367.

Thomas, M.A., Suntharalingam, P., Pozzoli, L., Rast, S., Devasthale, A., Kloster, S., Feichter, J., Lenton, T.M., 2010. Quantification of DMS aerosolecloudeclimate interactions using ECHAM5-HAMMOZ model in current climate scenario. Atmos. Chem. Phys., 10, 3087-3127.

van Curen, R.A., 2003. Asian aerosols in North America: extracting the chemical composition and mass concentration of the Asian continental aerosol plume from long-term aerosol records in the western United States. J. Geophys. Res., 108, 4623-4639.

van Donkelaar, A., Martin, R.V., Leaitch, W.R., Macdonald, A.M., Walker, T.W., Streets, D.G., Zhang, Q., Dunlea, E.J., Jimenez, J.L., Dibb, J.E., Huey, L.G., Weber, R., Andreae, N.O., 2008. Analysis of aircraft and satellite measurements from the Intercontinental Chemical Transport Experiment (INTEX-B) to quantify long-range transport of East Asian sulfur to Canada. Atmos. Chem. Phys., 8, 2999-3014.

van Dutkiewicz, V.A., Das, M., Husain, L., 2000. The relationship between regional $SO_2$ emissions and downwind aerosol sulfate concentrations in the northeastern US. Atmos. Environ., 34, 1821-1832.

Veldt, C., 1991. Emissions of SOx, NOx, VOC and CO from East European countries. Atmos. Environ., 25A, 2683-2700.

Vutukuru, S., Dabdub, D., 2008. Modeling the effects of ship emissions on coastal air quality: a case study of southern California. Atmos. Environ., 42, 3751-3764.

Wang, C., Firestone, J., Corbett, J.J., 2007. Modeling energy use and emissions from North American shipping: application of the ship traffic, energy, and environment model. Environ. Sci. Technol., 41, 3226-3232.

Wesely, M.L., 1989. Parameterization of surface resistances to gaseous dry deposition in regional-scale numerical models. Atmos. Environ., 23, 1293-1304.

Zhang, L., Brook, J.R., Vet, R., 2003. A revised parameterization for gaseous dry deposition in air-quality models. Atmos. Chem. Phys., 3, 2067-2082.

Table 4.1 Mean and standard deviation, root-mean-square error (RMSE), standard deviation of error (SDE), bias and correlation (R) for hourly averaged sea-level pressure (SLP), temperature (T), dew-point temperature ($T_d$), wind-speed (v) and direction (dir)

| Quantity | Simulated | Observed | RMSE | SDE | Bias | R |
|---|---|---|---|---|---|---|
| SLP (hPa) | 1005 ± 16 | 1007 ± 14 | 7.4 | 7.2 | -2 | 0.922 |
| T ($^o$C) | -13.5 ± 9.9 | -13.9 ± 15 | 11.6 | 11.5 | 0.4 | 0.638 |
| $T_d$ ($^o$C) | -15.9 ± 10.6 | -16.3 ± 15.7 | 11.4 | 11.9 | 0.4 | 0.654 |
| v (m s$^{-1}$) | 6.0 ± 3.5 | 1.7 ± 2.6 | 5.7 | 3.7 | 4.3 | 0.295 |
| dir ($^o$) | 156±86 | 153±98 | 118.6 | 119.3 | -3 | 0.166 |

Table 4.2 Fractional bias (FB), normalized mean-square-error (NMSE), correlation (R) and fraction of simulated values within a factor of two (FAC2) as obtained for $SO_2$ and $SO_4^{2-}$-aerosol

| | | Denali-IMPROVE | Denali-CASTNET | Poker-CASTNET |
|---|---|---|---|---|
| $SO_2$ | FB | No data | -1.03 | -0.72 |
| | NMSE | No data | 2.28 | 1.00 |
| | R | No data | 0.348 | 0.800 |
| | FAC2 | No data | 25% | 50% |
| $SO_4^{2-}$-aerosol | FB | 1.63 | -0.50 | 0.02 |
| | NMSE | 14.97 | 0.83 | 0.71 |
| | R | 0.477 | 0.232 | 0.315 |
| | FAC2 | 17% | 40% | 75% |
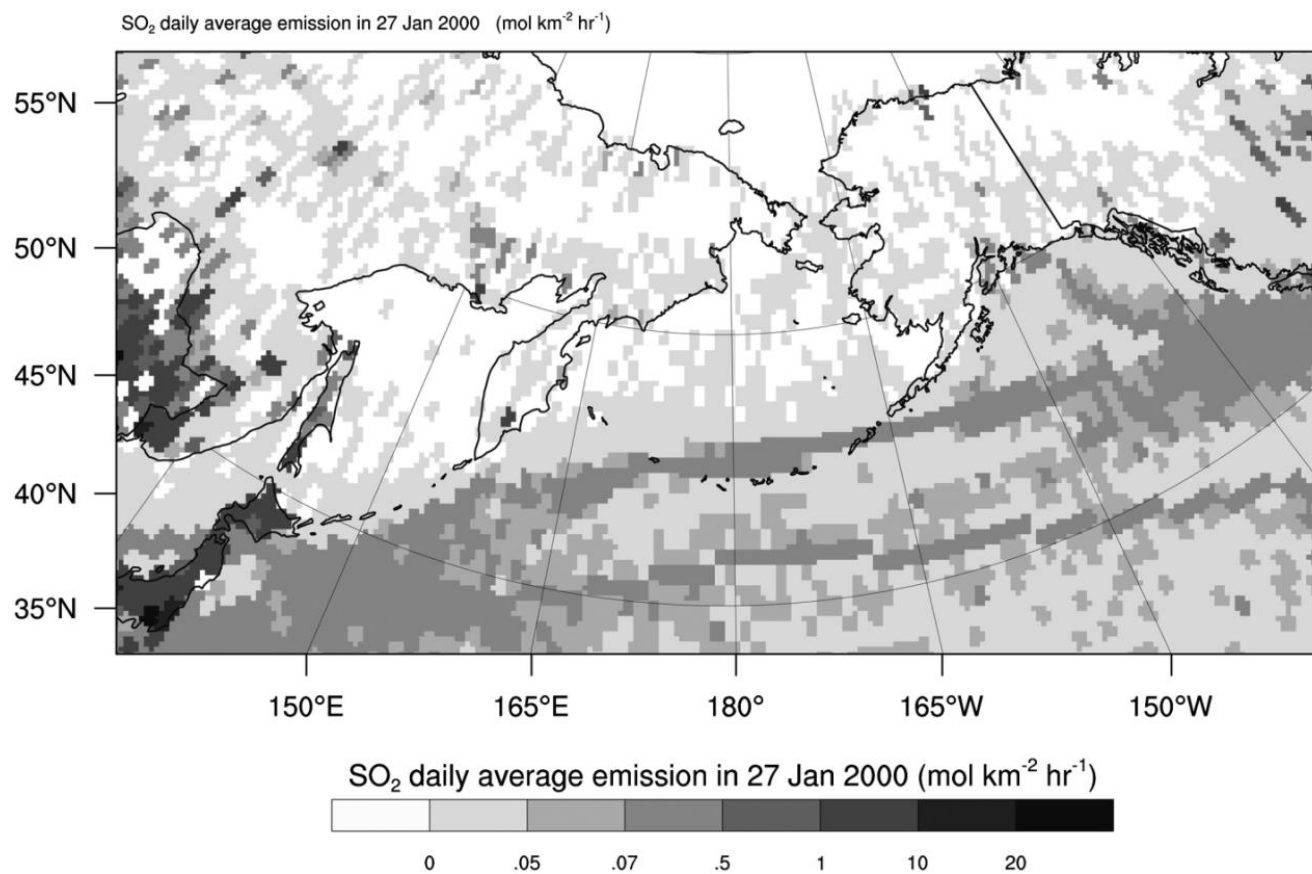
Fig. 4.1 Average emissions of $SO_2$ for 27 January 2000 as obtained from the combined EDGAR and RETRO data. See text for details.
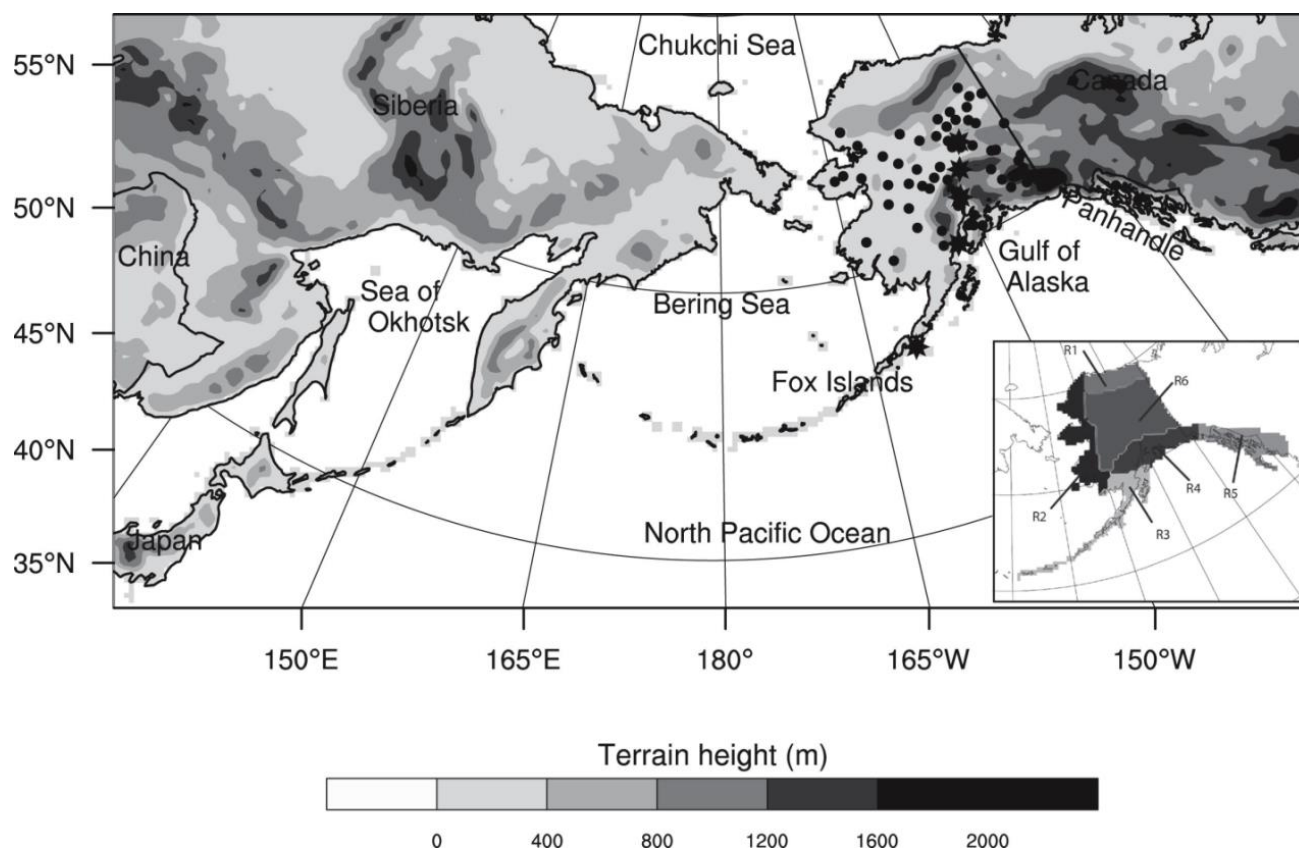
Fig. 4.2 Terrain height with locations of meteorological (dots) and aerosol-measurement sites (stars) superimposed. The panel in the right corner illustrates the regions of interest (R1–R6).
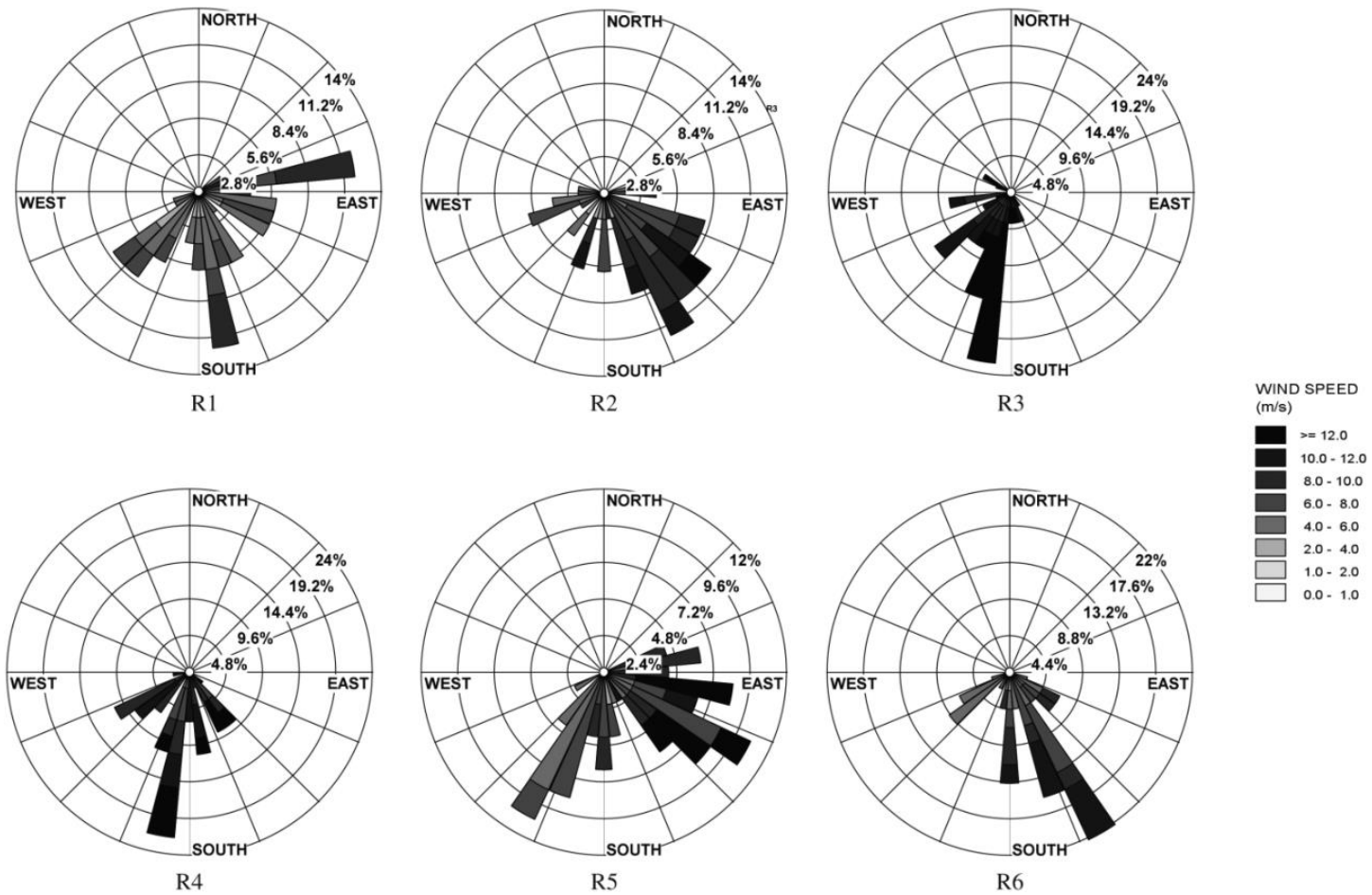
Fig. 4.3 Wind-roses for R1–R6 for 11–31 January, 2000. The circles show frequency. Data was taken from WRF-Chem simulations.
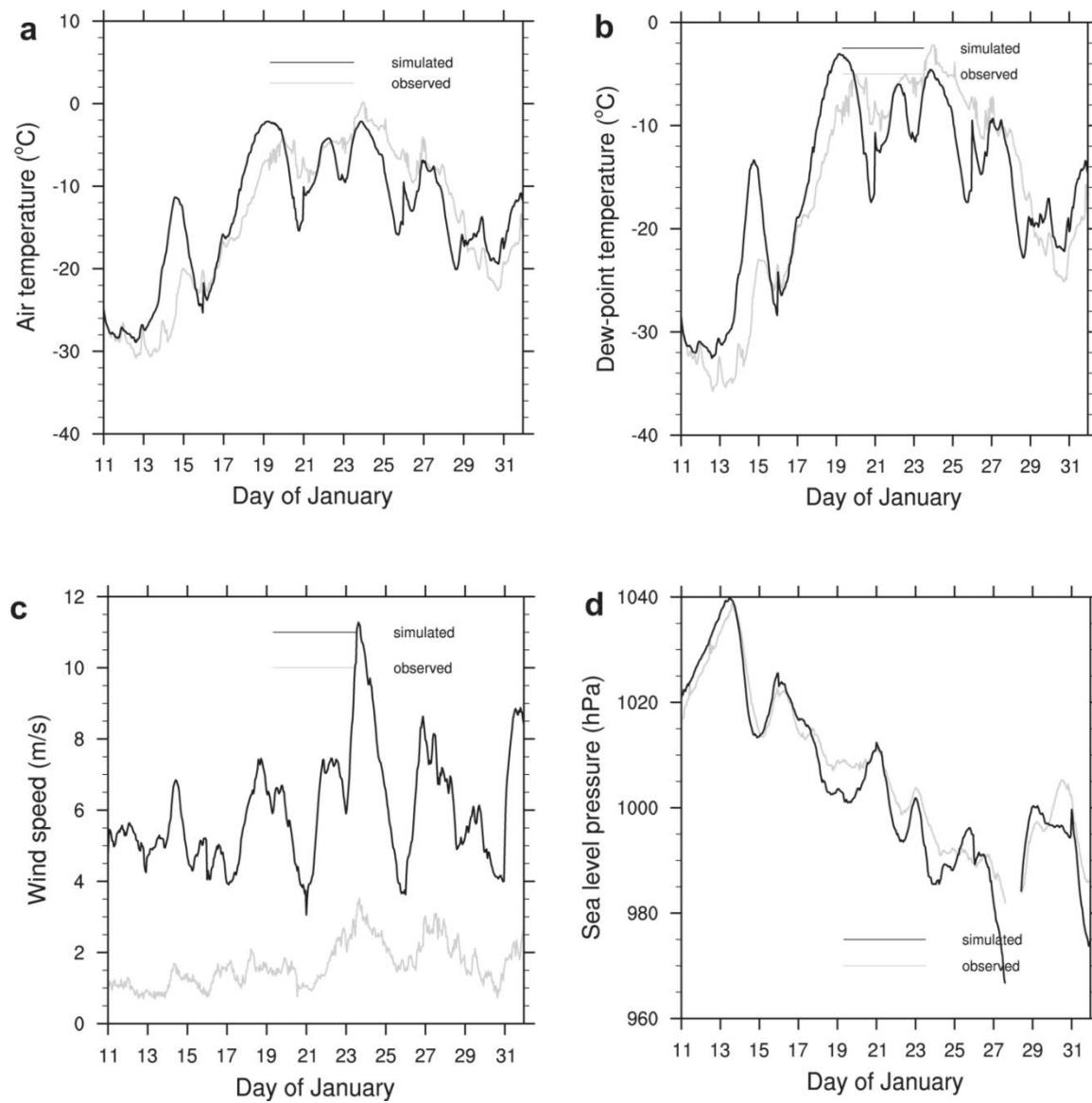
Fig. 4.4 Temporal evolution of hourly domain-averages of REF simulated and observed (a) air temperature, (b) dew-point temperature, (c) wind-speed, and (d) sea-level pressure. Data was averaged over all sites in Alaska for which data were available
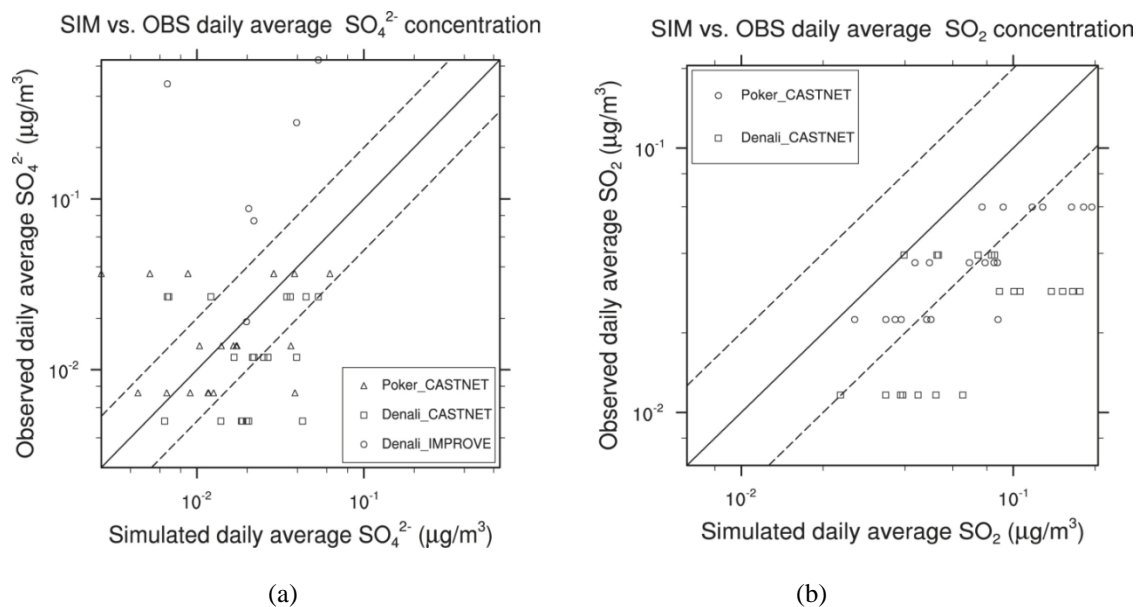
Fig. 4.5 Scatter plot of daily average concentrations of REF simulated (during January 11-31) and observed $SO_4^{2-}$-aerosols (a), and $SO_2$ (b) at Denali National Park and Poker Flat. Dashed lines indicate a factor of two agreements.
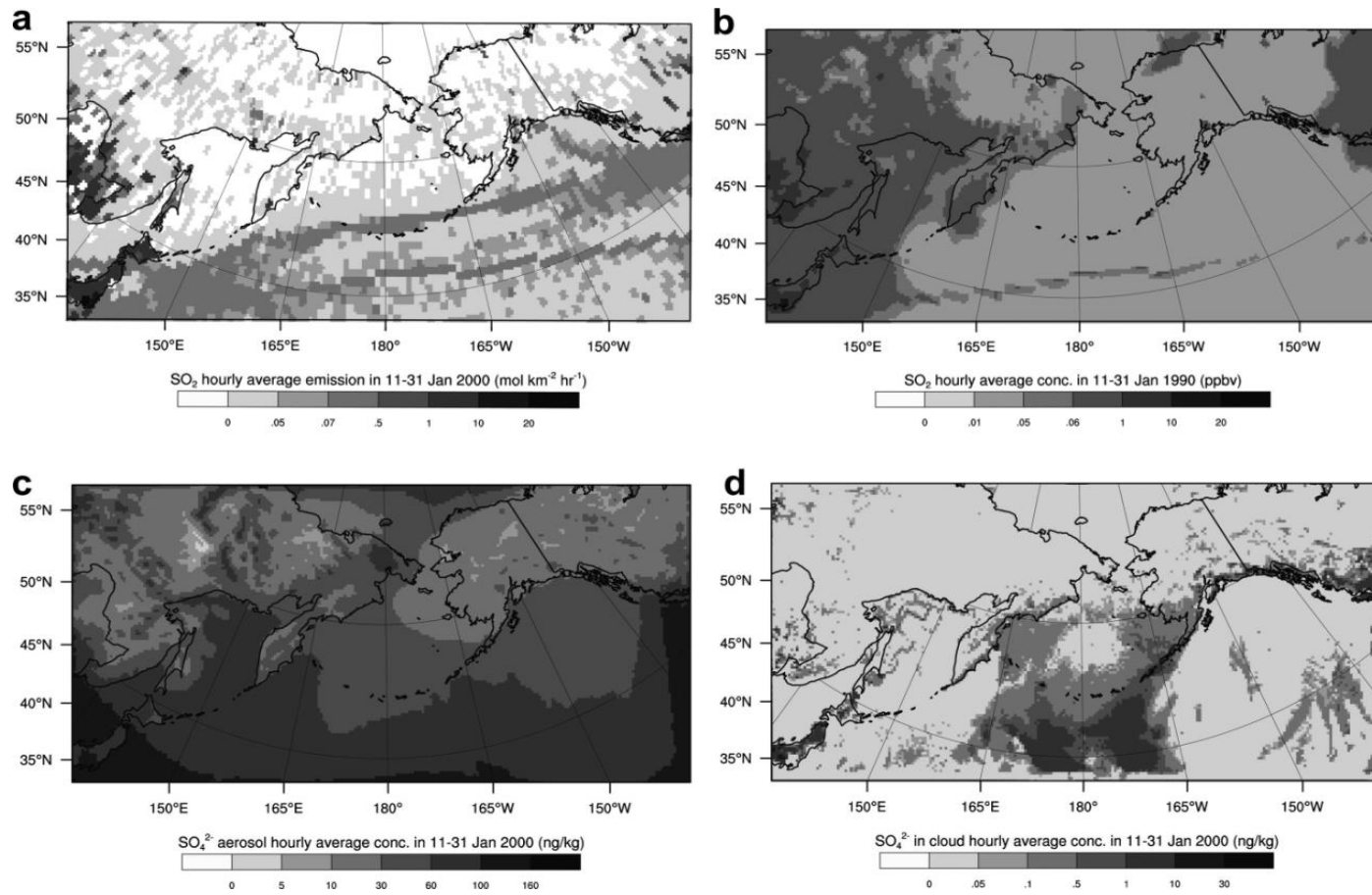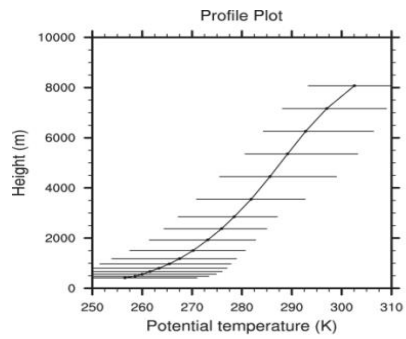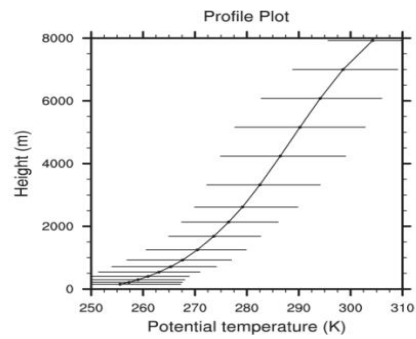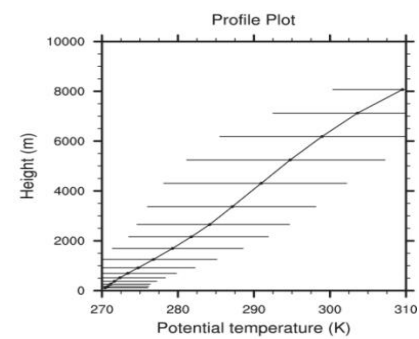
Fig. 4.6 Hourly average (a) SO$_2$-emissions, (b) SO$_2$, (c) SO$_4^{2-}$-aerosol and (d) SO$_4^{2-}$-in-cloud concentrations as obtained by REF for 11–31 January, 2000.
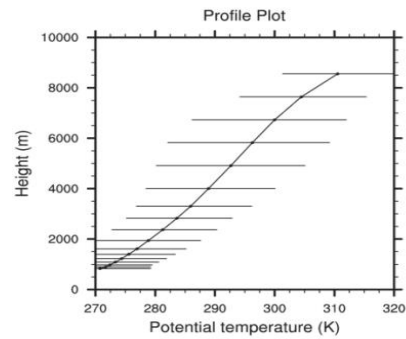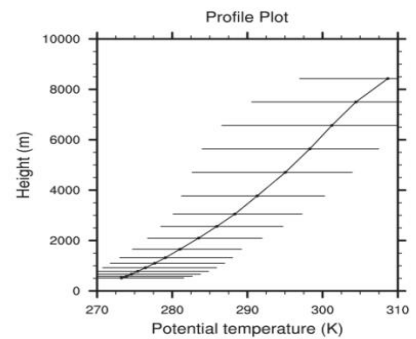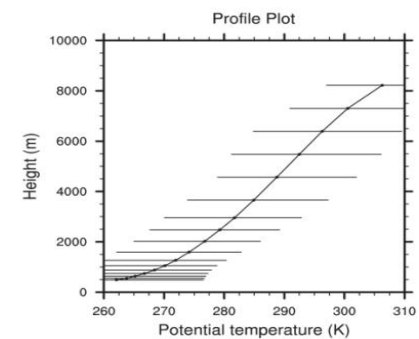
Fig. 4.7 Potential temperature profiles as obtained by REF during 11-31 January for R1–R6. The horizontal bars indicate the minimum and maximum values.
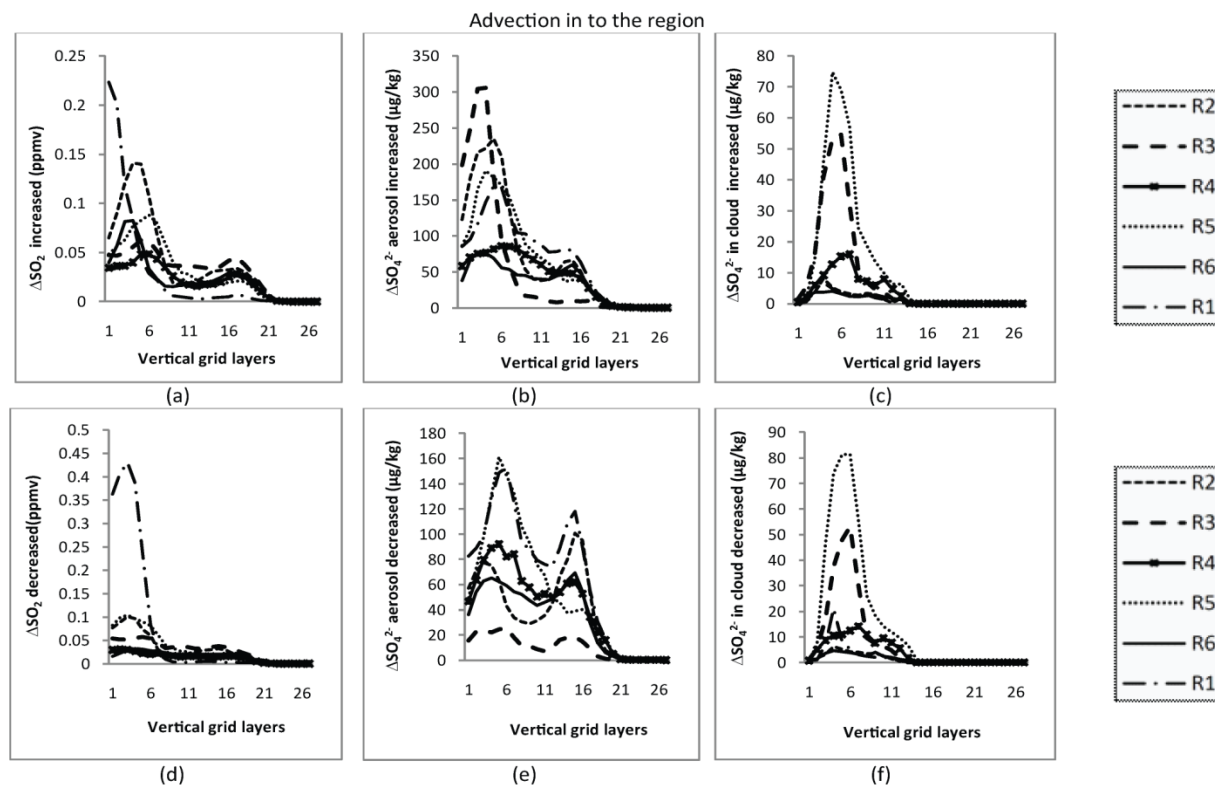
Fig. 4.8 Horizontal advection of SO$_2$, SO$_4^{2-}$-aerosol and SO$_4^{2-}$-in-cloud into (a–f) and out (g–l) of regions as obtained by REF for January 11-31. Increase (decrease) means advection of relatively higher polluted (cleaner) air into or out of the region. Plots for HIST look similar.
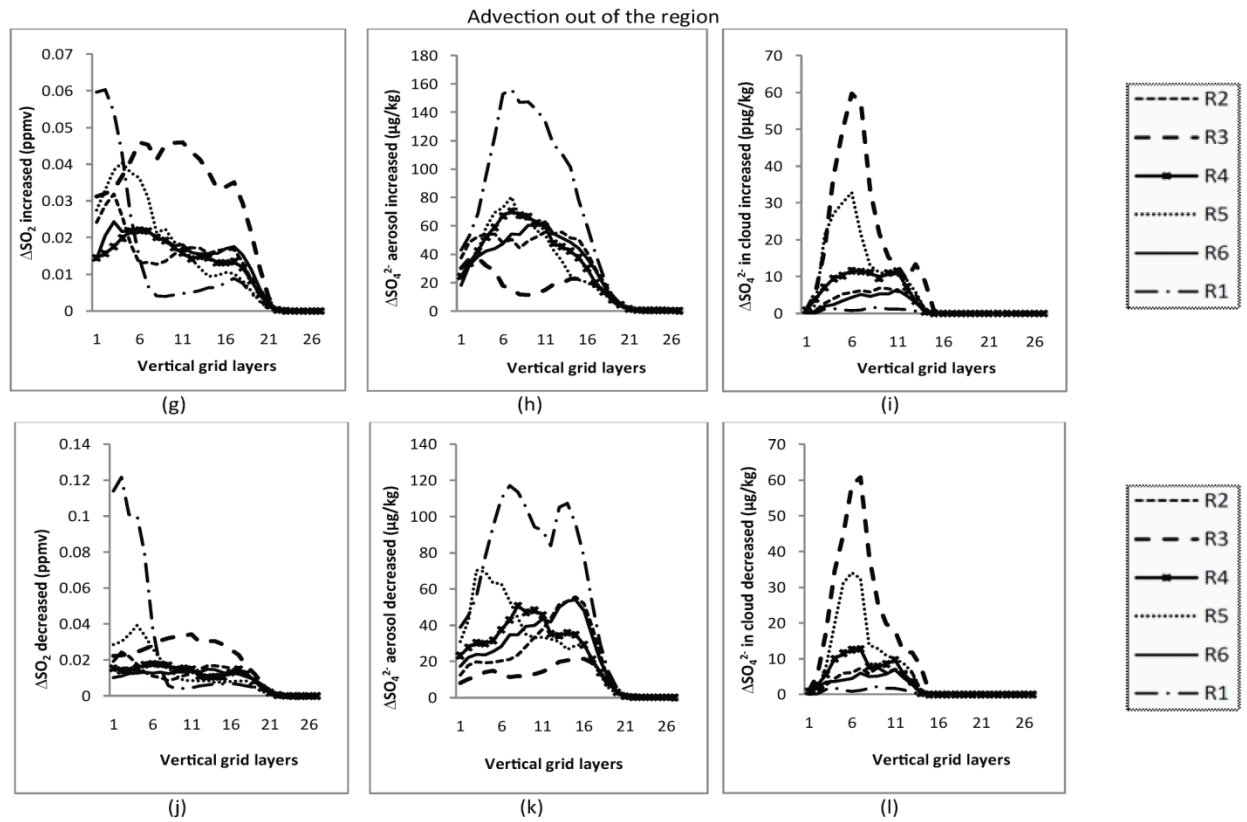
Fig. 4.8 (Cont.).
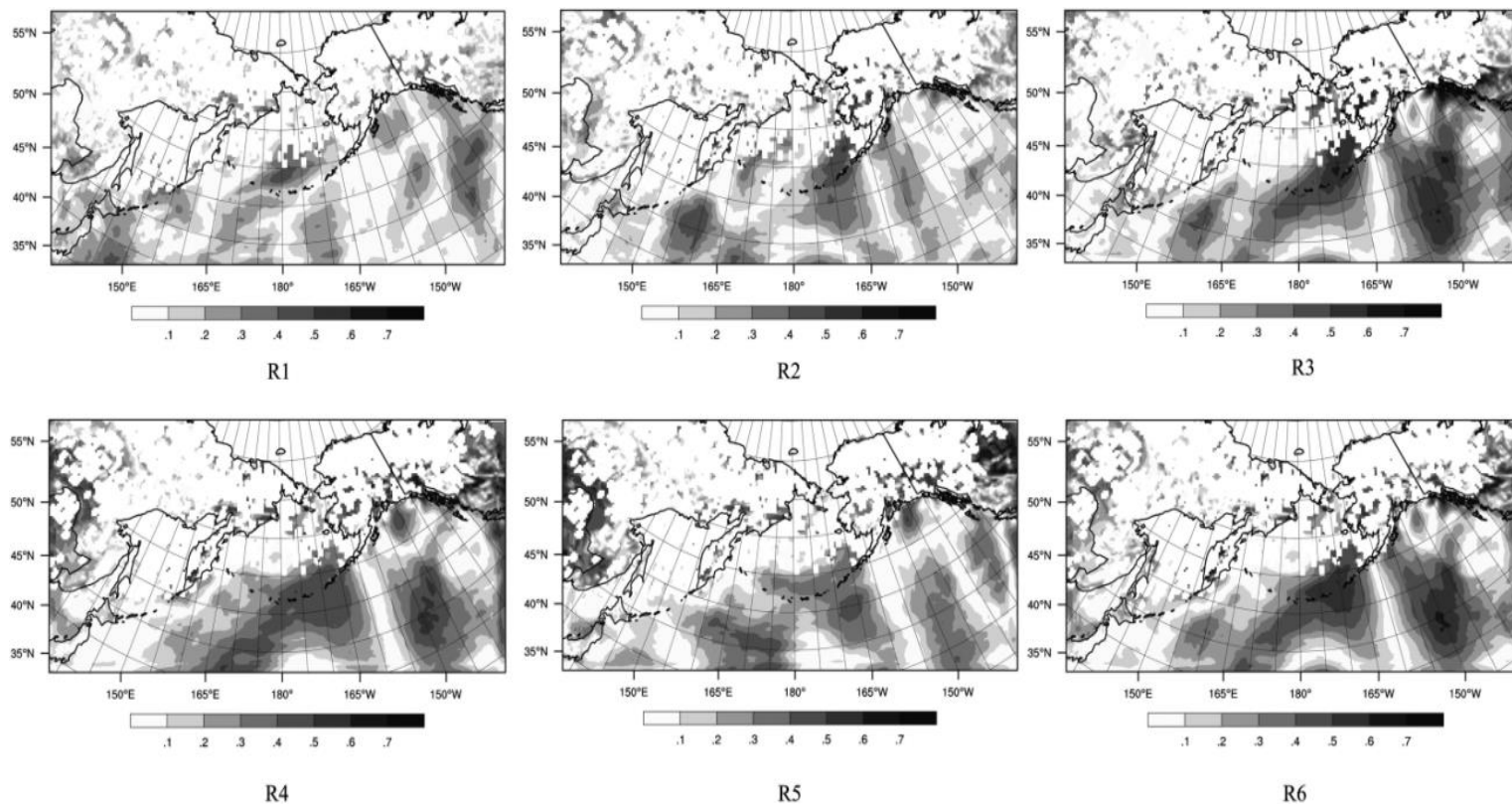
Fig. 4.9 Multi-correlation coefficients between the regional average SO$_2$-concentrations of R1–R6 and the SO$_2$-emission and wind-speed of each grid-cell as obtained by REF.
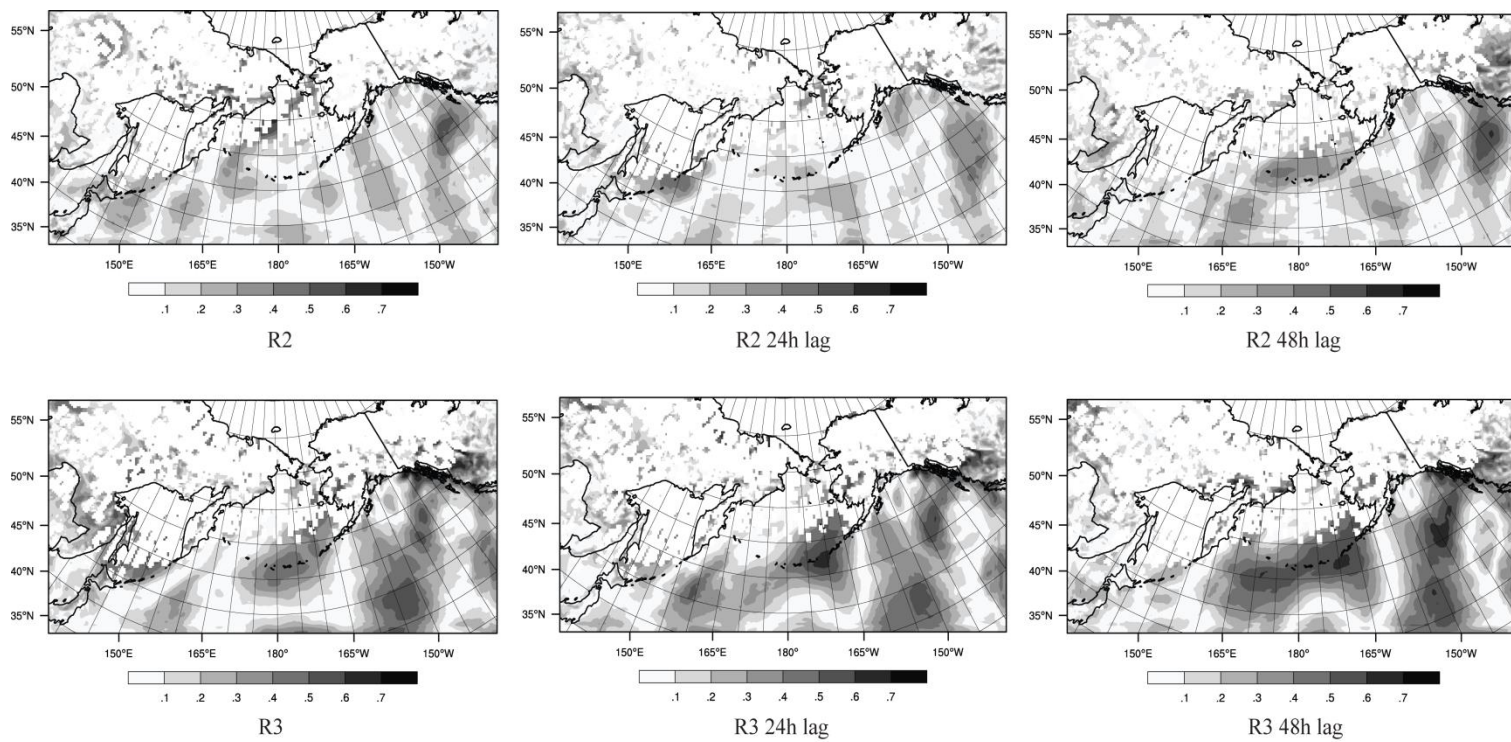
Fig. 4.10 Like Fig. 4.9, but for time-lagged multi-correlation coefficients of regional average $SO_4^{2-}$-aerosol concentrations of R2-R6 and the $SO_2$-emission and wind at each grid-cell.
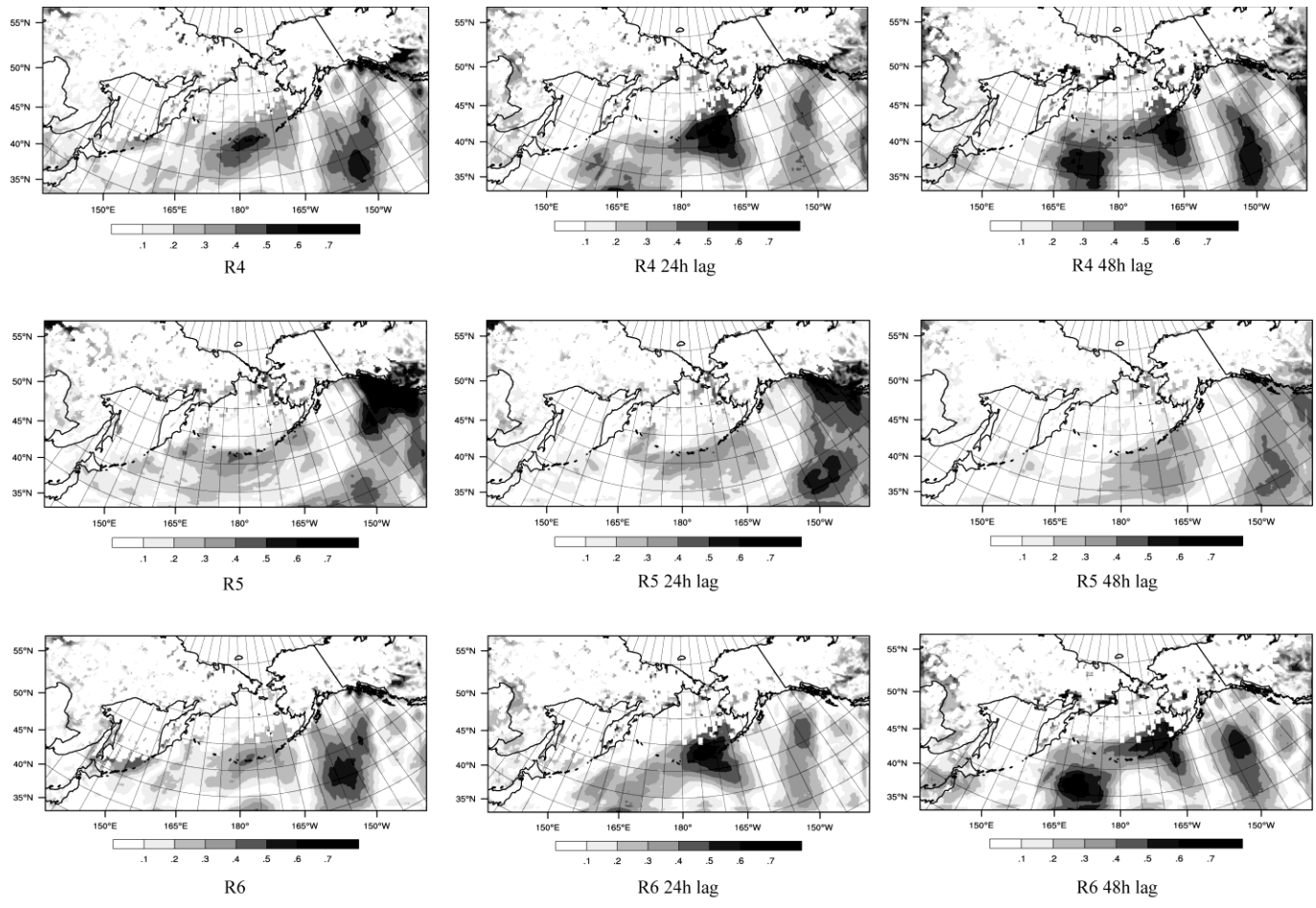
Fig. 4.10 (Cont.)
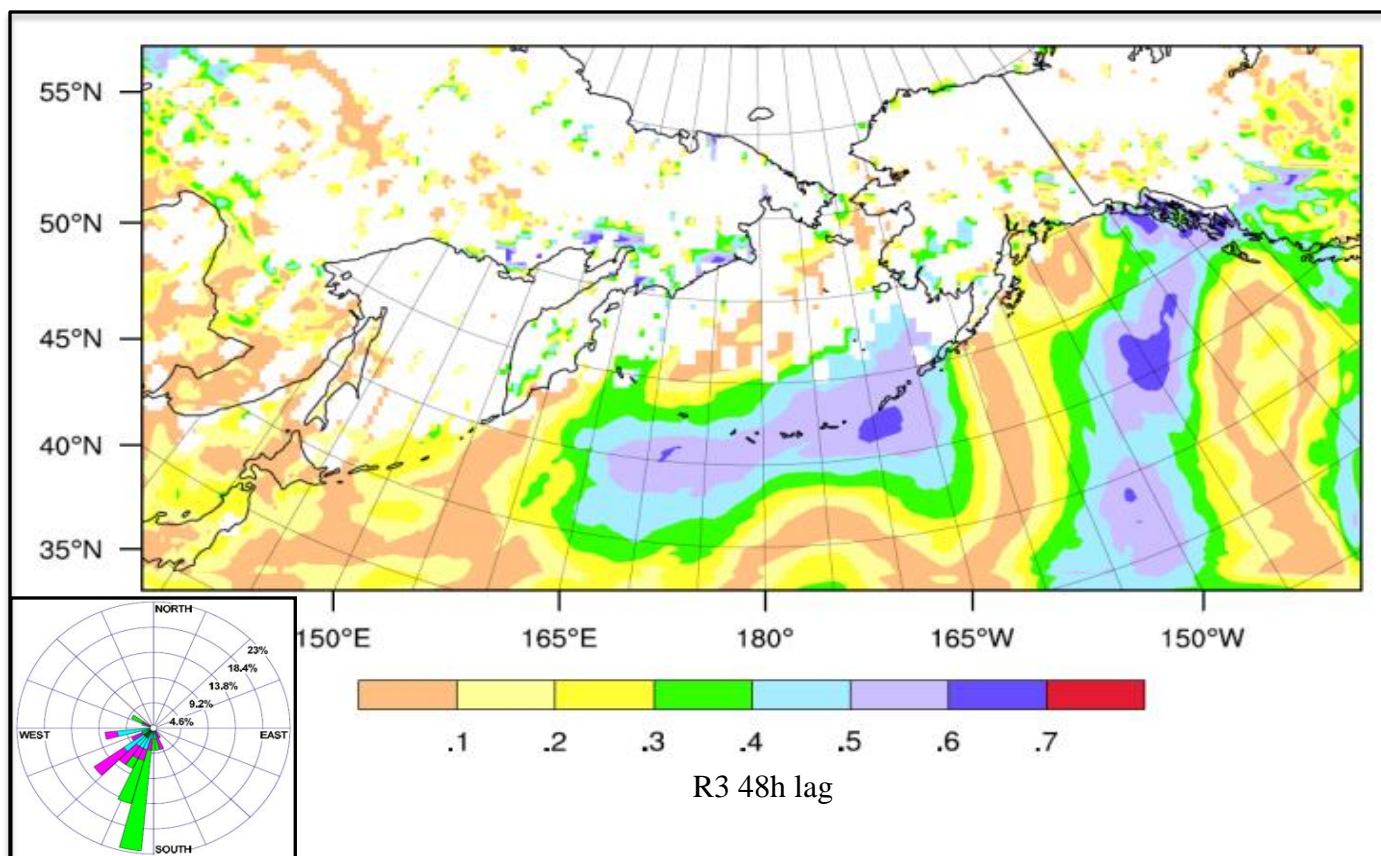
Fig. 4.11 Color version of Fig. 4.10 for R3, R4 and R5 at 48h, 24h and 0h time-lag, respectively. Wind roses indicated the main wind direction that confirmed the source regions of $SO_4^{2-}$-aerosol concentrations averaged over regions of interest.
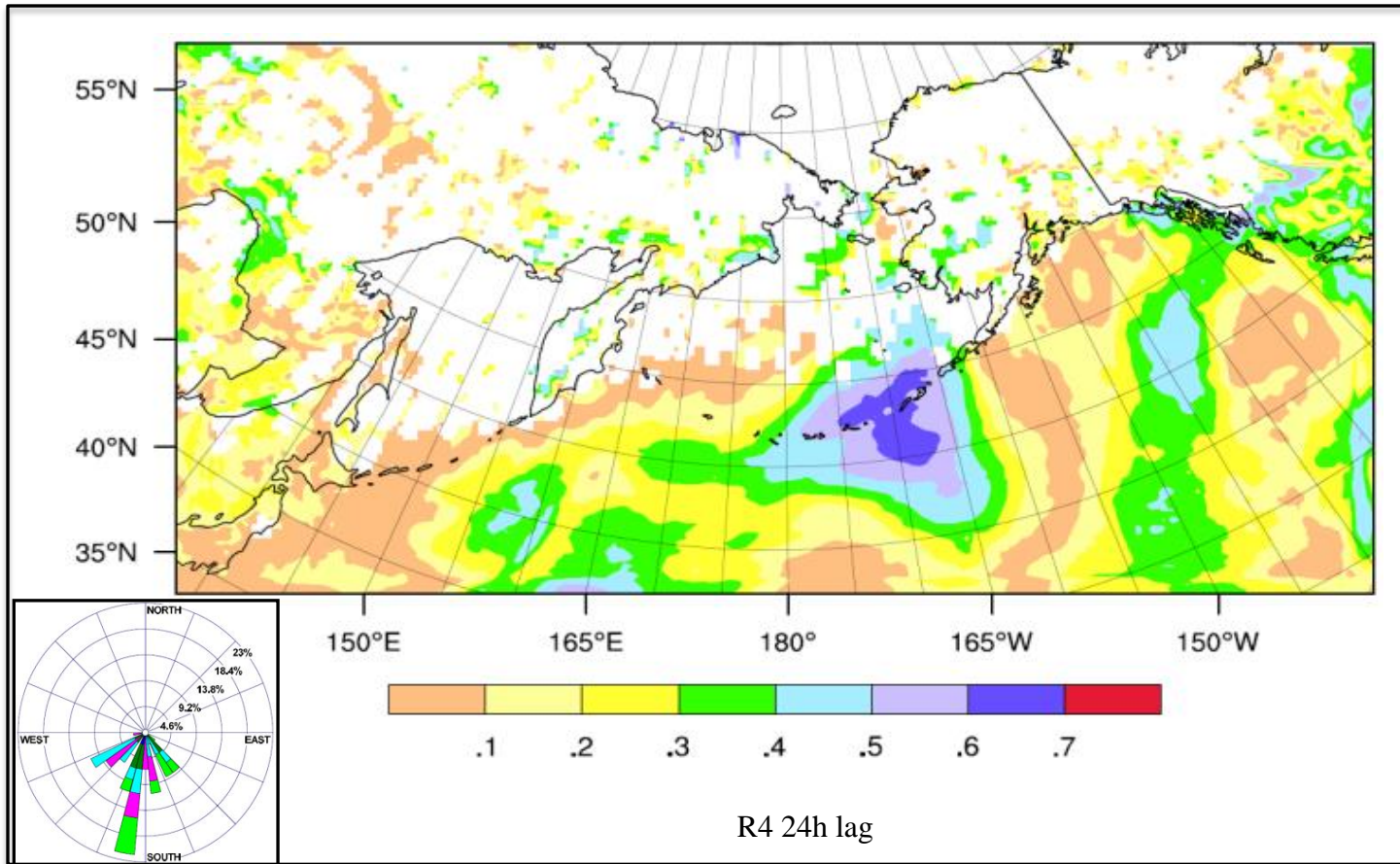
Fig. 4.11 (Cont.).
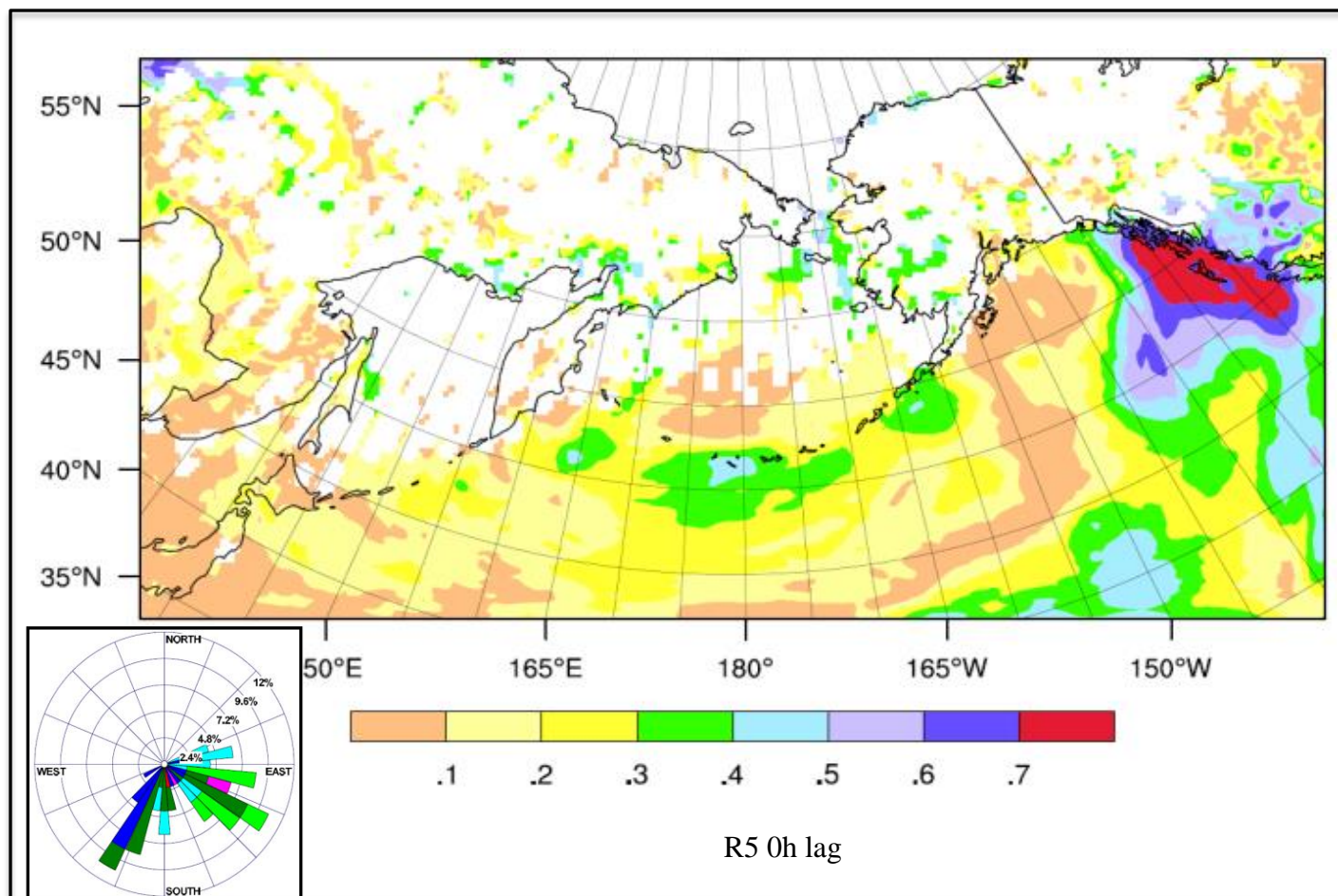
Fig. 4.11 (Cont.).
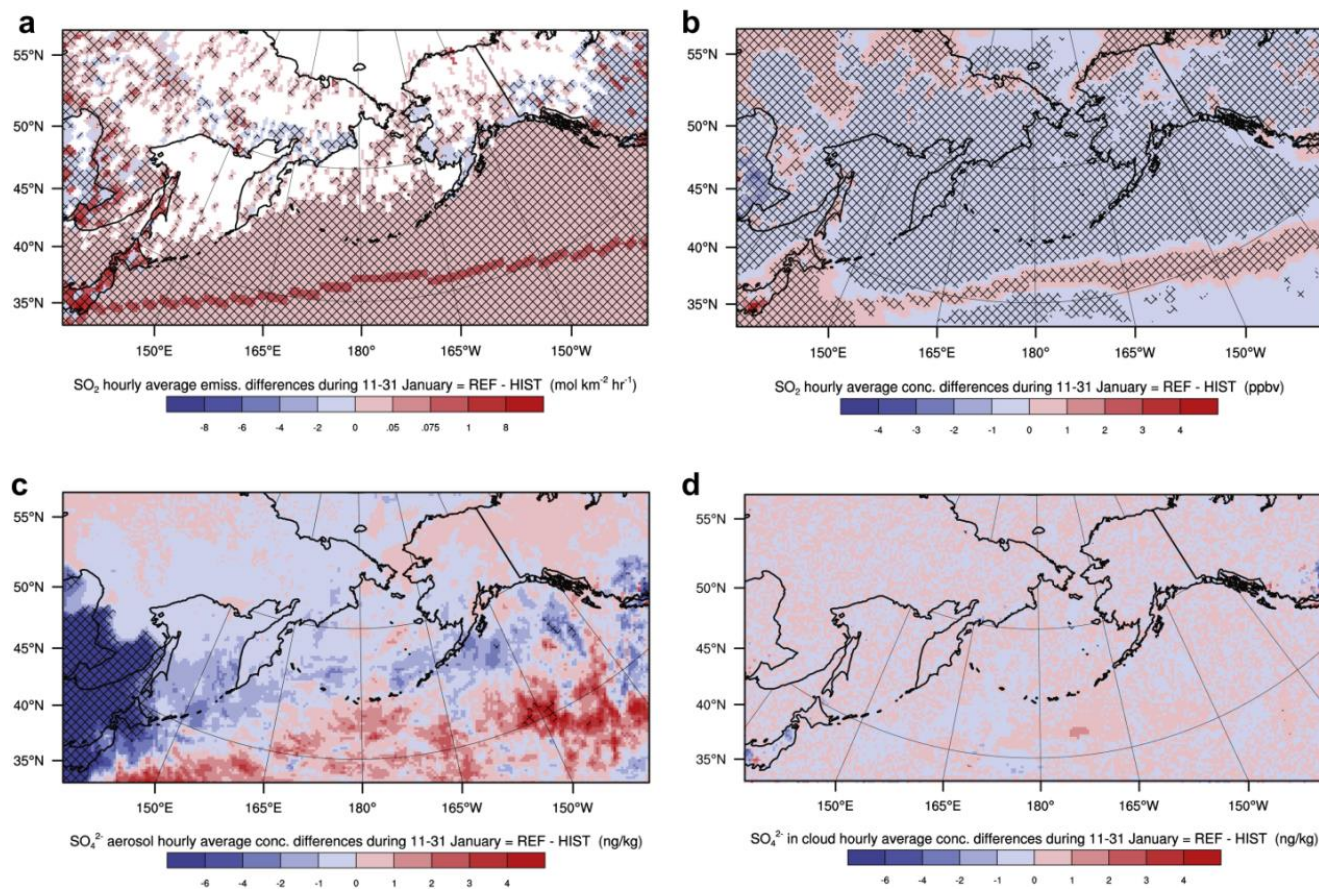
Fig. 4.12 Averaged differences of $SO_2$-emissions and sulfur-compound concentrations between REF and HIST for January 11–31. Hatching indicates significant differences at the 95% confidence level.
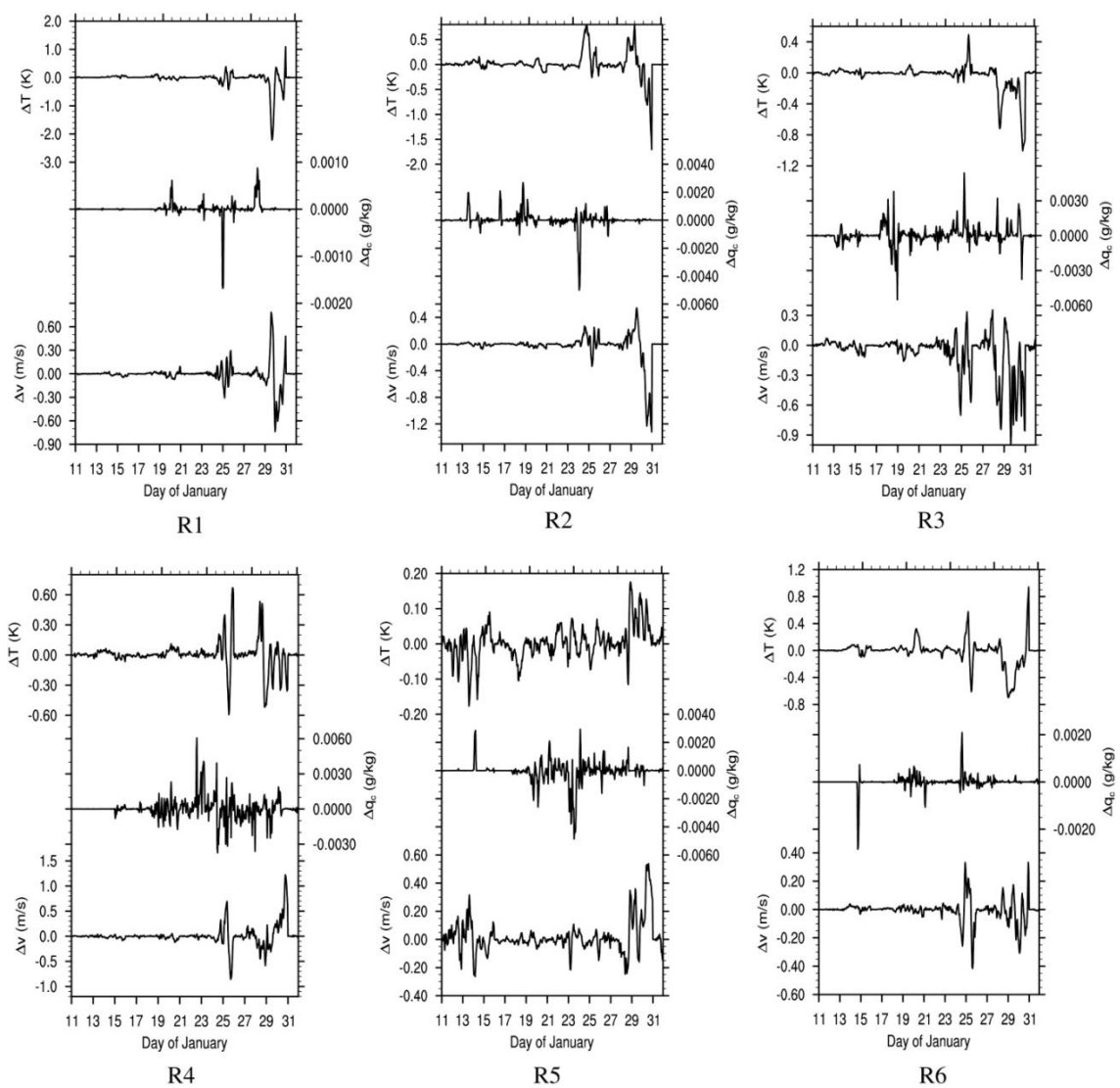
Fig. 4.13 Regionally averaged differences of near-surface temperature (T), cloud-water mixing ratio (qc) and wind-speed (v) between REF and HIST. Scaling differs among panels

## Chapter 5 Potential impacts of an Emission Control Area on air quality in Alaska coastal regions [1]

**Abstract**

The Alaska-adapted WRF-Chem was used to examine the benefits of the proposed North American Emission Control Area (ECA) for air quality along the Alaska coastlines. Simulations were performed alternatively assuming the emissions of 2000, and the emissions of 2000 reduced by the proposed ECA-reductions. In response to the emission reductions, reductions in sulfur (nitrogen) compounds reached up to 9 km (2 km) height above the ground (AGL). Reductions of sulfate- and nitrate-in-clouds were highest at the top of the atmospheric boundary layer. The strongest reductions occurred over the ECA and the international shipping lanes for sulfur- and nitrogen-compounds, respectively. Along the Gulf of Alaska, sulfur- and nitrogen-compound concentrations decreased significantly in response to the reduced ship-emissions. They decreased over all of Alaska despite the unchanged emissions in state of Alaska. $PM_{2.5}$-speciation only marginally changed in response to the reduced ship-emissions.

---

**5.1 Introduction**

Over the last decades, ship-traffic and ship-emissions have increased rapidly world-wide (Eyring et al., 2005). Ship-emissions critically impact air quality on various scales: satellite observations showed enhanced nitrogen-dioxide ($NO_2$) concentrations along the main shipping lanes over the Red Sea and Indian Ocean (Richter et al., 2004). The $NO_x$ (=$NO_2$ + NO (nitric oxide)) and sulfur dioxide ($SO_2$) from ship-emissions are important precursors for the formation of particulate matter (PM). Particles related to ship-emissions decrease the effective droplet radius and increase the droplet-number concentrations and optical thickness of stratus within ship-tracks (Schreier et al., 2006). On the regional scale, ship-emissions increase ozone ($O_3$) and PM-concentrations at many coastal sites in southern California significantly and at inland sites notably and the control of ship-emissions improved air quality at all these sites (Vutukuru and Dabdub, 2008). Increasing $NO_x$-emissions from ship-traffic led to burdensome near-surface $O_3$-concentrations mostly over the ocean (Eyring et al., 2007). Ship-emissions in the Eastern Atlantic strongly modify $NO_x$ in West-European coastal and even inland regions (Huszar et al., 2010). In most of Southeast Asia that experiences heavy ship-traffic, 10% of the annual sulfur deposition is due to ship-emissions (Streets et al., 2000).

To improve inland air quality downwind of shipping lanes the International Maritime Organization (IMO) issued regulations for $SO_2$- and $NO_x$-ship-emissions (IMO, 2009). By 2015, the global standard for the fuel-sulfur content is to be reduced from 4.5% m m$^{-1}$ to 3.5% m m$^{-1}$. Engine-based controls (Tier II) have to be implemented to reduce the $NO_x$-emissions by 20% as compared to the old standard (Tier I). Within

emission-control areas (ECAs), ships must comply with a 0.1% m m$^{-1}$ fuel-sulfur content and an 20% reduction in NO$_x$-emissions (Tier II) by 2015. The North America ECA is to be extended to the Gulf of Alaska by 2012.

The introduction of the North America ECA led to reduced near-surface O$_3$- and PM$_{2.5}$ (PM with diameter ≤2.5 μm) concentrations along the coast of the contiguous US (EPA, 2009) and over large areas of southern British Columbia, and along the Eastern coast (Environment and Transport Canada, 2009).

The insolation and meteorological conditions along Alaska's coastlines strongly differ from those along the coasts of the existing ECAs. Especially in January, temperatures are extremely low and there is hardly or only short period of daylight. Consequently, gas-phase chemistry is mainly nighttime chemistry, and the low temperatures favor particle formation. Thus, findings from the existing ECAs cannot be easily transferred to assess the potential benefits of an ECA in Alaska waters. Thus, the goal of this study was to exemplarily assess the impacts of the proposed ECA-extension on Alaska air quality in January.

## 5.2 Experimental design

### 5.2.1 Model description

The Weather Research and Forecasting model (Skamarock et al., 2008) inline coupled with a chemistry package (WRF/Chem; Peckham et al., 2009) was used with the physical and chemical schemes as described in Tran et al. (2011). They include Lin et al.'s (1983) parameterization of cloud-microphysical processes, an updated version of

Grell and Dévényi's (2002) cumulus-ensemble scheme, the long-wave and shortwave radiation parameterizations by Mlawer et al. (1997) and Chou and Suarez (1994), respectively, Janjić's (2002) viscous sub-layer and atmospheric boundary layer (ABL) parameterizations and the further-developed version of Chen and Dudhia's (2001) land-surface model that considers fractional sea-ice.

Gas-phase chemistry was calculated using Stockwell et al.'s (1990) mechanism with photochemical reaction rates calculated following Madronich (1987). The physical and chemical properties, dynamics of inorganic and secondary organic aerosols including aqueous-phase reactions were simulated by the Modal Aerosol Dynamics Model for Europe (Ackermann et al., 1998) and Secondary Organic Aerosol Model (Schell et al., 2001) (MADE/SORGAM). Interactions between aerosols, cloud-microphysics and radiation were also considered. Dry deposition of trace gases was calculated following Wesely (1989) with the modifications by Mölders et al. (2011).

## 5.2.2 Emissions

Biogenic emissions of volatile organic compounds (VOC) from vegetation and nitrogen from soil were calculated inline following Simpson et al. (1995). WRF/Chem calculated sea-salt and dust emissions (Peckham et al., 2009).

The Emission Database for Global Atmospheric Research (EDGAR; http://www.mnp.nl/edgar/) and Reanalysis of the Tropospheric (RETRO; http://retro.enes.org/data_emissions.shtml) data were merged to represent emissions from inland anthropogenic sources, international and domestic ship-traffic for carbon

monoxide, $SO_2$, $NO_x$, and non-methane VOC. The $1° \times 1°$-EDGAR-data was used for inland anthropogenic sources and ship-emissions along the international shipping lanes (ISL). The $1° \times 1°$-RETRO-data served to include domestic ship-emissions unavailable in the EDGAR-data (see Tran et al., 2011). The reference simulation (REF) used this merged emission data. Since Alaska (AK) had no ECA in 2000, the ship-emissions assumed for REF correspond to the global sulfur content (4.5% m m$^{-1}$) and Tier I global standards for $NO_x$.

Two emission datasets were created that only differ for ship-emissions from the emission-data described above. In doing so an ECA of 200 nautical miles extension was assumed in the waters off Alaska's coastlines (Fig. 5.1). We assumed a fuel-sulfur content of 0.1% m m$^{-1}$ in the ECA, and of 3.5% for the regions outside the ECA as proposed for 2015 (IMO, 2009). This emission-dataset is called ECA1 hereafter. The dataset ECA2 is identical to ECA1 expect that it assumes a 20% reduction in $NO_x$-ship-emissions compared to REF and ECA1.

### 5.2.3 Simulations

The model domain covers Alaska, Japan, and parts of Canada, Siberia, China, and the North Pacific (Fig. 5.1) by $240 \times 120$ grid-points in the horizontal direction with 30 km grid-increment. The vertically stretched grid has 28 layers that increase in thickness with height.

WRF-Chem-simulations were performed for January 1–31 with the three emission-scenarios. All simulations were initialized with the same meteorological

conditions and background concentrations on January 1. WRF-Chem was run in forecast-mode and the meteorology was initialized every 5 days. The $1° \times 1°$, 6 h global final analysis data of the National Centers for Environmental Prediction served as meteorological initial and boundary conditions. Alaska/Pacific specific background concentrations were used as boundary conditions for the chemical fields. The chemical distribution at the end of each simulation served as initial conditions for the subsequent simulation.

REF used the merged emission data of 2000. The first and second scenario-simulation called ECA1 and ECA2 hereafter, applied the ECA1- and ECA2-emission datasets. In the following, REF, ECA1 and ECA2 refer to the emission-datasets, simulations and their results. While ECA2 includes both reduced $SO_2$ and $NO_x$-ship-emissions as required for the ECA by 2015, the sensitivity study ECA1 served to investigate the effects of reductions from ship-emissions for $SO_2$ only.

### 5.2.4 Analysis

The first ten days of the simulations were discarded for spin-up of the chemical fields which leaves January 11–31 for the analysis.

WRF-Chem's performance in simulating nitrate-aerosol concentrations was evaluated by observations obtained from the Interagency Monitoring of Protected Visual Environment (IMPROVE) network for Denali Park and the Clean Air Status and Trends Network (CASTNET) for Denali Park and Poker Flat.

Hourly averaged horizontal and vertical distributions of nitrogen compounds, sulfate and ammonium-aerosol concentrations were analyzed, and the hourly averaged concentration differences ECA1-REF, ECA2-ECA1 and ECA2-REF of the sulfur and nitrate compounds to identify potential interactions between the impacts in response to reduced $SO_2$- or $NO_x$-ship-emissions. Differences between ECA1 and REF indicate effects of the reduced $SO_2$-ship-emissions. Analogously, comparison between ECA2 and ECA1 shows the effects of reduced $NO_x$-ship-emissions. The overall effects of concurrently reduced $SO_2$- and $NO_x$-ship-emissions can be examined by comparing ECA2 and REF. The concentration changes in the surface layer and the entire air columns over AK, ISL and ECA were analyzed to investigate how reduced ship-emissions affect local air quality at the locations of reductions (ISL, ECA) and remotely (AK).

To investigate how the reduced $SO_2$- and $NO_x$-ship-emissions affect $PM_{2.5}$, $PM_{2.5}$-speciation were examined with focus on sulfate ($SO_4^{2-}$), nitrate ($NO_3^-$), ammonium ($NH_4^+$), OC and elementary carbon (EC) in the domain, AK, along the ISL and within the ECA. Student's t-tests with a confidence level of 95% were applied to test the hypothesis that the reduced ship-emissions do not affect air quality.

**5.3 Results**

**5.3.1 General features**

**5.3.1.1 Evaluation**

Tran et al.'s (2011) evaluation of the reference simulation by meteorological observations from 59 sites showed that WRF-Chem performed well at capturing the meteorological conditions over Alaska with overall biases of 0.4 K, 0.4 K, 4.3 m s$^{-1}$ and -2 hPa in air temperature, dew-point temperature, wind-speed and sea-level pressure, respectively. Discrepancies were greatest after the passage of the cold fronts on January 13 and 16. WRF/Chem overestimated the $SO_2$-concentrations at the two $SO_2$-sites with a fractional bias (FB) of −1.03 and −0.72, but captured the temporal evolutions of $SO_2$ and sulfates acceptably or better. At the three sulfate-sites, the FBs were 1.63, −0.5, and 0.02. At the IMPROVE- and CASNET-sites in Denali Park and Poker Flat 17, 40 and 75% of the simulated and observed sulfate concentrations agreed within a factor of 2 (Table 5.1).

Nitrogen chemistry is more difficult to simulate than sulfur chemistry. Hence, WRF-Chem's performance in simulating nitrate-aerosols is not as good as its performance for sulfate-aerosols. At the three sites, 17, 20 and 55% of the simulated and observed values agreed within a factor of 2. WRF-Chem underestimated (overestimated) nitrate-aerosol concentrations at the Denali-Park IMPROVE (Denali-Park CASTNET, Poker-Flat CASTNET) site (Table 5.1). The differences in model performance were due to the sites' locations. The IMPROVE-site is downwind of Healy − a small community with a power plant. Models applied at the scale of this study cannot capture the sub-grid

scale dispersion of power-plant plumes. The CASTNET-sites are remote from any anthropogenic emissions. Low concentrations are difficult to simulate correctly.

### 5.3.1.2 Horizontal distributions

High $SO_2$- and $NO_x$-emissions occurred over the shipping lanes, and Chinese, Japanese, and Canadian industrial centers (Fig. 5.2a). $SO_2$- and $NO_x$-concentrations were high where the respective emissions were high (Fig. 5.2b) showing the local effects of the emissions on the $SO_2$- and $NO_x$-concentrations. Regionally, hourly averaged dry deposition fluxes of $SO_2$ and $NO_x$ were less than 2% of the emission flux, i.e. are a negligible sink. Wet deposition was also negligibly small as the regional daily-averaged precipitation was less than 1 mm day$^{-1}$.

Within Alaska, sulfate-aerosol concentrations were high along the coast of the Gulf of Alaska due to advection of polluted air from ship-emissions in the shipping lanes. Along the major shipping lanes, the highest sulfate-in-cloud concentrations occurred (cf. Tran et al.'s (2011) Fig. 4.6c, d).

$NO_x$ is a precursor for nitrate-aerosol. Nitrate-aerosols were more abundant in the southern part of the domain (Fig. 5.2c), as here the greater $NO_x$-concentration, insolation and water-vapor content than in the northern part triggered daytime (insolation-dependent) and nighttime (water-vapor dependent) gas-phase oxidation of $NO_x$ to nitrates. High nitrate-concentrations existed along the ISL and over Japan where $NO_x$-emissions were high. Despite the high $NO_x$-concentrations over China and Canada, nitrate-aerosol concentrations remained low in these regions (Fig. 5.2b, c). Unlike Japan

or the shipping lanes that received about 10 h of insolation, these regions had only 5–7 h of insolation. Nighttime oxidation of $NO_x$ requires water vapor that was also lower in these regions ($<2$ g $kg^{-1}$) than over the North Pacific ($>4$ g $kg^{-1}$).

Transport strongly affected the nitrate distribution, but not over long distances. High nitrate-concentrations occurred over the Pacific Ocean downwind of Japan and to both two sides of the shipping lanes. Sulfate-aerosols were transported over longer distances as they are more stable than nitrate-aerosols.

Nitrate-in-cloud concentrations were high over Japan and the North Pacific around 180°E (Fig. 5.2d). Nitrate-in-clouds was transported from the North Pacific into the Bering Sea, resulting into relatively high concentrations despite low $NO_x$-emissions in the Bering Sea.

The EDGAR and RETRO-data do not consider primary emissions of aerosols. Thus, in our study, all sulfates and nitrates stemmed from physio-chemical processes. Deposition is a sink for aerosols ($D$), but was negligibly small compared to the column-integrated advection ($A$) over AK ($A/D = 156$) and comparable to the advection in the surface layer ($A/D = 5$).

The sulfate and ammonium distributions were similar and differed from those of the nitrate distribution (e.g. Fig. 5.2c, e, f). The similarity between the sulfate and ammonium-distributions results from the fact that ammonia ($NH_3$) neutralizes $H_2SO_4$ first by irreversibly forming $(NH_4)_2SO_4$ before the excess $NH_3$ reacts with $HNO_3$ to reversibly form $NH_4NO_3$. Depending on the atmospheric conditions $NH_4NO_3$ formed or was destructed leading to the different distribution of $NH_4^+$ and nitrate. Neither EDGAR nor

RETRO has anthropogenic $NH_3$-emissions which led to low ammonium concentrations. In our study, $NH_4^+/SO_4^{2-}$ molar ratios are much lower than 2 (Fig. 5.2e, f) which indicates acidic particles. Acidic particles tend to enhance the volatility of nitrate. Therefore, nitrate-particle concentration are low in the source regions and hardly any nitrate-particles are transported to remote areas.

Surface and vertical-integrated $PM_{2.5}$-concentrations were highest over the ISL, followed by the ECA and AK (Table 5.2). Sulfate made up 85–89% of the total $PM_{2.5}$ over all three regions and the domain (Fig. 5.3). The fraction of EC and unspecified $PM_{2.5}$ were negligibly small compared with other $PM_{2.5}$-components (therefore not shown). Sulfate and nitrate contributed higher to $PM_{2.5}$ over the ocean (ISL, ECA) than over AK. Over AK, the ECA and ISL, OC made up 8.4, 5.0 and 4.0% of the total $PM_{2.5}$ reflecting that OC was more related to inland anthropogenic emissions than ship-emissions. Relatively high OC-concentrations existed west of 165°E along the ISL (~8%) due to the high anthropogenic emissions out of Japan. Over Japan, 15% of the total $PM_{2.5}$ was OC. Along the rest of the ISL, only 2% of the total $PM_{2.5}$ was OC.

## 5.3.1.3 Vertical distributions

No observed vertical profiles of $NO_x$, or $SO_2$ were available for the study time period. However, observed Arctic winter vertical profiles exist for 1987 for $SO_2$ (Möhler and Arnold, 1992) and for 2000 above 11 km for $NO_x$ (Payan et al., 2000). Simulated vertical profiles from WRF-Chem fall within the range of the typically observed $NO_2$ and

$SO_2$-profiles as presented in Möhler and Arnold (1992) and Payan et al. (2000). No observed nitrate and sulfate-aerosol profiles were available for Arctic winter.

Examined as a domain-average, the $NO_x$- and $SO_2$-concentrations decreased with height (Fig. 5.4a, b). Below 5 km (2 km) AGL, the $SO_2$ ($NO_x$) concentration-profiles differed between the ISL, ECA and AK with the ISL (AK) having the highest (lowest) concentrations. The differences in profiles established because of the different emissions in these regions. Above 5 km (2 km) AGL, the $SO_2$ ($NO_x$) profiles differed less distinct among the three regions than lower in atmosphere. The small differences in $SO_2$ ($NO_x$) concentrations among the three regions at these heights suggest that these heights were the upper limit to which the impact of the emissions reached. While the hourly near-surface and vertical-integrated $SO_2$-concentrations in AK and the ECA only slightly differed (Table 5.2), the near-surface (vertical-integrated) $NO_x$-concentrations amounted 74 ppt (626 ppt) and 144 ppt (1020 ppt) in AK and the ECA, respectively. The different distributions of $SO_2$- and $NO_x$-concentrations result from the fact that the gas-phase oxidation of $NO_x$ is ten times quicker than that of $SO_2$ (Stockwell et al., 1990). Thus, it was more likely for $SO_2$ to be transported from the ECA to AK prior to being oxidized than for $NO_x$. The slight $NO_x$-increase above 9 km AGL (Fig. 5.4a) resulted from photolysis of $NO_3$ that has relatively high background conditions above 9 km. Similar to the domain-averaged concentrations, $NO_x$-concentrations averaged over ISL, ECA, and AK decreased with height whereas $SO_2$-concentrations averaged over these regions had minima around 1 km AGL. This behavior of $SO_2$ can be associated with the loss of $SO_2$ via the production of sulfate-in-clouds.

Below 9 km AGL, nitrates (sulfates) decreased (increased) with height, while they both increased with height above this level (Fig. 5.4c, d). The vertical profiles relate to each other as follows. The $NO_x$-decrease with height reduced the nitrate-production via oxidation with OH leaving more OH for oxidization with $SO_2$. Thus, sulfate-production increased with height. Above 9 km, the extremely low temperatures (<-40 °C) enhanced the condensation of $HNO_3$ and $H_2SO_4$ to form nitrate- and sulfate-aerosols. The opposite trends in vertical profiles of the precursor $SO_2$ and the sulfate-aerosols above 5 km (Fig. 5.4b, d) resulted from the low volatility of sulfate-aerosols that prevents the evaporation of sulfate-aerosols to sulfate in the gas-phase to reproduce $SO_2$. This phenomenon indicates that above 5 km, where almost no clouds existed, gas-phase oxidation of $SO_2$ to sulfate-aerosols dominated. Below 5 km, $SO_2$ and sulfate showed similar trends with minima around 1 km. The vertical profiles of $NO_x$- and nitrate-aerosol concentrations showed similar trends at all heights (Fig. 5.4a, c). Since nitrate-aerosols are partially volatile, they easily converted back to $HNO_3$ in the gas-phase that can be photolyzed to produce $NO_2$.

Both nitrate- and sulfate-in-clouds were high at the top of the ABL around 800-1000 m (Fig. 5.4e, f). Their concentrations decreased gradually from the ISL, ECA to AK since more $SO_2$- and $NO_x$-precursors were emitted and more clouds existed over the ISL and ECA than over AK. The peaks of sulfate-in-clouds around 1 km height coincided with the $SO_2$-minimum (Fig. 5.4b, f). Below this height $SO_2$-oxidation in the aqueous phase dominated that produced sulfate-in-clouds rather than gas-phase oxidation to sulfate-aerosols.

**5.3.2 SO$_2$-reductions**

Averaged over the ISL and ECA, the reduction of SO$_2$-emissions was about 0.09 and 0.08 mol $(km^2\,h)^{-1}$, respectively. No changes in SO$_2$-emissions were assumed over AK in ECA1 or ECA2, and the NO$_x$-emissions were the same in ECA1 and REF.

In ECA1, the reduced SO$_2$-emissions resulted in reduced concentrations of all sulfur compounds over the three regions (Table 5.3). In ECA1, the hourly vertical-integrated SO$_2$-concentrations averaged over the ISL and ECA decreased about 5.6 and 9.6%, respectively, and negligibly over AK (0.4%) as compared to REF. Although the SO$_2$-emission reduction was lower in the ECA than ISL, the ECA experienced higher reductions of SO$_2$-concentrations (59 ppt) than the ISL (38 ppt). This behavior results from the advection of cleaner air from the ISL to the ECA in response to the reduced emissions. Advection from the ISL and ECA to AK led to reduced SO$_2$-concentrations in AK where the SO$_2$-emissions remained unchanged. Consequently, the reduction in sulfate-aerosols and sulfate-in-clouds showed the same gradient with the strongest reductions over the ECA and least over AK (Table 5.3). While SO$_4^{2-}$-aerosols were reduced less than 1% in all three regions, SO$_4^{2-}$-in-clouds were reduced about 4.4, 10.7 and 2.9% over the ISL, ECA and AK, respectively.

In response to the reduced SO$_2$-ship-emissions sulfur-compound concentrations were reduced in most of the vertical layers over the ISL, ECA and AK (Fig. 5.5a). Strong decreases occurred below 4 km AGL, while hardly any changes occurred above 10 km AGL. The reductions in SO$_2$ and SO$_4^{2-}$-aerosols decreased with height whereas strongest reductions of SO$_4^{2-}$-in-clouds occurred at the top of the ABL.

Although the $NO_x$-emissions were the same in ECA1 and REF, the nitrogen-compound concentrations changed due to the reduced $SO_2$-emissions (Fig. 5.5b, Table 5.3). Off-line simulations without consideration of feedbacks between meteorology and chemistry indicated that $SO_2$-emissions reductions increase nitrate-aerosols as more ammonium is available for ammonium nitrates formation (Matthias et al., 2010). Besides the inclusion of the feedbacks the different behavior in our study also partly results from the much drier and cooler conditions than in their study. The changes in $SO_4^{2-}$-aerosols slightly modified the meteorological conditions via radiative and thermal effects through cloud-microphysics and dynamics. The changed meteorological conditions led to changes in nitrogen-chemistry that is temperature-sensitive. Hourly vertical-integrated concentrations of $NO_3^-$-aerosols averaged over the ISL, ECA and AK decreased by 3.5, 1.9 and 1.9% whereas $NO_3^-$-in-clouds decreased by 3.0, 0.3 and 3.2%, respectively. On the contrary, $NO_x$-concentrations increased about 3.9, 7.6 and 8.2% over the ISL, ECA and AK, respectively. Similar to the sulfur-compounds, the changes of nitrogen-compounds reached up to 10 km height and were strongest below 4 km where hourly temperature averaged over the ISL, ECA and AK decreased in ECA1 as compared to REF (Fig. 5.5c). The average decreases over time and over the ISL, ECA and AK were of the order of 0.01 K, 0.01 K and 0.02 K, with local maximum decreases of up to 5, 4 and 12 K, respectively. The temperature decreases slowed down the thermal reaction rate for NO to $NO_2$-conversion. Since nitrates are formed by oxidation of $NO_2$, the decreased $NO_2$-formation reduced the nitrate-production. More NO remained and increased the $NO_x$-concentrations.

Since sulfate-aerosols were the main component of $PM_{2.5}$, and sulfate- and nitrate-aerosol concentrations decreased in response to reduced $SO_2$-ship-emissions, total $PM_{2.5}$ was reduced in all regions (Table 5.3). The ECA had the highest $PM_{2.5}$-reductions ($17.9 \, \text{ng m}^{-3}$) followed by the ISL ($12.8 \, \text{ng m}^{-3}$) and AK ($0.8 \, \text{ng m}^{-3}$). Like for the sulfate-aerosol reductions, the $PM_{2.5}$-reductions were less than 1% in all three regions.

### 5.3.3 $NO_x$-reductions

$NO_x$-emissions were the same over AK in REF, ECA1 and ECA2, and $SO_2$-emissions were the same over the whole domain in ECA2 and ECA1. Compared to REF in ECA2, the $NO_x$-emission reductions averaged over the ISL and ECA were about 0.08 and $0.02 \, \text{mol (km}^2\text{h)}^{-1}$, respectively.

Reducing $NO_x$-ship-emissions decreased the nitrogen-compound concentrations over the ISL, ECA and AK up to 198, 182, 89 ppt for $NO_x$, 3.5, 2.2, $0.2 \, \text{ng kg}^{-1}$ for nitrate-aerosols and 6.4, 3.2, $0.6 \, \text{ng kg}^{-1}$ for nitrate-in-clouds, respectively, on average over the episode and these areas (Table 5.3). The decreases of vertical-integrated nitrogen-compound concentrations were highest over the ISL which had the highest $NO_x$-emission reduction, followed by those over the ECA. Since nitrogen-compounds are less impacted by long-range transport than sulfur-compounds, the $NO_x$-concentration reductions gradually decreased from the ISL, ECA to AK like did the emission reductions. In the ISL, ECA and AK, $NO_x$, nitrate-aerosol and nitrate-in-clouds decreased about 13–16, 2–9 and 11–12%, respectively. In ECA2, over AK, the reductions of nitrate-aerosols that directly stem from the $NO_x$-emission reductions were about the same order

of magnitude as for the reduction of nitrate-aerosols in ECA1 that was caused indirectly by reduced $SO_2$-emissions (Table 5.3). The reductions of nitrogen-compounds reached up to 9 km with the strongest reductions below 2 km AGL (Fig. 5.6).

Reductions of $SO_2$-ship-emissions notably affected the nitrogen-compound concentrations as discussed before. However, the reductions of $NO_x$-ship-emissions only marginally affected the sulfur-compound concentrations. The reduction of sulfate-aerosols and/or sulfate-in-cloud caused indirectly in response to the reduced $NO_x$-emission was an order of magnitude lower than the sulfate reduction that occurred in direct response to the reduced $SO_2$-emissions (Table 5.3). In ECA2, $SO_2$-concentrations decreased about 2% as compared to ECA1 over the ECA that experienced the highest reduction rate for sulfur-compounds of the three regions. The reduction rates for the other sulfur-compounds were less than 1%. Since $SO_4^{2-}$-aerosols were the major component of total $PM_{2.5}$, the small changes in $SO_4^{2-}$-aerosols (0.1%) hardly reduced total $PM_{2.5}$ (0.5, 0.4 and 0.3% over the ISL, ECA and AK, respectively).

### 5.3.4 Concurrent $SO_2$- and $NO_x$-reductions

Compared to REF, ECA2 had both reduced $SO_2$- and $NO_x$-ship-emissions. The ISL had higher absolute reductions of $SO_2$- and $NO_x$-emissions (0.09, 0.08 mol $(km^2 h)^{-1}$) than the ECA (0.08, 0.02 mol $(km^2 h)^{-1}$).

All sulfur and nitrogen-compound concentrations decreased over the three regions in response to the reduced $SO_2$- and $NO_x$-ship-emissions (Table 5.3). Especially Alaska's air quality improved in response to the reduced ship-emission despite in Alaska emissions

remained the same. The vertical-integrated hourly concentration differences over the three regions indicated that the ISL had strongest decreases of nitrogen-compound concentrations whereas the ECA had strongest decreases of sulfur-compound concentrations. The total decreases of sulfur and nitrogen-compounds can be attributed directly to the reduced emissions of their precursors and indirectly to the changed meteorological conditions in response to the reduced emission of aerosol-precursors of other family compounds. Comparison of the changes due to reduced $SO_2$-emissions (ECA1-REF) and the changes due to additional $NO_x$-reductions (ECA2-ECA1) suggest that the sum of changes was nearly the change between ECA2-REF (Table 5.3). This means there seems to be a nearly linear behavior of impacts during the episode studied here. The reduced $SO_2$-ship-emissions contributed to more than 80% of the total reduction of all sulfur-compounds, whereas the reduced $NO_x$-ship-emissions reduced the nitrogen-compounds between 40 and 97%. The varying efficiency of the $NO_x$-reductions in reducing nitrate-compounds was due to the sensitivity of nitrogen chemistry to meteorological conditions, particularly temperature changes.

The reduced $SO_2$- and $NO_x$-emissions yielded $PM_{2.5}$-concentration decreases of about 1% over the ISL, and ECA, and less than 1% over AK. Hourly vertical-integrated $PM_{2.5}$-concentration reductions were highest over the ECA (22 ng m$^{-3}$), followed by the ISL (15 ng m$^{-3}$) and AK (0.8 ng m$^{-3}$).

Below 25 m or so, hourly differences showed that $SO_2$- and $NO_x$-concentrations decreased significantly over the North Pacific (Fig. 5.7a, b). Notable $SO_2$ ($NO_x$) reductions of up to 15 (28) ppt occurred over the ISL and ECA. Alaska experienced

small, non-significant $SO_2$ and $NO_x$-reductions except for the coastal areas along the Gulf of Alaska and the Aleutians where significant reductions up to 5 ppt occurred.

Sulfate-aerosol concentrations significantly decreased adjacent to the ECA, around 45°N, 135°W along the cyclone tracks that transported air over the ISL towards the ECA (Fig. 5.7c, d). Over the North Pacific, nitrate-aerosol reductions reached up to 5 ng kg$^{-1}$ and were less than the sulfate-aerosol reductions of up to 10 ng kg$^{-1}$. The pattern of the nitrate-reduction distribution lacks any obvious signs of nitrate-aerosol transport by cyclones, while those for sulfate- aerosol reduction do. This different behavior results as nitrate-aerosols are less stable than sulfate-aerosols.

The sulfate- and nitrate-in-cloud concentration differences were integrated over entire column of each of the three regions to account for all clouds therein. In ECA2, sulfate-in-clouds reduced strongly around 45°N, 135°W. Strong reductions of nitrate-in-clouds extended from the ISL around 170°E–170°W and 135°W northwards. Only the coastal areas along the Gulf of Alaska experienced reductions of sulfate- and nitrate-in-clouds (Fig. 5.7e, f).

In response to reduced $SO_2$- and $NO_x$-ship-emissions, sulfur (nitrogen) compound concentrations decreased at all heights up to 9 km (2 km) AGL in all three regions (Fig. 5.8). Like for the comparison REF-ECA1, in ECA2, reductions of sulfur-compounds reached farther in both horizontal and vertical directions than those of the less stable nitrogen-compounds. Except for the sulfate- and nitrate-in-cloud reductions that were highest at the top of the ABL, the magnitude of all sulfur- and nitrogen-compound reductions decreased with height (Fig. 5.8).

In ECA2, $PM_{2.5}$ decreased about 1.1, 1.3, and 0.3% over the ISL, ECA, and AK compared to REF. In the three regions and the domain, $PM_{2.5}$-speciation hardly changed (<1%) when the $SO_2$- and $NO_x$-ship-emissions were reduced at the IMO proposed rate for 2015.

## 5.4 Conclusions

Simulations with the Alaska-adapted WRF-Chem were performed for January 2000 alternatively applying three different emission-scenarios: The reference simulations used the emissions of 2000 (REF). ECA1 used the same emission-data as REF except that $SO_2$-ship-emissions were reduced by 22% and 98% outside and inside the ECA, respectively. ECA2 used the same emissions as ECA1 except that $NO_x$-ship-emissions were reduced by 20% outside and inside the ECA. All simulations used the meteorological conditions of 2000, so differences only result due to altered emissions. The impact of the ship-emission reductions for the planned North American ECA for $SO_2$ and $NO_x$ (ECA2) on air quality was investigated. The sensitivity simulation with the emissions of 2000 and the proposed $SO_2$-ship-emission reductions (ECA1) were used to examine interactions among the responses to the combined changes. The analysis focused on sulfur- and nitrogen-compounds and $PM_{2.5}$ over the ISL, ECA where emission were actually reduced, and over Alaska, where emissions remained the same.

All simulations showed the following features: local emissions governed the $NO_x$- and $SO_2$-concentration distributions. Nitrate-aerosol concentrations were high where insolation, $NO_x$-emissions and water-vapor content were relatively high. Since nitrate-

aerosols are less stable than sulfate-aerosols, nitrate-aerosol distributions were less governed by long-range transport than sulfate-aerosol distributions. Under supersaturated conditions, nitrate-aerosols were dissolved in cloud-droplets and became subject to long-range transport. Transport brought nitrate-in-clouds from the ISL where $NO_x$-emissions were high, to the Bering Sea, where $NO_x$-emissions were low.

In all three scenarios, sulfate-aerosol was the major component of total $PM_{2.5}$. Close to the land, the fraction of OC increased at the cost of sulfates and nitrates indicating the different influences of inland and ship-emissions on total $PM_{2.5}$.

In all scenarios, $SO_2$- and $NO_x$-concentrations decreased with height. Sulfate-aerosol concentrations increased with height whereas nitrate-aerosol concentrations decreased below and increased above 9 km. This different behavior is partly due to the high volatility of nitrate-aerosols. Nitrate-in-cloud and sulfate-in-clouds were highest at the top of the ABL where most of the liquid water existed.

The reduction of $SO_2$-ship-emissions led to reduced sulfur-compound concentrations in all three regions. In response to reduced $SO_2$-emissions the transport of less polluted air from the ISL to the ECA yielded higher reductions of sulfur-compound concentrations in the ECA than ISL despite of higher $SO_2$-emission reductions in the ISL. The advection of the relatively cleaner air to AK yielded decreased sulfur-compound concentrations over Alaska.

On the contrary, nitrogen-compounds showed high reductions where the $NO_x$-emission reductions were high. The reduced $NO_x$-ship-emissions led to decreases in nitrogen-compound concentrations of up to 198, 182, 89 ppt for $NO_x$, 3.5, 2.2,

0.2 ng kg$^{-1}$ for nitrate-aerosols and 6.4, 3.2, 0.6 ng kg$^{-1}$ for nitrate-in-clouds over the ISL, ECA and AK, respectively. These decreases correspond to a reduction of about 13–16% for NO$_x$, 2–9% for nitrate-aerosols and 11–12% for nitrate-in-clouds on average over the regions and episode.

The total reductions of all sulfur and nitrate-compounds in response to reduced SO$_2$- and NO$_x$-ship-emissions can be attributed partly directly to the reduced availability of their precursors and indirectly to the slight changes in meteorological conditions caused by radiative and cloud-microphysical feedbacks in response to the altered aerosol-concentrations. NO$_x$-emission reductions hardly affected the sulfur-chemistry whereas SO$_2$-emission reductions notably affected nitrogen-chemistry. Since nitrogen-chemistry is very temperature-sensitive, slight temperature changes due to the feedbacks between altered aerosol concentrations, cloud-microphysics and radiation led to changes in nitrogen-compound concentrations.

In response to the about 22% (98%) reductions in SO$_2$-ship-emissions outside (inside) the ECA and 20% reductions of NO$_x$-ship-emissions, the PM$_{2.5}$-concentrations decreased by slightly more than 1% over the ISL and ECA and less than 1% over AK. In these regions, PM$_{2.5}$-speciation hardly changed.

In conclusion, the proposed extension of the North America ECA has the potential to slightly improve air quality over Alaska as it can reduce the sulfur and nitrogen-aerosol compounds. However, significant decreases of sulfur and nitrogen compounds are most likely along the coast of the Gulf of Alaska.

**Acknowledgment**

150

## References

Ackermann, I.J., Hass, H., Memmesheimer, M., Ebel, A., Binkowski, F.S., Shankar, U., 1998. Modal aerosol dynamics model for Europe: Development and first applications. Atmos. Environ., 32, 2981-2299.

Chen, F., Dudhia, J., 2001. Coupling an advanced land-surface/ hydrology model with the Penn State/ NCAR MM5 modeling system. Part I: Model description and implementation. Mon. Wea. Rev., 129, 569–585.

Chou, M.-D., Suarez, M.J., 1994. An efficient thermal infrared radiation parameterization for use in general circulation models. NASA Tech. Memo., 104606, 85p.

Environment and Transport Canada, 2009. Canada/US emission control area (ECA) for ships. Consultation presentation. Vancouver, Ottawa, Halifax.

EPA, 2009. Proposal of emissions control area designation for geographic control of emissions from ships. EPA-420-F-09-015.

Eyring, V., Köhler, H.W., Lauer, A., Lemper, B., 2005. Emissions from international shipping: 1. The last 50 years. J. Geophys. Res., 110, D17305.

Eyring, V., Stevenson, D.S., Laurer, A., Dentener, F.J., Butler, T.M., Collins, W.J., Ellingsen, K., Gauss, M., Hauglustaine, D.A., Isaksen, I.S.A., Lawrence, M.G., Richter, A., Rodriguez, J.M., Sanderson, M., Strahan, S.E., Sudo, K., Szopa, S., van Noije, T.P.C., Wild, O., 2007. Multi-model simulations of the impact of international shipping on atmospheric chemistry and climate in 2000 and 2030. Atmos. Chem. Phys., 7, 757-780.

Grell, G.A., Dévényi, D., 2002. A generalized approach to parameterizing convection combining ensemble and data assimilation techniques. Geophys. Res. Lett., 29, 1693.

Huszar, P., Cariolle, D., Paoli, R., Halenka, T., Belda, M., Schlager, H., Miksovsky, J., Pisoft, P., 2010. Modeling the regional impact of ship-emissions on $NO_x$ and ozone levels over the Eastern Atlantic and Western Europe using ship plume parameterization. Atmos. Chem. Phys., 10, 6645-6660.

IMO, International Maritime Organization, 2009. Revised MARPOL Annex VI - Regulations for the prevention of air pollutions from ships and $NO_x$. Technical code 2008, CPI Books Limited, London.

Janjić, Z.I., 2002. Nonsingular implementation of the Mellor-Yamada level 2.5 scheme in the NCEP meso model. NCEP-Office-Note, 437, 61p.

Lin, Y.-L., Rarley, R.D., Orville, H.D., 1983. Bulk parameterization of the snow field in a Cloud Model. J. Appl. Meteor., 22, 1065-1092.

Madronich, S., 1987. Photodissociation in the atmosphere, 1, actinic flux and the effects of ground reflections and clouds. J. Geophys. Res., 92, 9740-9752.

Matthias, V., Bewersdorff, I., Aulinger, A. and Quante, M., 2010. The contribution of ship emissions to air pollution in the North Sea regions. Environ. Pol., 158, 2241-2250.

Mlawer, E.J., Taubman, S.J., Brown, P.D., Iacono, M.J., Clough, S.A., 1997. Radiative transfer for inhomogeneous atmospheres: RRTM, a validated correlated-k model for the longwave. J. Geophys. Res., 102D, 16663-16682.

Möhler, O. and Arnold, F., 1992. Gaseous sulfuric acid and sulfur dioxide measurements in the Arctic troposphere and lower stratospheres: implications for hydroxyl radical abundances. Geophys. Res. Lett., 19, 1763-1766.

Mölders, N., Tran, H.N.Q., Quinn, P., Sassen, K., Shaw, G.E., Kramm, G., 2011. Assessment of WRF/Chem to capture sub-Arctic boundary layer characteristics during low solar irradiation using radiosonde, SODAR, and station data, Atmos. Pol. Res., 2, 283-299.

Payan, S., Camy-Peyret, S., Jeseck, P., Té, Y., Pfeilsticker, K., Bösch, H., Fitzenberger, R., Rudiger, H. and Lefèvre, F., 2000. Arctic profiles of HCl, $HNO_3$ and $NO_2$ measured during THESEO 2000 by the LPMA/DOAS balloon payload. THESEO 2000 campaign. http://www.nilu.no/projects/theseo2000/palermo.html

Peckham, S.E., Fast, J.D., Schmitz, R., Grell, G.A., Gustafson, W.I., McKeen, S.A., Ghan, S.J., Zaveri, R., Easter, R.C., Barnard, J., Chapman, E., Salzmann, M., Wiedinmyer, C., Freitas, S.R., 2009. WRF/Chem Version 3.1 User's Guide, 78p.

Richter, A., Eyring, V., Burrows, J.P., Bovensmann, H., Lauer, A., Sierk, B., Crutzen, P.J., 2004. Satellite measurements of $NO_2$ from international shipping emissions. Geophys. Res. Lett., 31, L23110.

Schell, B., Ackermann, I.J., Hass, H., Binkowski, F.S., Ebel, A., 2001. Modeling the formation of secondary organic aerosol within a comprehensive air quality model system. J. Geophys. Res., 106, 28275-28293.

Schreier, M., Kokhanovsky, A.A., Eyring, V., Bugliaro, L., Mannstein, H., Mayer, B., Bovensmann, H., Burrows, J.P., 2006. Impact of ship emissions on the microphysical, optical and radiative properties of marine stratus: a case study. Atmos. Chem. Phys., 6, 4925–4942.

152

Simpson, D., Guenther, A., Hewitt, C.N., Steinbrecher, R., 1995. Biogenic emissions in Europe 1. Estimates and uncertainties. J. Geophys. Res., 100D, 22875-22890.

Skamarock, W.C., Klemp, J.B., Dudhia, J., Gill, D.O., Barker, D.M., Duda, M.G., Huang, X.-Y., Wang, W., Powers, J.G., 2008. A description of the Advanced Research WRF version 3. NCAR/TN, 125p.

Stockwell, W.R., Middleton, P., Chang, J.S., Tang, X., 1990. The second-generation regional acid deposition model chemical mechanism for regional air quality modeling. J. Geophys. Res., 95, 16343-16367.

Streets, D.G., Guttikunda, S.K., Carmichael, G.R., 2000. The growing contribution of sulfur emissions from ships in Asian waters, 1988-1995. Atmos. Environ., 34, 4425-4439.

Tran, T.T., Newby, G., Mölders, N., 2011. Impacts of emission changes on sulfate aerosols in Alaska. Atmos. Environ., 45, 3078-3090.

Vutukuru, S., Dabdub, D., 2008. Modeling the effects of ship emissions on coastal air quality: A case study of southern California. Atmos. Environ., 42, 3751–3764.

Wesely, M.L., 1989. Parameterization of surface resistances to gaseous dry deposition in regional-scale numerical models. Atmos. Environ., 23, 1293-1304.

Table 5.1 Fractional bias ($FB = \frac{(\overline{Co} - \overline{Cp})}{0.5(\overline{Co} + \overline{Cp})}$; where $\overline{Co}$ and $\overline{Cp}$ are observed and predicted mean values), normalized mean-square-error (NMSE), correlation (R) and factor of two agreement. Results for $SO_2$ and $SO_4^{2-}$-aerosol from Tran et al. (2011)

| | | Denali-Park IMPROVE | Denali-Park CASTNET | Poker-Flat CASTNET |
|---|---|---|---|---|
| $NO_3^-$-aerosol | FB | 0.98 | -1.17 | -0.22 |
| | NMSE | 3.04 | 3.16 | 0.78 |
| | R | 0.65 | 0.19 | 0.32 |
| | FAC2 (%) | 17% | 20% | 55% |
| $SO_2$ | FB | No data available | -1.03 | -0.72 |
| $SO_4^{2-}$-aerosol | FB | 1.63 | -0.50 | 0.02 |
| | FAC2 (%) | 17% | 40% | 75% |

Table 5.2 Hourly average $SO_2$- and $NO_x$-emissions, sulfur- and nitrogen-compound concentrations in the first WRF-Chem model layer above ground and vertical-integrated over the ISL, ECA and AK

| | | $SO_2$-emission (mol km$^{-2}$ h$^{-1}$) | $SO_2$ (ppt) | $SO_4^{2-}$-aerosol (ng kg$^{-1}$) | $SO_4^{2-}$-in-cloud (ng kg$^{-1}$) | $NO_x$-emission (mol km$^{-2}$ h$^{-1}$) | $NO_x$ (ppt) | $NO_3^-$-aerosol (ng kg$^{-1}$) | $NO_3^-$-in-cloud (ng kg$^{-1}$) | $PM_{2.5}$ (ng m$^{-3}$) |
|---|---|---|---|---|---|---|---|---|---|---|
| Near-surface | ISL | $39.5\times10^{-2}$ | 51.5 | 74.3 | 97.8 | $111\times10^{-2}$ | 194 | 7.5 | 1.2 | 106 |
| | ECA | $8.3\times10^{-2}$ | 34.0 | 59.1 | $2.7\times10^{-3}$ | $30.9\times10^{-2}$ | 144 | 5.7 | $7.9\times10^{-3}$ | 86.3 |
| | AK | $2.2\times10^{-2}$ | 33.0 | 24.6 | 18.3 | $7.9\times10^{-2}$ | 73.9 | 0.6 | 0.2 | 35.0 |
| Vertical-integrated | ISL | $39.5\times10^{-2}$ | 687 | 3490 | 97.4 | $111\times10^{-2}$ | 1150 | 40.5 | 52.2 | 2190 |
| | ECA | $8.3\times10^{-2}$ | 618 | 3220 | 51.4 | $30.9\times10^{-2}$ | 1020 | 34.5 | 29.4 | 1920 |
| | AK | $2.2\times10^{-2}$ | 601 | 2990 | 16.7 | $7.9\times10^{-2}$ | 626 | 14.2 | 5.8 | 1610 |

Table 5.3 Hourly vertical-integrated differences of sulfur- and nitrogen-compound and total $PM_{2.5}$ concentrations over various regions

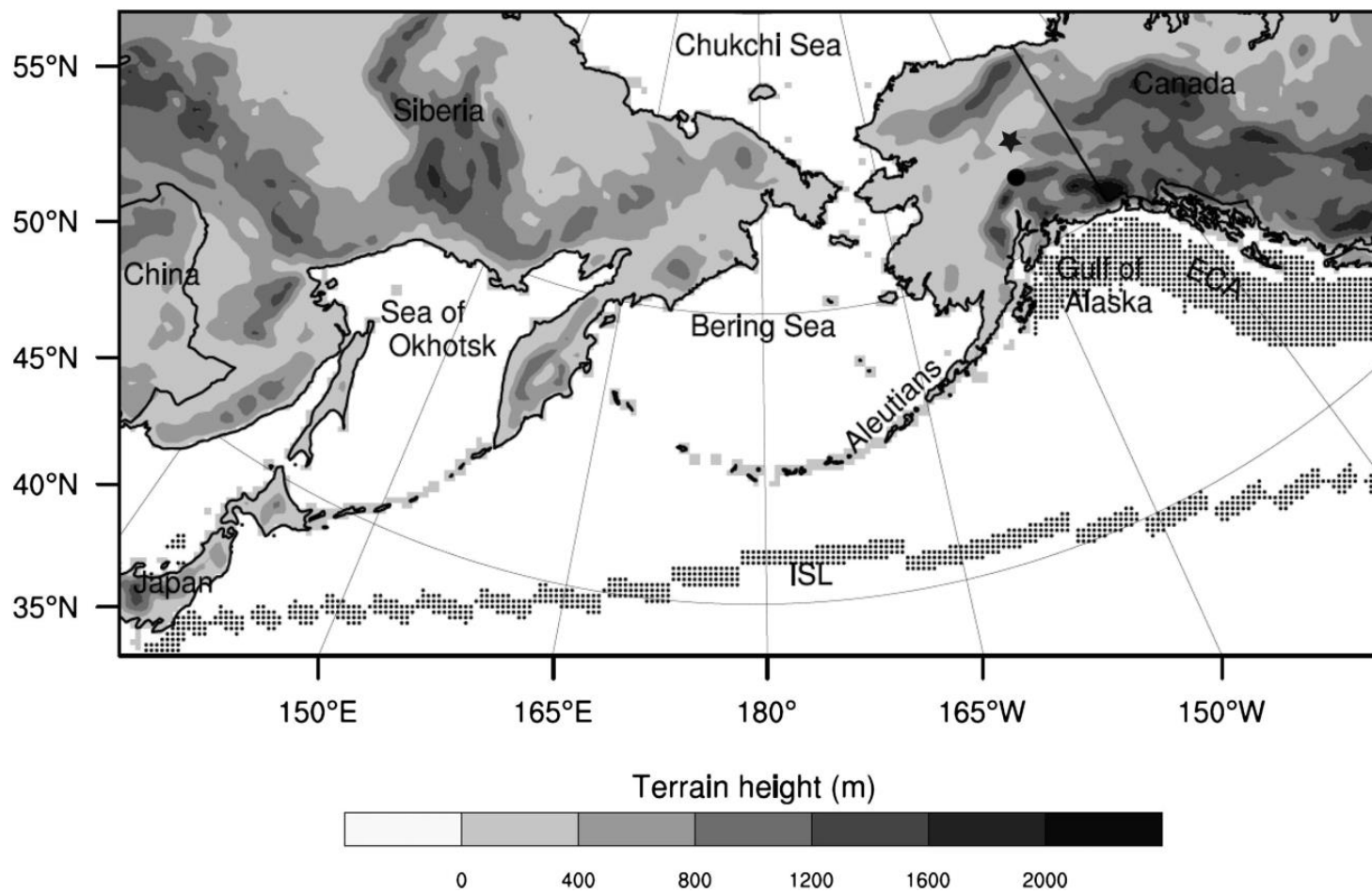| Species | ECA1-REF | | | ECA2-ECA1 | | | ECA2-REF | | |
|---|---|---|---|---|---|---|---|---|---|
| | ISL | ECA | AK | ISL | ECA | AK | ISL | ECA | AK |
| $\Delta SO_2$ (ppt) | -38.4 | -59.4 | -2.3 | -7.1 | -1.3 | -1.4 | -45.5 | -72.2 | -3.5 |
| $\Delta SO_4^{2-}$-aerosol (ng kg$^{-1}$) | -9.3 | -14.6 | -1.0 | -0.5 | -3.1 | $-3.3\times10^{-2}$ | -11.4 | -17.7 | -1.2 |
| $\Delta SO_4^{2-}$-in-cloud (ng kg$^{-1}$) | -4.3 | -5.5 | -0.5 | 0.4 | 0.4 | $3.9\times10^{-2}$ | -3.9 | -5.1 | -0.4 |
| $\Delta NO_x$ (ppt) | 44.5 | 77.4 | 5.2 | -198 | -182 | -88.7 | -153 | -104 | -37.5 |
| $\Delta NO_3^-$-aerosol (ng kg$^{-1}$) | -1.4 | -0.7 | -0.3 | -3.5 | -2.2 | -0.2 | -4.9 | -2.9 | -0.4 |
| $\Delta NO_3^-$-in-cloud (ng kg$^{-1}$) | -1.5 | $-9.2\times10^{-2}$ | -0.2 | -6.4 | -3.2 | -0.6 | -7.9 | -3.3 | -0.8 |
| $\Delta PM_{2.5}$ (ng m$^{-3}$) | -12.8 | -17.9 | -0.8 | -2.9 | -4.4 | $-1.7\times10^{-2}$ | -14.7 | -22.1 | -0.8 |

Fig. 5.1 Schematic view of the model domain, terrain height, and location of the ISL and assumed ECA. The dot and star indicate the grid-cells holding the Denali Park and Poker Flats chemical monitoring sites.
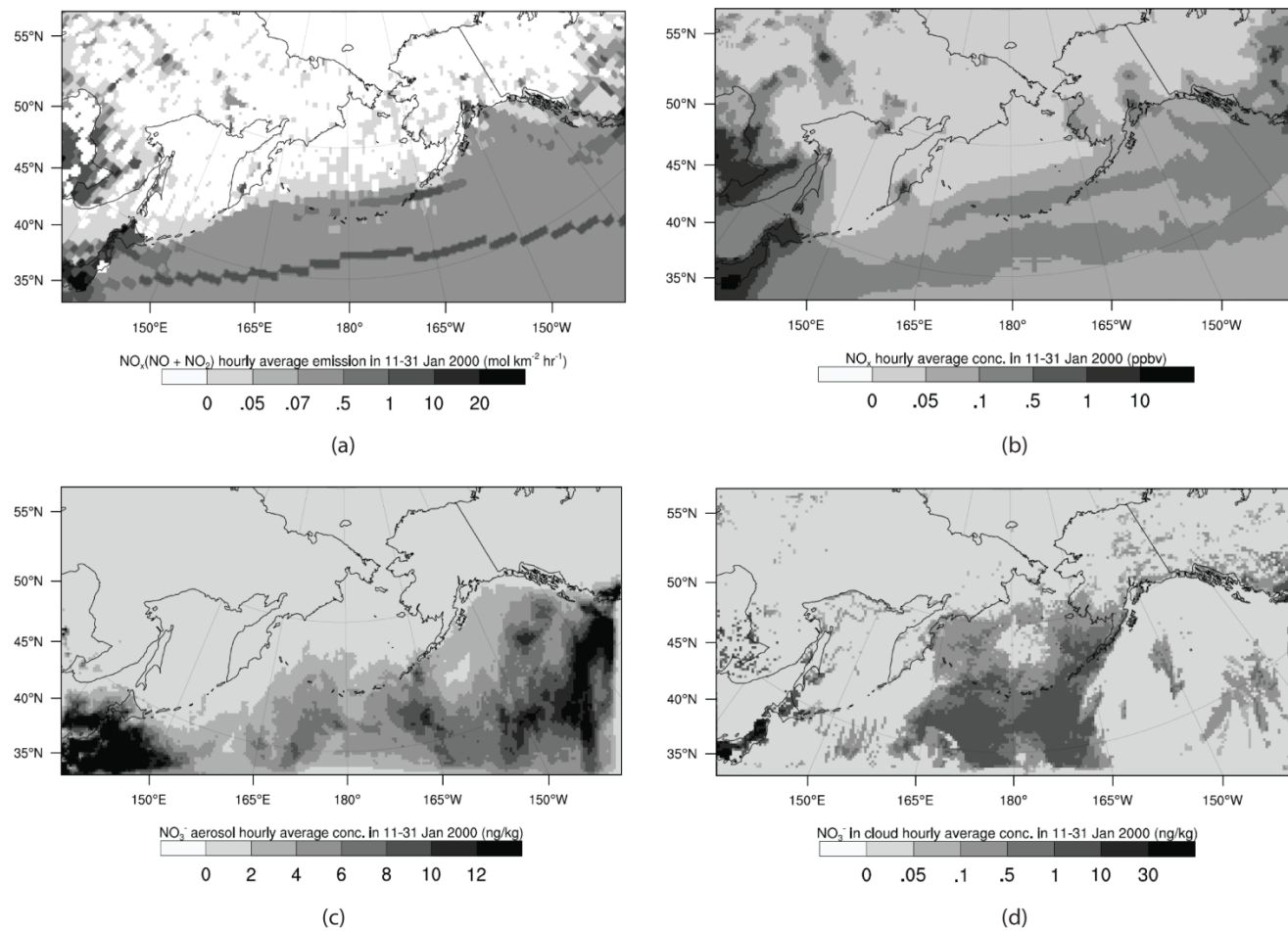
Fig. 5.2 Near-surface hourly averaged (a) NO$_x$-emissions, (b–d) nitrogen-compound concentrations, (e) sulfate-aerosol concentrations, and (f) ammonium-aerosol concentrations as obtained by REF. SO$_2$-emission and SO$_2$-concentration distributions look similar to those of NO$_x$.
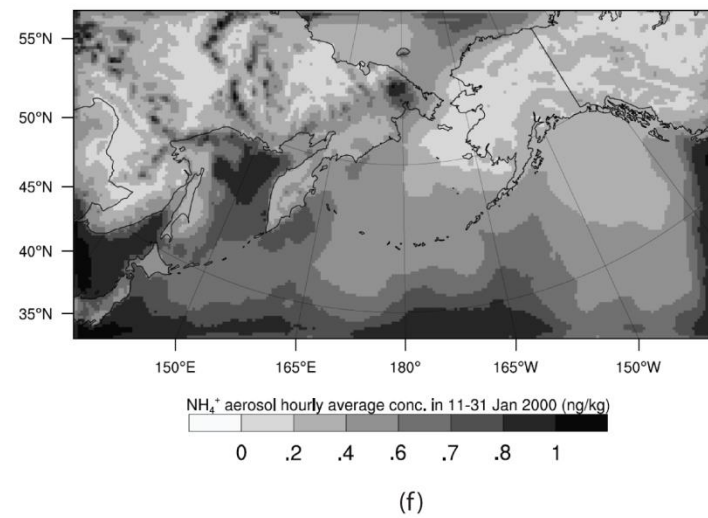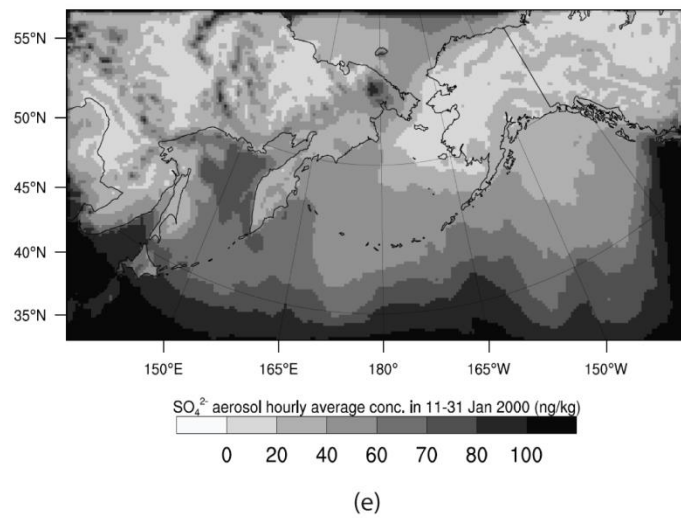
SO₄²⁻ aerosol hourly average conc. in 11-31 Jan 2000 (ng/kg)

0   20   40   60   70   80   100

(e)

NH₄⁺ aerosol hourly average conc. in 11-31 Jan 2000 (ng/kg)

0   .2   .4   .6   .7   .8   1
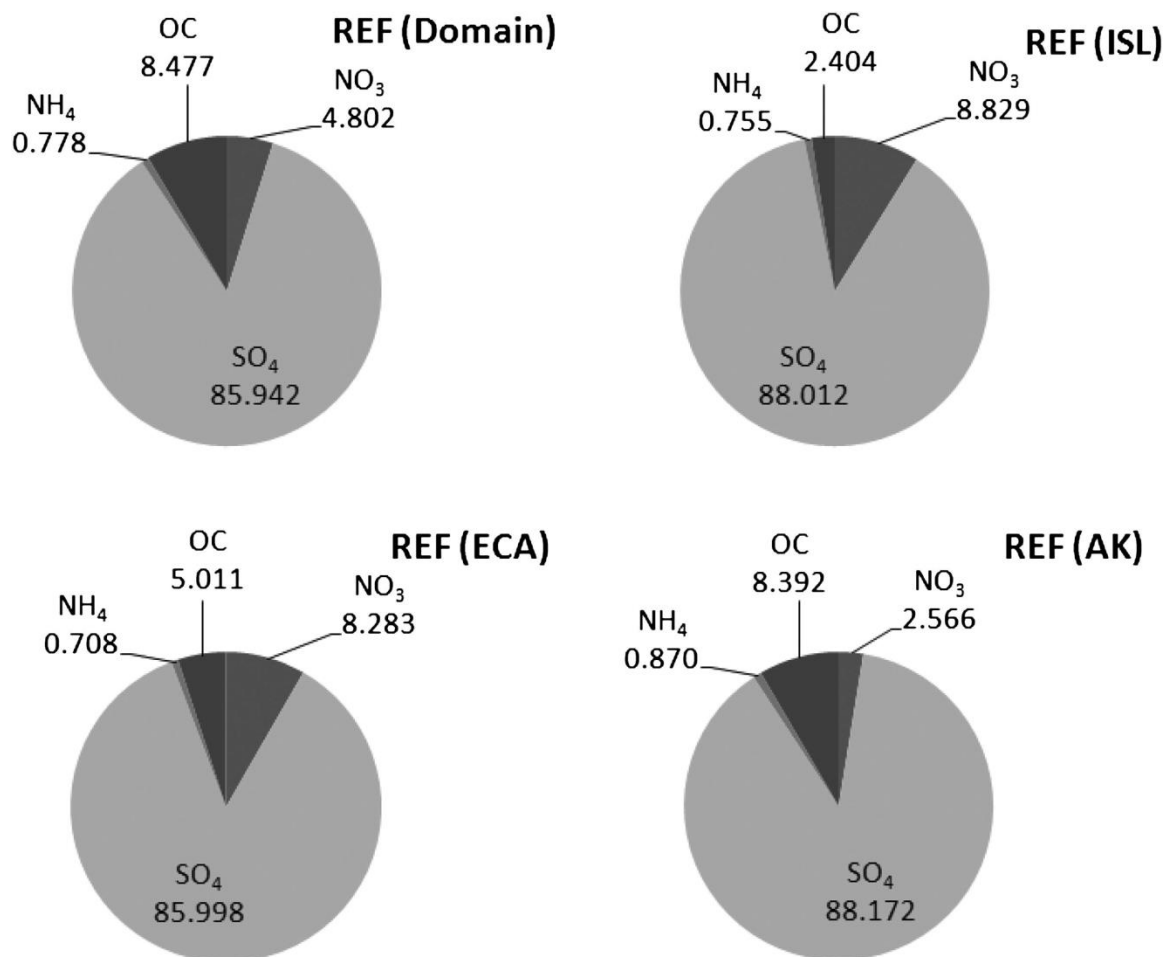
(f)

Fig. 5.2. (Cont.).

Fig. 5.3 PM$_{2.5}$-speciation in the first layer above ground as obtained by REF. Speciation for ECA1 and ECA2 looks similar.
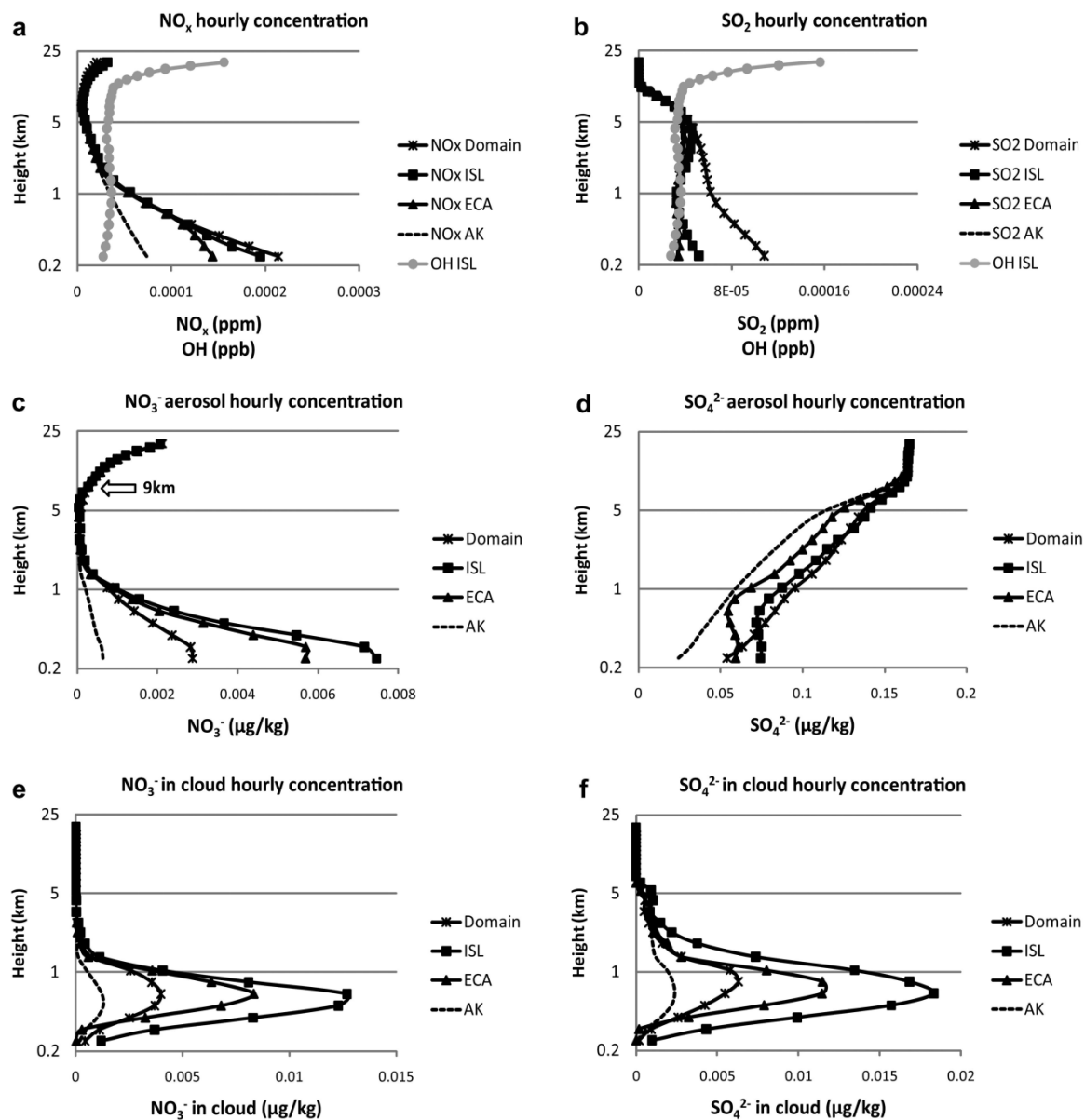
160



Fig. 5.4 Vertical profiles of OH over the ISL, sulfur-(right) and nitrate-compound (left) concentrations averaged over the regions and episode as obtained by REF. OH-profiles over the ECA and AK look similar to that over the ISL.
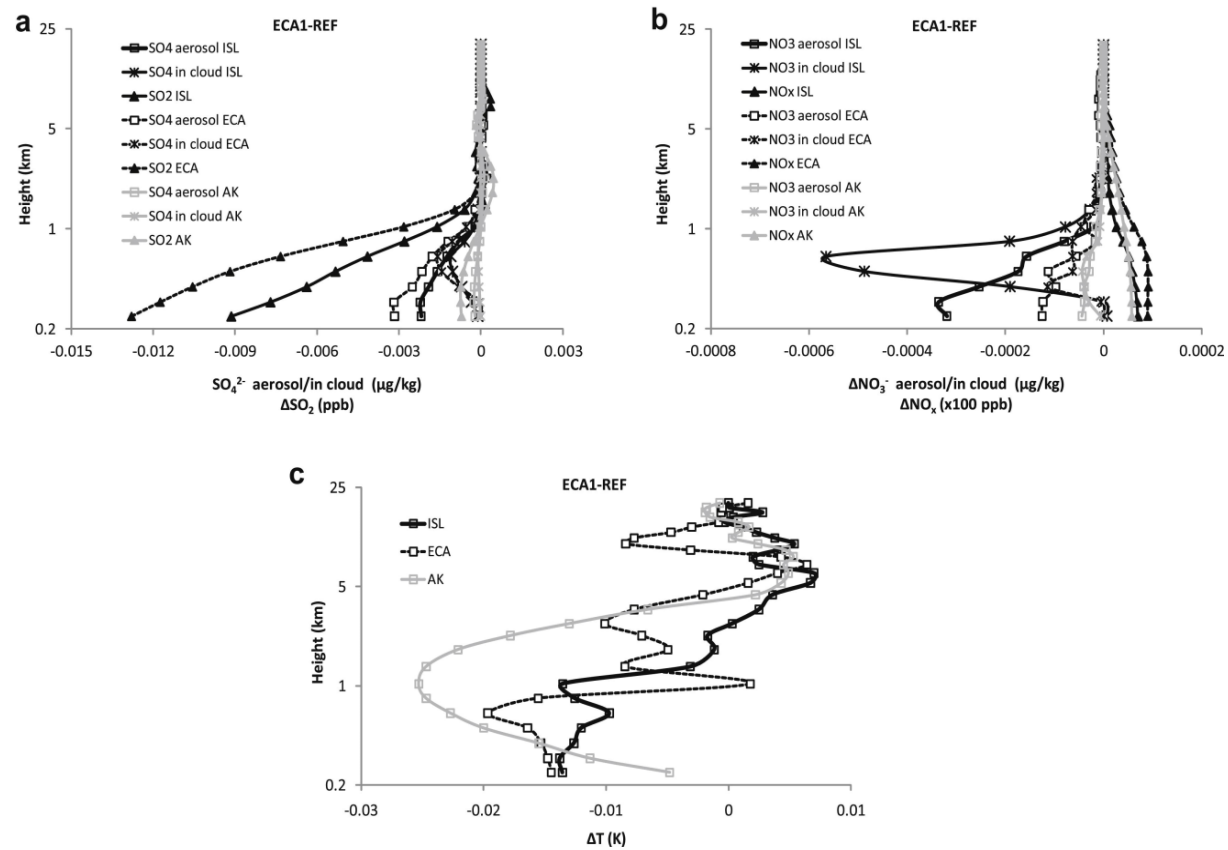
Fig. 5.5 Vertical profiles of hourly average differences ECA1-REF of various (a) sulfur-, and (b) nitrogen-compound concentrations, and (c) hourly average temperature differences ECA1-REF averaged over the ISL, ECA and AK.
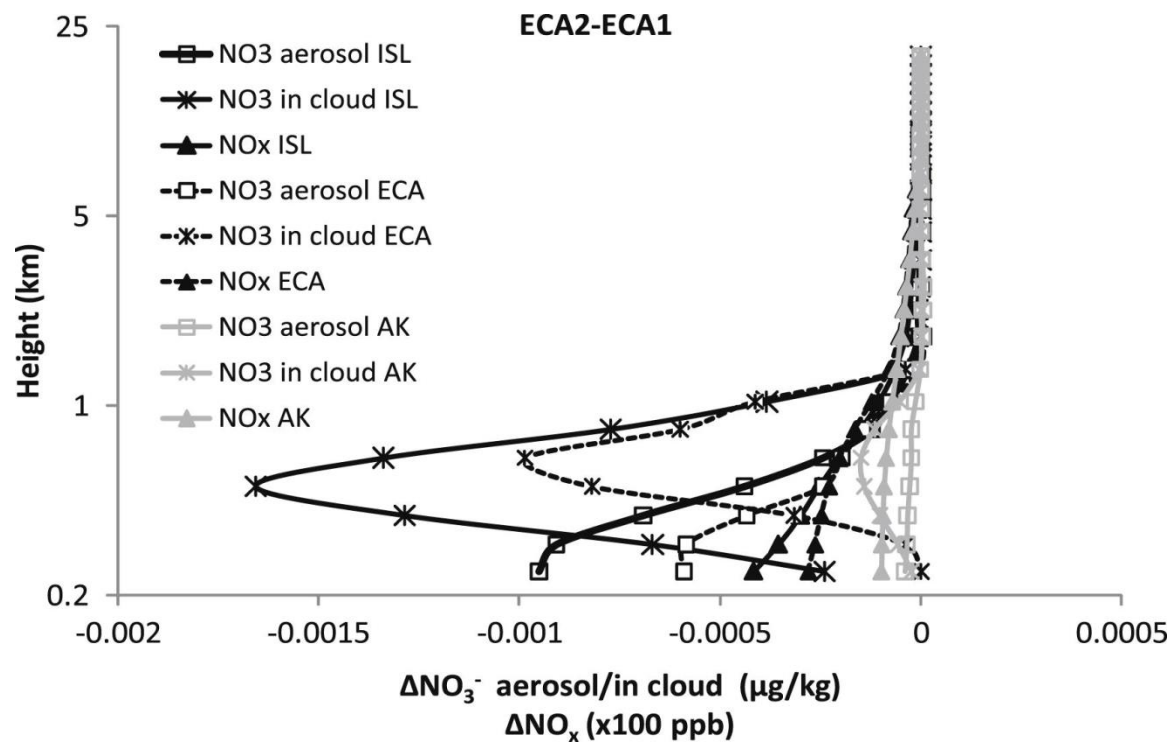
162



Fig. 5.6. Hourly average differences ECA2-ECA1 of various nitrogen-compound concentrations.
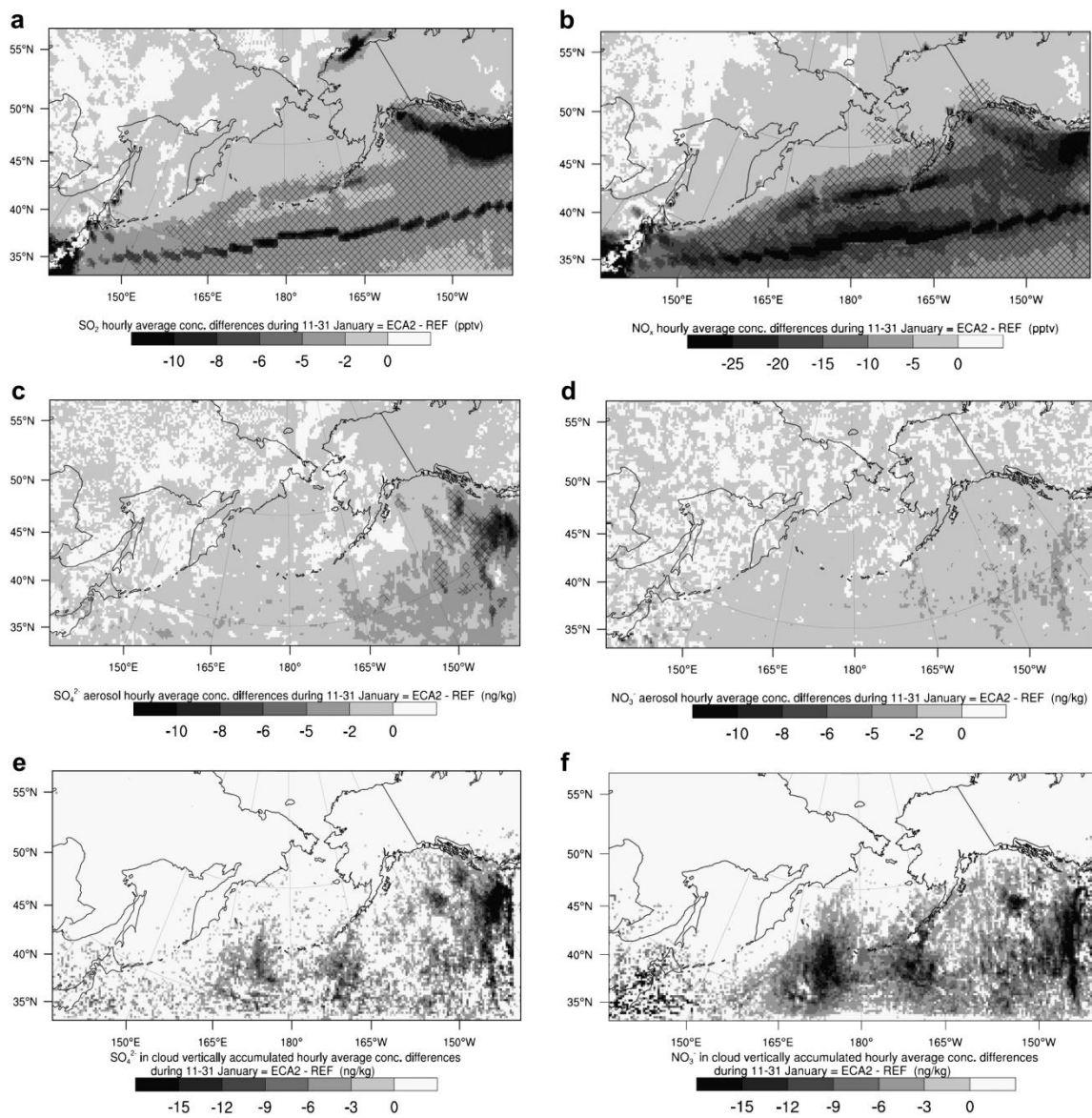
Fig. 5.7 (a–d) Average differences of sulfur-compound ECA2-REF (left) and nitrogen-compound (right) concentrations for January 11–31 in the first layer above ground. (e–f) Sulfate- and nitrate-in-cloud differences integrated over the grid-column. Hatching indicates significant differences at the 95% confidence level: (a) $SO_2$, (b) $NO_x$, (c) sulfate-aerosol, (d) nitrate-aerosol, (e) sulfate-in-cloud, and (f) nitrate-in-cloud
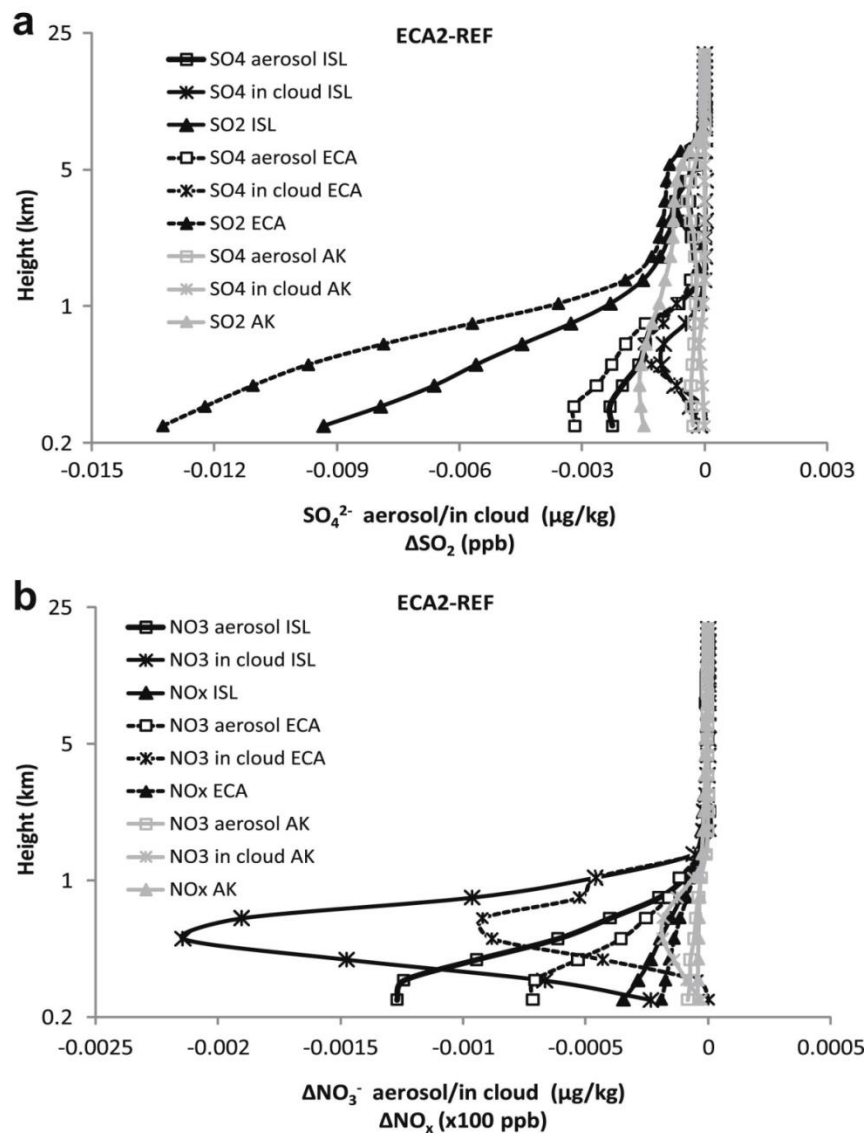
Fig. 5.8 Vertical profiles of hourly average differences ECA2-REF of (a) sulfur-compound and (b) nitrogen-compound concentrations averaged over the ISL, ECA and AK

# Chapter 6 Impacts of wildfire emissions and their changes on PM$_{2.5}$ concentrations and speciation in Alaska [1]

## Abstract

Alaska-modified Weather Research and Forecasting model coupled with an inline chemistry package (WRF/Chem) simulations were performed assuming biogenic, anthropogenic emissions and meteorological conditions for 2008 and alternatively wildfire emissions for weak (June 2008) and strong (June 2004) Alaska fire activities. These simulations were used to investigate the impacts of wildfire emission changes on PM$_{2.5}$ concentrations and speciation in Alaska. The relative importance of wildfire versus anthropogenic emissions was also examined under weak and strong fire activity scenarios for various regions of Alaska. The analysis focused on Interior Alaska and three coastal regions. Wildfire emission increases in Interior Alaska led to dramatic increases in PM$_{2.5}$ concentrations and percentages of organic carbon components of PM$_{2.5}$ speciation in Interior Alaska, and the northern and western coastal regions whereas the PM$_{2.5}$ distributions along the southern coast were less impacted. Siberian wildfire emission changes did not significantly impact aerosol concentrations in Alaska during this period. Under the strong fire activity scenario, local wildfires contributed 52% of PM$_{2.5}$ concentrations with the maxima $\geq$ 90% during extreme wildfire events in Interior Alaska. Interior wildfire emissions contributed to PM$_{2.5}$ concentrations comparable to

[1] Tran, T.T, Cahill, C.F., 2013. Impacts of wildfire emissions and their changes on PM$_{2.5}$ concentrations and speciation in Alaska. Atmos. Environ., in preparation for submission.

anthropogenic emission contributions along the northern coast of Alaska. Wildfire emission contributions to $PM_{2.5}$ concentrations were small across the western coast and negligible along the southern coast of Alaska even under strong fire activity scenarios. Under the weak fire activity scenario, anthropogenic emissions contributed ≥70% and ~43% of $PM_{2.5}$ concentrations in the coastal regions and Interior Alaska, respectively. Interior wildfires contributed ~16% to $PM_{2.5}$ concentrations in Interior Alaska and ~0% in the coastal regions.

**6.1. Introduction**

Denali National Park in Alaska is one of the most pristine areas of the United States (Karl et al., 2011). It is categorized as a Class I Area under the Clean Air Act impacted by the Regional Haze Rule (EPA, 2013). According to National Park Service (2013), Denali NP has the best visibility and cleanest air measured in the country. Wildlife and the natural ecosystem in the Denali NP are a valuable asset to the state and nation. At this Class I Area, a national visibility goal as "the prevention of any future and remedying of any existing impairment of visibility in mandatory Class I Federal areas, which impairment results from man-made air pollution" stated in Clean Air Act Amendments of 1977 must be attained (ADEC, 2012). However, concentrations of sulfate ($SO_4^{2-}$) and organic carbon (OC) containing aerosol particles with diameters $\leq 2.5$ $\mu$m (fine aerosols) measured during high insolation periods (June-August) at the Interagency Monitoring of Protected Visual Environment (IMPROVE) networks have increased in Denali NP over the last decades, whereas the concentrations of these two components have decreased in the wilderness areas along the Gulf of Alaska (Malm et al., 1994; IMPROVE, 2013) (Fig. 6.1). The rate of OC-concentration changes were about an order of magnitude larger than the rate of $SO_4^{2-}$-concentration changes (Fig. 6.1). Fine aerosols could cause adverse impacts to human health such as heart and lung diseases that could lead to premature deaths (Kappos et al., 2004; Dominici et al., 2006; Pope and Dockery, 2006) or cause adverse impacts to the ecosystem such as increasing acid deposition onto the vegetation or acid loading into the water bodies and impaired visibility impairment (Bulger et al., 1998; NAPAP, 2005; Han et al., 2012). In wilderness

areas like Denali NP, where the human population density is extremely low but wildlife is a valuable possession, the environmental impacts of fine aerosols on the ecosystem are of more concern than their human health impacts. The increasing trends in these compounds at Denali NP are of concern because degrading air quality at this site could cause adverse impacts to the park's ecosystem and visibility. Therefore, the reasons for the observed increases in aerosol concentrations in the park need to be quantified to determine if it is possible to control the sources of the aerosol and return the park's visibility to 'pristine'.

While the air in Denali NP is to be protected from emissions due to anthropogenic activities; it cannot be protected from the impacts of emissions from natural wildfires in Interior Alaska. Most of fires in Alaska are due to naturally occurring lightning ignitions (Barney, 1971; Bieniek, 2007). It is well known that local wildfire emissions strongly affect air quality of Alaska (Duck et al., 2007; Grell et al., 2011; Hecobian et al., 2011). Wildfire smoke plumes are subject to long-range transport, especially at upper altitudes due to the high injection height of fire emissions (Grell et al., 2011; Hecobian et al., 2011; Sessions et al., 2011). Located downwind of the prevailing westerlies from Siberia, Alaska's air quality could be impacted not only by local wildfire emissions, but also potentially by Siberian wildfire emissions. For a typical year in Siberia, Belov (1976) and Furyaev (1996) reported that 80% of all fires were surface fires with relatively low injection heights (~1300 m above sea level (Jet Propulsion Laboratory, 2013)), advection of Siberian wildfire plumes to Alaska would be subject to more intense lower

atmospheric scavenging mechanisms, and less impact on Alaskan aerosol particle concentrations may be expected.

Wildfire emissions in both Alaska and Siberia have been increasing over the last decades (Barney, 1971; Soja et al., 1997; Juday et al., 2004) partly due to climate change effects including increases in temperature and decreases in summer precipitation in the boreal regions (Stocks et al., 1998; Stafford et al., 2000). The increases of wildfire emissions are potential cause of observed increases of aerosol concentrations in the Interior Alaska. This study investigates the impacts of Siberian and Alaskan wildfire emissions on the concentration and speciation of particulate matter with aerodynamic diameter $\leq 2.5\mu m$ ($PM_{2.5}$) during summertime (high insolation) conditions in several regions of Alaska. In order to assist air quality protection efforts, the relative importance of wildfire versus anthropogenic emissions under weak versus strong Alaska fire activity scenarios is addressed by calculating the contribution of anthropogenic and wildfire emissions to $PM_{2.5}$ concentrations in various regions across Alaska.

## 6.2. Experimental design

### 6.2.1 Model description

The Alaska-modified Weather Research and Forecasting model (Skamarock et al., 2008) coupled with an inline chemistry package (WRF-Chem; Grell et al., 2005; Peckham et al., 2009) was used in this study, since this model was proved by previous studies to capture extreme weather situations and chemistry in Arctic and sub-Arctic regions well (Mölders, 2008; Hines and Bromwich, 2008; Mölders et al., 2012; Tran et

al., 2011). The following model setup was selected. Lin et al.'s (1983) cloud microphysical parameterization, which considers cloud-water, rainwater, cloud-ice, snow, graupel and hail, served to describe clouds on the resolvable scale. Cumulus convection was parameterized using a modified version of the 3D Grell-Dévényi ensemble scheme (Grell and Dévényi, 2002). The Rapid Radiative Transfer Model (Mlawer et al., 1997) and the Goddard scheme (Chou and Suarez, 1994) were used to simulate long-wave and shortwave radiation, respectively. Direct and indirect radiative impacts of aerosols were considered according to Barnard et al. (2010). Janjić's (2002) parameterizations served to consider the processes in the viscous sub-layer and surface layer. The Mellor-Yamada-Janjić scheme was selected to calculate the turbulence in the atmospheric boundary layer (ABL) and free atmosphere (Mellor and Yamada, 1982; Janjić, 2002). Surface heat and moisture fluxes were calculated by the further-developed version of the NOAH land-surface model (Chen and Dudhia, 2001) that considers frozen soil physics in calculating the soil temperature and moisture states, one canopy layer, fractional snow-cover and fractional sea-ice.

Gas-phase chemistry mechanisms (Stockwell et al., 1990) were simulated by the Regional Acid Deposition Model (RADM2; Chang et al., 1991). Photolysis rates were determined according to Madronich (1987). The Modal Aerosol Dynamics Model for Europe (MADE; Ackermann et al., 1998) in conjunction with the Secondary Organic Aerosol Model (SORGAM; Schell et al. 2001) served to predict mass concentrations of fine aerosol components including sulfate ($SO_4^{2-}$), nitrate ($NO_3^-$), ammonium ($NH_4^+$), sea salt ($Na^+$ and $Cl^-$), organic carbon (OC), black carbon (EC) and unspeciated-$PM_{2.5}$.

Unspeciated-$PM_{2.5}$ was an artificial tracer aerosol species that was considered in WRF-Chem simulations to account for all potential emissions contributing to the total $PM_{2.5}$. This species stemmed from the unspeciated-$PM_{2.5}$ primary emissions, and did not participate in chemical processing and were assumed to be non-absorbing. Soil aerosols were not included in the simulations due to known large errors in WRF-Chem's online calculations of wind-blown dust (Zhao et al., 2010; Saide et al., 2012). Because there were no identifiable dust-emission sources in the model domain (e.g. a desert), including dust calculations in the simulations was unnecessary. MADE/SORGAM treats aerosol physics and chemistry including both gas-phase and aqueous-phase aerosol formation and secondary organic aerosol formation. The treatment of dry deposition is based on Weseley (1989) with the modifications of Mölders et al. (2011).

### 6.2.2 Emissions

Simpson et al.'s (1995) biogenic emission scheme served to calculate the emissions of volatile organic compounds from vegetation and nitrogen from soil inline depending on temperature and photosynthetic active radiation using the U.S Geological Survey land-use classification.

The updated version of Emission Database for Global Atmospheric Research (EDGAR v4.2; EC-JRC/PBL, 2011) $0.1°\times0.1°$ data for 2008 was used for anthropogenic emissions. This dataset included emissions of CO, sulfur dioxide ($SO_2$), nitrogen oxides (NO and $NO_2$), ammonia ($NH_3$) and non-methane volatile organic carbon species (NMVOC). Primary aerosol emission data including elementary carbon (EC), OC, $SO_4^{2-}$,

nitrate ($NO_3^-$) and unspeciated-$PM_{2.5}$ were also included in our simulations. Monthly, weekday/weekend and hourly allocation functions were applied for inland anthropogenic emissions following Mölders (2009) and Veldt (1991) for Alaska and the rest of the domain, respectively. Uniform weekday/weekend and hourly variations for ship emissions were assumed.

Wildfire emissions were estimated by the Brazilian Biomass Burning Emissions Model (3BEM) (Freitas et al., 2005; Longo et al., 2010). 3BEM used near real-time remote sensing fire products as the source for determining fire locations. In the study MOderate-Resolution Imaging Spectrometer (MODIS; Giglio, 2003) datasets were used for wildfire locations due to its high spatial resolution of about 1 km. 3BEM used land use (Belward, 1996; Sestini et al., 2003) and carbon in vegetation (Olson et al., 2000) datasets to determine emission factors, combustion factors and carbon densities for each vegetation type in accordance with the approaches of Ward et al. (1992) and Andreae and Merlet (2001). The mass of each emitted gas or aerosol species was calculated from those factors (see Longo et al. (2010) for more detail). Uniform hourly emissions during each 24h-period were applied for wildfire emissions.

Anthropogenic and biogenic emissions were assigned as surface fluxes in the lowest layer above the ground, since these sources emit pollutants at a temperature close to the ambient air temperature resulting in negligible buoyancy. However, wildfire emissions are always emitted with strong buoyancy due to the hot air released by the burns. Therefore, the effect of plume rise on the wildfire emissions needs to be included. For this, a 1-D time-dependent cloud model (Freitas et al., 2007) with appropriate

boundary conditions provided by WRF-Chem was applied (the host model) to explicitly simulate the plume rise and determine the injection height of the fire smoke plumes. Wildfire emissions were then assigned throughout the vertical column at fire locations from the near-surface layer up to the layer corresponding to the simulated injection height.

### 6.2.3 Simulations

The WRF-Chem model domain in this study encompasses eastern Siberia, Alaska, northwestern Canada, Japan and the North Pacific with 240×120 horizontal grid-points of 30 km grid-increment and 28 vertical stretched layers (Fig. 6.2).

Typically, June has intense wildfire activity in Alaska and Siberia (Mölders, 2008; Stocks et al., 1998). Moreover, the nearly continuous daylight of June leads to unique atmospheric chemistry that could enhance the aerosol formation via photochemical reaction pathways. Reference simulations (REF) were performed that included all emission sources for June 2008 and increased-wildfire activity simulations (IFA) with the same emissions of REF but greater wildfire emission from a different year. Both REF and IFA were initiated with the same meteorological initial and boundary conditions. Therefore, differences between REF and IFA aerosol concentrations are only due to wildfire emission changes.

Alaskan wildfires had minimum and extreme fire activities in 2008 and in 2004, respectively, with the areas burned of 103,649 acres in 2008 and 6,523,182 acres in 2004 (Alaska Department of Forestry, 2012). Therefore, wildfire emission scenarios were

selected from June 2008 (REF) and June 2004 (IFA) for the study because these episodes provided excellent opportunity to exammine the changes in wildfire emissions and their impacts on $PM_{2.5}$ concentration in Alaska.

Contributions of each emission sector to $PM_{2.5}$ concentrations were calculated by comparing results of simulations with and without that emission sector. This method is a commonly applied in most of numerical modeling studies (Chapman et al., 2009; Davis et al., 2001; Tran and Mölders, 2012; Tran, 2012). All of these simulations were initialized with the same meteorological conditions and background concentrations of June 2008. The meteorological conditions were initialized every five days with the $1° \times 1°$, 6 h global final analysis (FNL) data from the National Centers for Environmental Prediction. The FNL data also provided the meteorological boundary conditions. Vertical profiles of background gas and aerosol concentrations representative of Alaska and the North Pacific (Mölders et al., 2011) gave the chemical initial and boundary concentrations. Subsequent simulations were initialized with the chemical fields from the previous simulation.

### 6.2.4 Analysis

The first five days of the simulations served as spin-up of the chemical fields; hence, were discarded from the analysis. The Western Regional Climate Center (WRCC, 2012) meteorological surface station data available at 83 sites within Alaska and standard meteorological data from National Data Buoy Center (NDBC, 2012) available at 15 sites over the North Pacific were used to evaluate the model's performance on simulating the

meteorological quantities of June 2008. Observational data of June 2008, daily-averaged $PM_{2.5}$ concentrations available from the IMPROVE network once every three days at Denali NP and the coastal sites of Tuxedni, Trapper Creek and Simeonof served to evaluate WRF-Chem performance with respect to aerosol emissions and their chemical transformations.

The analysis focused on four regions of Alaska (Fig. 6.2): Interior Alaska, the northern coast of Alaska (NAK), the southern coast of Alaska (SAK) and the western coast of Alaska (WAK). Interior Alaska was considered a wildfire-emission source region whereas three coastal areas (NAK, SAK and WAK) were considered receptors impacted by the transport of compounds from source regions.

Siberia and Japan were considered in the analysis as potential emission-source regions. Because air mass from Siberian and Japan normally cross over the ocean and shipping lanes to reach Alaska (e.g. westerly flows from Siberia occur over the Bering Sea, storms track from southwest to northeast spread through the Aleutians into the Bering Sea (Fett et al., 1993)), an oceanic region around Alaska was included as an "intermediate-zone" (hereafter called INTE; Fig. 6.2) to strengthen the discussion of whether Siberian and Japanese emissions impact Alaskan air quality.

This study focuses on investigating the impact of wildfire emissions on $PM_{2.5}$ concentrations. Therefore, the total $PM_{2.5}$ concentrations discussed in this study included all $PM_{2.5}$ components (i.e., sulfate, nitrate, ammonium, organic carbon, elementary carbon and unspeciated-$PM_{2.5}$) except sodium and chloride components which were considered to be originated from oceanic emissions, not from wildfire emissions in our

simulations. However, when PM$_{2.5}$ speciation is discussed in section 3.4.2, sodium and chloride components are included in the discussion to provide the broader picture of how PM$_{2.5}$ speciation varied in different regions of Alaska with respect to the distances between their locations and the emission sources. Emissions of PM$_{2.5}$ in terms of the primary PM$_{2.5}$ emissions and sum of all precursor gas emissions including SO$_2$, NO$_x$, NH$_3$ and NMVOC are discussed.

The temporal evolution of hourly, regionally averaged, PM$_{2.5}$ concentrations and PM$_{2.5}$ speciation between REF and IFA are compared to investigate the impact of wildfire emissions on PM$_{2.5}$ distributions in our four regions over Alaska. A Student's t-test (Student, 1908) at the 95% confidence level was applied to hourly averaged concentration differences (IFA-REF) of PM$_{2.5}$ to test the null hypothesis that the changing wildfire emissions did not affect PM$_{2.5}$ concentrations and speciation in Alaska.

The contribution of wildfire emissions to PM$_{2.5}$ concentrations in Alaska was examined by comparing the PM$_{2.5}$ concentrations between the simulations with and without wildfire emissions (Eq. 6.1). Similar calculations were used to estimate the anthropogenic emission contributions. These calculations were conducted for both the REF and IFA cases.

$$Contribution = \frac{C_{Base} - C_{Test}}{C_{Base}} \times 100\% \qquad\qquad (Eq.\ 6.1)$$

Here $C_{Base}$ were the PM$_{2.5}$ concentrations obtained from the simulations including all emission sources (REF or IFA) and $C_{Test}$ were the PM$_{2.5}$ concentrations obtained from the test simulations without the emissions of the source of interest (i.e. anthropogenic or wildfires).

## 6.3. Results

### 6.3.1 Model performance evaluation

WRF-Chem performed well at simulating the meteorological conditions over Alaska. It successfully captured the temporal evolutions of sea-level pressure (SLP), air temperature (T), downward shortwave radiation (SW) and relative humidity (RH) with very high to high correlation skill-scores of 0.900, 0.714, 0.567 and 0.500, respectively (Table 6.1; Fig. 6.3). WRF-Chem underestimated T by 0.5 K and overestimated SLP, SW, RH, precipitation and wind-speed (v) by 1 hPa, 66 W m$^{-2}$, 1.6 %, 3.3 mm and 2.1 m s$^{-1}$, respectively. WRF-Chem performed well to capture the main wind-direction over Alaska with a small bias of 7$^o$, but only broadly captured the temporal evolution. The relatively low correlation skill-scores for precipitation may partly be related to the large number of missing values in the observational data. Wind-speed and direction are strongly affected by topography. WRF-Chem uses the grid-cell average terrain height and hence cannot capture any subgrid-scale local terrain effects that influence the observed wind-speed and direction. In general, WRF-Chem had a better performance at simulating meteorological quantities over the ocean than over inland areas (e.g. Alaska) because there was no sub-grid scale terrain over the ocean to impact the model performance's (Table 6.1). WRF-Chem was better at simulating the wind-speed and wind direction over the NDBC stations in the North Pacific than over Alaska with higher correlation skill-scores (0.651 for v and 0.431 for wind direction) and lower biases (-0.9 m s$^{-1}$ for v and -4$^o$ for wind direction). Model performance in simulating temperature over NDBC sites (ocean), however, was slightly weaker than over WRCC sites (land).

WRF-Chem simulated the daily averaged $PM_{2.5}$ concentrations averaged over the coastal sites in the Gulf of Alaska better than in Denali NP site (Fig. 6.4). On average over the three coastal IMPROVE sites, the fractional bias ($FB = \frac{(\overline{Co} - \overline{Cp})}{0.5(\overline{Co} + \overline{Cp})} \times 100\%$) and % of the simulated $PM_{2.5}$ concentrations within a factor of two (FAC2 = $0.5 \leq \frac{C_p}{C_o} \leq 2$) of observed values were -27% and 88%, respectively, indicating very good performance for an air-quality model (Chang and Hanna, 2004). However, FB and FAC2 for the Denali NP site were 60% and 20%, respectively, which were outside the defined "good" performance ranges (FB within ±30% and FAC2 ≥50%, Chang and Hanna, 2004). The overestimation of $PM_{2.5}$ concentrations at the Denali NP site may be due to overestimating the advection of compounds to Denali by the model's ignoring the impacts of sub-grid scale terrain complexity on at the highly topographically variable region around the Denali NP site.

### 6.3.2 Emissions and synoptic situation

### 6.3.2.1 Synoptic situation of June 2008

Surface weather analysis maps of the West-East Pacific and Alaska provided by National Climatic Data Center (NCDC; http://nomads.ncdc.noaa.gov/ncep/NCEP) indicated that the synoptic situation over the entire model domain for June 2008 had the common features of the typical summer climatology regime of storm tracks and surface winds for the Bering Sea, Aleutian Islands and Gulf of Alaska as described by Fett et al. (1993), for instance, westerly flows occur over the Bering Sea, storms track from

southwest to northeast spread through the Aleutians into the Bering Sea and storms track occurred into the Gulf of Alaska from the region south of the Aleutians. The model captured those features very well except that it slightly overestimated wind-speed (as discussed in section 3.1).

The surface analysis maps showed a westerly flow over Siberia and across the Bering Sea that occurred during 8-15 June. This flow could potentially transport aerosols and aerosol precursors from Siberia toward Alaska. Over the Aleutian Islands, during the entire study period, the wind directions were mostly from the southwest. These flows could carry the air masses potentially polluted by Japan or ship emissions. The Gulf of Alaska regularly experienced storms moving from south of the Aleutians (days 6 to 9, 14 to 16, and 21 to 23 June). Therefore, the air over the coastal areas along the Gulf of Alaska would be strongly impacted by maritime air masses containing shipping lane emissions. WRF-Chem performed well at capturing very well the main wind direction and the storm appearances over the Pacific (Fig. 6.5).

The same meteorological initial and boundary conditions of REF were applied for IFA to exclude the impact of meteorological changes on $PM_{2.5}$ distributions from our analysis, i.e. assumption made that over Alaska, synoptic conditions between June 2008 and June 2004 were approximately the same. Surface analysis synoptic maps of Alaska (Plymouth State Weather Center, 2012) indicated that June 2004 and June 2008 had similar wind patterns with calm to light winds (<5 m/s) over Interior Alaska and stronger winds (7.5-10 m/s) over the coastal areas (Fig. 6.6).

**6.3.2.2 Emissions**

In REF, the emission situation was characterized by high anthropogenic emissions over Japan and the North Pacific shipping lanes and high wildfire emissions over Siberia. Anthropogenic emissions over Alaska were relatively small compared to the Japanese and ship emissions (Fig. 6.7a$_1$, a$_2$).

Anthropogenic PM$_{2.5}$ could be from gas-to-particle conversion of precursor gases (SO$_2$, NO$_x$, NH$_3$ and NMVOC) and primary PM$_{2.5}$ (SO$_4^{2-}$, NO$_3^-$, EC, OC, unspeciated-PM$_{2.5}$; emission data for NH$_4^+$ were not available). The sum of hourly, regionally-averaged emissions of all PM$_{2.5}$ precursor gases ($Emis._{(SO_2+ NH_3+NO_x+NMVCO)}$) from anthropogenic sources over Japan, INTE, SAK, WAK, Interior Alaska and NAK were 12.85, 0.34, 0.27, 0.22, 0.19 and 0.18 mol km$^{-2}$ hr$^{-1}$, respectively. Primary PM$_{2.5}$-aerosol emissions ($Emis._{(SO_4^{2-}+NO_3^-+EC+OC+unspec\_PM_{2.5})}$) were 18.14, 0.66, 0.19, 0.09, 0.02 and 0.02 g km$^{-2}$ hr$^{-1}$ over Japan, INTE, SAK, WAK, Interior Alaska and NAK, respectively.

While anthropogenic emissions occurred only in the near-surface layer, wildfire emissions occurred throughout the vertical column from near-surface layer up to the layer corresponding to simulated smoke plume injection height. In the WRF-Chem simulations, the daily-averaged injection heights of the wildfire emissions over Siberia varied from ~750 to 8000 m above ground level depending on fire size and meteorological conditions, which were higher the observed injection heights of wildfire emissions over Siberia in 2008 reported by Jet Propulsion Laboratory (2013) (~ 719 to 1820 m above sea level). Over Siberia the column-integrated PM$_{2.5}$ precursor emissions from wildfires were 6.55 mol km$^{-2}$ hr$^{-1}$, whereas the anthropogenic sources emitted only

0.46 mol $km^{-2}$ $hr^{-1}$. Also, the primary $PM_{2.5}$ emissions from wildfires were 21.60 g $km^{-2}$ $hr^{-1}$ over Siberia. In June 2008, there was no noticeable wildfire emission in Alaska (Fig. 6.7$a_2$) except for some relatively low wildfire emissions on 14-15 and 21-22 June (Fig. 6.8b).

Anthropogenic sources emitted higher amounts of inorganic $PM_{2.5}$ precursor gases (e.g., $SO_2$, $NO_x$ and $NH_3$) than organic $PM_{2.5}$ precursor gases (NMVOC), whereas wildfire sources emitted higher amounts of NMVOC than inorganic $PM_{2.5}$ precursors. The sum of $SO_2$, $NO_x$ and $NH_3$ anthropogenic emissions was approximately 4 times higher than the NMVOC anthropogenic emissions. Conversely, the NMVOC emissions from wildfires were approximately 4.5 times higher than the sum of those inorganic gases from wildfires. Therefore, the speciation of $PM_{2.5}$ impacted by anthropogenic sources would be indicated by higher percentages of inorganic species (i.e., $SO_4^{2-}$, $NO_3^-$ and $NH_4^+$) than organic species (i.e., OC); whereas, high OC percentages in $PM_{2.5}$ speciation would be an indicator of wildfire emission impacts. It is well known that the low ratio EC/OC due to high OC concentrations is usually used as wildfire smoke tracer (Andreae and Merlet, 2001; Park et al., 2003; Ames et al., 2004).

IFA was assumed to have the same anthropogenic emissions as REF; however, the wildfire emission situation of IFA was very different from the wildfire emission situation in REF. In IFA, there were very high wildfire emissions in Alaska and almost no wildfire emissions in Siberia (Fig. 6.7$b_1$, $b_2$). In IFA, over Interior Alaska the hourly averaged, column-integrated $PM_{2.5}$ precursor and primary $PM_{2.5}$ emissions from wildfires were 4.57 mol $km^{-2}$ $hr^{-1}$ and 28.80 g $km^{-2}$ $hr^{-1}$, respectively. In this emission scenario,

$PM_{2.5}$ precursor emissions from wildfires were 25 times higher than those of anthropogenic sources in Interior Alaska. There were no wildfire emissions in NAK, SAK and WAK during this period. Wildfire emissions over Siberia in REF and over Interior Alaska in IFA increased toward the end of the month (Fig. 6.8a).

### 6.3.3 Description of the situation in REF

For REF simulations, in Alaska, $PM_{2.5}$ concentrations were distributed homogeneously among the regions of interest. Over the entire episode, near-surface hourly, regionally-averaged $PM_{2.5}$ concentrations for SAK, WAK, Interior Alaska and NAK were 0.22, 0.17, 0.16 and 0.13 $\mu g\ m^{-3}$, respectively. Whereas, such concentrations averaged over entire column were 2.70, 2.56, 2.42 and 2.31 $\mu g\ m^{-3}$ for SAK, WAK, Interior Alaska and NAK, respectively. The slightly higher $PM_{2.5}$ concentrations over SAK were partly due to slightly higher local anthropogenic emissions of precursors and primary $PM_{2.5}$ in SAK compared to WAK, Interior Alaska and NAK as described in 6.2.2. The meteorological conditions of SAK were also more favorable for the oxidation of precursor gases to $PM_{2.5}$. While downward shortwave radiation (SW) was similar among all regions of interest, SAK had lower temperatures and higher cloud water contents that promoted aqueous-phase oxidation reactions in cloud droplets more than in other regions of Alaska (Table 6.2). Moreover, SAK is located closer to the trans-Pacific shipping lanes; therefore, stronger ship-emission impacts also contributed to the higher $PM_{2.5}$ concentrations in SAK. The impacts of shipping lane emissions on SAK were clearest during 8 to 13 June 2008 (Fig. 6.9a – green line). During this period, advection of

the pollutants from shipping lanes to SAK (Fig. 6.10a) caused hourly, column-averaged $PM_{2.5}$ concentrations double those in NAK, SAK and Interior Alaska (Fig. 6.9a). Hourly column-averaged $PM_{2.5}$ concentrations averaged over the INTE remained quite constant, while those over Japan and Siberia strongly varied throughout the period (Fig. 6.9b). This indicated that the air flow crossing shipping lanes on its way to SAK was not impacted by Japanese anthropogenic emissions or Siberian wildfires. $PM_{2.5}$ concentrations over SAK decreased with height and were negligible above 5 km above ground level (AGL) (Fig. 6.10b, as representative example). The vertical distributions indicate that the emissions had a minor effect on $PM_{2.5}$ concentrations above 5 km altitude over SAK.

Analogously, in WAK during 14 to 19 June the peaks in $PM_{2.5}$ concentrations were due to advection from the shipping lanes in the Bering Sea (Fig. 6.9a – red line). Horizontal distributions of near-surface $PM_{2.5}$ concentrations over the entire domain on day 15 showed obvious advection from INTE into Alaska (Fig. 6.11a$_1$). 15 June was selected as an example for the period of 14 to 19 June to illustrate that Siberian wildfire smoke plumes did not reach to Alaska, even when they were transported by the strongest westerly flows observed during the study period toward Alaska. Above the atmospheric boundary layer (~2 km AGL), the stronger wind-speed (~11 m s$^{-1}$) still did not transport Siberian wildfire $PM_{2.5}$ plumes far enough to reach Alaska (Fig. 6.11a$_2$). Horizontal distributions of $PM_{2.5}$ concentrations at 2 km altitude on the following day (Fig. 6.11a$_3$) provided additional evidence that wildfire $PM_{2.5}$ plumes were transported only within the vicinity of Siberia. Since Japanese anthropogenic emissions were treated as surface fluxes, Japanese $PM_{2.5}$ plumes were not transported far enough in either vertical or

horizontal directions to reach Alaska. Moreover, the near-surface (not shown) and column-averaged $PM_{2.5}$ concentrations over INTE remained unchanged during 14 to 19 June (Fig. 6.9b) indicated that throughout the entire column over INTE there was no transport of $PM_{2.5}$ from Japan or Siberia to this region; hence, no transport of $PM_{2.5}$ to WAK. In WAK, $PM_{2.5}$ concentrations were homogeneously distributed from the surface up to 3 km altitude and then dramatically decreased, suggesting that there was no transport of $PM_{2.5}$ to WAK above 3 km, although the simulated injection heights of Siberian wildfire smoke emissions were up to ~5 km AGL on this day. Since OC aerosols are the major component of wildfire smoke plumes as observed in the ARCTAS/CARB-2008 field campaign (Hecobian et al., 2011) and as simulated by the WRF-Chem model in this study (discussed later in section 6.4.2), their relatively short life-times (~ few days, Schauer et al., 1996; Rogge et al., 1993) could be the reason for the removal of the Siberian wildfire plume aerosols before reaching Alaska. Sessions et al. (2011) also noted that Siberian wildfire smoke plumes did not to reach Alaska during 28 June to 8 July 2008, confirming the WRF-Chem simulations.

Over NAK, the temporal evolution of column-averaged $PM_{2.5}$ concentrations fluctuated with peaks/dips appearing every 7 days (Fig. 6.9a – black line). This evolution coincided with the temporal profile of local anthropogenic emissions with lower emissions on weekends, suggesting that local anthropogenic emissions were the major sources of $PM_{2.5}$ over NAK.

In Interior Alaska, two peaks of $PM_{2.5}$ concentrations appeared during 14 to 16 and 20 to 23 June coincided with the emissions from small local wildfire events in this

region (Fig. 6.9a – blue line; Fig. 6.8b). The injection heights of the small wildfires in Interior Alaska were low ($\leq 1$ km AGL). Therefore, impacts of emissions on $PM_{2.5}$ concentrations were negligible above 2 km (Fig. 6.12b, as representative example). Another peak in $PM_{2.5}$ concentrations over Interior Alaska occurred during 18 to 20 June was due to the advection of $PM_{2.5}$ from the shipping lanes, across WAK, to Interior Alaska (Fig. 6.12a). The mountain ranges located along the southern coast of Alaska prevented the advection of $PM_{2.5}$ from the shipping lanes across SAK to Interior Alaska during 8 to 13 June.

**6.3.4 Impact of increased wildfire emissions on $PM_{2.5}$ distributions in Alaska**

**6.3.4.1 Impact of increased wildfire emissions on $PM_{2.5}$ concentrations in Alaska**

In IFA, wildfire emissions over Siberia dramatically decreased compared to REF (Fig. 6.8a). In Interior Alaska, vertically-integrated emissions of $PM_{2.5}$ precursor gases averaged over the entire region were about 25 times higher than those in REF due to local wildfire emission increases. Over NAK, SAK and WAK the emissions remained unchanged between IFA and REF (Table 6.2). In REF, hourly averaged, in Alaska $PM_{2.5}$ concentrations were extremely low compared with Siberia, Asia and oceanic regions (Fig. 6.13a). In response to increased wildfire emissions over Interior Alaska not only Interior Alaska, but also coastal regions of Alaska, experienced statistically significant and dramatic increases in $PM_{2.5}$ concentrations in the near-surface layer (Fig. 6.13b), indicating advection of smoky air from Interior Alaska to the coastal regions. In IFA,

near-surface-layer (column-averaged), hourly averaged $PM_{2.5}$ concentrations over Interior Alaska, NAK and WAK increased 3.01 (17.99), 0.83 (12.19) and 0.09 (1.46) µg m$^{-3}$, respectively. In IFA, near-surface hourly, regionally-averaged $PM_{2.5}$ concentrations over Interior Alaska, NAK and WAK increased 3.01, 0.83 and 0.09 µg m$^{-3}$, respectively. Such increases averaged over entire column were 17.99, 12.19 and 1.46 µg m$^{-3}$ over Interior Alaska, NAK and WAK, respectively. $PM_{2.5}$ concentrations marginally increased in SAK in response to Interior wildfire emission increases (Table 6.2).

In IFA, throughout the entire vertical column over regions of interest in Alaska, $PM_{2.5}$ concentrations were always highest in Interior Alaska; followed by NAK, SAK and SAK, respectively (Fig. 6.14a). This order differed from the situation in REF in which $PM_{2.5}$ concentrations in Interior Alaska and NAK were notably lower than those in SAK and WAK (Fig. 6.14b). In IFA, $PM_{2.5}$ concentrations in NAK and WAK were higher than in SAK implying that Interior wildfire emissions had a greater impact on air quality over NAK and WAK than SAK. The high terrain of the mountain ranges along the southern coast eliminated the exchange of the air masses between Interior Alaska and the SAK, limiting the impact of Interior Alaska emissions on SAK.

In Alaska, in both REF and IFA, $PM_{2.5}$ concentrations averaged over the entire study period decreased with height (Fig. 6.14). From this point on, the discussions focus on near-surface $PM_{2.5}$ concentrations because they directly affect ecosystems and human health. In the simulations, the simulated thickness of the near-surface layer averaged over all of Alaska was about 27 m AGL.

In IFA, in Interior Alaska $PM_{2.5}$ concentrations strongly increased from 16 June toward the end of the month in response to the increasing local wildfire emissions (Fig. 6.15a). Over NAK and WAK, the impact of wildfire smoke plume advection from Interior Alaska was obvious during 20 to 30 June (Fig. 6.15b, c). Over SAK, there were hardly any impacts from Alaskan wildfire emissions on $PM_{2.5}$ concentrations until the last day of the studied period (Fig. 6.15d). Over NAK, WAK and SAK, in the days when there was no advection from Interior Alaska to these regions, the $PM_{2.5}$ concentrations were almost identical between IFA and REF, suggesting that $PM_{2.5}$ concentrations in Alaska were not impacted by Siberian wildfire emissions during the studied episode. Otherwise, lower $PM_{2.5}$ concentrations would have been expected in IFA than in REF in response to the dramatic decrease in Siberian wildfire emissions between the two years.

### 6.3.4.2 Impact of increased wildfire emissions on $PM_{2.5}$ speciation in Alaska

In REF, sea-salt aerosols (sodium and chloride) were the big components of $PM_{2.5}$ composition over SAK, WAK and NAK because these coastal regions were impacted by oceanic air masses (Fig. 6.16$b_1$, $c_1$, $d_1$). In SAK, the simulated hourly, regionally-averaged chloride and sodium concentrations were 1020 and 660 ng m$^{-3}$, respectively, which were within the range of measured values during March and April 2001 in Adak Island (Cahill, 2003). However, those simulated concentrations were much higher than the measured values at Simeonof (chloride: 117 ng m$^{-3}$; sodium: 85 ng m$^{-3}$) and Tuxedni (chloride: 349 ng m$^{-3}$; sodium: 264 ng m$^{-3}$) as obtained by IMPROVE during June 2008. Over Interior Alaska, sea-salt aerosols were also large components (up to 60% and 40%

for chloride and sodium aerosols, respectively) except on those days when wildfires occurred in the Interior (14 to 15 and 20 to 23 June) (Fig. 6.16$a_1$). Such high percentages of sea-salt aerosol component are not expected for $PM_{2.5}$ speciation in a continental atmosphere like in the Interior Alaska, suggesting WRF-Chem strongly overestimated sea-salt aerosols over Interior Alaska. At Denali NP, the sum of simulated, hourly averaged chloride plus sodium aerosol concentrations were 2.05 µg m$^{-3}$, two orders of magnitude larger than the concentrations observed at this site by IMPROVE. Overestimations of sea-salt aerosol concentrations in Alaska by WRF-Chem were also found in other studies further confirming this study WRF-Chem results (Yang et al., 2011; Saide et al., 2012). However, sea salt is emitted by natural processes that are the same between the REF and IFA simulations so the differences between the observed and simulated concentrations can be neglected since this study does not focus on sea salt changes.

In REF, the strong impact of anthropogenic emissions on $PM_{2.5}$ formation caused sulfate-aerosols to be the major component of $PM_{2.5}$ composition in all four regions of interest in Alaska. Ammonium and nitrate concentrations were extremely low relatively to sulfate concentrations (Fig. 6.16$a_1$, $b_1$, $c_1$, $d_1$). In Alaska, 100% of the total sulfur was in aerosol phase. Also, almost 100% of $NH_3$ was converted to ammonium. In all four regions of interest in Alaska, hourly molar ratios of $NH_4^+/SO_4^{2-}$ varied from 0.2 to 0.6 (i.e. much less than the theorical ratio of 2 of $(NH_4)_2SO_4$ (Brown et al., 2005)) throughout entire studied period indicating that there is not enough ammonia to neutralize the available sulfur compounds. Because there was little $NH_3$ available for nitrate formation,

the conversion efficiency of $NO_x$ to nitrate aerosols was much lower than the conversion effciency of $SO_2$ to sulfate aerosols in throughout Alaska (Table 6.3). Higer nitrate conversion efficiencies in SAK (12%) and WAK (8%) than in NAK (4%) and Interior Alaska (3%) (Table 6.3) may result from higher cloud water contents in SAK and WAK that promoted aqueous-phase oxidation reactions in cloud droplets more than in NAK and Interior Alaska (Table 6.2). The cloud water increase may allow more aerosol nitrate by diluting the acid that is present and making the pH more neutral. That increase neutrality allows more nitric acid to stick to the particle as nitrate.

According to measured data from the Arctic Research of the Composition of the Troposphere from Aircraft and Satellites - studies for the California Air Resources Board (ARCTAS-CARB-2008) field campaign, OC was the major component of $PM_{2.5}$ in smoke from biomass burning (Hecobian et al., 2011). Hence, the increased OC percentage in $PM_{2.5}$ must be related to increases in wildfire smoke emissions. WRF/Chem captured this behavior well. In REF, although the wildfire events that happened in Interior Alaska during 14 to 15 and 20 to 23 June were relatively small, they yielded dramatic increases in the OC percentage in $PM_{2.5}$ over Interior Alaska (Fig. 6.16a$_1$). During these wildfire events, the increases in unspeciated-$PM_{2.5}$ percentages also indicated wildfire emissions impacts on $PM_{2.5}$, as unspeciated-$PM_{2.5}$ comes from primary wildfire $PM_{2.5}$ emissions.

In IFA, before 15 June, there was little change in $PM_{2.5}$ speciation throughout Alaska because local wildfire emissions in Interior Alaska were very low (Fig. 6.8). During 16 to 30 June, in Interior Alaska, OC, unspeciated-$PM_{2.5}$ and EC components

increased dramatically in response to large increases in local wildfire emissions. Over this region, the OC component comprised up to 65% of aerosol mass (Fig. 6.16a$_2$), which was very close to the observed PM$_{2.5}$ OC emission from biomass burning reported in the literature (Yamasoe et al., 2000; Mayol-Bracero et al., 2002).

As discussed previously, NAK and WAK received strong advection of Interior wildfire plumes during 16 to 30 June in IFA. Consequently, in these regions the PM$_{2.5}$-speciation in IFA differed substantially from the PM$_{2.5}$-speciation in REF especially in OC and unspeciated-PM$_{2.5}$ percentages during this period (Fig. 6.16b$_2$, c$_2$). Over SAK PM$_{2.5}$-speciation marginally changed (Fig. 6.16d$_2$).

## 6.3.4.3 Impact of increased wildfire emissions on the relative importance of wildfire versus anthropogenic emissions to PM$_{2.5}$ concentrations in Alaska

In Alaska, except for sea-salt aerosols (sodium and chloride) all other PM$_{2.5}$ components were contributed by biogenic, anthropogenic and wildfire emissions. Biogenic emissions are natural whereas wildfire emissions could be both natural and human-initiated. In the perspective of eliminating emissions to improve air quality, only anthropogenic and wildfire emissions are of concern. Our discussions therefore only focus on the relative importance of wildfire versus anthropogenic emissions during different emission situation: weak (REF) versus strong (IFA) fire activity.

In REF, on average over the entire study period and over each region of interest, anthropogenic emissions contributed about 78, 75, 70 and 43% to PM$_{2.5}$ concentrations over WAK, SAK, NAK and Interior Alaska, respectively. Wildfire emissions contributed

negligibly to $PM_{2.5}$ concentrations in the three coastal regions (Fig. 6.17b$_1$, c$_1$, d$_1$). Small wildfire events occurred in June 2008 and contributed noticeably (16%) to $PM_{2.5}$ concentrations on average over the entire episode in Interior Alaska (Fig. 6.17a$_1$). Biogenic emissions were responsible for the rest of the $PM_{2.5}$ mass (Fig. 6.17).

In IFA, in response to local wildfire emission increases, the contribution of wildfire emissions to $PM_{2.5}$ concentrations dominated the contributions of anthropogenic emissions in Interior Alaska. In this region, on average over the entire studied period, wildfire emissions contributed to 52% of $PM_{2.5}$ concentrations with maxima of more than 90% during those days toward the end of the month (Fig. 6.17a$_2$). On average over the entire study period, anthropogenic emissions contributed only ~24% to $PM_{2.5}$ concentrations in this region.

Over NAK, in response to the advection of smoky air masses from Interior Alaska, the contributions of wildfire emissions to $PM_{2.5}$ concentrations became more comparable to the contributions of anthropogenic emissions (Fig. 6.17b$_2$). In this region, wildfire and anthropogenic emissions contributed 39 and 38% to $PM_{2.5}$ concentrations, respectively.

Similarly, in IFA on average over the entire study period, wildfire emissions contributed 18 and 3% to $PM_{2.5}$ concentrations over WAK and SAK, respectively. However, anthropogenic emissions were still the major sources of $PM_{2.5}$ concentrations in these two coastal regions, even when extreme wildfire events occurred in Interior Alaska (Fig. 6.17c$_2$, d$_2$). In IFA, anthropogenic emissions contributed 72 and 62% of $PM_{2.5}$ concentrations over SAK and WAK, respectively.

**6.4. Conclusions**

To investigate the impact of increased wildfire emissions on $PM_{2.5}$ concentrations across Alaska, two simulation sets (REF and IFA) performed by WRF-Chem using same meteorological initial and boundary conditions and emissions except that wildfire emissions were switched between 2008 (REF) and 2004 (IFA) were compared. The effects of wildfire smoke plume rise were included in the simulations. The analysis focused on Interior Alaska and three coastal regions. The relative importance of wildfire versus anthropogenic emissions was also addressed for both REF and IFA.

WRF-Chem performed well at simulating the meteorological conditions over Alaska and the North Pacific. It captured temporal evolutions of SLP, T, SW and RH very well with small biases; however, it overpredicted wind-speed with a bias of 2.1 m s$^{-1}$. WRF-Chem simulated wind fields over the North Pacific much better than over Alaska with smaller biases of -0.9 m s$^{-1}$. Performance skill-scores for WRF-Chem on simulating $PM_{2.5}$ concentrations for the coastal monitoring sites along the Gulf of Alaska were within the ranges of a state-of-the-science air-quality model performance.

In REF, over SAK, WAK and Interior Alaska, $PM_{2.5}$ concentrations were occasionally impacted by ship emissions. Over NAK, $PM_{2.5}$ concentrations were more impacted by local anthropogenic emissions than by long-range transport from outside the region. Small wildfire events in Interior Alaska did not impact air quality in the coastal regions. Japanese anthropogenic and Siberian wildfire $PM_{2.5}$ plumes were strongly diluted before reaching Alaska.

In IFA, wildfire emission increases in Interior Alaska led to increases in $PM_{2.5}$ concentrations not only in the Interior but also in Alaska's coastal regions. The impacts of increased wildfire emissions on concentrations are more obvious over NAK and WAK than SAK. On average over the entire study period, near-surface hourly, regionally averaged $PM_{2.5}$ concentrations over Interior Alaska, NAK and WAK increased 3.01, 0.83 and 0.99 $\mu g\ m^{-3}$, respectively and remained unchanged in SAK when compared to REF. Such increases in column-averaged, hourly, regionally averaged $PM_{2.5}$ concentrations were 17.99, 12.19 and 11.46 $\mu g\ m^{-3}$ over Interior Alaska, NAK and WAK, respectively and also remained unchanged in SAK. Interior wildfire emission increases also led to obvious increases in OC, unspeciated-$PM_{2.5}$ and EC percentages over Interior Alaska, NAK and WAK. The observed increases of aerosols concentrations, especially the OC component, in Interior Alaska (e.g. the Denali NP site) were mostly related to the increases in local wildfire emissions. Siberian wildfire emission changes were unlikely to impact the $PM_{2.5}$ concentration changes in all regions of interest in Alaska, at least during our studied period (June).

Under weak local fire activity scenario (REF), anthropogenic emissions were the major contributor of $PM_{2.5}$ concentrations in the coastal regions of Alaska. Wildfire emission contributions to $PM_{2.5}$ concentrations were negligible in the coastal regions and less important compared to anthropogenic emissions in Interior Alaska. Under the strong fire activity scenario (IFA), wildfire emissions were the biggest contributor to $PM_{2.5}$ concentrations in Interior Alaska. The contributions of wildfire emissions to $PM_{2.5}$ were competitive to anthropogenic emissions in NAK. However, anthropogenic emissions

194

were still the major contributor to PM$_{2.5}$ concentrations over SAK and WAK under the strong fire activity scenario. This was especially true over SAK, where two Class I preserve areas (Simeonof and Tudxedni Wilderness) are located; therefore, wildfire emissions were much less important than anthropogenic emissions in contributing to PM$_{2.5}$ distributions at these sites. In conclusion, controlling wildfire emissions would benefit air quality for not only Interior Alaska but also the North Slope regions. However, since this study does not distinguish the impacts of human-initiated and natural wildfires on PM$_{2.5}$ distributions. A future study that explicitly examines the benefit of controlling human-initiated wildfire emissions on air quality in Interior Alaska needs to be conducted. This could help to determine whether it is worth spending more efforts with respect to economic and labor expenses in controlling human-initiated wildfire emissions to prevent the air quality of the Denali NP from any further degradation. For the southern coast, to protect air quality from degradation, the anthropogenic emissions (e.g., ship and local–inland emission sources) should be targeted for the controlling mitigation.

## Acknowledgment

**References**

Ackermann, I.J., Hass, H., Memmesheimer, M., Ebel, A., Binkowski, F.S., Shankar, U., 1998. Modal aerosol dynamics model for Europe: Development and first applications. Atmos. Environ., 32, 2981-2299.

ADEC, 2012. Regional haze trans-boundary monitoring study report. Air Quality Division, Air Monitoring and Quality Assurance Program. Available at http://www.dec.state.ak.us/air/am/am_projects.htm

Alaska Department of Forestry, 2012. Fire statistics. Retrieved June 17, 2012, from http://forestry.alaska.gov/firestats/index.htm

Ames, R., Fox, D.G., Malm, W.C., Schichtel, B.A., 2004. Preliminary apportionments of carbonaceous aerosols to wild fire smoke using observations from the IMPROVE network. Paper #76, Conference on Regional Haze, AWMA, Asheville, NC.

Andreae, M., Merlet, P., 2001. Emission of trace gases and aerosols from biomass burning, Glob. Biogeochem. Cy., 15(4), 955–966.

Barnard, J.C., Fast, J.D., Paredes-Miranda, G., Arnott, W.P., Laskin, A., 2010. Technical note: evaluation of the WRF-Chem "aerosol chemical to aerosol optical properties" module using data from the MILAGRO campaign. Atmos. Chem. Phys., 10, 7325-7340.

Barney, R.J., 1971. Wildfires in Alaska-some historical and projected effects and aspects. Proceedings of Fire in the Northern Environment - A Symposium - Fairbanks, AK 13-14 April 1971. 51-59.

Belov, S.V., 1976. Forest Pyrology. Leningrad Forestry Academy of the USSR, St. Petersburg, Russia.

Belward, A., 1996. The IGBP-DIS global 1 km land cover dataset (DISCover)-proposal and implementation plans, IGBP-DIS Working Paper No. 13, Toulouse, France.

Bieniek, P., 2007. Climate and predictability of Alaska wildfires. Master thesis, Uni. of Alaska Fairbanks.

Brown S. S., Ryerson,T.B., Wollny, A. G., Brock, C. A., Peltier, R., Sullivan, A. P., Weber, R. J., Dube´, W. P., Trainer, M., Meagher, J. F., Fehsenfeld, F. C., Ravishankara, A. R., 2005. Variability in nocturnal nitrogen oxide processing and its role in regional air quality. Sci., 311, 67-70.

Bulger, A., Cosby, J., Webb, R., 1998. Acid Rain: current and projected status of coldwater fish communities in the Southeastern US in the context of continued acid deposition. Coldwater conservation fund report for Trout Unlimited. Available at http://swas.evsc.virginia.edu/Assests/Docs/Current-and-Projected-Status.pdf

Cahill, C. F., 2003. Asian aerosol transport to Alaska during ACE-Asia. J. Geophys. Res., 108(D23), 8664.

Chang, J. S., Binkowski, F. S., Seaman, N. L., McHenry, J. N., Samson, P. J., Stockwell, W. R., Walcek, C. J., Madronich, S., Middleton, P. B., Pleim, J. E., Lansford, H. H., 1991. The regional acid deposition model and engineering model. State-of-Science/Technology, Report 4, National Acid Precipitation Assessment Program, Washington, DC.

Chang, J.C., Hanna, S.R., 2004. Air quality model performance evaluation. Meteor. Atmos. Phys., 87, 167-196.

Chapman, E.G., Gustafson, W.I.Jr., Easter, R.C., Barnard, J.C., Ghan, S.J., Pekour, M.S., Fast, J.D., 2009. Coupling aerosol-cloud-radiative processes in the WRF-Chem model: Investigating the radiative impact of elevated point sources. Atmos. Chem. Phys., 9, 945-964.

Chen, F., Dudhia, J., 2001. Coupling an advanced land-surface/ hydrology model with the Penn State/ NCAR MM5 modeling system. Part I: Model description and implementation. Mon. Wea. Rev., 129, 569–585.

Chou, M.-D., Suarez, M.J., 1994. An efficient thermal infrared radiation parameterization for use in general circulation models. NASA Tech. Memo., 104606, 85pp.

Davis, D.D., Grodzinsky, G., Kasibhatla, P., Crawford, J., Chen, G., Liu, S., Bandy, A., Thornton, D., Guan, H., Sandholm, S., 2001. Impact of ship emissions on marine boundary layer $NO_x$ and $SO_2$ distributions over the Pacific Basin. Geophys. Res. Lett., 28, 235-238.

Dominici, F., Peng, R.D., Bell, M.L., 2006. Fine particulate air pollution and hospital admission for cardiovascular and respiratory diseases. J. Ameri. Med. Assoc., 295(10), 1127-1134.

Duck, T.J., Firanski, B.J., Millet, D.B., Doldstein, A.H., Holzinger, R., Worsnop, D.R., White, A.B., Stohl, A., Dickinson, C.S., van Donkelaar, A., 2007. Transport of forest fire emissions from Alaska and the Yukon Territory to Nova Scotia during summer 2004. J. Geophys. Res., 112, doi:10.1029/2006JD007716.

EC-JRC/PBL, 2011. Emission Database for Global Atmospheric Research version 4.2. http://edgar.jrc.ec.europa.eu/.

EPA, 2013. List of 156 Mandatory Class I Federal Areas. U.S. Environmental Protection Agency website, retrieved Feb 5th 2013 from http://www.epa.gov/visibility/class1.html

Fett, R.W., Englebretson, R.E., Perryman, D.C., 1993. Forecasters handbook for the Bering Sea, Aleutian Islands and Gulf of Alaska. Final report - Science Applications International Corp., Monterey CA 93940. NRL/PU/7541-93-0006.

Freitas, S. R., Longo, K. M., Silva Dias, M., Silva Dias, P., Chatfield, R., Prins, E., Artaxo, P., Grell, G., Recuero, F., 2005. Monitoring the transport of biomass burning emissions in South America, Environ. Fluid Mech., 5(1–2), 135–167.

Freitas, S. R., Longo, K. M., Chatfield, R., Latham, D., Silva Dias, M. A. F., Andreae, M. O., Prins, E., Santos, J. C., Gielow, R., Carvalho Jr., J. A., 2007. Including the sub-grid scale plume rise of vegetation fires in low resolution atmospheric transport models. Atmos. Chem. Phys., 7, 3385–3398.

Furyaev, V.V., 1996. Fire Ecology of Siberian Boreal Forests. Fire in Ecosystems of Boreal Eurasia. Eds: Goldammer, J.G., Furyaev, V.V.. Kluwer Academic Publishers, Netherlands, 168–185.

Giglio, L., Descloitres, J., Justice, C. O., Kaufman, Y. J., 2003. An enhanced contextual fire detection algorithm for MODIS. Remote Sens. Environ., 87, 273–282.

Grell, G.A., Dévényi, D., 2002. A generalized approach to parameterizing convection combining ensemble and data assimilation techniques. Geophys. Res. Lett., 29, 1693.

Grell, G.A., Peckham, S.E., Schmitz, R., McKeen, S.A., Frost, G., Skamarock, W.C., Eder, B., 2005. Fully coupled "online" chemistry within the WRF model. Atmos. Environ., 39, 6957-6975.

Grell, G.A., Freitas, S.R., Stuefer, M., Fast, J., 2011. Inclusion of biomass burning in WRF-Chem: impact of wildfires on weather forecasts. Atmos. Chem. Phys., 11, 5289–5303.

Han, S., Bian, H., Zhang, Y.m Wu, J., Wang, Y., Tie, X., Li, Y., Li, X., Yao, Q., 2012. Effect of aerosols on visibility and radiation in spring 2009 in Tianjin, China. Aeros. A.Q. Res., 12, 211–217.

Hines, K.M., Bromwich, D.H., 2008. Development and testing of Polar Weather Research and Forecasting (WRF) model. Part I: Greenland ice sheet meteorology. Mon. Wea. Rev., 136, 1971-1989.

Hecobian, A., Liu, Z., Hennigan, Z., Huey, L. G., Jimenez, J. L., Cubison, J. L., Vay, S., Diskin, G. S., Sachse, G. W., Wisthaler, A., Mikoviny, T., Weinheimer, A. J., Liao, J., Knapp, D. J., Wennberg, P. O., K¨urten, A., Crounse, J. D., St. Clair, J., Wang, Y., Weber, R. J., 2011. Comparison of chemical characteristics of 495 biomass burning plumes intercepted by the NASA DC-8 aircraft during the ARCTAS/CARB-2008 field campaign. Atmos. Chem. Phys., 11, 13325–13337.

Interagency Monitoring of Protected Visual Environments (IMPROVE), 2013. Online IMPROVE Database Access; retrieved in Mar 2009 and Oct 2012 from IMPROVE website at http://views.cira.colostate.edu/fed/DataWizard/Default.aspx

Janjić, Z.I., 2002. Nonsingular implementation of the Mellor-Yamada level 2.5 scheme in the NCEP meso model. NCEP-Office-Note 437, 61pp.

Jet Propulsion Laboratory, 2013. MISR plume height project – Siberia 2008. Retrieved July 24, 2013, from http://www-misr.jpl.nasa.gov/getData/accessData/MisrMinxPlumes/projectArea/index.cfm?ProjectArea=16

Juday, G.P., Barber, V., Duffy, P., Linderholm, H., Rupp, S., Sparrow, S., Vaganov, E., Yarie, J., 2004. Forests, land management, and agriculture. Chapter 14 – Arctic climate impact assessment. Cambridge University Press., ISBN 0-521-86509-3.

Kappos, A.D., Bruckmann, P., Eikmann, T., Englert, N., Heinrich, U., Höppe, P., Koch, E., Krause, G.H.M., Kreyling, W.G., Rauchfuss, K., Rombout, P., Schulz-Klemp, V., Thiel, W.R., Wichmann, H.-E., 2004. Health effects of particles in the ambient air. Inter. J. Hyg. Environ. Heal., 207, 399-407.

Karl J., Morrison, P., Swope, L., Ackley, K., 2011. Wildlands of the United States. Pacific Biodivesity Institute's report for the Pew Wilderness Center.

Lin, Y.-L., Rarley, R.D., Orville, H.D., 1983. Bulk parameterization of the snow field in a Cloud Model. J. Appl. Meteor., 22, 1065-1092.

Longo, K. M., Freitas, S. R., Andreae, M. O., Setzer, A., Prins, E., Artaxo, P., 2010. The Coupled Aerosol and Tracer Transport model to the Brazilian developments on the Regional Atmospheric Modeling System (CATT-BRAMS) – Part 2: Model sensitivity to the biomass burning inventories, Atmos. Chem. Phys., 10, 5785–5795.

Madronich, S., 1987. Photodissociation in the atmosphere, 1, actinic flux and the effects of ground reflections and clouds. J. Geophys. Res., 92, 9740-9752.

Malm, W.C., Sisler, J.F., Huffman, D., Eldred, R.A., Cahill, T.A., 1994. Spatial and seasonal trends in particle concentration and optical extinction in the United States. J. Geophys. Res., 99, 1347-1370.

Mayol-Bracero, O.L., Guyon, P., Graham, B., Roberts, G., Andreae, M.O., Decesari, S., 2002. Water-soluble organic compounds in biomass burning aerosols over Amazonia: 2. Apportionment of the chemical composition and importance of the polyacidic fraction. J. Geophy. Res., 107:8091-106.

Mellor, G.L. and Yamada, T., 1982. Development of a turbulence closure model for geophysical fluid problems, Rev. Geophys. Space Phys., 20, 851-875.

Mlawer, E.J., Taubman, S.J., Brown, P.D., Iacono, M.J., Clough, S.A., 1997. Radiative transfer for inhomogeneous atmospheres: RRTM, a validated correlated-k model for the longwave. J. Geophys. Res., 102D, 16663-16682.

Mölders, N., 2008. Suitability of the Weather Research and Forecasting (WRF) model to predict the June 2005 fire weather for Interior Alaska. Wea. Forecast., 23, 953-973.

Mölders, N., 2009. Alaska Emission Model (AkEM) Description Internal Report, Fairbanks, 10 p.

Mölders, N., Porter, S.E., Tran, T.T., Cahill, C.F., Mathis, J., Newby, G.B., 2011. The effect of unregulated ship emissions for aerosol and sulfur-dioxide concentrations in southwestern Alaska. In: Criddle, K., Eicken, H., Lovecraft, A., Metzger, A. (Eds.), North by 2020: Perspectives on a Changing North. Alaska University Press, Fairbanks, 14p.

Mölders, N., Tran, H.N.Q., Cahill, C.F., Leelasakultum, K., Tran, T.T., 2012. Assessment of WRF/Chem $PM_{2.5}$-forecasts using mobile and fixed location data from the Fairbanks, Alaska winter 2008/09 field campaign, Atmos. Pol. Res., 3, doi: 10.5094/APR.2012.018

NAPAP, 2005. National acid precipitation assessment program report to Congress: an integrated assessment. Available at
 http://ny.water.usgs.gov/projects/NAPAP/NAPAPReport2005.pdf

National Data Buoy Center (NDBC), 2012. Alaska Historical Marine Data. Retrieved at http://www.ndbc.noaa.gov/maps/alaska_hist.shtml

National Park Service, 2013. Air quality, Denali National Park and Preserve, Alaska. Available at http://www.nps.gov/dena/naturescience/airquality.htm

Olson, J. S.,Watts, J. A., Allison, L. J., 2000. Major world ecosystem complexes ranked by carbon in live vegetation: A database (revised November 2000), NDP-017, available at: http://cdiac.esd.ornl.gov/ndps/ndp017.html, Carbon Dioxide Information Analysis Center, Oak Ridge National Laboratory, Oak Ridge, Tennessee, USA.

Park, R.J., Jacob, D.J., Chin, M., Martin, R.V., 2003. Sources of carbonaceous aerosols over the United States and implications for natural visibility. J. Geophys. Res., 108, doi:10.1029/2002JD003190

Peckham, S.E., Fast, J.D., Schmitz, R., Grell, G.A., Gustafson, W.I., McKeen, S.A., Ghan, S.J., Zaveri, R., Easter, R.C., Barnard, J., Chapman, E., Salzmann, M., Wiedinmyer, C., Freitas, S.R., 2009. WRF/Chem Version 3.1 User's Guide. 78p.

Plymouth State Weather Center, 2012. Retrieved July 20, 2012, from http://vortex.plymouth.edu/sfcwx-u.html

Pope, C.A., Dockery, D.W., 2006. Health effects of fine particulate air pollution: Lines that connect. J. Air & Waste Manag. Assoc., 56, 709-742.

Rogge, W.F., Mazurek, M.A., Hildemann, L.M., Cass, G.R., Simoneit, B.R.T., 1993. Quantification of urban organic aerosols at a molecular level: identification, abundance and seasonal variation. Atmos. Environ., 27, 1309–1330.

Saide, P. E. , Spak, S. N., Carmichael, G. R., Mena-Carrasco, M. A., Yang, Q., Howell, S., Leon, D. C., Snider, J. R., Bandy, A. R., Collett, J. L., Benedict, K. B., de Szoeke, S. P., Hawkins, L. N., Allen, G., Crawford, I., Crosier, J., Springston, S. R., 2012. Evaluating WRF-Chem aerosol indirect effects in Southeast Pacific marine stratocumulus during VOCALS-Rex. Atmos. Chem. Phys., 12, 3045–3064.

Schauer J.J., Rogge W.F., Hildemann L.M., Mazurek M.A., Cass G.R., 1996. Source apportionment of airborne particulate matter using organic compounds as tracers. Atmos. Environ., 30:3837–55.

Schell, B., Ackermann, I.J., Hass, H., Binkowski, F.S., Ebel, A., 2001. Modeling the formation of secondary organic aerosol within a comprehensive air quality model system. J. Geophys. Res., 106, 28275-28293.

Sessions, W. R., Fuelberg, H. E., Kahn, R. A., Winker D. M., 2011. An investigation of methods for injecting emissions from boreal wildfires using WRF-Chem during ARCTAS. Atmos. Chem. Phys., 11, 5719–5744.

Sestini, M., Reimer, E., Valeriano, D., Alvalá, R., Mello, E., Chan, C., and Nobre, C.: Mapa de cobertura da terra da Amazônia legal para uso em modelos meteorológicos, Anais XI Simpósio Brasileiro de Sensoriamento Remoto, 2901–2906, 2003.

Soja, A.J, Tchebakova, M.N, French, N.H.F, Flannigan, M.D., Shugart, H.H., Stocks, B.J. Sukhinin, A.I. Parfenova, E.I., Chapin III F.S., Stackhouse Jr.P.W., 1997. Climate-induced boreal forest change: predictions versus current observations. Glob. Planet. Chan., 56, 274–296.

Simpson, D., Guenther, A., Hewitt, C.N., Steinbrecher, R., 1995. Biogenic emissions in Europe 1. Estimates and uncertainties. J. Geophys. Res., 100D, 22875-22890.

Skamarock, W.C., Klemp, J.B., Dudhia, J., Gill, D.O., Barker, D.M., Duda, M.G., Huang, X.-Y., Wang, W., Powers, J.G., 2008. A description of the Advanced Research WRF version 3. NCAR/TN, 125pp.

Stafford, J.M., Wendler, G., Curtis, J., 2000. Temperature and precipitation of Alaska: 50 year trend analysis. Theor. Appl. Climatol., 67, 33-44.

Stocks, B.J., Fosberg, M.A., Lynham, T.J., Mearns, L., Wotton, B.M., Yang, Q., Jin, J.Z., Lawrence, K., Hartley, G.R., Mason, J.A., McKenney, D.W., 1998. Climate Change and Forest Fire Potential in Russian and Canadian Boreal Forests. Clim. Chan., 38, 1-13.

Stockwell, W.R., Middleton, P., Chang, J.S., Tang, X., 1990. The second-generation regional acid deposition model chemical mechanism for regional air quality modeling. J. Geophys. Res., 95, 16343-16367.

Student, 1908. The probable error of a mean. Biomet., 6, 1-25.

Tran, H.N.Q., 2012. Analysis of model and observation data for the development of a public $PM_{2.5}$ Air-Quality Advisories Tool (AQuAT). Ph.D. dissertation. University of Alaska Fairbanks.

Tran, H.N.Q., Mölders, N., 2012. Numerical investigations on the contribution of point-source emissions to the $PM_{2.5}$-concentrations in Fairbanks, Alaska. Atmos. Pol. Res., 5, 199-210.

Tran, T.T., G. Newby, Mölders, 2011. Impacts of emission changes on sulfate aerosols in Alaska. Atmos. Environ., 45, 3078-3090.

Veldt, C., 1991. Emissions of SOx, NOx, VOC and CO from East European countries. Atmos. Environ., 25A, 2683-2700.

Ward, E., Susott, R., Kaufman, J., Babbit, R., Cummings, D., Dias, B., Holben, B., Kaufman, Y., Rasmussen, R., Setzer, A., 1992. Smoke and fire characteristics for cerrado and deforestation burns in Brazil: BASE-B Experiment. J. Geophys. Res., 97(D13), 14601–14619.

202

Weseley, M.L., 1989. Parameterization of surface resistances to gaseous dry deposition in regional-scale numerical models. Atmos. Environ., 23, 1293-1304.

Western Regional Climate Center (WRCC), 2012. RAWS USA climate archive. Retrieved from http://www.raws.dri.edu/index.html

Yamasoe, M.A., Artaxo, P., Miguel, A.H., Allen, A.G., 2000. Chemical composition of aerosol particles from direct emissions of vegetation fires in the Amazon Basin: water-soluble species and trace elements. Atmos. Environ., 34:1641-53.

Yang, Q., W. I. Gustafson Jr., Fast, J. D., Wang, H., Easter, R. C., Morrison, H., Lee, Y.-N., Chapman, E. G., Spak, S. N., Mena-Carrasco, M. A., 2011. Assessing regional scale predictions of aerosols, marine stratocumulus, and their interactions during VOCALS-REx using WRF-Chem. Atmos. Chem. Phys., 11, 11951–11975.

Zhao, C., Liu, X., Leung, L.R, Johson, B., McFarlane, S.A., Gustafson, W.I.Jr., Fast, J.D., Easter, R., 2010. The spatial distribution of mineral dust and its shortwave radiative forcing over North Africa: modeling sensitivities to dust emissions and aerosol size treatments. Atmos. Chem. Phys., 10, 8821–8838.

Table 6.1. Mean and standard deviation, root-mean-square error (RMSE), standard deviation of error (SDE), bias and correlation (R) for hourly averaged sea level pressure, temperature (T), shortwave radiation (SW), relative humidity (RH), precipitation, wind speed (v) and wind direction (Dir)

| | Quantity | Simulated | Observed | RMSE | SDE | Bias | R |
|---|---|---|---|---|---|---|---|
| Model evaluation with WRCC data | SLP (hPa) | 1011 ± 8 | 1012 ± 8 | 4 | 4 | 1 | 0.900 |
| | T ($^o$C) | 11.5± 4.0 | 12.0 ± 3.7 | 3.0 | 3.0 | -0.5 | 0.714 |
| | SW(W m$^{-2}$) | 278 ± 68 | 212 ± 88 | 131 | 95 | 66 | 0.567 |
| | RH(%) | 67.9 ± 13.7 | 66.3 ± 14.8 | 14.7 | 14.6 | 1.6 | 0.500 |
| | Precip. (mm) | 4.2 ± 6.6 | 0.9 ± 5.2 | 9.5 | 9.1 | 3.3 | 0.100 |
| | v (m s$^{-1}$) | 4.1 ± 1.7 | 2.0 ± 1.3 | 2.8 | 1.7 | 2.1 | 0.336 |
| | Dir ($^o$) | 160 ± 97 | 180 ± 64 | 96 | 80 | -7 | 0.222 |
| Model evaluation with NDBC bouy data | SLP (hPa) | 1014± 6 | 1016 ± 7 | 3.9 | 3.2 | -2 | 0.903 |
| | T ($^o$C) | 8.2 ± 2.1 | 9.1 ± 2.6 | 3.0 | 2.8 | -0.9 | 0.512 |
| | v (m s$^{-1}$) | 5.0 ± 2.3 | 4.1 ± 2.9 | 2.5 | 2.0 | 0.9 | 0.651 |
| | Dir ($^o$) | 152 ± 92 | 163 ± 66 | 102 | 90 | -4 | 0.431 |

Table 6.2. Hourly average SW, near-surface T, cloud-water content ($Q_c$), column-integrated emissions of $PM_{2.5}$ precursor and $PM_{2.5}$ concentrations averaged over regions of interest in Alaska during 6 to 30 June

| Parameter | | NAK | SAK | WAK | Interior Alaska |
|---|---|---|---|---|---|
| SW (W m$^{-2}$) | | 302 | 274 | 277 | 281 |
| Near-surface T ($^{o}$C) | | 11 | 7 | 9 | 11 |
| Column-averaged Qc (g kg$^{-1}$) | | 0.06 | 0.19 | 0.12 | 0.08 |
| Total column-integrated $Emis._{(SO_2+NH_3+NO_x+NMVCO)}$ (mol km$^{-2}$ hr$^{-1}$) | REF | 0.18 | 0.27 | 0.22 | 0.19 |
| | IFA | 0.18 | 0.27 | 0.22 | 4.76 |
| Near-surface $PM_{2.5}$ concentrations (µg m$^{-3}$) | REF | 0.13 | 0.22 | 0.17 | 0.16 |
| | IFA | 0.96 | 0.24 | 0.26 | 3.17 |
| Column-averaged $PM_{2.5}$ concentration (µg m$^{-3}$) | REF | 2.31 | 2.70 | 2.56 | 2.42 |
| | IFA | 14.50 | 2.79 | 4.02 | 20.41 |

Table 6.3. Hourly regionally average conversion efficiency of sulfate, ammonium and nitrate from their precursors in regions of interest as obtained by REF.

| Conversion efficiency | NAK | SAK | WAK | Interior Alaska |
|---|---|---|---|---|
| $\dfrac{[SO_4^{2-}]aerosol}{[SO_4^{2-}]aerosol + [H_2SO_4]gas + [SO_2]} \times 100\%$ | 100 | 100 | 100 | 100 |
| $\dfrac{[NH_4^+]}{[NH_4^+] + [NH_3]} \times 100\%$ | 100 | 100 | 100 | 100 |
| $\dfrac{[NO_3^-]aerosol}{[NO_3^-]aerosol + [HNO_3]gas + [NO_x]} \times 100\%$ | 4 | 12 | 8 | 3 |
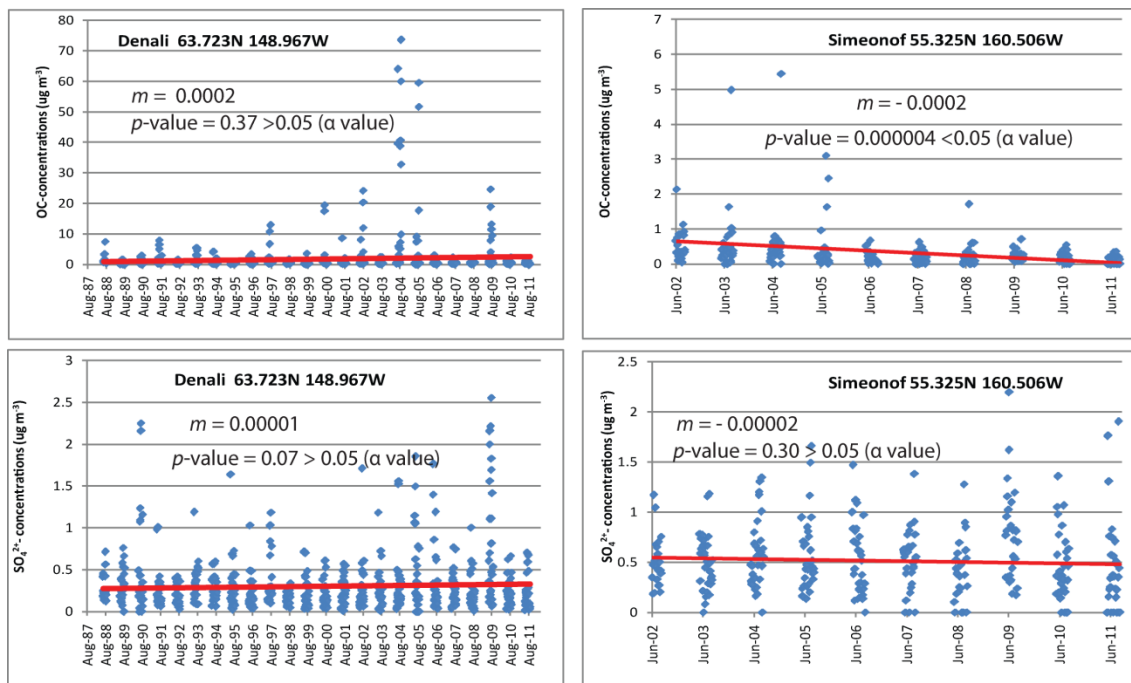
Fig. 6.1. Temporal evolution of observed organic carbon and sulfate-concentrations (blue dots) and linear trends (red lines) at the Denali NP (a, b) and Simeonof (c, d). Data are extracted for summer (June-July-August) from the IMPROVE network. The Trapper Creek and Tuxedni sites demonstrated similar trends to Simeonof (therefore not shown). Noted that x-axes are shown in different timescales due to more data available at Denali NP than at Simeonof site. $m$ indicates slope of the linear trends. Probability ($p$-value) was calculated to examine the statistical significance of the trends at the 95% confidence level (i.e. $\alpha = 0.05$)

.
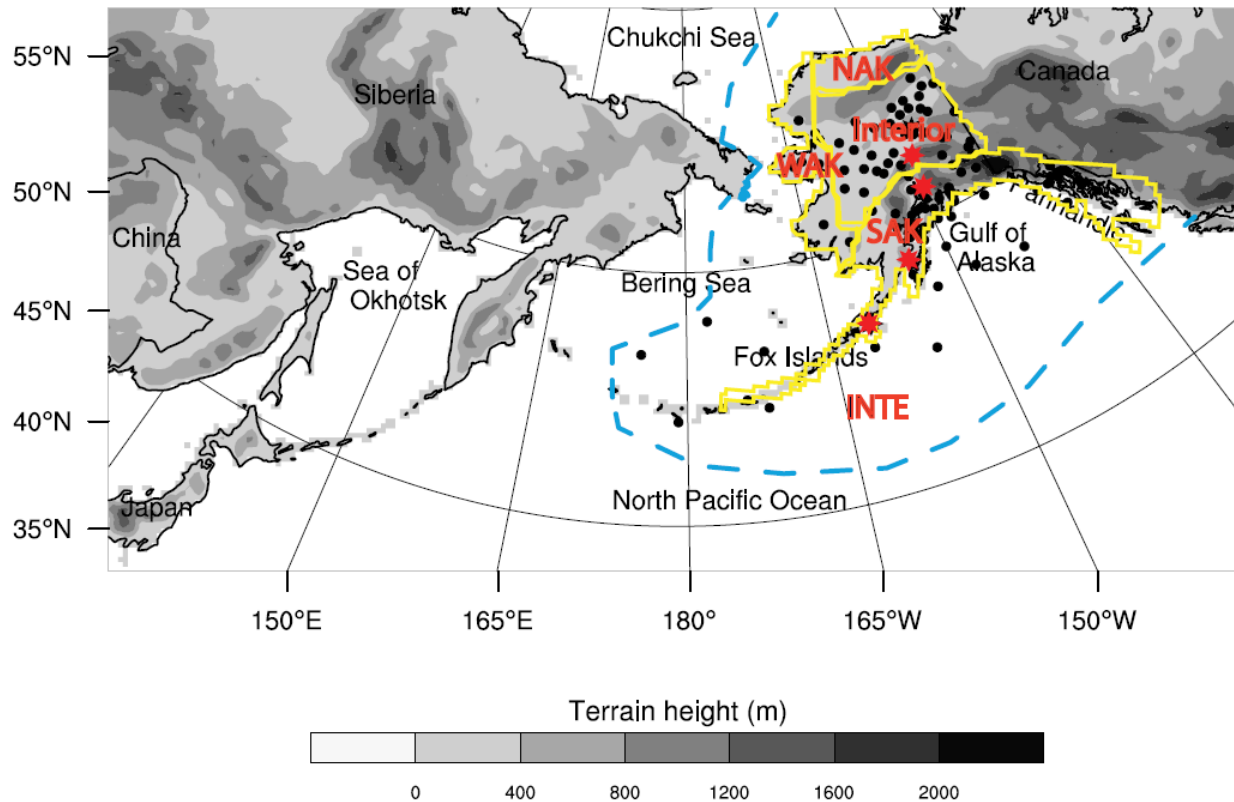
Fig. 6.2. Terrain height and location of WRCC and NDBC meteorological (black-dots) and aerosol-measurements (red-stars). Yellow lines distinguish the modeled regions of interest in Alaska. Blue-dash lines indicate the vicinity of intermediate-zone (INTE).
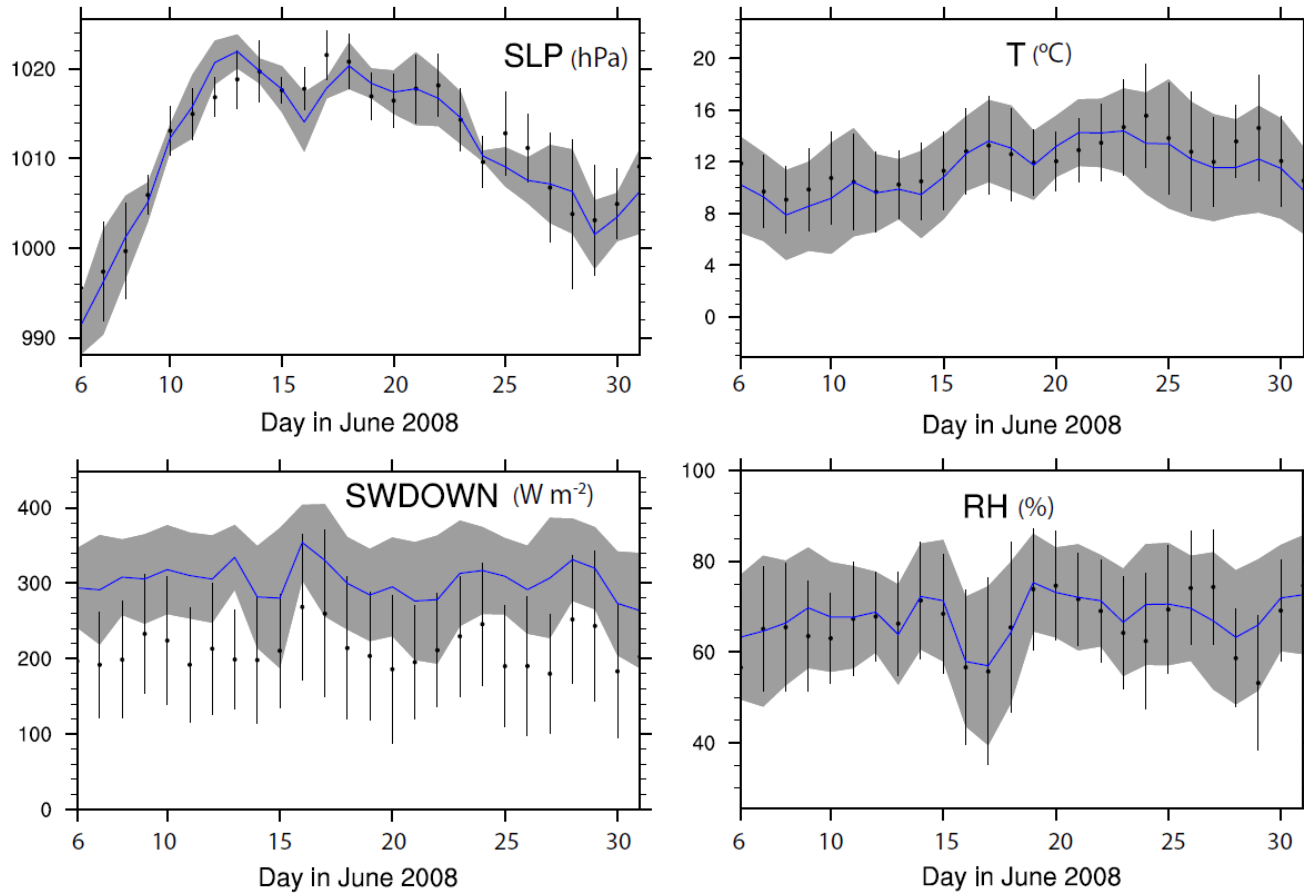
Fig. 6.3. Temporal evolution of daily averaged sea level pressure (SLP), temperature (T), shortwave radiation (SWDOWN) and relative humidity (RH) averaged over 84 observational sites for 6 - 30 June 2008. Blue lines (black dots) and grey-shading (vertical bars) indicated simulated (WRCC-observed) data and their variances, respectively.
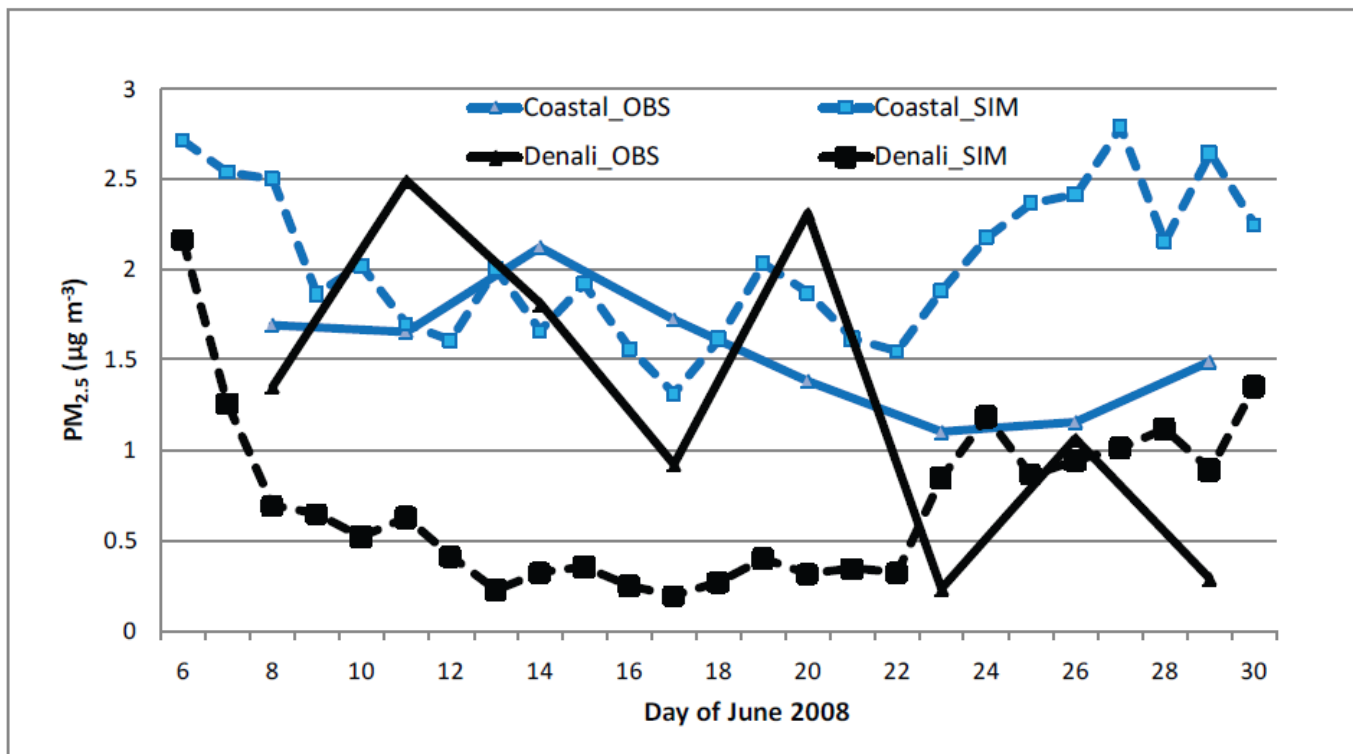
Fig. 6.4. REF simulated (dash) and IMPROVE observed (solid) daily-averaged PM$_{2.5}$ concentrations at Denali NP (black) and averaged over the three coastal IMPROVE sites (blue) for which data were available for 6 - 30 June 2008.

(a)

(b)
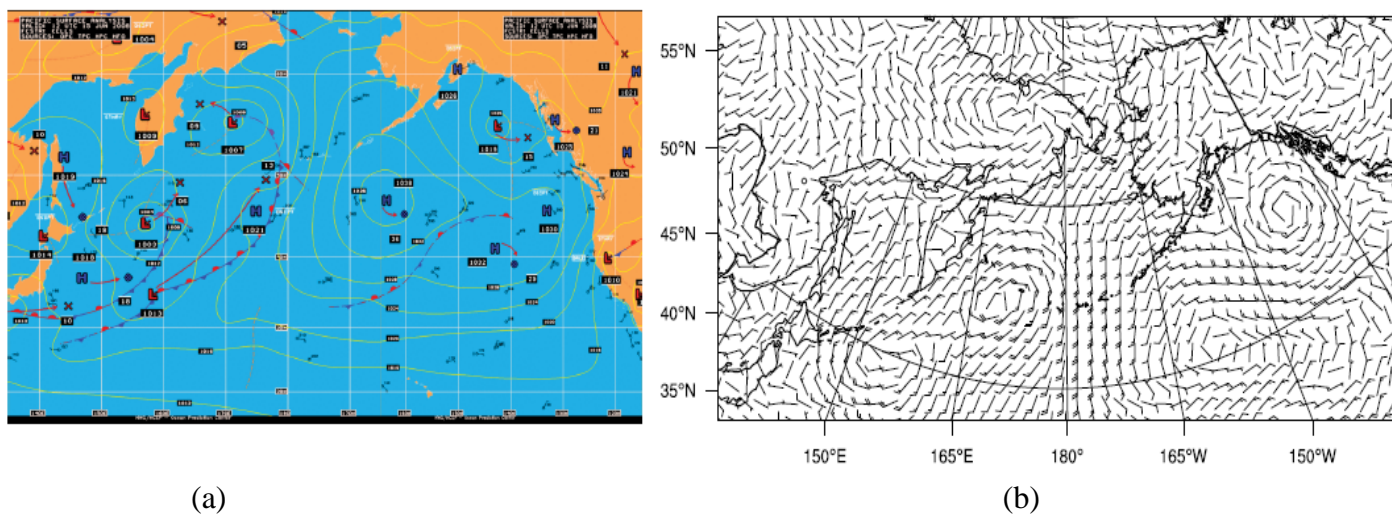
Fig. 6.5. West-East Pacific surface analysis map at 12UTC (a) (NCDC; http://nomads.ncdc.noaa.gov/ncep/NCEP) and WRF-Chem daily-averaged simulated wind field (b) on 15 June, 2008, as a representative.
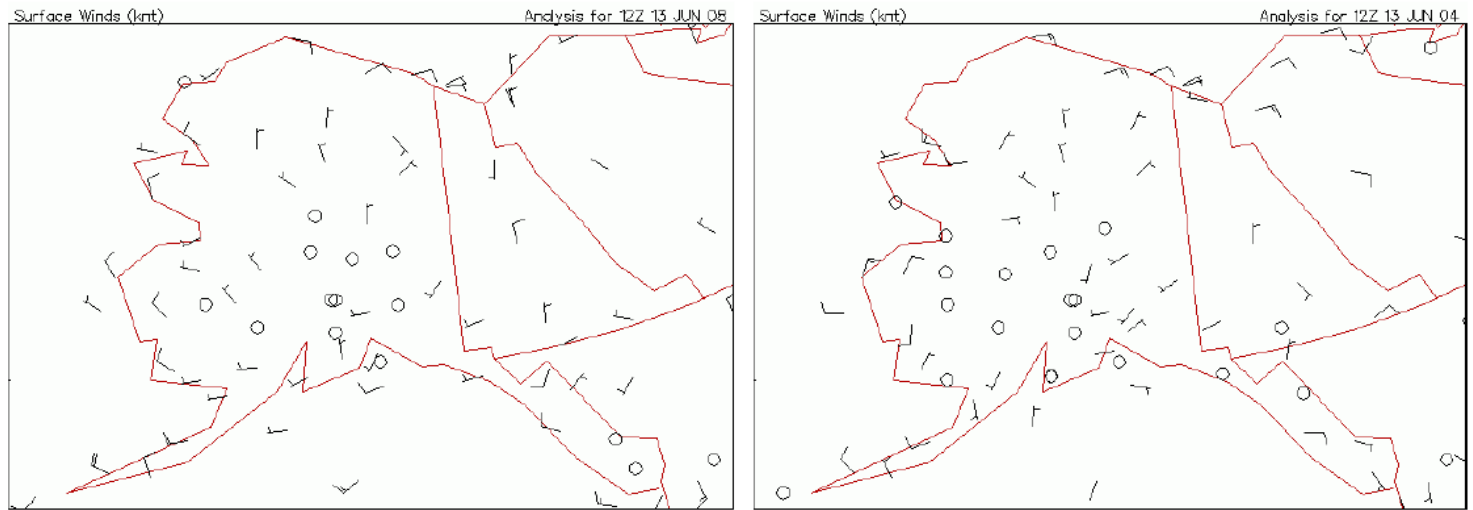
Fig. 6.6. Surface analysis synoptic maps of Alaska at 12UTC on 13 June, 2008 (a) and 2004 (b) (Source: Plymouth State Weather Center, 2012; http://vortex.plymouth.edu/sfcwx-u.html).

(a₁)

(a₂)
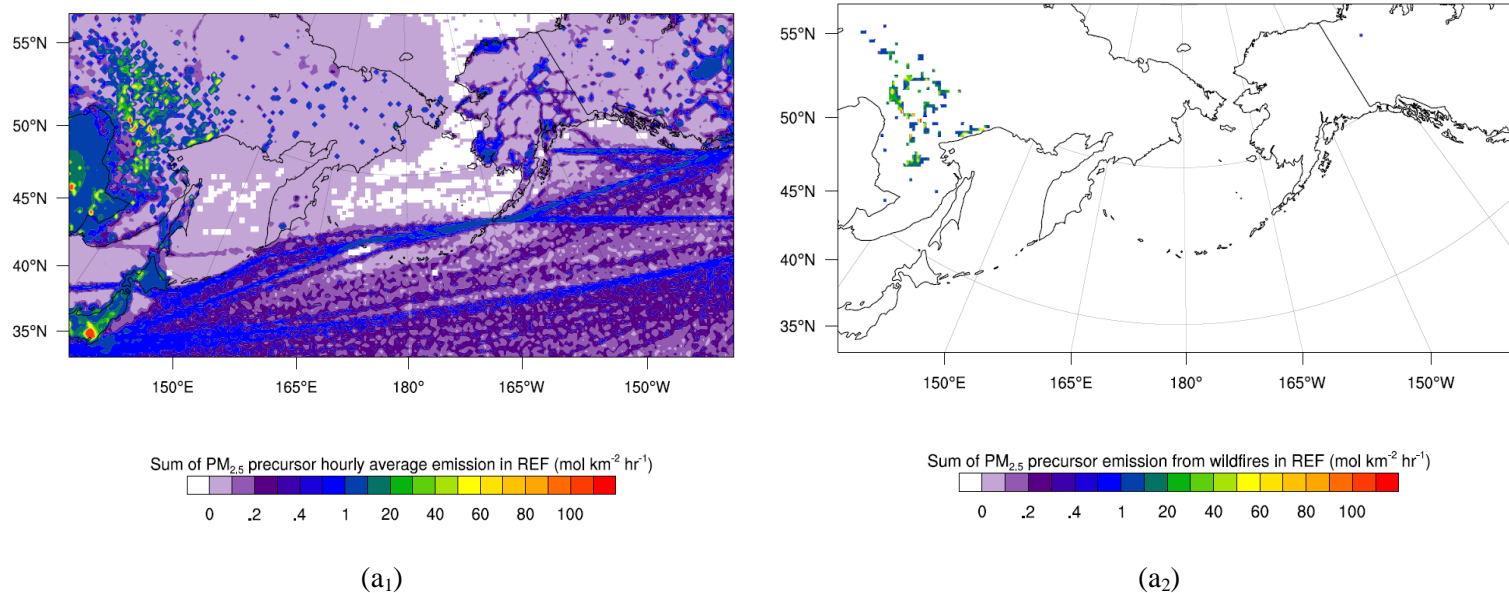
Fig. 6.7. Near-surface average emissions of total $PM_{2.5}$ precursors during 6-30 June for combined anthropogenic-wildfire sources (a₁) and wildfire emissions only (a₂) as obtained from REF (a₁, a₂) and in IFA (b₁, b₂).
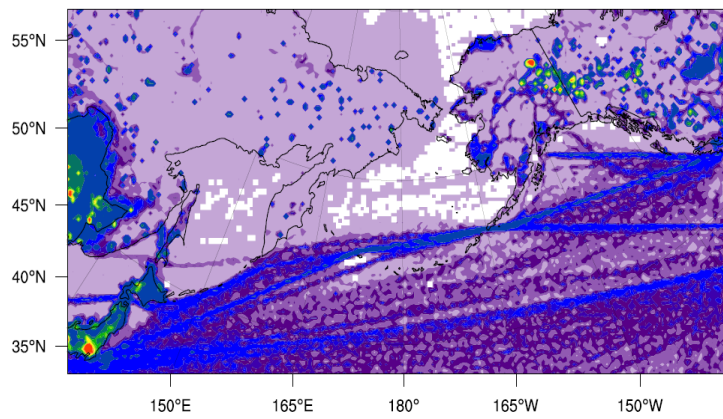
Sum of PM$_{2.5}$ precursor hourly average emission in IFA (mol km$^{-2}$ hr$^{-1}$)

0    .2    .4    1    20    40    60    80    100
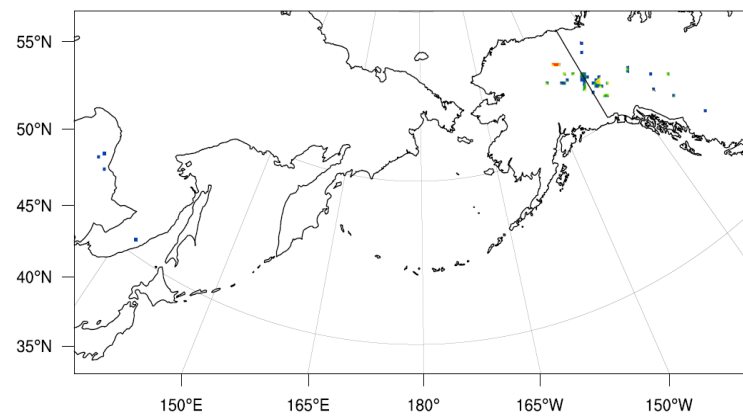
Sum of PM$_{2.5}$ precursor emission from wildfires in IFA (mol km$^{-2}$ hr$^{-1}$)

0    .2    .4    1    20    40    60    80    100

(b$_1$)

(b$_2$)

Fig. 6.7. (Cont.)
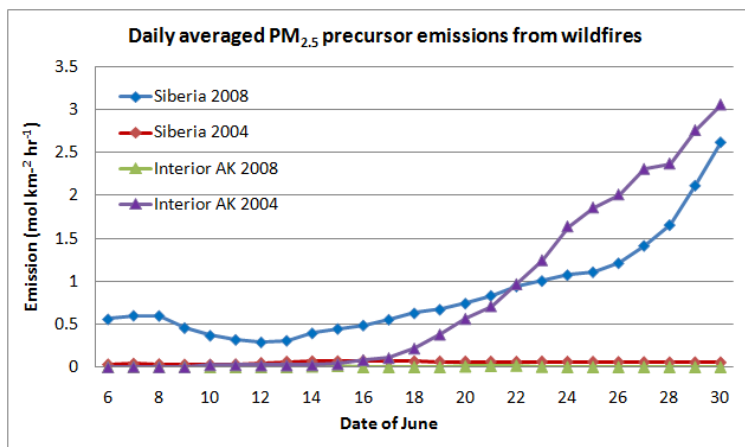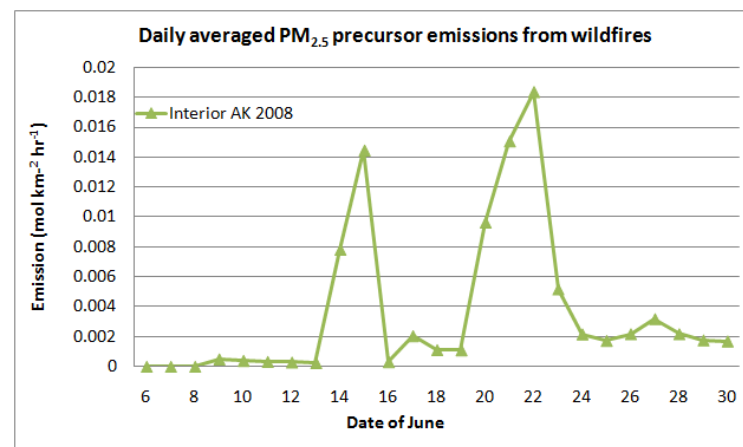
(a)                                                                 (b)

Fig. 6.8. Temporal evolution of daily-averaged PM$_{2.5}$ precursor emissions in the near-surface layer as derived by the 3BEM model.
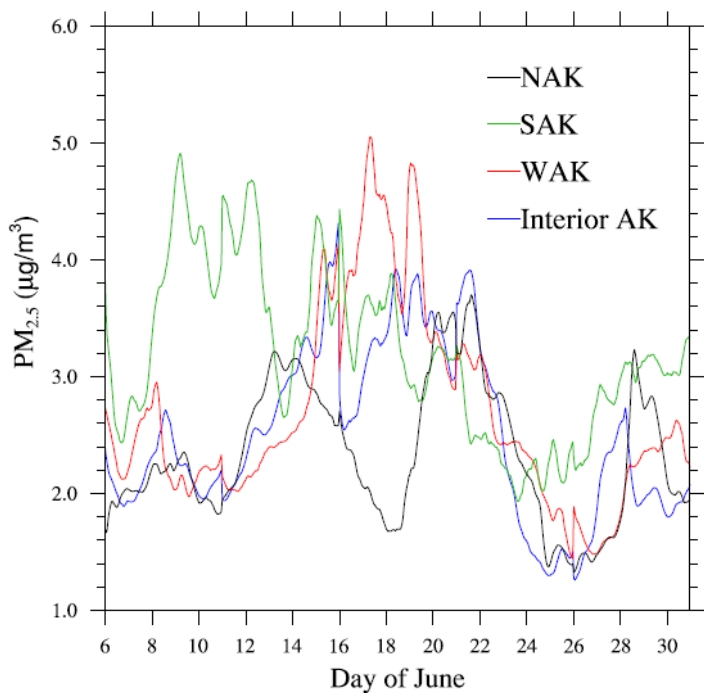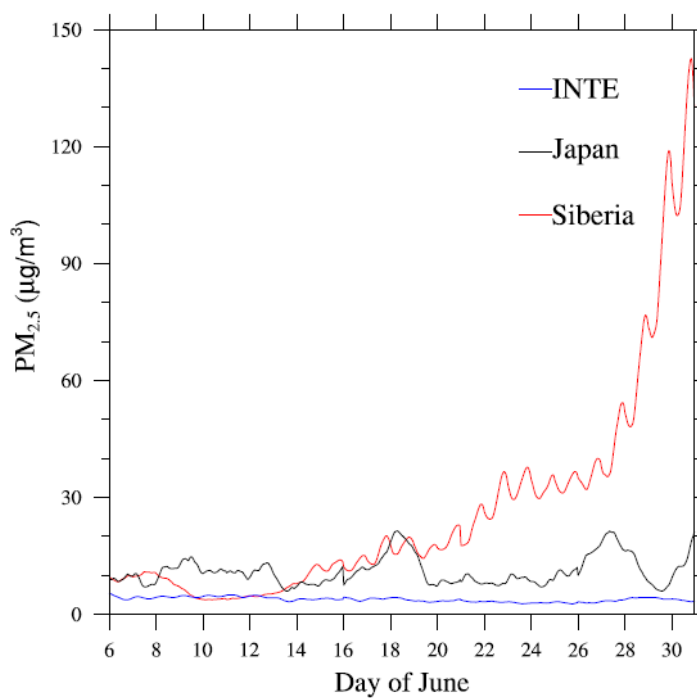
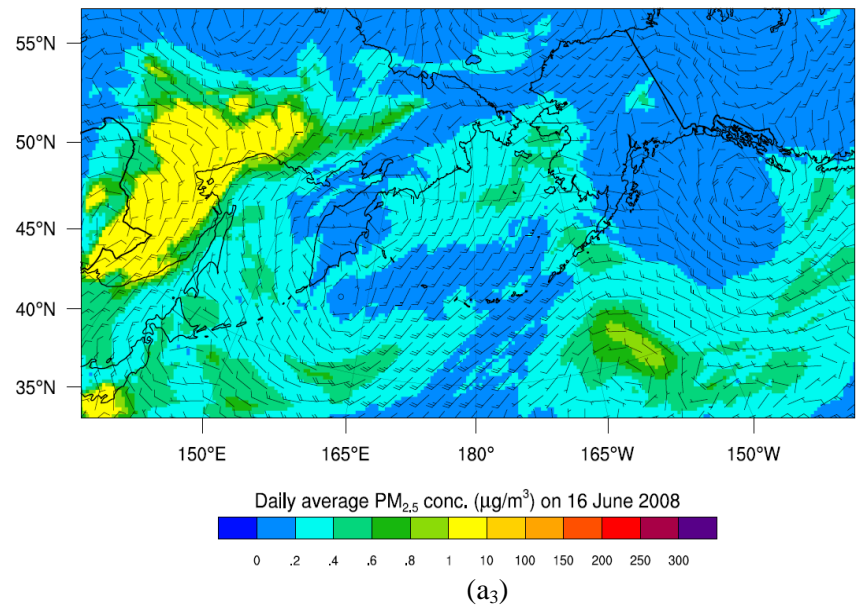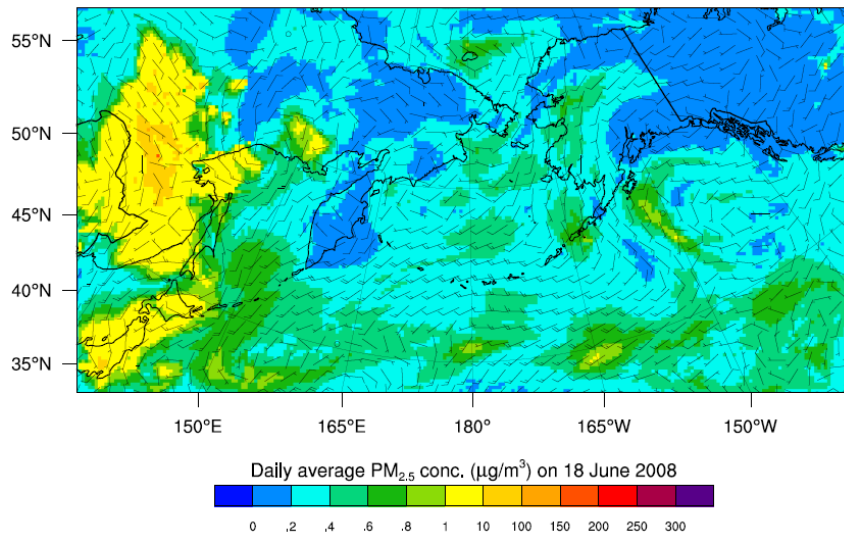Fig. 6.9. Temporal evolution of column-averaged hourly PM$_{2.5}$ concentrations averaged over the regions of interest as simulated by REF.
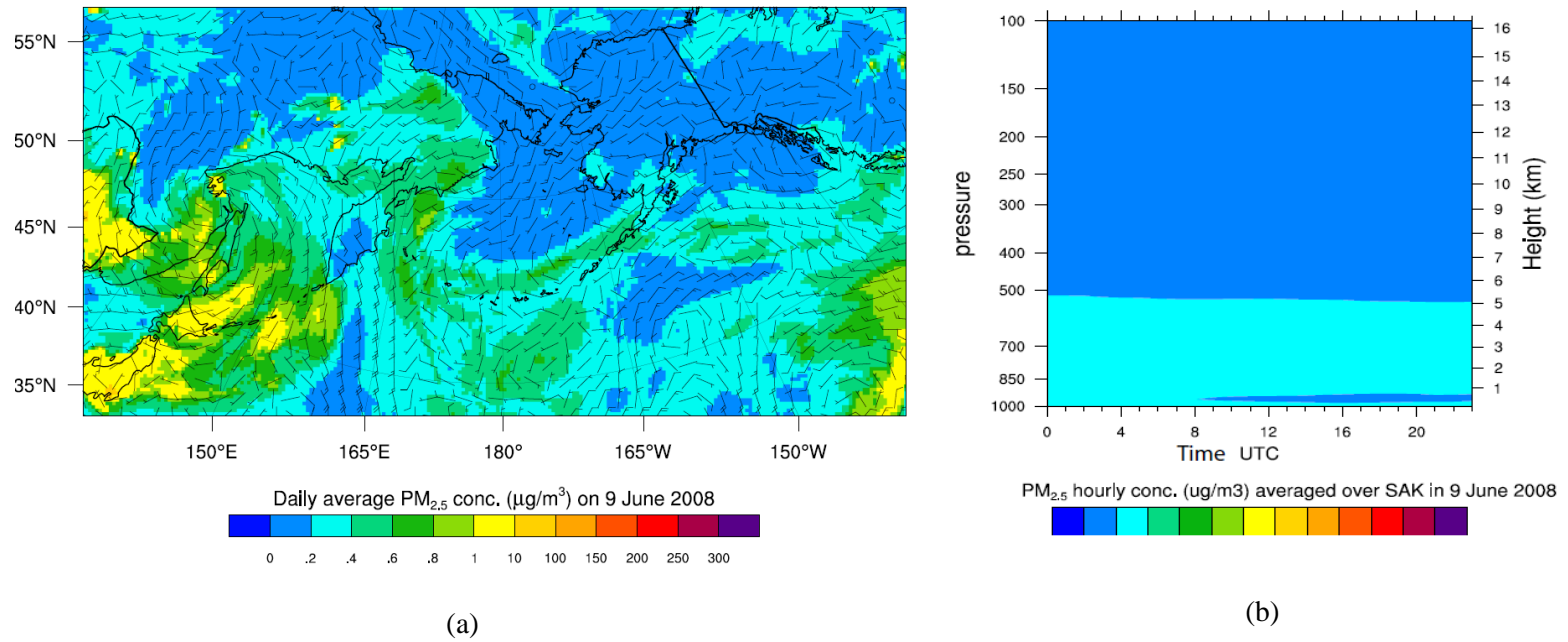
Fig. 6.10. Daily-averaged, near-surface PM$_{2.5}$ (a), and diurnal cycle of PM$_{2.5}$ vertical profile averaged over SAK (b) on 9 June as simulated by REF.
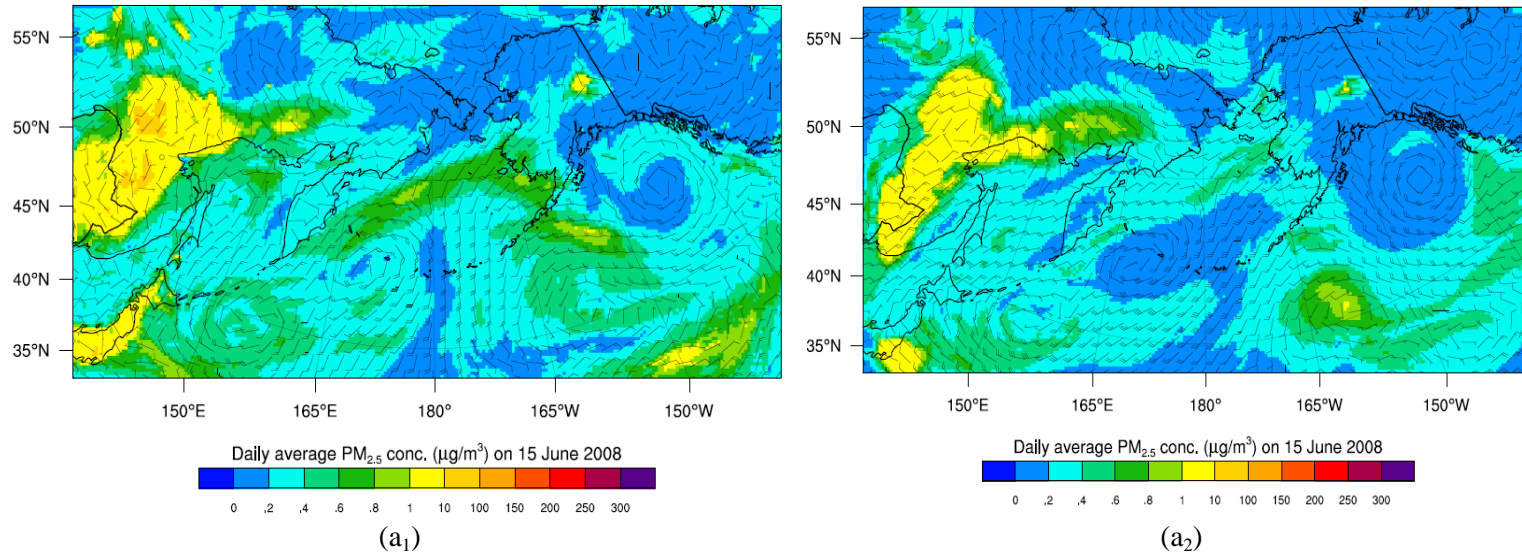
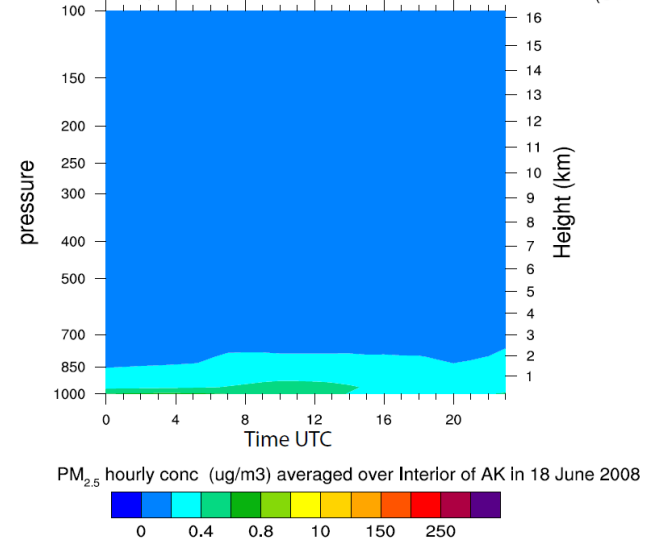Fig. 6.11. Daily-averaged, near-surface ($a_1$) and 2km-($a_2$, $a_3$) $PM_{2.5}$, and diurnal cycle of the $PM_{2.5}$ vertical profile averaged over WAK (b) on 15 and 16 June as simulated by REF.

Daily average PM$_{2.5}$ conc. (µg/m$^3$) on 16 June 2008

0   .2   .4   .6   .8   1   10   100   150   200   250   300

(a$_3$)

PM$_{2.5}$ hourly conc  (ug/m3) averaged over WAK in 15 June 2008

0   0.4   0.8   10   150   250

(b)
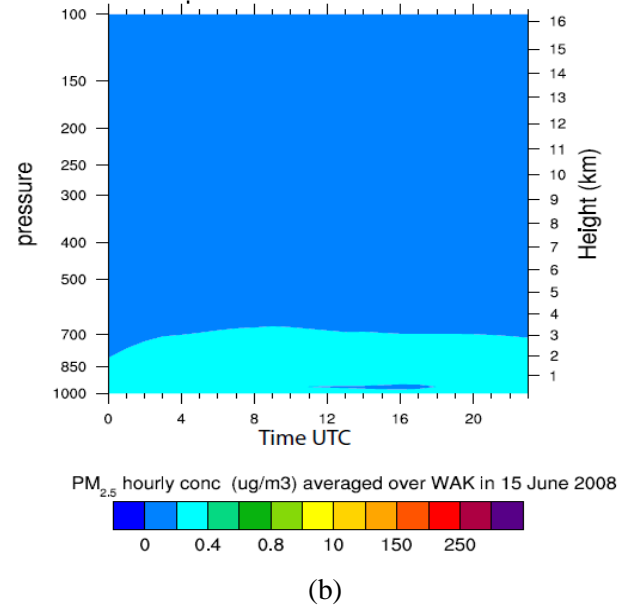
Fig. 6.11. (Cont.)

(a)                                                    (b)

Fig. 6.12. Daily-averaged, near-surface PM$_{2.5}$ (a) and diurnal cycle of PM$_{2.5}$ vertical profile averaged over Interior Alaska (b) on 18 June as simulated by REF.
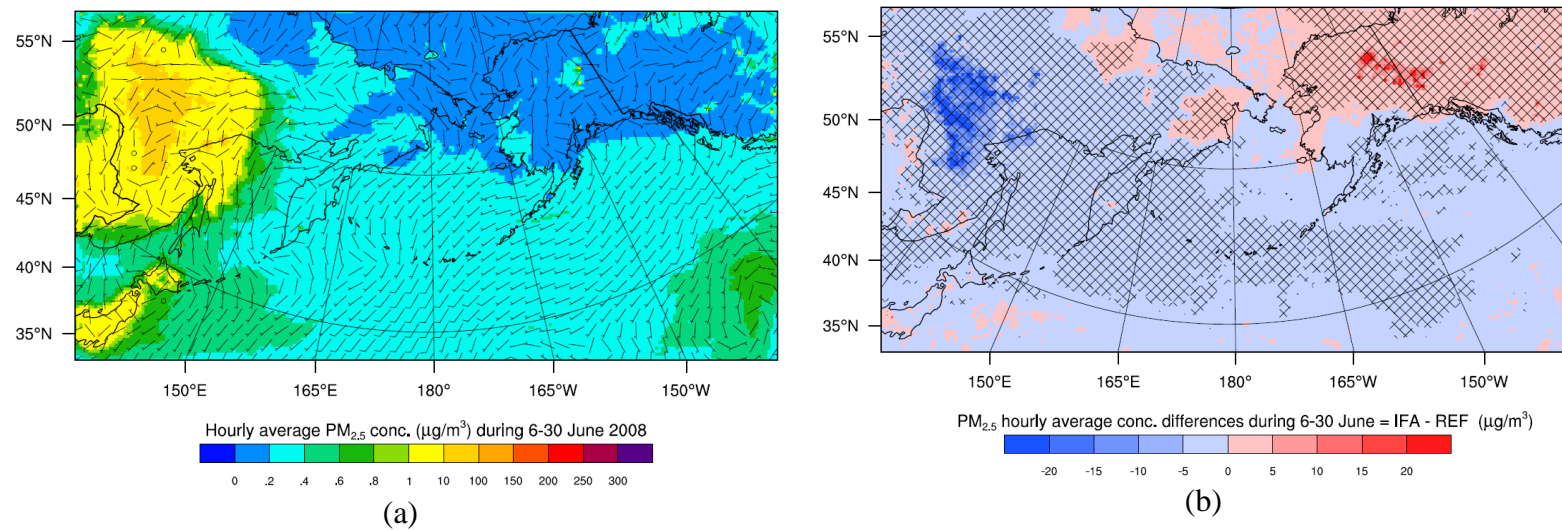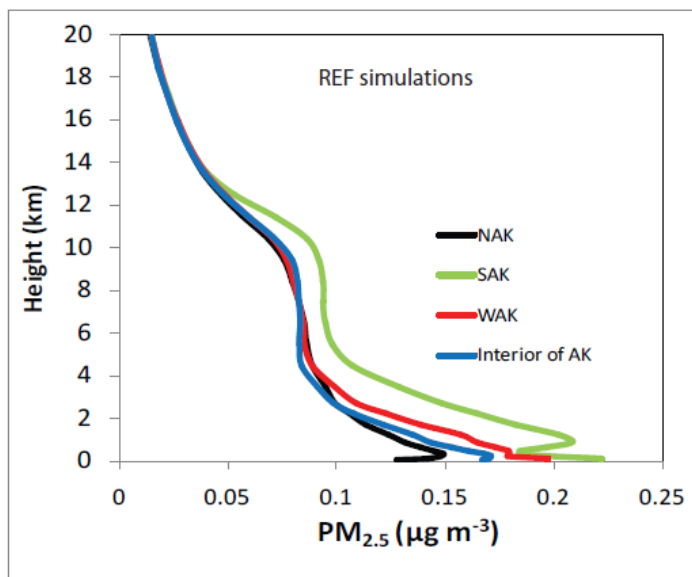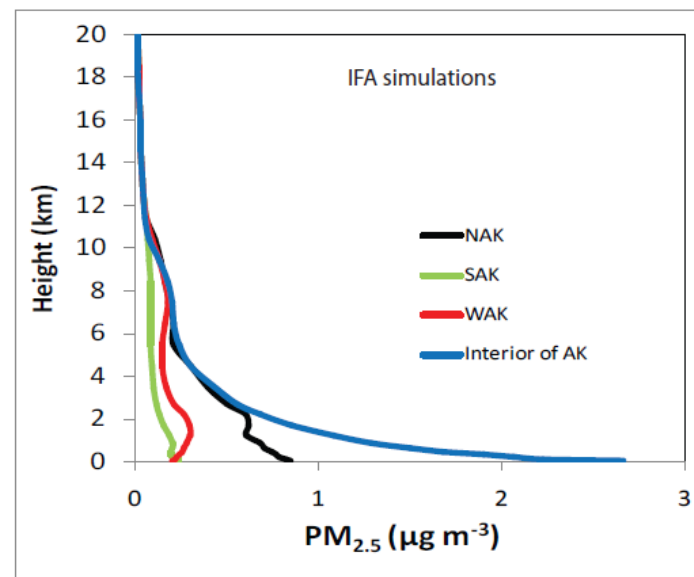
Fig. 6.13. Hourly averaged, near-surface PM$_{2.5}$ concentration simulated by REF (a) and PM$_{2.5}$ concentration differences between IFA and REF (b) for 6-30 June. Hatching indicates significant differences at the 95% confidence level.

(a)  (b)

Fig. 6.14. Vertical profiles of PM$_{2.5}$ averaged over the regions of interest and the entire study period as simulated by IFA (a) and REF (b).
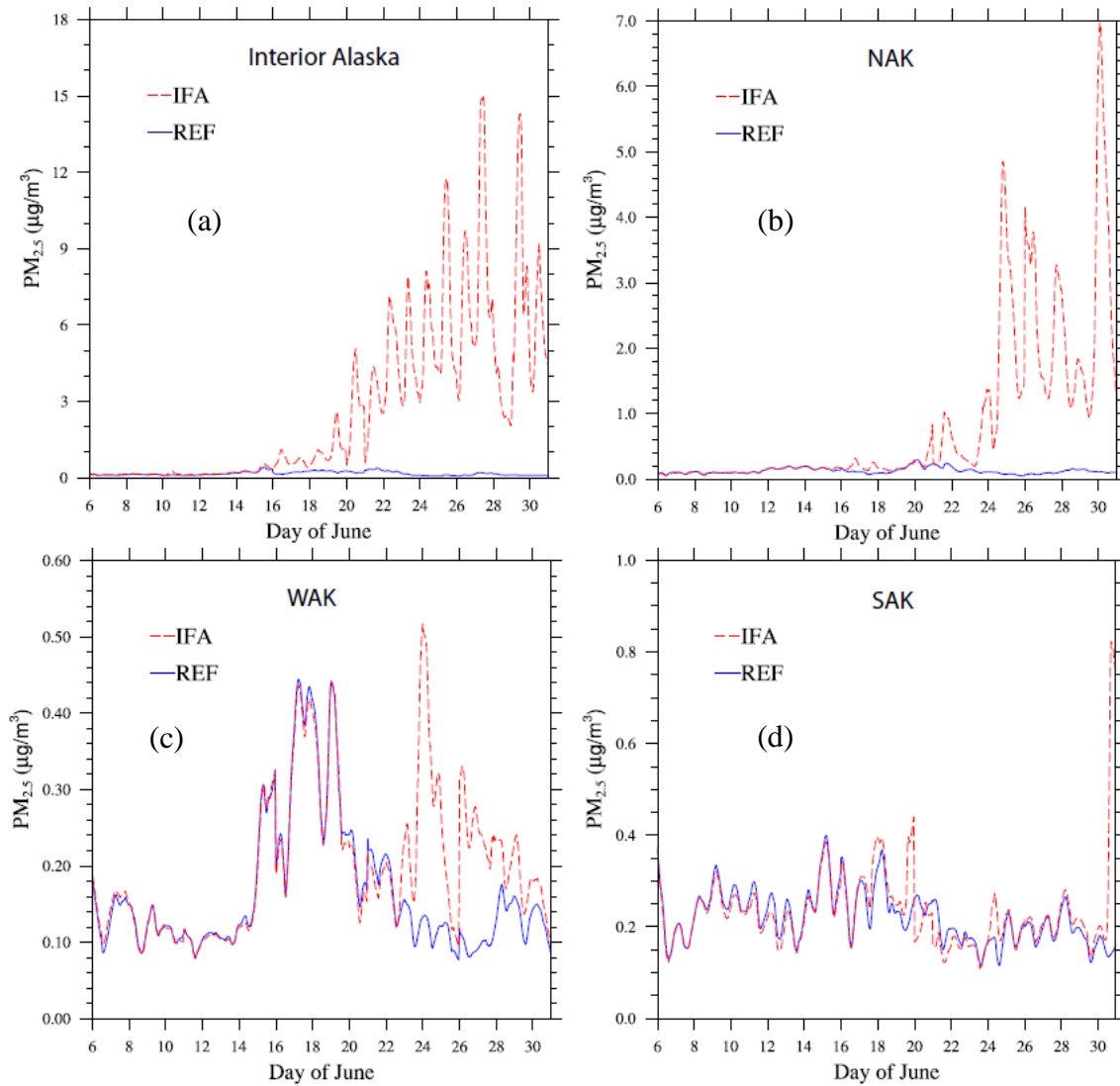
Fig. 6.15. Temporal evolution of near-surface hourly PM$_{2.5}$ concentrations averaged over the regions of interest as simulated by REF and IFA: (a) Interior Alaska, (b) NAK, (c) WAK and (d) SAK.
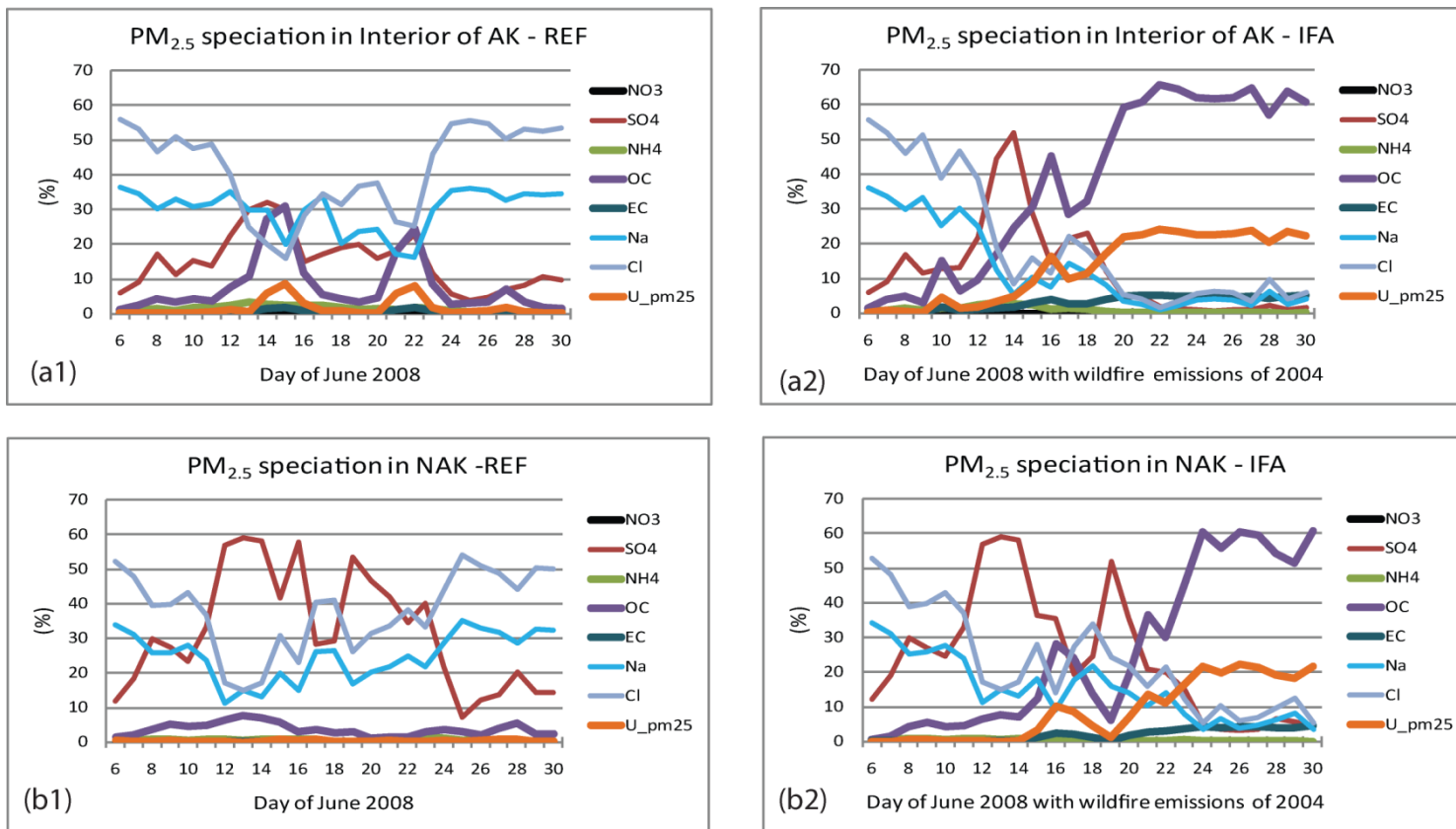
Fig. 6.16. Daily regionally-averaged near-surface $PM_{2.5}$ speciation over regions of interest in Alaska: $a_1$ ($a_2$), $b_1$ ($b_2$), $c_1$ ($c_2$), $d_1$ ($d_2$) refer to $PM_{2.5}$ speciation for Interior Alaska, NAK, WAK and SAK as simulate by REF (IFA), respectively.
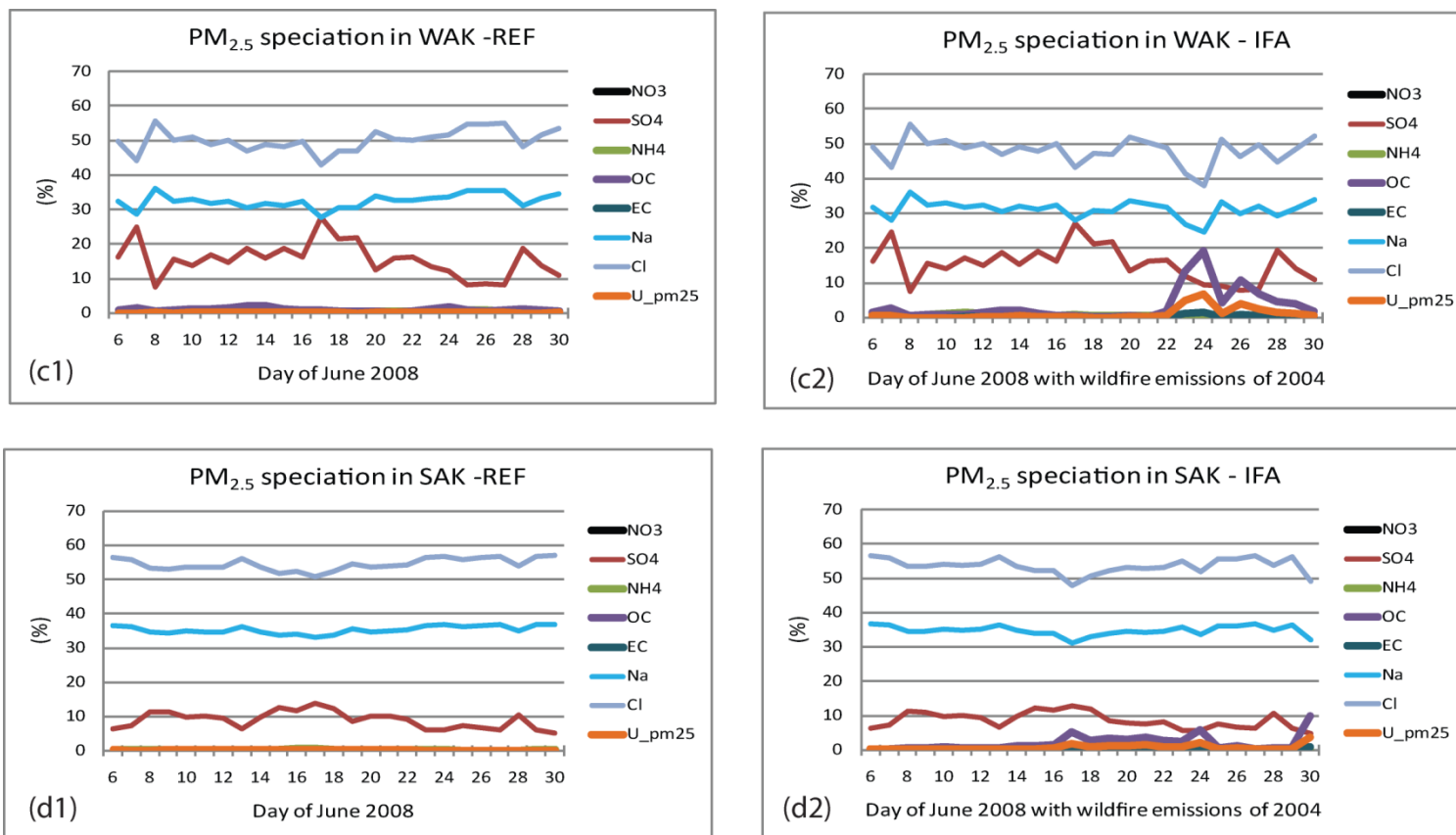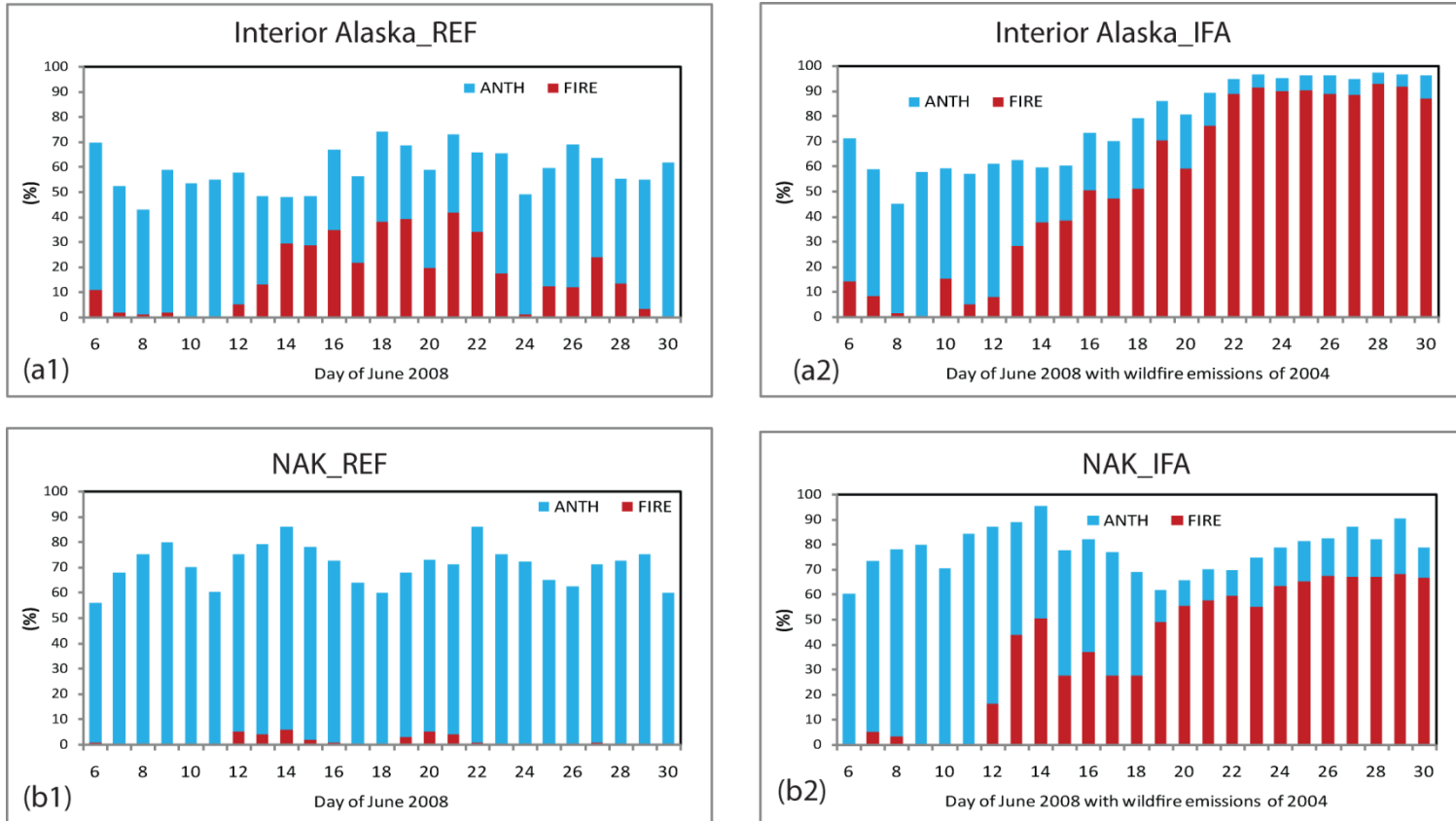
Fig. 6.16. (Cont.)

Fig. 6.17. Contributions of anthropogenic and wildfire emissions to near-surface $PM_{2.5}$ concentrations over regions of interest in Alaska: $a_1$ ($a_2$), $b_1$ ($b_2$), $c_1$ ($c_2$), $d_1$ ($d_2$) show the results for Interior Alaska, NAK, WAK and SAK as simulate by REF (IFA), respectively.
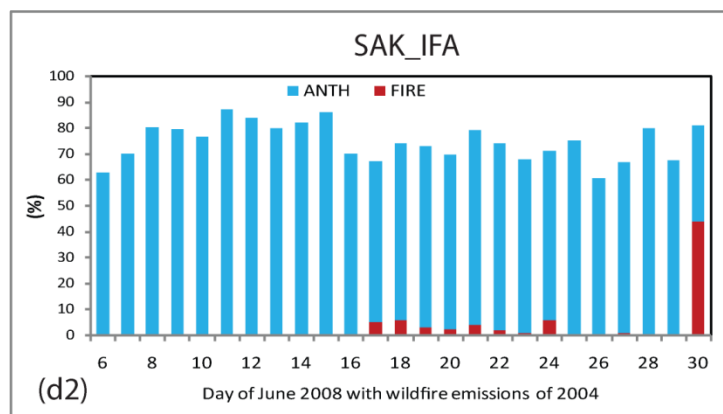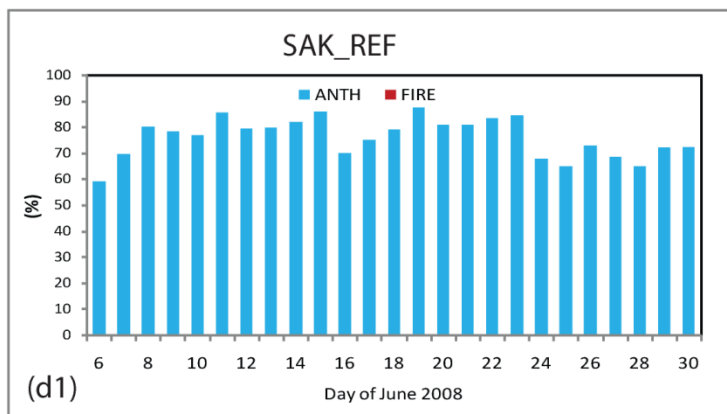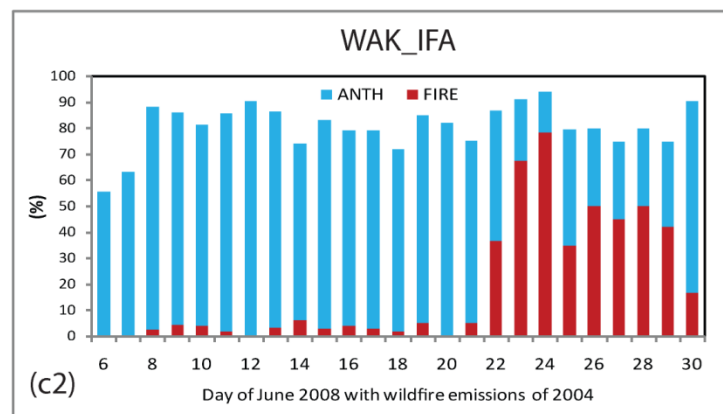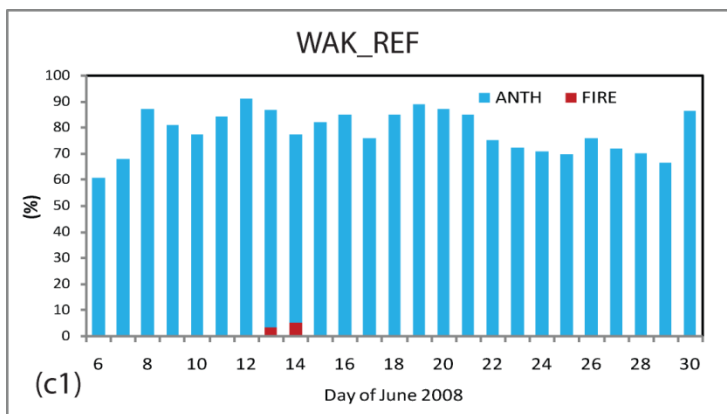
Fig. 6.17. (Cont.)

**Chapter 7 Conclusions**

The increasing trends of aerosol concentrations observed by the Interagency Monitoring of Protected Visual Environments network (IMPROVE, 2013) in the wilderness areas along the Gulf of Alaska during low insolation periods and in Denali National Park (Denali NP) during high insolation periods identified the concerns regarding air quality degradation and visibility impairment in these areas. The small slope values of the observed sulfate concentration trend lines indicate the slow rate of change in sulfate concentrations for both low and high insolation conditions. The observed trends were statistically significant for low insolation conditions and insignificant for high insolation conditions at the 95% confidence level. The large variability of wildfire emissions during high insolation conditions might affect the statistical significance of the linear trends. These wilderness areas and Denali NP are classified as Class I areas of the Clean Air Act. Here, the air quality must be strictly protected to prevent future and remedy existing visibility impairment due to man-made air pollution (ADEC, 2012). In Alaska, aerosol concentrations can be affected by various emission sources such as anthropogenic (e.g. ship, residential, transport, and industrial emissions), wildfire, or long-range transport of pollution from Asian and/or Siberian sources. Therefore, to protect the visibility and air quality of these Class I areas from degradation due to increases in man-made emissions, it is important to investigate which emission sectors are important contributors to the aerosol concentrations in Alaska. We also seek to determine whether the emission increases of those sectors may have caused the increasing trends in aerosol concentrations observed in these areas. A numerical

modeling approach using the Alaska-adapted WRF-Chem model was selected for this study. WRF-Chem allows comparison of model results from simulations with different emission scenarios but the same meteorological conditions, which ensures that modeled aerosol concentration changes stem from changes in modeled emissions.

As the trends of aerosol concentrations differ in regions of Alaska and vary between low and high insolation periods, investigating the relationship between emission changes and aerosol concentrations changes in Alaska were conducted exclusively for low (January) and high (June) insolation periods. For low insolation periods, simulations were performed with three emission scenarios: emissions of January 2000 (referred as reference simulations, REF_Jan), emissions of January 1990 and emissions of January 2000 with applied reductions rate for the ship emissions in accordance with North American Emission Control Areas' (ECA) regulations. For high insolation periods, simulations were performed with two emission scenarios: emissions of June 2008 (referred as reference simulations, REF_Jun) and emissions same as with REF_Jun except wildfire emissions of 2008 substituted wildfire data of June 2004.

Evaluations of model performance were performed for reference simulations for REF_Jan and REF_Jun to examine their accuracy and reliability. The evaluation results showed that WRF-Chem performed well at simulating meteorological conditions over Alaska and the North Pacific under both low and high insolation periods. It captured the temporal evolutions of SLP, T, SW and RH over Alaska with small biases of 1 to 2 hPa, $\sim 0.5$ K, 66 W m$^{-2}$ and $\sim 2\%$, respectively. However, it overpredicted near-surface wind-speed over Alaska during both insolation periods with higher bias for low insolation

period (4.3 m s$^{-1}$) than for the high insolation period (2.1 m s$^{-1}$). The overprediction of near-surface wind-speed was attributed to the coarse resolution of the model domain, which has deficient representations of the surface roughness. In high insolation periods, WRF-Chem better simulated wind speeds with smaller bias of -0.9 m s$^{-1}$ over the North Pacific than over Alaska. WRF-Chem performed well at capturing the main wind-direction over Alaska for both low and high insolation periods with a small bias of 3$^{o}$ and 7$^{o}$, respectively. Performance skill-scores of WRF-Chem model in simulating aerosol concentrations for the coastal monitoring sites along the Gulf of Alaska were within the ranges of a state-of-the-science air-quality model performance.

For low insolation simulations, Alaska was divided into six regions for analysis. The discussion focused on SO$_2$ concentrations, which acted as sulfate aerosol precursors and sulfate aerosol concentrations. These regions were very similar to Alaska climate regions including the Arctic (R1), the west coast (R2), the western maritime (R3), the south central (R4), the eastern maritime (R5) and the Interior Alaska (R6) regions. In the coastal regions along the Gulf of Alaska (R3, R4 and R5), dominant winds came from regions with high ship emissions, suggesting potential advection of the pollutants from ship emissions to these coastal regions. Whereas, in the Arctic, the west coast and Interior Alaska (R1, R2 and R6), the winds were mostly directed from low-emission regions. The SO$_2$ concentration distribution in Alaska was impacted by local emissions. Most regions of Alaska had relatively low SO$_2$ concentrations compared to other areas within the model domain except for R1 that had relatively high SO$_2$ concentrations due to oil production in Prudhoe Bay. On the other hand, sulfate aerosols were strongly

subjected to long-range transport due to long lifetime (e.g. ~ a week (Moore et al., 1980; Bondietti and Papastefanou, 1993)). In the coastal regions along the Gulf of Alaska (R3, R4 and R5), the prevailing wind was from south-southwest and advected sulfate aerosols from the areas of high ship emissions into these regions. Therefore, sulfate aerosol concentrations were higher in R3, R4 and R5 (39, 24, 31 ng kg$^{-1}$, respectively) than in the west coast (R2; 18 ng kg$^{-1}$) and the Interior Alaska (R6; 16 ng kg$^{-1}$). Hence, the western maritime region (R3) located closest to the major shipping lanes had highest sulfate concentrations. In R3, R4 and R5, sulfate aerosol concentrations had high multi-correlation coefficients (R>0.6) with SO$_2$ emissions and wind-speed from the regions with high ship emissions. This finding provides more evidence that emissions from domestic and international shipping lanes were important contributors to aerosol concentrations in these coastal regions. Except for the North Slope (R1) where oil productions were the major contributor to sulfate aerosol concentrations, low multi-correlation coefficients (R<0.5) of sulfate aerosol concentrations in all remaining regions of Alaska versus SO$_2$ emissions and wind speed in Asia and Alaska indicated that Asian and Alaska local anthropogenic emissions were not important contributors to near-surface aerosol concentrations in Alaska. According to Alaska Department of Environment Conservation (ADEC, 2011), at low altitudes, pollutants from China and Japan follow a northeastern track towards the Arctic and encounter the Aleutian Low, and then are easily scavenged due to high precipitation in the cyclonic conditions. The horizontal distribution of simulated hourly averaged sulfate concentrations over the entire domain also showed no evidence of sulfate advection from Asian to Alaska at near-surface layer. Therefore,

despite their high anthropogenic emissions, the Asian plumes did not impact near-surface sulfate concentrations in Alaska during the study period.

Therefore, from my studies and current literature, I find that the answer to scientific question 1 (Chapter 1) is _under low insolation periods, domestic and international ship emissions were the most important contributors to aerosol concentrations in the coastal regions along the Gulf of Alaska._

Emission changes between January of 1990 and 2000 were characterized by strong $SO_2$ emission increases along the shipping lanes, Japan and the northeastern part of China. In Alaska, the inland anthropogenic emission changes were relatively small compared to those changes in the aforementioned areas. There was no correlation existing between the changes of Alaska inland anthropogenic emissions and the changes of sulfate aerosol concentrations. This finding suggests that the change in Alaska inland anthropogenic emissions between these two years was not the main cause for the changes of aerosol concentrations over entire Alaska. Since Asian anthropogenic emissions did not affect sulfate aerosol concentrations at near-surface layer in all regions of Alaska, the increases of $SO_2$ emission in Japan and China did not impact the changes in near-surface sulfate concentrations in Alaska. Therefore, by the process of elimination, we find that the significant increase of international ship emissions led to significant increase of sulfate aerosol and its precursor ($SO_2$) concentrations along the major shipping lanes. The notable increase of sulfate aerosol concentrations in the eastern maritime region (R5) resulted from advection of more strongly polluted air from the international shipping lanes where the emissions increased between 1990 and 2000. The advection of air flow

with increased $SO_2$ and/or sulfate-aerosol concentrations from the shipping lanes to the western maritime region (R3) led to the increase of sulfate-in-cloud concentrations despite the decreases of local $SO_2$ emissions in this region.

According to the WRF-Chem model results, the decreases in $SO_2$- and $NO_x$-ship emissions in compliance with emission reduction rates, introduced by the International Maritime Organization for shipping transports inside and outside the Emission Control Areas (ECA), potentially improved air quality over Alaska with respect to the decreases in sulfate and nitrate-aerosol concentrations. However, significant decreases of sulfate and nitrate aerosols and their precursors are only found along the coast of the Gulf of Alaska, not in the regions further inland. In response to 22% (98%) reductions in $SO_2$-ship-emissions outside (inside) the ECA and 20% reductions of $NO_x$-ship-emissions at all locations over the ocean, the total $PM_{2.5}$ concentrations decreased by slightly greater than 1% over the international shipping lanes and the ECA regions, and less than 1% over entire Alaska, implying that the gas-to-particle conversion was low due to the lack of sunlight under low insolation conditions. The calculated values of

$$\frac{[SO_4^{2-}]aerosol}{[SO_4^{2-}]aerosol+[H_2SO_4]gas+[SO_2]} \times 100\% \quad \text{and} \quad \frac{[NO_3^-]aerosol}{[NO_3^-]aerosol+[HNO_3]gas+[NO_x]} \times 100\%$$

averaged over entire Alaska and over studied episode of 11-31 January 2000 as obtained by REF simulations were 33% and less than 1%, respectively, confirming very weak gas-to-particle conversion in Alaska under low insolation conditions.

Therefore, from my studies, I find that the answer to scientific question 2 (Chapter 1) is *the changes, either increases or decreases in ship emissions led to the*

*increases or decreases in aerosol concentrations in the coastal areas along the Gulf of Alaska under low insolation periods.*

For high insolation periods, for the analysis Alaska was divided in to four regions including Interior Alaska, the northern coast of Alaska, the southern coast of Alaska and the western coast of Alaska. Alaskan wildfire events only occurred within Interior Alaska. The analysis focused on the emissions of $PM_{2.5}$ precursor gases, $PM_{2.5}$ concentrations and speciation. The relative importance of wildfire emissions versus anthropogenic emissions on aerosol concentrations in Interior Alaska was examined for weak (June 2008) and strong (June 2004) Alaskan wildfire activity years. In contrast with Alaska fire activities, Siberian fire activity was strong in 2008 and weak in 2004.

The analysis results of temporal evolution of hourly $PM_{2.5}$ concentrations in Interior Alaska combined with the analysis of corresponding daily averaged wind fields and horizontal distributions of aerosol concentrations over entire domain indicated that in Interior Alaska aerosol concentrations were mostly impacted by local anthropogenic, Alaskan wildfire and occasionally by ship emissions coming from the west. The high terrain of the Alaska ranges along the southern coast prevented the sea breezes coming from the intensive ship-emission areas (i.e., from the Gulf of Alaska) to reach Interior Alaska. The analysis results also showed that Japanese-anthropogenic and Siberian-wildfire emissions minimally affected air quality in all regions of Alaska during the entire study episode as they were strongly diluted before reaching Alaska. Under the weak fire activity scenario, anthropogenic emissions were the major contributor to $PM_{2.5}$ concentrations in Interior Alaska. This sector contributed 43% of hourly regionally

averaged $PM_{2.5}$ concentrations in the region. Although there were only few small wildfire events occurring during June 2008, the contributions of Alaskan wildfire emissions to hourly regionally-averaged $PM_{2.5}$ concentrations were notable (up to ~16%). Under the strong fire activity scenario, Alaskan wildfire emissions were the biggest contributor to $PM_{2.5}$ concentrations in Interior Alaska. In this region, on average over the entire study episode, Alaskan wildfire emissions contributed ~52% to regionally near-surface $PM_{2.5}$ concentrations with the maximum contributions up to ~90% during the day when extreme fire events occurred. In this strong fire activity scenario, anthropogenic emission contributions to $PM_{2.5}$ concentrations averaged over entire study period were about ~24%, which was much less than wildfire emission contributions.

Therefore, from my studies, I find that the answer to scientific question 3 (Chapter 1) is *in Interior Alaska the contributions of local wildfire emissions to aerosol concentrations were notable even under weak Alaska fire activity scenario. Under strong Alaska fire activity, local wildfire emissions were the dominant source  of aerosols Interior Alaska*. Anthropogenic emissions were only important contributors to $PM_{2.5}$ concentrations in Interior Alaska under weak wildfire activity scenario. Siberian wildfire and Japanese anthropogenic emissions did not affect aerosol concentrations in Interior Alaska during the entire study period.

In Interior Alaska under strong Alaskan wildfire activity scenarios (IFA), the vertically-integrated emissions of $PM_{2.5}$ precursor gases averaged over the region increased about 25 times compared with weak Alaska fire activity scenarios (REF_Jun). In response to these increases, in Interior Alaska the vertically hourly averaged $PM_{2.5}$

concentrations averaged over the region increased about nine times, with the strongest increases occurring in the near-surface layer (~19 times). In this region, the differences of daily regionally-averaged $PM_{2.5}$ concentrations and $PM_{2.5}$ speciation responded with the increases in daily regionally-averaged $PM_{2.5}$ precursor emissions between IFA and REF_Jun. This result indicates that the increases in Alaskan wildfire emissions lead to obvious increases of total $PM_{2.5}$ concentrations and altered $PM_{2.5}$ speciation in concert with the increases in organic carbon, unspeciated-$PM_{2.5}$ and elementary carbon percentages.

Therefore, from my studies, I find that the answer to scientific question 4 (Chapter 1) is *under high insolation periods the increases in Alaskan wildfire emissions led to the increases in aerosol concentrations in the Interior Alaska.*

The above answers to the scientific questions 1-4 verified the research hypothesis that *in the wilderness areas along the Gulf of Alaska, the increases in aerosol concentrations observed during low insolation periods mostly stemmed from the increases in domestic and international ship emissions in the North Pacific; whereas in Denali NP, the increases in aerosol concentrations observed during high insolation period might be contributed by the increases in Alaskan wildfire emissions.* However, since the increasing trends in aerosol concentrations during high insolation conditions are statistically insignificant (Chapter 1), wildfire emission increases might not be the only cause for all of the observed aerosol trends. Further study that examines the historical trend in wildfire emissions only and then the efficiency that those emitted amount become sulfate aerosols would be an appropriate approach to quantiatively explain the

magnitude of the observed increases in aerosol concentrations. Similar approach would also be applicable to quantiatively explain how ship emission increases contribute to the magnitude of the observed increases in aerosol concentrations during low insolation conditions.

To prevent degradation of the air quality in wilderness areas along the Gulf of Alaska from enhanced aerosol concentrations, it is recommended that emissions from shipping lanes be reduced. Under low insolation periods, the reduction rates for emissions of $PM_{2.5}$ precursor gases ($SO_2$ and $NO_x$) in accordance with current ECA regulations only marginally improved air quality of Alaska with respect to the reductions in $PM_{2.5}$ concentrations. This poor improvement may be due to the low photochemical gas-to-particle conversion because of the lack of sunlight. Therefore, the reductions of primary $PM_{2.5}$ directly emitted from ships should benefit the air quality in Alaska more than the reductions of $PM_{2.5}$-precursor emissions. Such hypotheses should be tested in further studies of the ECA regulation benefits on air quality in high latitude areas like Alaska.

A future study that explicitly examines the benefit of controlling human-initiated wildfire emissions on air quality in Interior Alaska needs to be conducted.  This study should examine whether it is worthwhile to apply more funding towards economic and labor expenses to help control human-initiated wildfires and their emissions.  This may be the key factor to preventing the air quality of the Denali NP from any further degradation.

## References

ADEC, 2011. Overview of Alaska and air quality. Amendments to state air quality control plan, appendix to Section III.K: Areawide pollutant control program for regional haze. Available at http://dec.alaska.gov/air/anpms/rh/rhdoc2/Appendix%20III.K.3.pdf

ADEC, 2012. Regional haze trans-boundary monitoring study report. Air Quality Division, Air Monitoring and Quality Assurance Program. Available at http://www.dec.state.ak.us/air/am/am_projects.htm

Bondietti, E.A., Papastefanou, C., 1993. Estimates of residence times of sulfate aerosols in ambient air. Sci. of Total Environ., 136, 25-31.

Interagency Monitoring of Protected Visual Environments (IMPROVE), 2013. Online IMPROVE Database Access; retrieved in Mar 2009 and Oct 2012 from IMPROVE website at http://views.cira.colostate.edu/fed/DataWizard/Default.aspx

Moore, H.E., Poet, S.E., Martell, E.A., 1980. Size distribution and origin of Lead-210, Bismuth-210 and Polonium-210 on airborne particles in the troposphere. Proc. Int. Symp. On Natural Radiation Environment III, 1, 415-429.